Crystals in Supramolecular Chemistry

Edited by Alicia M. Beatty

Proceedings from the Symposium

Crystals in Supramolecular Chemistry

ACA TRANSACTIONS
VOLUME 39

Hyatt Regency Chicago, IL
July 17 – 22, 2004

Editor

Alicia M. Beatty
Dept of Chemistry
Mississippi State University
Mississippi State, MS 39762
Tel: 662 325 0032
Fax: 662 325 1618
abeatty@ra.msstate.edu

Notice of Copyright for Volume 39

TABLE OF CONTENTS

INTRODUCTION

Crystals in Supramolecular Chemistry

The contributions to this volume stem from the two-day Transactions symposium held at the annual ACA meeting, Chicago, IL, July, 2004. Each of the four half-day sessions represented diverse aspects of a crystallographic/chemical approach to supramolecular chemistry. This volume is organized to reflect the sessions of the symposium: Crystal Structure Prediction, Crystal Growth Mechanisms, Crystal Structure Design, and Applications of Crystal Design.

Many scientists are still trying to answer Gavezzotti's question "Are Crystal Structures Predictable?"[1] in the affirmative, so it seems appropriate that 10 years later the first paper in this volume is a report by Price *et al.* on the current state of methods used for predicting crystal structures. Joel Bernstein's contribution follows, in which he lends his unique historical and scientific perspective to a discussion of crystal structure prediction and polymorphism. A more statistical view of how molecules crystallize is provided by Pidcock and Motherwell, in which they describe a molecular box model for crystal packing. Along these lines, Lauher contributes a discussion of the use of subperiodic groups in analyzing molecular assemblies. The following paper, from Davis *et al.* provides a description of experimental methods for predicting whether a particular co-crystalline phase is possible.

From the question of crystal structure prediction, we move to the mechanisms for crystal growth. The first contribution in this section is from Kahr *et al.*, who probe crystal growth from the fluorophore luminescence observed during confocal laser scanning microscopy. Methods for *in situ* studies of the crystal growth of a Cu(II) coordination complex are given by Palmore *et al.* Swift *et al.* discuss the crystal structure and growth of uric acid, including an analysis of epitaxial growth of two different crystalline phases. Finally, Seaton and Blagden examine interfaces and epitaxy of benzoic acid and benzamide from both computational and experimental points of view.

The third section of the volume is concerned with the design of supramolecular assemblies. Hosseini *et al.* provide examples of tectons that, when combined with metal ions, lead to 1-D coordination networks. Hydrogen bonding produces a 1-D organic assembly in a paper by MacGillivray *et al.* Next, Brammer *et al.* discuss inorganic and organic halogens as design tools, including electrostatic potential calculations and experimental results. Finally, Aakeröy *et al.* demonstrate that boronic acids are not just for cross-coupling reactions anymore, they also can be used to create hydrogen-bonded networks.

Crystalline material applications are being achieved through crystal design, as demonstrated by the final two papers. Braga *et al.* provide examples of reactions performed with crystalline organometallic solids, while Ward *et al.* describe host compounds that facilitate selective inclusion from isomeric mixtures of methylated benzene guests.

The four sessions of the 2004 ACA Transactions symposium and the four sections in this volume demonstrate the ways in which chemists look at crystals, from computational methods of crystal structure prediction to practical uses of crystalline materials. The topic was inspired by Ray Davis, then the ACA President, who has for years been dedicated to both Chemistry and Crystallography. I thank him, as well as the Donors of The American Chemical Society Petroleum Research Fund, for the partial support of the 2004 ACA Transactions Symposium.

Alicia Beatty
Mississippi State University
Starkville, Mississippi
August 2, 2005

---

[1] A. Gavezzotti, *Acc. Chem. Res*. **27** (1984) 309-314.

CRYSTAL STRUCTURE PREDICTION AND POLYMORPHISM - SOME MUTUAL INSIGHTS

Sarah (Sally) L. Price, Binal Patel, Pinky Pridhanani-Jethani and Antonio Torrisi
Dept. of Chemistry, University College London, 20 Gordon St, London WC1H 0AJ, UK

1. ABSTRACT

Computational crystal structure prediction seeks to predict the crystal structure of an organic molecule from the chemical diagram. The blind test of crystal structure prediction, organized by CCDC in spring 2004, gives an independent measure of the current state of development of such methods. However, interpreting the results is complicated by the possible polymorphism of the test molecules.

Most methods of crystal structure prediction are based on a search for the crystal structure that corresponds to the global minimum in the lattice energy. This generates a set of hypothetical crystal structures that are energetically feasible, which usually includes many structures that are not observed. Some of the variety that can be displayed in the types of hypothetical low energy structures is illustrated by the low energy structures obtained for imidazole, uric acid and 2,6-diamino-3,5-dinitro pyrazine, and discussed in terms of their crystallization behaviour. Progress towards a reliable method for computational crystal structure prediction raises many questions about the factors that determine polymorphism, whilst providing insight into the crystallization options for specific molecules.

2. INTRODUCTION

The ultimate aim of computational scientists working on organic crystal structure prediction is to find a methodology of predicting the full crystal structure (i.e. space group, cell constants and fractional atomic coordinates), given just the chemical diagram of the molecule. Once we have a reliable method for crystal structure prediction, it would be a practical aid in the design of new molecular materials with desired supramolecular properties. It would also have to quantify the factors that determine which crystal structures are adopted by organic molecules. Our progress towards this aim has been charted by the blind tests [1,2] of crystal structure prediction which have been organized by the Cambridge Crystallographic Data Centre. The results of the test held in 2004 [3] actually had fewer correct predictions than in previous years, possibly because of the increased complexity in the crystal structures used within the test (particularly the removal of the Z'=1 restriction). Nevertheless, there have been some correct predictions, even under such blind test conditions. The polymorphism amongst the blind test molecules (one case known for the test [1], another polymorph found later [4]) clearly demonstrates some of the fundamental challenges in crystal structure prediction.

Most of the successful predictions of crystal structures in the blind test have been based on searches for the global minimum in the lattice energy. This corresponds to searching for the thermodynamically most stable crystal structure, but approximating the free energy by the lattice energy. The assumption that the observed crystal structure will be the most thermodynamically stable one is clearly a good starting point, as we expect that most slow crystallization methods would yield the thermodynamically stable structure. However, since there are many examples of molecules that have two or more polymorphs that appear to be stable under the same thermodynamic conditions, including concomitant polymorphs that crystallize in the same batch [5], we clearly need to go beyond just thermodynamic considerations and also consider kinetic factors. The cases where a thermodynamically more stable polymorph has not been discovered until a pharmaceutical compound has been in production for some time (such as ritonavir [6,7]), or after the metastable form has been known for over a century [8], clearly are a complication to assessing the success of crystal structure prediction. However, they also point to a major potential benefit of such work – to warn of the potential existence of a more stable polymorph. Crystallization strategies to search for this hypothetical form could then be developed [9]. Thus, although crystal structure prediction studies tend to

find more energetically feasible crystal structures than known (or expected) polymorphs, consideration of the set of such structures can aid the understanding of the supramolecular behaviour of the molecule.

This paper reports some examples of searches for the minima in the lattice energy for small rigid molecules, chosen to illustrate some of the different types of crystal energy landscapes that have been observed, as well as the challenges facing computational crystal structure prediction.

3. METHOD

Essentially the same methodology was applied to generate a set of lattice energy minima for imidazole, uric acid, and 2,6-diamino-3,5-dinitropyrazine, with any variations discussed in the specific section. Molecules that would normally be considered as rigid were chosen, as the modeling method uses rigid molecules, to avoid requiring an intramolecular potential to model the deviations in the molecular structure caused by the packing forces. The experimental molecular structure was taken from the most accurate determination in the Cambridge Structural Database [10]. For X-ray determinations, the bonds to hydrogen atoms were elongated to standard neutron values [11]. The MP2 6-31G** wave function for this molecular structure was calculated using GAUSSIAN [12], and analyzed by GDMA [13] to give a distributed multipole [14,15] (DMA) representation of the charge density. This molecular structure was then optimized at the same level of *ab initio* theory to give an approximation to the gas-phase molecular structure, and the corresponding DMA obtained.
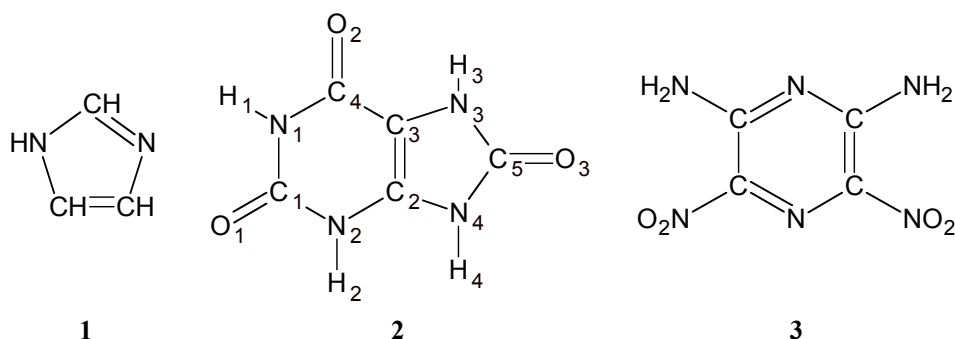
Scheme 1. Imidazole (1), Uric acid (2), 2,6-diamino-3,5-dinitropyrazine (3).

The DMA model of the molecular charge density was used to calculate the electrostatic contribution to the lattice energy within DMAREL [16,17], with the charge-charge, charge-dipole and dipole-dipole terms being evaluated by Ewald summation and the remaining terms in the multipole expansion up to R^{-5} calculated by direct summation up to a molecule-molecule separation of 15 Å. Thus, this approach is modeling the electrostatic contribution to the lattice energy essentially to the accuracy of the wave function, and thus automatically modeling the electrostatic directionality [18] in hydrogen bonding and $\pi-\pi$ stacking arising from lone pair and π [18] electrons. All other contributions to the intermolecular forces were assumed to be represented by an empirical repulsion-dispersion potential of the form

$$U = \sum_{i \in 1, k \in 2} U_{ik} = \sum_{i \in 1, k \in 2} (A_{\iota\iota} A_{\kappa\kappa})^{1/2} \exp(-(B_{\iota\iota} + B_{\kappa\kappa})R_{ik}/2) - \frac{(C_{\iota\iota} C_{\kappa\kappa})^{1/2}}{R_{ik}^{6}} \tag{1}$$

where atom i in molecule 1 is of type ι, and atom k in molecule 2 is of type κ. The parameters were those of the FIT potential [19], which extended the empirically fitted potential of Williams *et al.* [20,21] for C, H_C, N and O atoms to also cover hydrogen bonding (H_N), except where the transferability of the C parameters proved unsatisfactory. The adequacy of the intermolecular potential was tested by comparing the experimental crystal structure with the closest lattice energy minimum obtained with the intermolecular potential, keeping the experimental molecular crystal conformation rigid (ExptMinExpt). This was

contrasted with ExptMinOpt, the corresponding lattice energy minimum obtained using the *ab initio* optimized molecular structure (and corresponding DMA), to determine the effects of the differences in conformation between the crystal and the "gas-phase" molecules.

The search for the low energy minima in the lattice energy used the *ab initio* optimized molecular structure in the program MOLPAK [22] to generate up to 200 densely packed crystal structures in each of 29 most commonly found packing types with Z'=1, including the *P*1, $P\bar{1}$, *P*2$_1$, *P*2$_1$/*c*, *P*2$_1$2$_1$2, *P*2$_1$2$_1$2$_1$, *Pna*2$_1$, *Pca*2$_1$, *Pbca*, *Pbcn*, *C*2/*c*, *Cc* and *C*2 space groups. Each of these crystal structures was then lattice energy minimized using DMAREL, using the same intermolecular potential. Thus the closest approximation to the experimental crystal structure that it would be possible to find in the search would be equivalent to ExptMinOpt. Any minima that did not correspond to a true minimum in the lattice energy, as judged from the second derivative properties, were excluded.

4. RESULTS

4.1 Imidazole

Imidazole is an ideal system for this particular method of modeling the molecular crystal, as it is undoubtedly rigid and there is a published crystal structure [23] determined by neutron diffraction at 103 K. The crystal comprises chains of N−H···N hydrogen bonded molecules. The FIT+DMA model potential satisfactorily reproduces this crystal structure and the frequencies of the low energy *k*=0 intermolecular lattice vibrations both by lattice energy minimization and lattice dynamics [24] and in a Molecular Dynamics simulation [25]. This is confirmed in Table 1, where it is also clear that the minor differences between the *ab initio* optimized and neutron molecular structures have a very small effect on the structure obtained by lattice energy minimization.

Table 1

The modeling of the experimental crystal structures by lattice energy minimization

		a/Å	b/Å	c/Å	β /°	Density g cm^{-3}	Lattice Energy kJ mol^{-1}
Imidazole [23]	Expt *P*2$_1$/*c*	7.569	5.366	9.785	119.08	1.302	-67 -85[a]
	ExptMinExpt	7.718	5.461	9.814	120.69	1.270	-78.4
	ExptMinOpt	7.721	5.501	9.839	121.05	1.263	-75.1
	Closest in search	7.721	5.501	9.839	121.05	1.263	-75.1
Uric Acid [26]	Expt *P*2$_1$/*c*	6.208	7.403	14.464	114.90	1.852	
	ExptMinExpt (A$_{CC}$)	6.187	7.151	14.477	113.81	1.905	-181.6
	Closest in search (Expt)	6.187	7.152	14.477	113.81	1.906	-181.6
	ExptMinOpt (A$_{CC}$)	6.926	7.390	14.126	112.72	1.842	-164.9
	Closest in search (Opt)	6.296	7.390	14.125	112.72	1.842	-164.9
2,6-diamino-3,5-dinitropyrazine [27]	Expt *P*2$_1$/*c*	9.014	12.960	6.394	100.77	1.812	
	ExptMinExpt (SCF)	8.875	12.882	6.161	94.03	1.891	-145.3
	ExptMinOpt (SCF)	8.919	13.025	6.139	91.40	1.864	-135.8
	Closest in search	8.918	13.023	6.141	91.79	1.865	-135.9

a Range of measured heats of sublimation [28]. Where required, cells have been transformed to the same axis setting using PLATON [29]
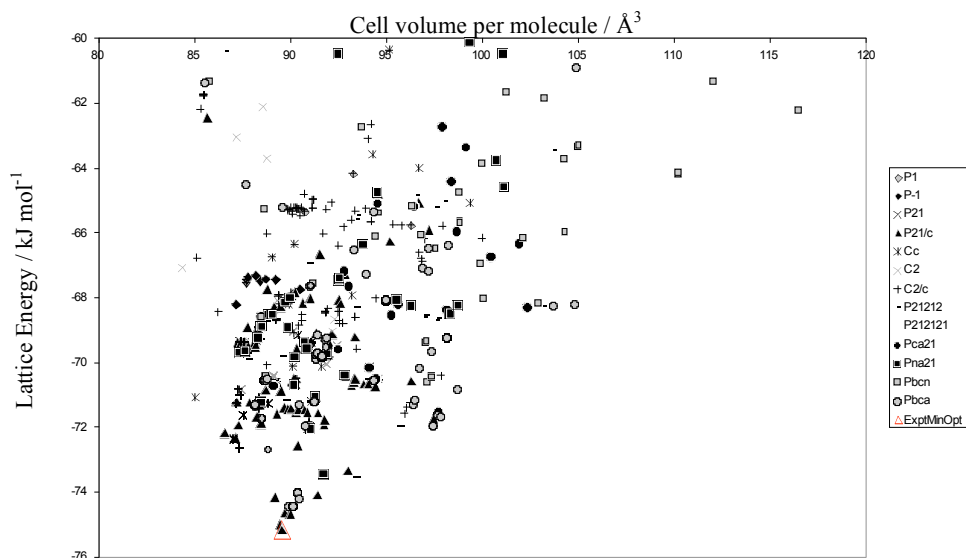
Figure 1. The distribution of low energy structures found in a search for minima in the lattice energy of imidazole. The minimum corresponding to the known crystal structure (ExptMinOpt) is denoted by the open triangle.

The low energy minima in the lattice energy found in the search **(Figure 1)** show the typical result of there being a large number of crystal structures within 10 kJ mol^{-1} of the global minimum (an estimate of the likely maximum energy difference between polymorphs [30]), with a small variation in density. Nevertheless, the search has found ExptMinOpt as the global minimum.

Comparison of the unique low energy crystal structures shows a range of variations from the known crystal structure. Some of the crystal structures that are very close to the global minimum are virtually indistinguishable by visualization, though differences are apparent in the powder pattern. However, within less than 2 kJ mol^{-1}, there are structures where hydrogen bonded molecules are coplanar, whereas the tilt between adjacent molecules in the experimental structure is over 50 °. Other structures show considerable variations on the simple anti-parallel stacking of the hydrogen bonding chains in the observed structure, and yet are only 3 to 5 kJ mol^{-1} less stable. This includes some polar crystals, which could have a destabilising dipole moment [31] if grown under unusual conditions. Nevertheless, all the low energy crystal structures are based on the same hydrogen bonding network, and the anti-parallel arrangement of the chains is favoured.

Concluding, the known crystal structure of imidazole is found as the thermodynamically most stable static structure at 0 K. Although other crystal structures are thermodynamically feasible, they have the same dominant hydrogen bonding motif. Hence, it seems unlikely that the conditions of crystallization could be readily manipulated to give a kinetic advantage in nucleation and growth to an alternative structure that could result in a long-lived polymorph.

4.2 Uric Acid

Uric acid contrasts with imidazole in that it has 4 hydrogen bond donors and 3 acceptors, and thus can form a variety of hydrogen bonds. It is medically relevant as it is found in human kidney stone deposits, in both the monoclinic anhydrate form and the less stable dihydrate form. The latest crystal structure determinations in the Cambridge Structural Database by Ringertz [26,32] date back to the mid 1960s. Thus, when the experimental crystal structure was found to differ from the essentially planar *ab initio* optimized structure in that the N2−H2 bond deviated by 17 ° from planarity **(Figure 2a)**, it seemed likely that this deviation could have been an artefact of the X-ray determination. Attempts to reproduce the experimental crystal structure using the FIT potential revealed that it appeared to overestimate the repulsion due to the carbon atoms, and so A_{CC} in equation (1) was empirically reduced by 35 % to 240335 kJ mol^{-1}. This gives an acceptable reproduction of the crystal structure with either molecular model (Table 1, **Figure 2b**),

though the differences in the molecular structure made a reasonable difference to the reproduction of the crystal structures and hydrogen bond lengths, with the most marked effect being the lower lattice energy with the non-planar N2–H2 bond.
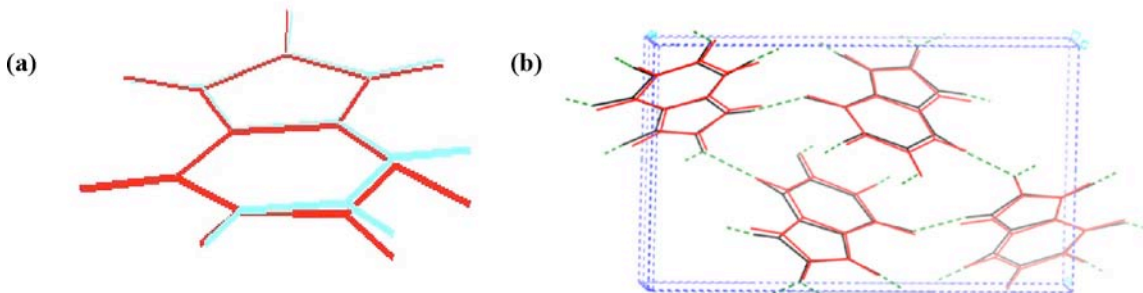
Figure 2. (a) Overlay of the experimental (red) and *ab initio* optimized (cyan) molecular structures of uric acid. (b) Overlay of the experimental crystal structure (black) of uric acid [26] with ExptMinOpt (red), the minimum obtained with the *ab initio* optimized molecular structure and same potential used in the search.

The search for minima in the lattice energy, with the *ab initio* optimized molecular model **(Figure 3a)**, found the experimental structure as one of the less dense structures almost 5 kJ mol^{-1} above the global minimum. Many of the denser, more energetically favourable structures used different combinations of hydrogen bond donors and acceptors. For example, a hypothetical structure only 1.1 kJ mol^{-1} above the global minimum has the same N1–H1···O1=C1 cyclic double hydrogen bond motif as the experimental structure, but the five membered ring forms a double hydrogen bond motif using N4–H4···O3=C5 instead of N3–H3···O3=C5, and the single hydrogen bonds also differ in nature and orientation (**Scheme 1** defines the atom labelling). This implies that should a route be found to form such crystal structures, there is likely to be a significant barrier for a solid state transformation to the known structure.
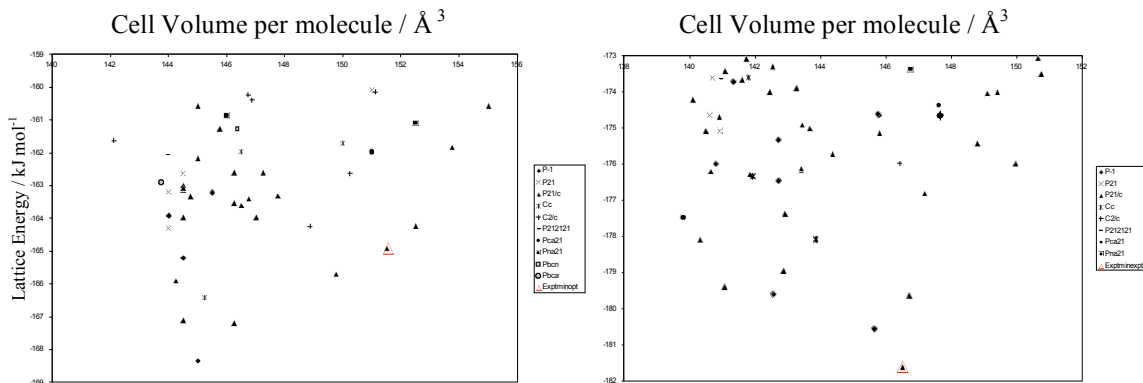
Figure 3. The distribution of low energy structures found in a search for minima in the lattice energy of uric acid with (a) the *ab initio* optimized molecular structure and (b) the molecular structure found in the known crystal structure. The minima corresponding to the known crystal structure (ExptMinOpt for (a), ExptMinExpt for (b)) are denoted by the open triangles.

Given the uncertainty in the computational model being used for the molecular structure and intermolecular forces of uric acid, another search was performed using the experimental molecular structure **(Figure 3b)**. This time, the known structure was found at the global minimum in the lattice energy. The structures that were previously predicted more stable than the known structure were also found again within about 6 kJ mol^{-1} of the minimum. This significant change in the relative energies of the crystal structures was consistent with the distortion of N2–H2 forming a shorter hydrogen bond in the known structure.

Thus, the quality of the computational model for uric acid considerably limits the confidence that can be placed in the relative energies of the hypothetical structures. The *ab initio* optimized structure was generated at the correlated MP2 6-31G** (d,p) level, which gives marked pyramidalization of the amino

groups and very slight non-planarity to the structures of guanine and adenine [33], in contrast to the less realistic SCF wavefunctions. Thus the *ab initio* method used is certainly likely to be correct in that the large deviation of N2–H2 from the plane would not be found in the true gas phase structure, but it is difficult to give a reliable estimate of the energy penalty for the conformational distortion. It is quite likely to be much less than one kJ mol^{-1}. Hence, the known crystal structure is one of the lowest in energy, and may well be the thermodynamically preferred structure. The calculations also show that hypothetical structures with different hydrogen bonding motifs are competitive in energy.
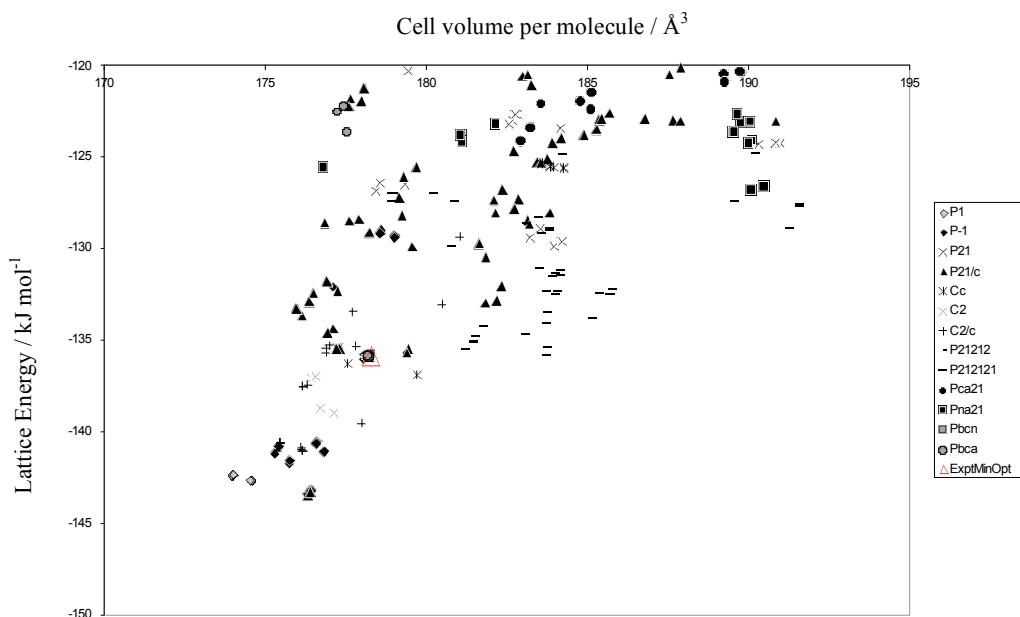
We attempted to grow crystals of uric acid suitable for X-ray diffraction by solvent evaporation, slow cooling and vapour diffusion, but this was unsuccessful, as were attempts to repeat a gel-filtration method [34]. Such experiments were severely limited by the low solubility of uric acid in many solvents. Uric acid crystals up to 250 µm can be grown from hot aqueous solutions [35]. Thus crystallization conditions for growing good uric acid crystals are limited, and hence it is not yet possible to say whether this has prevented us from finding new polymorphs.

4.3 2,6-diamino-3,5-dinitropyrazine

This molecule **(Scheme 1)** involves hydrogen bonding groups that are often used in energetic materials, and is closely related to stable insensitive explosives that are under development. The recently determined X-ray crystal structure [27] at 204 K, shows extensive inter- and intramolecular hydrogen bonding forming sheets in the *ab* plane. These sheets are stacked along the *c* direction in a $P2_1/c$ structure. The intramolecular hydrogen bonding ensures that the molecule is almost planar within the crystal, and so the differences in using the *ab initio* optimized molecular structure and the experimental molecular structure were small. The FIT model potential was able to reproduce the structure of the hydrogen bonded sheets well **(Figure 4a)**, and their parallel stacking, but produced a significant error in the β angle (Table 1, **Figure 4b**). Since the distributed multipoles of an SCF wave function produced a somewhat better reproduction of the crystal structure than the MP2 wave function, possibly because the potential was parameterized in conjunction with an SCF electrostatic model, this less realistic electrostatic model was used for the search. It seemed unlikely that any minor modifications of the FIT potential would improve the close layer stacking in this dense crystal structure. Thus, the reproduction of this crystal structure limits the confidence that can be placed in the modeling.
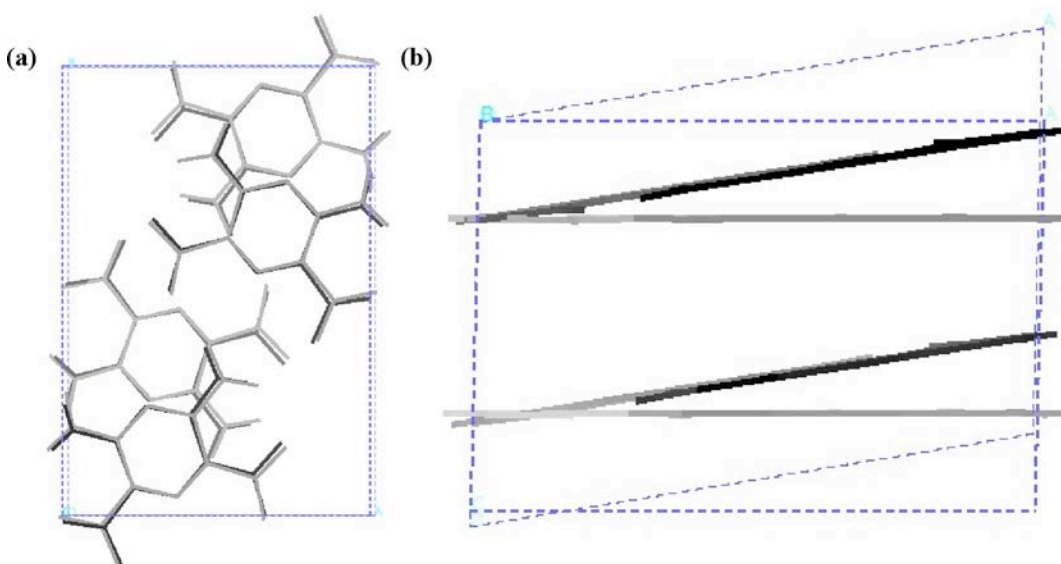
Figure 4. Overlay of the experimental crystal structure (black) of 2,6-diamino-3,5-dinitropyrazine [27] with ExptMinOpt (grey), the minimum obtained with the *ab initio* optimized molecular structure and same potential used in the search. (a) View showing sheet structure (b) overlay of cell perpendicular to the sheets.

Sarah (Sally) L. Price, Binal Patel, Pinky Pridhanani-Jethani and Antonio Torrisi

Cell volume per molecule / Å³

Figure 5. The distribution of low energy structures found in a search for minima in the lattice energy of 2,6-diamino-3,5-dinitropyrazine. The minimum corresponding to the known crystal structure (ExptMinOpt) is denoted by the open triangle.

The search for minima in the lattice energy, using the *ab initio* optimized molecular structure, found the experimental structure (ExptMinOpt) 7.5 kJ mol⁻¹ above the global minimum **(Figure 5)**. Virtually all the more stable structures are based on the stacking of sheets, although there are marked differences between the hydrogen bonding motifs within the sheets. **Figure 6** contrasts the sheet found in the most stable structure, with that found experimentally. The experimental sheet contains a distortion of a plausible dimer structure, with a NH_2 group intermolecularly hydrogen-bonded to both the NO_2 groups of one neighbour. However, this is compromised with a NO_2 group hydrogen bonded to a N–H of another neighbour producing a close N=O⋯O=N contact. The sheet in the global minimum structure has a NO_2 to NH_2 distorted double hydrogen bond, and a NH_2 hydrogen bonding to NO_2 groups in different molecules which produces a short N=O⋯N(pyrazine) contact. Many of the hydrogen bonds are quite long, and vary in length with the small rearrangements that occur in the different crystal structures based on similar sheets. Thus, the hydrogen bonding in both sheets in **Figure 6** is compromised by the inevitable proximity of close interactions between electronegative atoms. The relative energies of the structures would change further if the modeling allowed low energy distortions of the NH_2 and NO_2 groups. Indeed, when the experimental molecular structure was used in the search, the energy gap between the most stable crystals structure with either sheet shown in **Figure 6** reduced from 7.5 to 4.3 kJ mol⁻¹. This shows that the minor conformational distortions favour the observed sheet. However, the global minimum sheet found by the computational model is certainly thermodynamically competitive to the known sheet.

There are many low energy structures in **Figure 5** because the sheets can overlay in a variety of ways. **Figure 7** shows some of the different stackings found for the sheet **(Figure 6a)** which was predicted to give the most stable structure. Whilst the pyrazine rings are not vertically stacked, they may overlay various hydrogen bonding regions, with partial overlap with either amino or nitro groups. In most cases, the sheet dipole moments alternate, though there are cases (e.g. **Figure 7b** and **c**) where the packing produces a polar crystal structure. It is also worth noting that the small scale of the search (Z'=1 in limited space groups) will limit the number of alternative stackings of the sheets that could be found. It is likely that other crystals structures could be constructed that mixed the modes of stacking to give more complicated structures of similar energy.

(a)   (b)
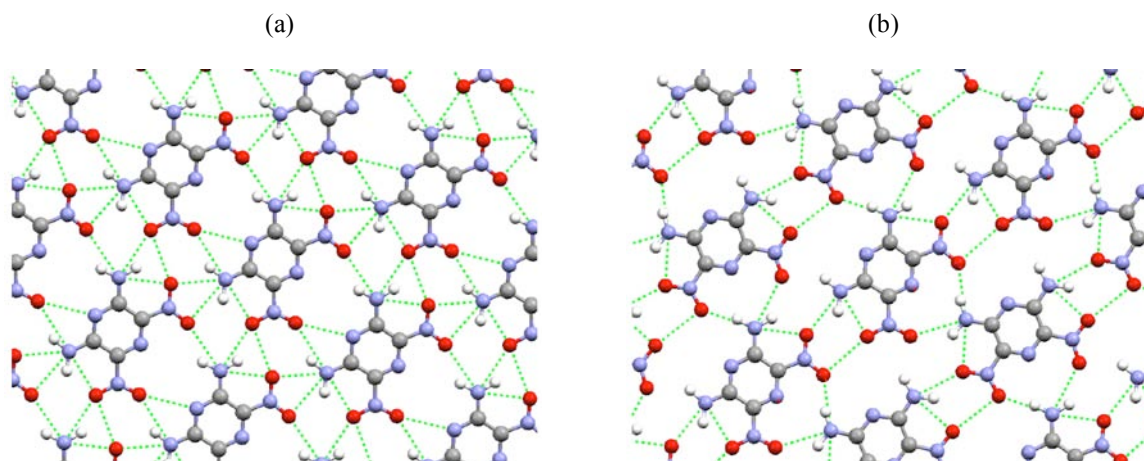
Figure 6. The sheet structure of 2,6-diamino-3,5-dinitropyrazine found in (a) the global minimum energy structure in the search, contrasted with (b) the corresponding model of the experimental sheet structure (ExptMinOpt). The dotted lines denote contacts between nitrogen and oxygen that are less than the sum of the van der Waals radii, which includes both hydrogen bonds and short intermolecular contacts between heteroatoms, drawn using Mercury [36].
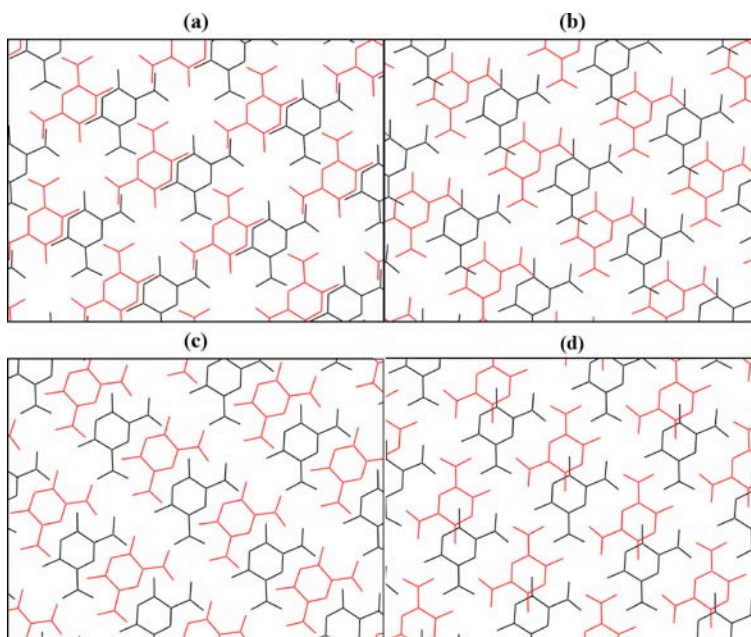
Figure 7. Some of the alternative sheet stackings found for 2,6-diamino-3,5-dinitropyrazine, based on the same sheet structure (a) global minimum AM93 ($P2_1/c$), lattice energy, U_{latt}= -143.4 kJ mol^{-1}, (b) AA91 ($P1$), U_{latt}=-142.6 kJ mol^{-1}, (c) AV79 ($Pna2_1$), U_{latt}=-136.9 kJ mol^{-1}, (d) AB88 ($P\bar{1}$) U_{latt}=-135.5 kJ mol^{-1}. Hydrogen atoms have been removed for clarity.

Given the problems in reproducing the experimental crystal structure, and the sensitivity to low energy distortions of the molecular structure, we can have little faith in the relative energies of the different structures that fall within this small energy range of 7.5 kJ mol^{-1} of the global minimum. However, given the nature of the hydrogen bonded sheets, it is very plausible that there are a variety of positions for stacking the sheets above each other. The bumpiness of the repulsive wall above the molecule, as modelled by the isotropic atom-atom potential is likely to be unrealistic because the π electron density etc. may well flatten this shape. The high density of 2,6-diamino-3,5-dinitropyrazine and related energetic materials probably implies that a specific, non-empirical, anisotropic atom-atom repulsive potential (c.f. the recently developed model for the chlorobenzenes [37]) would be worth developing for more realistic computational modeling. Nevertheless, whilst improving the intermolecular potential may well reproduce the stacking in the known structure better, and reorder the energies, it is likely that there will remain alternative hydrogen

bonded sheets of 2,6-diamino-3,5-dinitropyrazine, and alternative stackings of the sheets that are energetically competitive.

An experimental search for new polymorphs of 2,6-diamino-3,5-dinitropyrazine was carried out in conjunction with the theoretical search. It is soluble in dimethylformamide (DMF), dimethylsulfoxide (DMSO) and 1-methyl-2-piperidinone (NMP), and partially soluble in water, methanol, 1,4-dioxane and tetrahydrofuran. From a range of crystallization experiments, the only crystals formed which were suitable for single crystal X-ray diffraction were the known structure [27] (by crystallization from NMP), and the known DMSO solvate [38]. A large number of the microcrystals obtained from DMF and 1,4-dioxane were heavily layered or twinned, consistent with the twinning problems encountered in the original structure determination [27].

5. DISCUSSION

This paper studies the crystal energy landscapes of three contrasting small polar molecules. This clearly reveals how the problems of crystal structure prediction studies can vary with the molecule. Imidazole is an ideal example for computational work as it has been very widely studied both experimentally, to give an accurate molecular and crystal structure with reliable proton positions, and computationally, in the development of model potentials. The other two examples are of molecules chosen for their own intrinsic interest, which appeared to fall within the capabilities of the computational methodology. Uric acid demonstrates the sensitivity of the lattice energies to the position of a hydrogen bonding proton. The dense, stacked sheet structure of 2,6-diamino-3,5-dinitropyrazine proved too challenging for the interactions between stacked molecules to be accurately modelled by the transferable isotropic atom-atom repulsion-dispersion model. Thus, in both cases, there is more uncertainty in the relative lattice energies than for imidazole. Nevertheless, the three molecules have very different crystal energy landscapes, which can cautiously be interpreted as having rather different implications for the likelihood of polymorphism in these systems.

The only distribution of lattice energy minima that can be unambiguously interpreted is when the known structure is found at the global minimum, with no other structures within the energy range of polymorphism, allowing for the inherent inaccuracies in the intermolecular potential, the molecular model and the use of lattice energy rather than free energy. In such a case, the prediction is clear that no other crystal structure is thermodynamically feasible, and it is predicted that no polymorphs are possible. An example of this is Pigment Yellow 74, where the known structure was predicted [39] to be 12 kJ mol^{-1} more stable than any hypothetical structure generated in the search. Despite many crystallizations of Pigment Yellow 74, through various synthetic routes, no polymorphs have been detected.

When the energy gap between the global minimum and other hypothetical structures is smaller, so that there are hypothetical structures that are thermodynamically plausible as potential polymorphs, the kinetic aspects of polymorph formation have to be considered. Does a metastable structure have such a kinetic advantage in nucleation and crystal growth, and difficulty in transforming to the more stable crystal structure, that it is likely to be an observed polymorph? The dynamical motions of molecules within crystals also complicate the thermodynamic argument. Are the differential effects of temperature and pressure on the different crystal structures likely to change the order of thermodynamic stability relative to the 0 K lattice energies? Whilst we cannot answer these questions in general, we can make tentative predictions in the cases of specific energy landscapes.

Imidazole has the known crystal structure as the global minimum in the lattice energy, and rigid-body harmonic phonon estimates suggest that it is likely to remain the thermodynamically most stable structure under reasonable variations in temperature. The low energy hypothetical structures all adopt the same hydrogen-bonding chain motif. Thus, given that forming these hydrogen bonds is likely to be a key step in the nucleation process, and that transformation between different low energy structures would not necessitate changing the hydrogen bonding motif, it seems unlikely that crystallization conditions could be readily devised that would give a long-lived alternative polymorph. (If crystallization conditions could be devised so that the hydrogen bonded chains were parallel and the crystal polar, it would be more difficult

for the structure to rearrange to the more thermodynamically stable structure, so this seems the most probable hypothetical route to a metastable polymorph.)

In contrast, uric acid is predicted to have a variety of low energy structures, with different combinations of donors and acceptors used in the hydrogen bonding. Thus, if the hypothetical structures could be formed, there is likely to be a significant barrier to a solid state transformation to the known form. The key to forming polymorphs is to get alternative hydrogen bonds to form a nucleus which then grows. However, experimentally, the ability to nucleate one of the hypothetical crystal structures is clearly limited by the poor solubility of uric acid. It is tempting to speculate that the specificity of the conditions required to grow even small crystals of uric acid could be a result of the molecule's complex choices of possible hydrogen bonds. Polymorphism in uric acid, with diverse supramolecular structures and properties, is thermodynamically feasible, and we need to understand its nucleation and growth before it will be clear what kinetic factors determine the lack of polymorphs found to date.

The low energy crystal structures of 2,6-diamino-3,5-dinitropyrazine show a strong preference for forming hydrogen bonding sheets. However, there are at least two hydrogen bonded sheet motifs **(Figure 6)** that are unlikely to interconvert easily. Thus, it is possible that the observed sheet structure might be kinetically rather than thermodynamically preferred, although the sensitivity of hydrogen bonding to low energy changes in molecular structure means that it could be the thermodynamically most stable form. The relative energy differences for different stackings of the same sheet, and the energy barriers for transformation by slipping the sheets, are too small to be given meaningfully by the transferable intermolecular potential used in this study. Hence, it is impossible to say whether, once formed, any differences in the position of stacking of the sheets would be quickly lost by transformation to the most stable stacking of these sheets. An alternative possibility is that a variety of sheet stackings are energetically and kinetically feasible, and therefore this system could exhibit organic polytypism. This phenomenon has been demonstrated in picryl bromide (2,4,6-trinitrobromobenzene), where five of six polymorphs have recently been solved by X-ray diffraction by Gilardi [40]. All contain planar sheets with identical packing motifs, but the sheets stack in different ways, giving between 3 and 18 molecules in the asymmetric unit. Thus, the energy landscape of 2,6-diamino-3,5-dinitropyrazine suggests the possibility of polymorphs that differ in both the hydrogen bonding motif, and the possibility of many related polymorphs based on polytypic stackings of the same sheet. No polymorphs have yet been characterized, though there are problems in growing untwinned crystals, and also in trying a wide range of different crystallization conditions. Thus, the crystal structure of 2,6-diamino-3,5-dinitropyrazine is particularly hard to predict because the range of low energy structures includes both different hydrogen bonded sheets and various ways of stacking these sheets. Kinetic factors are likely to play a major role in determining which crystal structures are found.

6. CONCLUSION

Computational crystal structure prediction is still far from its goal of being able to predict the crystal structure of an organic molecule from just the chemical diagram. Nevertheless, it is clear that whilst some crystal structures can be predicted by just searching for the global minimum in the lattice energy, many molecules have such a variety of low energy crystal structure packings, that even predicting the thermodynamically most stable crystal structure remains a challenge. The current study illustrates the problems of accurately evaluating the lattice energy when there are small, low energy distortions which affect the positions of hydrogen atoms, and in accurately modeling the intermolecular forces involved in the dense stacking sheets of planar molecules. Improving on lattice energy minimization to model free energies [24] is also required before we can predict relative thermodynamic stabilities sufficiently accurately for molecules which have a variety of crystal structures within the energy range of polymorphism.

To use computational methods to predict polymorphism clearly requires computational modeling of kinetic effects. Whilst simple models for crystal growth can be applied [41], a method of predicting relative ease of nucleation is a major experimental and theoretical challenge. However, as this paper illustrates, crystal structure prediction calculations do at least show the types of low energy crystal structures that are available to the molecule. There may be only one predominant motif, which can then be predicted with

confidence. The structures of the hypothetical crystals may help devise strategies for obtaining new polymorphs [9,42], or at least encourage the successful search for new forms [43,44]. It may suggest that simple new polymorphs with very different structures and supramolecular properties are unlikely. It is conceivable that having a complex set of solid state packing possibilities may hinder the nucleation and growth of good crystals, though this would be hard to establish. Although computational crystal structure "prediction" studies raise more questions than answers, they certainly contribute to the fun of studying polymorphism.

7. ACKNOWLEDGEMENTS

8. REFERENCES

[1]   J.P.M.Lommerse, W.D.S.Motherwell, H.L.Ammon, J.D.Dunitz, A.Gavezzotti, D.W.M.Hofmann, F.J.J.Leusen, W.T.M.Mooij, S.L.Price, B.Schweizer, M.U.Schmidt, B.P.van Eijck, P.Verwer, and D.E.Williams. *Acta Crystallogr. B*, **56** (2000) 697-714.

[2]   W.D.S.Motherwell, H.L.Ammon, J.D.Dunitz, A.Dzyabchenko, P.Erk, A.Gavezzotti, D.W.M.Hofmann, F.J.J.Leusen, J.P.M.Lommerse, W.T.M.Mooij, S.L.Price, H.Scheraga, B.Schweizer, M.U.Schmidt, B.P.van Eijck, P.Verwer, and D.E.Williams. *Acta Crystallogr. B*, **58** (2002) 647-661.

[3]   G.M.Day, W.D.S.Motherwell, H.L.Ammon, S.X.M.Boerrigter, R.G.Della Valle, E.Venuti, A.Dzyabchenko, J.D.Dunitz, B.P.van Eijck, P.Erk, J.C.Facelli, V.E.Bazterra, M.B.Ferraro, D.W.M.Hofmann, F.J.J.Leusen, C.Liang, C.C.Pantelides, P.G.Karamertzanis, S.L.Price, T.C.Lewis, A.Torrisi, H.Nowell, H.Scheraga, Y.Arnautova, M.U.Schmidt, B.Schweizer, and P.Verwer. A Third Blind Test of Crystal Structure Prediction, *Acta Crystallogr. B*, submitted.

[4]   R.K.R.Jetti, R.Boese, J.Sarma, L.S.Reddy, P.Vishweshwar, and G.R.Desiraju. *Angew. Chem. Int. Edit.*, **42** (17) (2003) 1963-1967.

[5]   J.Bernstein, R.J.Davey, and J.O.Henck. *Angew. Chem. Int. Edit.*, **38** (23) (1999) 3441-3461.

[6]   J.Bauer, S.Spanton, R.Henry, J.Quick, W.Dziki, W.Porter, and J.Morris. *Pharmaceut. Res.*, **18** (6) (2001) 859-866.

[7]   S.R.Chemburkar, J.Bauer, K.Deming, H.Spiwek, K.Patel, J.Morris, R.Henry, S.Spanton, W.Dziki, W.Porter, J.Quick, P.Bauer, J.Donaubauer, B.A.Narayanan, M.Soldani, D.Riley, and K.McFarland. *Organic Process Res. Dev.*, **4** (5) (2000) 413-417.

[8]   P.K.Thallapally, R.K.R.Jetti, A.K.Katz, H.L.Carrell, K.Singh, K.Lahiri, S.Kotha, R.Boese, and G.R.Desiraju. *Angew. Chem. Int. Edit.*, **43** (9) (2004) 1149-1155.

[9]   N.Blagden and R.J.Davey. *Cryst. Growth Des.*, **3** (6) (2003) 873-885.

[10]   F.H.Allen. *Acta Crystallogr. B*, **58** (2002) 380-388.

[11]   F.H.Allen, O.Kennard, D.G.Watson, L.Brammer, A.G.Orpen, and R.Taylor. *J. Chem. Soc. Perk. T. 2*, (12) (1987) S 1-S 19.

[12]   M.J.Frisch, G.W.Trucks, H.B.Schlegel, G.E.Scuseria, M.A.Robb, J.R.Chesseman, V.G.Zakrzewski, J.A.Montgomery, R.E.Stratmann, J.C.Burant, S.Dapprich, J.M.Millam, A.D.Daniels, K.N.Kudin, M.C.Strain, O.Farkas, J.Tomasi, V.Barone, M.Cossi, R.Cammi, B.Mennucci, C.Pomelli, C.Adamo, S.Clifford, J.Ochterski, G.A.Petersson, P.Y.Ayalla, Q.Cui, K.Morokuma, D.K.Malick, A.D.Rabuck, K.Raghavachari, J.B.Foresman, J.Cioslowski, J.V.Ortiz, B.B.Stefanov, G.Liu, A.Liashenko, P.Piskorz, I.Komaromi, R.Gomperts, R.L.Martin, D.J.Fox, T.Keith, M.A.Al-Laham, C.Y.Peng, A.Nanayakkara, C.Gonzalez, M.Challacombe, P.M.W.Gill,

B.G.Johnson, W.Chen, M.W.Wong, J.L.Andres, M.Head-Gordon, E.S.Replogle, and J.A.Pople. GAUSSIAN 98. [A6]. 1998. Pittsburgh, Gaussian Inc. Computer Program

[13] A.J.Stone. GDMA: a program for performing Distributed Multipole Analysis of wavefunctions calculated using the Gaussian program system. [1.0]. 1999. University of Cambridge (U. K.). Computer Program

[14] A.J.Stone and M.Alderton. *Mol. Phys.*, **56** (5) (1985) 1047-1064.

[15] A.J.Stone. *The Theory of Intermolecular Forces*. Clarendon Press, Oxford, 1996.

[16] D.J.Willock, S.L.Price, M.Leslie, and C.R.A.Catlow. *J. Comput. Chem*., **16** (5) (1995) 628-647.

[17] S.L.Price, D.J.Willock, M.Leslie, and G.M.Day. DMAREL 3.02. 2001. http://www.ucl.ac.uk/~ucca17p/dmarelmanual/dmarel.html.

[18] S.L.Price. Toward more accurate model intermolecular potentials for organic molecules. In K.B.Lipkowitz and D.B.Boyd (eds.), Reviews in Computational Chemistry, **14**, John Wiley & Sons, New York, 2000, PP: 225-289.

[19] D.S.Coombes, S.L.Price, D.J.Willock, and M.Leslie. *J. Phys. Chem.*, **100** (18) (1996) 7352-7360.

[20] D.E.Williams and S.R.Cox. *Acta Crystallogr. B*, **40** (1984) 404-417.

[21] S.R.Cox, L.Y.Hsu, and D.E.Williams. *Acta Crystallogr. A*, **37** (1981) 293-301.

[22] J.R.Holden, Z.Y.Du, and H.L.Ammon. *J. Comput. Chem*., **14** (4) (1993) 422-437.

[23] Y.Kim and K.Machida. *Chem. Pharm. Bull.*, **34** (8) (1986) 3087-3096.

[24] G.M.Day, S.L.Price, and M.Leslie. *J. Phys. Chem. B*, **107** (39) (2003) 10919-10933.

[25] A.E.Gray, G.M.Day, M.Leslie, and S.L.Price. *Mol. Phys.*,**102** (2004) 1067-1083.

[26] H.Ringertz. *Acta Crystallogr.*, **20** (1966) 397-403.

[27] R.D.Gilardi and R.J.Butcher. *Acta Crystallogr. E*, **57** (2001) O738-O740.

[28] J.S.Chickos. Heat of Sublimation Data. In W.G.M. and P.J.Linstrom (eds.), NIST Chemistry WebBook, NIST Standard Reference Databse, National Institute of Standards and Technology, Gaithersburg MD, 20899 (http://webbok.nist.gov),. 1998.

[29] A.L.Spek. PLATON, A Multipurpose Crystallographic Tool. 2002. Utrecht, University of Utrecht.

[30] J.Bernstein. *Polymorphism in Molecular Crystals*. Clarendon Press, Oxford, 2002.

[31] B.P.van Eijck and J.Kroon *Phys. Chem. B*, **104** (33) (2000) 8089.

[32] H.Ringertz. *Acta Crystallogr.*, **19** (1965) 286-287.

[33] J.Sponer and P.Hobza. *J. Phys. Chem. B*, **98** (12) (1994) 3161-3164.

[34] S.N.Kalkura, V.K.Vaidyan, M.Kanakavel, and P.Ramasamy. *J. Cryst. Growth*, **132** (3-4) (1993) 617-620.

[35] R.E.Sours, D.A.Fink, and J.A.Swift. *J. Am. Chem. Soc.*, **124** (29) (2002) 8630-8636.

[36] CCDC. Mercury. http://www.ccdc.cam.ac.uk/products/csd_system/mercury/.

[37] G.M.Day and S.L.Price. *J. Am. Chem. Soc.*, **125** (52) (2003) 16434-16443.

[38] R.D.Gilardi and R.J.Butcher. *Acta Crystallogr. E*, **57** (2001) O757-O759.

[39] M.U.Schmidt. Energy minimization as a tool for crystal structure determination of industrial pigments. In D.Braga, F.Grepioni, and A.G.Orpen (eds.), Crystal Engineering: From Molecules and Crystals to Materials, Kluwer, Dordrecht, 1999, PP: 331-348.

[40] R.Gilardi. 2004. Personal Communication

[41] D.S.Coombes, C.R.A.Catlow, J.D.Gale, and S.L.Price. 2005, *Cryst. Growth Des.* **5** (3) (2005) 879-885.

[42] W.I.Cross, N.Blagden, R.J.Davey, R.G.Pritchard, M.A.Neumann, R.J.Roberts, and R.C.Rowe. *Cryst. Growth Des.*, **3** (2) (2003) 151-158.

[43] A.T.Anghel, G.M.Day, and S.L.Price. *CrystEngComm*, **4** (62) (2002) 348-355.

[44] T.C.Lewis, D.A.Tocher, and S.L.Price. *Cryst. Growth Des.*, **4** (5) (2004) 979-987.

CRYSTAL STRUCTURE PREDICTION AND POLYMORPHISM

Joel Bernstein

Dept. of Chemistry, Ben-Gurion University of the Negev, Beer Sheva, Israel 84120

1. ABSTRACT

to predict: to foretell, prophesy, announce beforehand
                                            Oxford English Dictionary

Since the early days of structure determination by diffraction methods the prediction of crystal structures of small to medium-sized organic molecules from a structural formula has been a goal and a constantly recurring theme of crystallographers. The challenge is even greater when considering the additional factor of the possible existence of polymorphic forms of the material, since true predictive capability requires accounting for all crystal forms and their relative stability. While considerable progress has been made and some practitioners have even claimed that the goal has been achieved, a great deal still needs to be learned and done before one can state with any degree of confidence the ability to predict a crystal structure from a structural formula alone, much less its polymorphic forms. An even greater challenge is the prediction of solvates, including hydrates. This contribution attempts to summarize some of the current thinking on the subject.

2. INTRODUCTION

At the outset to this contribution, I want to make it clear that I am an enthusiastic believer in the importance of computational approaches to the understanding of interactions within molecular crystals and their potential for aiding in the solution of crystal structures, as well as for surveying the energy landscape for possible, even as yet unknown, structures. I have been following the development of this field for nearly forty years, even with occasional personal forays into it. I am impressed by the progress that has been made, and I enthusiastically support and encourage those who are attempting to develop and refine the field in general and its applications to polymorphs in particular. The rapidly increasing interest in polymorphism in recent years, from the purely scientific point of view to the commercial and intellectual property aspects has led to increasing (perhaps more correctly intense) interest in our ability to predict *ab initio* the existence of multiple crystal forms for a particular compound. I do think that some of the hyperbole and optimism of the past decade concerning our ability to predict even the possible existence of polymorphs was misplaced, and this paper is an attempt to present my perspective on the current situation. Although I have attempted to be objective, this minireview is the view from one person's perspective, which must per force carry some bias.

As with many aspects of chemistry, much discussion and debate surround our definition of terms, and the associated frame of reference. In this case, what do we mean by the term "to predict"? The Longman's Dictionary has a slightly different definition from that given by the OED above: "to see or describe in advance as a result of knowledge, experience, thought, etc." Using classical physics we can predict the path of a cannon shell or an interplanetary space probe. In chemistry we can often predict the outcome of a reaction or the bonding geometry around an atom. In the current context I view a prediction as the ability to see or describe in advance a crystal structure simply on the basis of its molecular structure. The key phrase in this definition is 'in advance'. For a sound scientific prediction we don't have to do the experiment to know what the result will be. It may be technologically challenging or difficult to carry out the experiment, but we expect the known scientific truths to be valid and the accepted scientific laws to be obeyed. By either dictionary definition above the notion of a prediction in scientific terms carries with it some degree of confidence, implied in the Longman's definition "as a result of knowledge, experience, thought, etc." That is, we expect the prediction to be proven.

In the context of the historical development of "predicting" crystal structures of small to medium molecules, 1994 was a particularly notable year, with two nearly simultaneous publications. One was the official announcement by Molecular Simulations Inc. (now Accelrys) in July of the availability of the "Polymorph Predictor" program [1]. The second event was the publication in October of the stimulating paper by Angelo Gavezzotti [3] entitled "Are crystal structures predictable?" to which he gave the emphatic one word opening response "No!" The dichotomy is glaring. How can there be a program for *predicting* multiple crystal structure (i.e. polymorphs) if we can't even predict a single crystal structure? Part of the problem arises, of course, from how each author interprets of the definition of *predict*, and we will attempt to address that aspect of the question as well as making a general assessment of the current situation as seen from the perspective of this viewer.

3. SOME HISTORICAL BACKGROUND

In the current context of automated CCD diffractometers and "black box" programs for the solution, refinement and presentation of crystal structures it may be difficult to imagine (or to recall) the days when the few text books on crystal structure analysis (e.g. 4,5]) contained whole chapters on "Trial and Error Methods" for solving crystal structures, more correctly for providing the initial model. In many ways these were essentially means for describing the crystal structure in advance as a result of knowledge experience, thought, etc., i.e. predicting the crystal structure. Much thought and effort went into these methods, since the cost in time and work (often on the order of months) in getting it wrong could be frustrating, if not disastrous. With the advent of powerful desktop or laptop computers armed with efficient software for structure solution (generally by direct methods) and refinement, those chapters have disappeared from the textbooks. However, the earlier need to use every means possible to arrive at a possible crystal structure spawned some pioneering work and led to considerable understanding of the nature of crystals and crystal structures.

The classic work in this area is Kitaigorodskii's *Organic Chemical Crystallography* [6], which contains many still-valuable observations and insights on the nature of intermolecular interactions in molecular crystals. Kitaigorodskii also built a "structure seeker" for the prediction/solution of crystal structures by incorporating the principles of van der Waals radii and closest packing into a mechanical model. In the middle 1960's many of these ideas were incorporated by (the late) Don Williams into his PCK5 program [7], various versions of which he used as an aid for solving the structures of dibenzoylmethane [8], 2,4,6-triphenylverdazyl [9] and others employed in solving the structures of some monosaccharides [10].[*] A

---

[*]A personal note. In 1968 I was a postdoctoral fellow in Ken Trueblood's lab at UCLA. He was working with Don Cram on the structures of paracyclophanes. One of these that came into the lab was the hydrocarbon [2.2]*meta,para* cyclophane, which crystallized in the space group $P2_12_12_1$. In those days (before the birth of MULTAN, SHELX, etc.) such a light atom noncentrosymmetric structure was considered non-routine at best and often not solvable, and it might have been laid it to rest. However, the rigid molecule is very similar to [2.2]*para,para* cyclcophane which crystallizes in tetragonal space group $P4_2/mnm$, and we had been reinvestigating the structure originally reported by Kathleen Lonsdale [11]. The cell constants of the two structures were also very similar; however, whereas the *para,para* derivative had crystallographic site symmetry *mmm* (a very rare case for molecular crystals [6]), in space group $P2_12_12_1$ Z'=1, the *meta,para* derivative was required to have crystallographic site symmetry *1*. The four arrangements possible for the *meta* and *para* rings were generated as input into the Williams PCK5 program at the locations suggested by the tetragonal structure. One of the four produced a significantly lower packing energy than the others as a trial structure, and refined smoothly on data collected manually on a General Electric quarter-circle diffractometer. However, the exocyclic C-C single bonds were approximately 1.62Å, a value much larger than any previously published. Another set of data led to identical results, which we felt could not be published due to this anomalously long bond. Sometime later, Renault *et al.* published another structure of the compound[12, also] in $P2_12_12_1$, but with Z'=2, in which 3 out of 4 of the C-C single bonds exceeded 1.54, and subsequently many C-C single bonds exceeding the 'standard' 1.54Å have been reported.

parallel development at the time was Bill Busing's WMIN program [13], which was used by Kvick and Noordik to aid in solving the structure of 2-amino-4-methylpyridine [14].

The field has expanded rapidly over the past thirty years, with an increasing number of practitioners developing a variety of methods. At least three useful summaries with many references to the historically important and current developments have been given by Verwer and Leusen [2], Gavezzotti and Filippini [15] and Price [16]. Price et al. also compiled a useful 'atlas' of organic molecules which have been used in crystal structure prediction studies carried out by lattice energy calculations [17]. Of the ~190 structures reported in this survey 9 are denoted by the authors as having been carried out "in advance of an experimental investigation" – much in the way that traditional predictions would be made.

The title of this paper involves the confluence of two subjects – the calculation of crystal structures on the one hand and polymorphism on the other hand. Some historical developments of the former were noted above. In many ways the beginning of modern systematic study of polymorphism also can be traced to the 1960's with two landmark papers by McCrone [18, 19]. In the first of these McCrone made an oft-quoted provocative statement about the occurrence of polymorphism:

"Every compound has different polymorphic forms, and the number of forms known for a given compound is proportional to the time and energy spent in research on that compound."

In spite of the implied universalism of this statement, there are many very well researched compounds for which polymorphism has not been discovered: naphthalene, sucrose and the pigment perylene red are but a few notable examples. Statistics on the occurrence of polymorphism are hard to come by, because almost any data set is biased, and many instances of polymorphism are not properly reported (this includes false positives as well as false negatives). For instance, a survey of the Cambridge Structural Database on the keywords "polymorph," "form," "phase" and "modification" indicates that about 4% of the included structures are polymorphic. A search on "hydrates and "solvates" results in about 23% hits. This survey is biased by the fact that it includes only compounds for which the crystal structures have been reported. Perhaps closer to the other extreme, Steve Byrn recently summarized work from SSCI on over 150 compounds for which >87% had more than one form, 37% were hydrates and 31% were solvates [20]. These statistics may be biased by the fact that some samples at least were known to be polymorphic when received, or special efforts were made to identify multiple crystal forms, even if relatively unstable. Additional statistical surveys have been reported [21].

The general situation is somewhere in between these two sets of statistics: the existence of multiple crystal forms (polymorphs and/or solvates) is not surprising when found, but cannot be foreseen or expected for any compound. Essentially, this has been the state of our knowledge and understanding for many years, and given the increasing interest and importance of multiple crystal forms, it is not surprising that considerable efforts would be made to "predict" the possible existence of polymorphs in particular, and multiple crystal forms in general. One result was the announcement of the "Polymorph Predictor" program in 1994.

4. WHAT WE CAN DO; WHAT WE CAN'T DO

In the introduction to a chapter in a 1997 book entitled *Theoretical Aspects and Computer Modeling of the Molecular Solid State* edited by Angelo Gavezzotti, Robert Gdanitz, one of the authors of the Polymorph Predictor program, quoted three authorities on their view of our ability to predict crystal structures [22]. In a since oft-quoted statement John Maddox, past editor of *Nature,* wrote in 1988 [23]:

"One of the continuing scandals in the physical sciences is that it remains in general impossible to predict the structure of even the simplest crystalline solids."

Similar skepticism was voiced by F. Hawthorne [24]:

"Thus a rigorous general solution to the question of crystal structure prediction may not be forthcoming in the near future."

and Fagan and Ward [25]:

"Unfortunately, the molecular interactions in a lattice become too complicated for any human or computer to handle."

Nevertheless, in the same opening paragraph, Gdanitz [22] concluded that:

"….quite a few articles on predicting molecule crystal structures have been published, showing that *the problem has now become a rather routine task*" (emphasis added).

Perhaps the telltale hint of the author's true estimation of one's predictive ability is the title of the chapter, "*Ab Initio* Prediction of Possible Crystal Structures". The prediction of *possible* crystal structures may be routine, but the prediction of *the* crystal structure clearly is not.

A similarly over optimistic view of the situation may be found in the chapter by Verwer and Leusen [2] in stating that

"…computational methods and algorithms that allow packing simulations with many degrees of freedom,…were not developed until this decade (e.g. the 1990's), making true 'ab initio' crystal structure predictions possible on the basis of molecular information alone."

Possible, perhaps, but the rate of success still leaves a lot to be desired before it can be claimed that the problem has been solved, and crystal structures in general, or polymorphic structures in particular, can be reliably predicted. In reviewing the general situation of the predictability of polymorphs in general, Gavezzotti's emphatic "No" in 1994 and subsequent developments, Dunitz succinctly summarized the situation in 2003. His current answer to the question is [26]:

"…still 'No', although at certain levels of discussion a 'Maybe' or even a conditional 'Yes', may be entertained as possible responses".

Perhaps the greatest service to this effort of developing methods to computationally survey possible crystal structures has been performed by the Cambridge Crystallographic Data Centre, with a series of competitional "blind tests." Developers and practitioners of these methods have been invited three times since 1998 to apply their methods to attempting to predict the crystal structures of three compounds on the basis of molecular information alone. The crystal structures of the candidate compounds have been done but not published. The results of two of these blind tests have been published [27, 28]. The rules for the competition say as much about our current ability to computationally predict crystal structures as do the results of the competition. These rules were laid out, "[t]o give a reasonable chance of success within the practical limits of known computer programs[*]…":

- maximum number of atoms including H atoms did not exceed 40;
- space group required to be one of the ten most frequently encountered (i.e. *P2₁/c*, *P-1*, *P2₁2₁2₁*, *C2/c*, *P2₁*, *Pbca*, *Pna2₁*, *Cc*, *Pbcn*, *C2*);
- one molecule in the asymmetric unit;[**]

---

[*] The ground rules for the second blind test are quoted here. They differ only slightly from the first.

[**] Most of the programs used for computing the lattice energy can not take into account the possibility of the molecule lying on a crystallographic special position (Wyckoff position). In a recent survey [29] it was shown that for Z'=1 approximately 71% of the molecules lack molecular symmetry, while those that have an inversion center retain that in more than 80% of the cases, those with a rotation axis retain it in approximately 50% of the cases, while those with mirror plane retain that element in about 30% of the cases. Most of these structures with retention of symmetry would not be included in the computed crystal structures since the programs are not capable of handling them. In some algorithms, especially those that compare the calculated powder pattern with an experimental one, the proper spatial arrangement of the molecules might be found, but the space group would not be correctly assigned. Such was the case, for

- no solvent molecules or co-crystals;
- no disorder in the determined structure;
- hydrogen atoms located experimentally in the determined structure.

In addition, the three candidate molecules were categorized by perceived increasing difficulty for prediction:

- rigid molecule with only C, H, N and O atoms, less than 25 atoms;
- rigid molecule with some less common elements (e.g. Br), less than 30 atoms;
- flexible molecule with two degrees of acyclic torsional freedom, less than 40 atoms.

What classes or features of structures are considered too difficult or too challenging for such a competition? "Medium" or "large" molecules (>~40 atoms), all of the metal-containing complexes, most of the compounds with less common elements, molecules with more than two conformational degrees of freedom, salts, solvates, and structures with more than one molecule in the asymmetric unit, or molecules lying on special crystallographic positions (inversion center, 2-fold axis, etc.). While the eight allowed space groups comprise approximately 80% of the CSD, by adopting such a restriction one is already reducing one's chance of success by 20%. This is a considerable fraction of the compounds that are of interest to "small molecule" chemists.

What kind of success was achieved for the two blind tests for which results have been published? There were three molecules (but four structures – see below) and 11 participants in the first blind test, for a total of 44 chances of success. Each participant was allowed three choices for each solution, so actually there were 132 possible solutions. There were seven correct predictions, five of them being the first of the three choices. 7/44 is a 16% success rate.

It turned out that the behavior of one of the compounds was particularly relevant to the title of this paper. The compound is a liquid at room temperature, and was crystallized (in orthorhombic *Pbca) in situ* at low temperature in a capillary on a diffractometer for the data collection and structure determination, which served as the first structure of reference for the first blind test. A breakdown in the cooling system led to melting, and all subsequent attempts at crystallization yielded a monoclinic *P2₁/c* structure [29,30]. The sequence of events suggests that the monoclinic form is the more stable one, in accord with Ostwald's Rule of Stages, and that the orthorhombic form should be classified as a disappearing polymorph [31]. In terms of the computational prediction of crystal structures, the important point here is that four out of the seven correct responses in the first blind test were for the orthorhombic structure (the less stable form) and if it had not been found initially, the number of correct predictions would be reduced to three (7% success rate). Moreover, if the monoclinic structure had initially crystallized one might never have known about the existence of polymorphs in this system.

Seventeen groups participated in the second blind test, carried out on three structures for a total of 51 possible correct answers. The structures were correctly predicted by two groups for the first molecule, by four groups for the second molecule, with no correct answers for the conformationally flexible third molecule. The success rate is therefore 6/51 or 12%. The participants did conclude that there had been significant progress on the ability to generate crystal structures for rigid molecules, and if the solution were to be found among the top six, rather than the top three, solutions the success rate would rise significantly. The failure of all participants to find a solution for the third molecule in the second round led to additional attempts to prepare a polymorphic structure which might be found among the higher ranked computed ones [32]. The authors determined that the blind test reference structure exhibited an unusual conformation, which made the calculations less likely to succeed. After determining the cell constants of more than 80 crystals they obtained a second polymorph of the material crystallized from nitromethane; however, it crystallizes with two molecules in the asymmetric unit with two different molecular conformations, so that

---

instance, for the original version of the "Polymorph Predictor", which yielded a solution for benzene in space group *P2₁2₁2₁* (Z=4, Z'=1, molecules on general positions), when it should have been *Pbca* (Z=4, Z'=0.5, molecules on inversion centers).

it would not have been included in any of the possible structures for the blind test calculated at the current level of capability.

The example of acetic acid demonstrates one of the major difficulties and challenges still to be overcome. An attempt to computationally predict the crystal structure(s) of acetic acid using both the grid-search method [33] and the Monte Carlo approach [34-36] led to ~100 structures within a narrow energy range of 5 kJ/mol. With various modifications the experimental structure always had a low energy, but it was not possible to distinguish it from the many other solutions. This led the authors to suggest that "other factors need to be considered for genuine structure prediction." In the realm of synthetic organic chemistry, a parallel situation would be to claim that one has carried out the synthesis of the desired product which indeed may be found in the reaction mixture along with ~100 other products, but we don't know how to independently identify or isolate that desired product.

All the methods for calculating lattice energies of possible crystal structures lead to a list that must be ranked. Ideally, the real or possible polymorphic forms appear as the most stable forms in that list. Historically, success has been measured by whether a structure, or polymorphic structures can be properly accounted for, or predicted in that list and subsequently found. I would like to suggest an alternative developmental approach, which I believe has been applied to a much lesser extent, but may be more systematic and fruitful in terms of the long term development of these methods.

The polymorphic systems to be studied should be very well characterized in terms of the relative thermodynamic stability of the various forms, monotropism, enantiotropism, heats of transition, and heats of sublimation, etc., if possible. In the end, the lattice energies that are calculated can and should be benchmarked against those experimental quantities. I do not underestimate the difficulties in obtaining good quality thermodynamic data for all of these quantities, especially sublimation enthalpies, and the paucity of laboratories where such measurements are made. The least demanding benchmark for one of these calculations is that it reproduces the experimentally determined energetic ranking of the various polymorphic forms, without regard to the actual quantities involved. At the next level of stringency, the computed differences in energy between the various polymorphic forms should conform to the experimentally determined differences. As the most demanding test, the computed lattice energies should match the experimentally determined ones. Such a developmental process should result in a force field and search procedure that are at least suitable for a class of functional groups and molecules similar to those of the test molecule or group of molecules. Attempts to develop 'universal' methods or force fields are reminiscent of the search for the Holy Grail.

The computational "proof of concept" experiment would then be to use that force field and those computational methods to generate, ab initio, the crystal structures of all of the known polymorphs in the energetic order in which they are known to exist. Suitable (albeit demanding) test systems, might be a compound like ROY, for which seven polymorphs have been identified and characterized [37,38], or *p'*-methylchalcone, for which 13 polymorphic forms have been reported [39] and at least 5 structures have been determined [40].

Table 1

Crystal forms obtained for N,N'dithiobisphthalimide [from 41]

Form	Solvent for crystallization	Space group	Z'
Solvent-free polymorphs			
(1)	$CH_3COOC_2H_5$	$P2_1/c$	2
(4)	CH_3OH	$Pna2_1$	1
(5)	CH_3CN or $HCON(CH_3)_2$	$P2_1/c$	2
Polymorphs with solvent hydrogen-bonded to (I)			
(6)	CH_3NO_2	$P2_1/c$	1
Solvent molecules are in isolated cavities			
(7)	C_6H_5Cl	$P\bar{1}$	1
(8)	$C_6H_5C_2H_5$	$P2_1/c$	2
Solvent molecules are non-localized in channels			
(2)	CH_2Cl_2	$C2/c$	0.5
(3)	C_2H_5OH	$C2/c$	0.5
(9)	C_4H_8O	$C2/c$	0.5
(10)	$(CH_3)_3COH/H_2O$	$C2/c$	0.5
Solvent molecules are localized in channels			
(11)	$1,4\text{-}(CH_3)_2C_6H_4$	$P2_1/n$	1
(12)	$C_6H_5CH_3$	$P2_1/n$	1

This process for developing reliable computational methods does not deal with any of the simplifying limiting assumptions made for the blind tests. For crystal structure prediction those will have to be dealt with as well. Some of the challenges are represented by the variety of polymorphs and solvates reported for the relatively simple molecule N,N'-dithiobisphthalimide, summarized in Table 1 [41]. The three solvent-free polymorphs represent a challenge that might be considered possible today, but "predicting" the other four solvated motifs is way beyond our current capabilities.

The description above might leave the impression that computational methods have not progressed sufficiently to provide useful chemical and structural information. As noted at the outset, the contrary is true. In conjunction with a variety of analytical techniques, these methods can provide guidelines and confirming parameters for modeling possible crystal structures. We are still a long way from crystal structure or polymorph *prediction*, but we can learn something about what we might want to look for and obtain structural information when crystal structure analysis is difficult or not possible. The recent case history of acetaminophen illustrates this synergism.

Acetaminophen/paracetamol (e.g. Tylenol®) is the most widely used analgesic and antipyretic which has been known to be dimorphic for many years [42]. The commercially used Form I requires binders for formulation; Form II does not require binders, but transforms to Form I. Considerable effort has gone into improving the solid state properties of acetaminophen, including the search for additional crystal forms that might have improved formulation and stability properties, and these efforts included a computational search for possible new forms. Verwer and Leusen [2] completed one such study with the conclusion that

"Recalculation of the lattice energetic…established that this third structure is actually too unstable to exist."

Chemists often see the prediction of the nonexistence of a substance as a challenge to make it,[*] and this case was no different. In fact, at the time the statement was made there was already evidence in the

---

[*] Philosophers of science have also argued against this approach. For instance, the relevant quotation in a recent book by the father-philosopher/son-scientist, Buddhist monk team: "But not to be able to find something is no proof of its nonexistence."[43].

literature for a third form, detected by microscope hot stage methods [44-46]. Beyer et al. carried out another set of calculations on the possible crystal structure of the compound [47]. Almost simultaneously, a set of experiments based on high throughput crystallizations found evidence for a third form, which was characterized by hot stage microscopy and Raman spectroscopy [48]. The X-ray powder diffraction pattern measured by Peterson et al. [48] also closely matches one of the low energy computed structures of Beyer et al., although the latter had ruled it out as a possible structure on the basis of packing considerations. In any event, the combination of experimental and computational techniques led to significant advances in the characterization and understanding of this system, and it is this synergism, especially between computationally-derived models for crystal structures and powder diffraction [49] which promises to provide the greatest immediate and near term benefit.

5. THE CHALLENGES

What is the current status of our ability to predict crystal structures in general and polymorphs in particular? The situation was recently summarized by S.L. Price, one of the leading practitioners in the field [16]:

> "We cannot yet computationally predict the possible polymorphs of any given organic molecule."

As we have pointed out above, and as Price further notes, the computational studies can provide useful information about polymorphs that we might want to look for. They say nothing about their existence or how they might be prepared. In fact, as Dunitz has noted in the same vein [26]:

> "We have a long way to go before we can think of predicting which polymorph will be
> obtained under any given circumstances."

From the computational point of view it must be shown that calculated lattice energies can truly reflect or reproduce experimentally determined energetics. This will require much more work on force fields, and the development of computational tools for determining lattice energies. Good thermodynamic data are also required on polymorphic systems to provide the standards against which these calculations can be measured. It is still difficult to distinguish between the global minimum and local minima in computational studies, which means that it is not always possible to computationally determine which polymorphic form is the most stable, and how others may be thermodynamically related to it. Price has also pointed out the necessity for assessing and modeling kinetic factors in the growth of different polymorphs.

In order for the computational techniques to be truly predictive, they must be more comprehensive. Hence, on the more practical level some of the computational challenges that must be met along the way were noted above. (In the following the numbers in parentheses are the current percentages of entries in the CSD). Molecules containing only C,H,N,O comprise about %18.5 of the CSD. Provision must be made for modeling crystals with conformationally flexible molecules, molecules larger than ~40 atoms, crystals of salts, solvates (14.3% of CSD) and hydrates (10.1% of CSD), cocrystals, crystals of organometallic compounds (56%), crystals with more or less than one molecule in the asymmetric unit (35%), crystals in the 'less common' space groups (12.7%) – in short the technique must be generalized to cover all the possibilities that are regularly encountered in laboratory situations.

By noting our current limitations Price and Dunitz have touched on some of the exciting challenges facing those studying the chemistry of crystal forms – polymorphs and solvates. I would define them with three rather general questions which we would like to be able to answer for any specific system:

- How many different crystal forms can we expect?
- How do we go about preparing those different crystal forms?
- What will be the properties of those different crystal forms if and when I obtain them?

This contribution made an attempt to assess where we are with regard to the computational tools used to address the first question. There has indeed been significant progress since Kitaigorodskii's pioneering

work in the area, and in closing I was reminded of Martin Luther King's inspiring remarks in a memorable speech at the Lincoln Memorial 41 years ago:

"We've come a long way, but we've got a long, long way to go."

6. REFERENCES

[1]   Later referenced [2] as follows: Cerius^2 User Guide, March 1997, Molecular Simulations, Inc. 9685 Scranton Road, San Diego, CA; http://www.msi.com/.

[2]   P. Verwer and F.J.J. Leusen, in *Reviews in Computational Chemistry*1998, eds. K.P. Lipkowitz and D.B. Boyd (Wiley-VCH, John Wiley and Sons, Inc., New York 1998), p 327.

[3]   A. Gavezzotti, *Acc. Chem. Res.* **27** (1994), 309.

[4]   H. Lipson and W. Cochran, *The Determination of Crystal Structures,* ed. W.L. Bragg, *The Crystalline State,* Vol 3, (Cornell University Press, Ithaca, 1966), Chapter 6.

[5]   C.W. Bunn, *Chemical Crystallography*, (Oxford University Press, Oxford, The Clarendon Press, Oxford, 2nd. Edition, 1961), p. 204

[6]   A.I. Kitaigorodskii, *Organic Chemical Crystallography,* (Consultants Bureau, New York, 1961).

[7]   D.E. Williams, *Acta Crystallogr., Sect. A* **25** (1969), 464.

[8]   D.E. Williams, *Acta Crystallogr.,* **21** (1966), 340.

[9]   D.E. Williams, *Acta Crystallogr., Sect. B* **29** (1973), 96.

[10]   P. Zugenmaier and A. Sarko, *Acta Crystallogr., Sect. B* **28** (1972), 3158.

[11]   H. Hope, J. Bernstein and K.N. Trueblood, *Acta Crystgallogr. Sect.B* **28** (1972), 1733.

[12]   A. Renault, C, Cohen-Addad, J. Lajzerowicz-Bonneteau, J.P. Dutasta and M.J. Crisp, *Acta Crystallogr., Sect. B* **38** (1987), 480.

[13]   W.R. Busing, *Acta Crystallogr., Sect. A* **28** (1972), S252.

[14]   Å. Kvick and J.H. Noordik, *Acta Crystallogr., Sect. B* **38** (1977), 2862.

[15]   A. Gavezzotti and G. Filippini, in *Theoretical Aspects and Computer Modeling of the Molecular Solid State*1997, ed. A. Gavezzotti (John Wiley and Sons, Inc., New York 1997), p 61.

[16]   S.L. Price, *Adv. Drug Delivery Revs.,* **56** (2004), 301.

[17]   T. Beyer, T. Lewis and S. Price, *Cryst. Eng. Comm.* **44** (2001), 1.

[18]   W.C. McCrone, in *Physics and Chemistry of the Organic Solid State*,1965 eds. D. Fox, M.M. Labes and A. Weisberger (Wiley Interscience., New York 1965), p 725.

[19]   J. Haleblian and W.C. McCrone, *J. Pharm. Sci.* **58** (1969), 911.

[20]   S.R. Byrn, presented at the 35th Erice School on Crystallography, "Diversity Amidst Similarity: A Unified Approach to Polymorphs, Solvates and Phase Changes", Erice, Sicily, June, 2004.

[21]   J.A.R.P. Sarma and G.R. Desiraju, in *Crystal Engineering. The Design and Applications of Functional Solids*, eds. K.R. Seddon and M. Zaworotko (Klewer, Dordrecht 1999), pp. 325-356; U.J. Griesser and A. Burger, "Statistical Aspects of the Occurrence of Crystal Forms Among Organic Drug Substances" Poster P09.013 at the International Union of Crystallography Congress and General Assembly, Glasgow, Scotland, Aug. 4-13, 1999. Book of Abstracts, p. 533; U.J. Griesser, *Acta Crystallogr., Sect. A* **58** Supplement (2002), C241.

[22]   R.J. Gdanitz, in *Theoretical Aspects and Computer Modeling of the Molecular Solid State*1997, ed. A. Gavezzotti (John Wiley and Sons, Inc., New York 1997), p 18.

[23]   J. Maddox, *Nature,***335** (1988), 201.

[24]   F.C. Hawthorne, *Nature,***345** (1990), 297.

[25]   P.J. Fagan and M.D. Ward, *Scientific American,* **267**(1) (1992), 28.

[26]   J.D. Dunitz, *Chem. Comm.*, (2003), 545.

[27]   J.P.M. Lommerse, W.D.S. Motherwell, H.L. Ammon, J.D. Dunitz, A. Gavezzotti, D,W,M. Hofmann, F.J.J. Leusen, W.T.M. Mooij, S.L.Price, B. Schweizer, M.U. Schmidt, B.P. van Eijck, P. Verwer and D.E. Williams, *Acta Crystallogr., Sect. B* **56** (2000), 697.

[28]   W.D.S. Motherwell, J.P.M. Lommerse, H.L. Ammon, J.D. Dunitz, A. Dzyabchenko, P. Erk, A. Gavezzotti, D,W,M. Hofmann, F.J.J. Leusen, J.P.M. Lommerse, W.T.M. Mooij, S.L.Price, H. Scheraga, B. Schweizer, M.U. Schmidt, B.P. van Eijck, P. Verwer and D.E. Williams, *Acta Crystallogr., Sect. B* **58** (2002), 647.

[29]   E. Pidcock, W.D.S. Motherwell and J.C. Cole, *Acta Crystallogr., Sect. B* **59** (2003), 634.

[30]   R. Boese, private communication.

[31]   J.D. Dunitz and J. Bernstein, *Acc. Chem. Res.* **28** (1995), 193.

[32]   R.K.R. Jetti, R. Boese, J.A.R.P. Sarma, L.S. Reddy, P. Vishweshwar and G.R. Desiraju, *Angew. Chem. Int. Ed.* **42** (2003), 1963.

[33]   W.T.M. Mooij, B.P. van Eijck, S.L. Price, P. Verwer and J. Kroon, *J. Comput. Chem.* **19** (1998), 459.

[34]   H.R. Karfunkel and F.J.J. Leusen, *Speedup* **6** (1992), 43.

[35]   H.R. Karfunkel, F.J.J. Leusen and R.J. Gdanitz, *J. Comput.-Aid Mat. Des.,* **1** (1993), 177.

[36]   H.R. Karfunkel, and R.J. Gdanitz, *J. Comput. Chem.,* **13** (1992), 1171.

[37]   L. Yu, G.A. Stephenson, C.A. Mitchell, C.A. Bunnell, S.V. Snorek, J.J. Bowyer, T.B. Borchardt, J.G. Stowell and S.R. Byrn, *J. Am. Chem. Soc.* **122** (2000), 585.

[38]   L. Yu, *J. Phys. Chem.* **A106** (2002), 544.

[39]   C. Weygand and H. Baumgärtel, *Lieb. Ann.* **469**, (1929) 251.

[40]   J. Bernstein and J.-O. Henck, *Cryst. Eng.* **1** (1998), 119.

[41]   D.M.M. Farell, C. Glidewell, J.N. Low, J.M.S. Skakle and C.M. Zakaria, *Acta Crystallogr., Sect. B* **58** (2002), 289.

[42]   G. Nichols and C.S. Frampton, *J. Pharm. Sci.* **87** (1998), 684.

[43]   J.-F. Revel and M. Ricard, *The Monk and the Philosopher*, (Thorsons, London, 1998), p. 57.

[44]   A. Burger*, Acta Pharm. Technol.* 28 (1982), 1.

[45]   P. Di Martino, P. Conflant, M. Drache, J.-P. Huvenne and A.-M. Guyot-Hermann*, J. Therm. Anal.* **48** (1997), 447.

[46]   M. Szelagiewicz, *Therm. Anal.* **57** (1999), 23.

[47]   T. Beyer, G.M. Day and S.L. Price *J. Am. Chem. Soc.* **123** (2001), 5086.

[48]   M.L. Peterson , S.L. Morissette, C. McNulty, A. Goldsweig, P. Shaw, M. LeQuesne, J. Monagle, N. Encina, J. Marchionna, A. Johnson, J. Gonzalez-Zugasti, A.V. Lemmo, S.J. Ellis, M.J. Cima and Ö. Almarsson, *J. Am. Chem. Soc.* **124** (2002), 10958.

[49]   W.I.F. David, K. Shankland , L. McCusker and Ch. Baerlocher, (eds.) *Structure Determination from Powder Diffraction Data* (Oxford University Press, Oxford, 2000).

A NEW AND SIMPLE DESCRIPTION OF CRYSTAL PACKING

Elna Pidcock and W.D. Sam Motherwell
Cambridge Crystallographic Data Centre, 12 Union Rd, Cambridge, UK CB2 1EZ

1. ABSTRACT

The distribution of values obtained by taking ratios of cell length to molecular dimension for thousands of crystal structures shows a remarkable degree of order and consistency amongst space group and Z subsets. A model has been proposed to rationalise these findings which is based upon the consideration of the close-packing of three-dimensional objects, in this case, boxes. The box model of crystal packing has been shown to reproduce key features of the distribution of cell length/ molecular dimension ratios and is proposed to be a viable description of molecular crystal packing. Thousands of experimental structures have been assigned to the "packing patterns" of the box model and analysis of these subsets of molecules has led to some interesting observations about crystal packing. For example, it has been shown that the position of the molecular centre in the unit cell (in fractional coordinates) is correlated with the packing pattern assigned to the structure. It is found that the packing patterns are not populated equally by experimental structures; the packing patterns characterised by low surface area are populated to a greater extent. Unit cell dimensions have been shown to be related to molecular dimensions in a systematic way. Thus a new understanding of crystal structures is emerging where molecular shape is of primary importance. A brief outline of applications of the model to crystal structure prediction and polymorphism is given.

2. INTRODUCTION

The seminal work of Kitaigorodskii [1] established the theory of close-packing as being a fundamental rule governing the structure of molecular crystals. Kitaigorodskii used the principle of close-packing to elucidate relationships between molecular and crystallographic symmetry and to propose which space groups allowed the efficient packing of molecules of particular point group symmetries. Despite the success of close-packing in helping to rationalise many aspects of molecular crystal structures, close-packing as a "structure-directing" force has largely been ignored. Thus it is known that all crystal structures are close-packed but the impact of close-packing on the structure of the unit cell and contents is not understood. In this paper we present a summary of recent work that has concentrated on the parameterisation of close-packing in molecular crystal structures.

3. THE SEARCH FOR CLOSE PACKING

A close-packed structure is a regular structure. Thus for an array of close-packed spheres, the positions of the centres of touching spheres are evenly spaced in all directions. Molecules are not generally spherical and molecular shape has to be taken into consideration when looking for similar patterns in a network of molecular centres. Our approach to searching for close-packing within a unit cell is fundamentally geometrical: each cell axis is divided by a molecular dimension to establish the amount of "linear space" required by the molecule[2,3]. To perform this analysis, the length of the unit cell axes, the molecular dimensions and the orientation of the molecule within the unit cell are required pieces of information. Datasets of crystal structures belonging to space group $P2_1/c$, $P-1$, $P2_1$, $P2_12_12_1$ and $C2/c$ were obtained from searching the Cambridge Structural Database [4] using Conquest [5]. To perform the searches, the space group and Z were specified, and the number of chemical entities in the structure was restricted to one. For each structure, the molecule was described by three dimensions and these were determined from using the three, perpendicular principal axes of inertia (PAI) of the molecule. The extent of the molecule along each of the three perpendicular axes (including van der Waals radii) was measured (difference between the maximum and minimum coordinates along each axis), hence three molecular dimensions, L, M and S where L>M>S. For the purpose of the calculation of cell length/molecular dimension each molecular

dimension was paired with the unit cell axis to which it was most closely aligned. Thus, the angles between each PAI and all cell axes (for an orthogonalised cell) were calculated. For two of the PAIs the smallest angle between the PAI and the cell axes was chosen thus pairing two molecular dimensions with two (different) unit cell axes, the third pairing being assumed. For each cell axis - molecular dimension pairing, the ratio of cell length to molecular dimension was calculated. Thus, each crystal structure is characterised by three ratios, henceforth pattern coefficients.[3]

Graphs of pattern coefficient vs. frequency, calculated for structures belonging to $P2_1$ (Z= 2), $P2_1/c$ (Z = 4) and $C2/c$ (Z=8) are given in **Figure 1**. There are a number of interesting observations to be made regarding **Figure 1**. Firstly the graphs are clearly very structured: the ratios of cell lengths to molecular dimensions do not give rise to a random distribution of values, rather the data cluster in discrete ranges. Secondly the graphs of **Figure 1** show a reasonable degree of similarity to one another: the corresponding peaks between the graphs are centred at approximately the same values of pattern coefficient. A result of these findings is that molecular dimensions are systematically related to cell dimensions (cell dimension = molecular dimension (D_{mol}) * pattern coefficient). Molecules in crystal structures form a regular array and the graphs of **Figure 1** show that there is a fundamental structure to the unit cell that is independent of space group, and to a first approximation, Z.
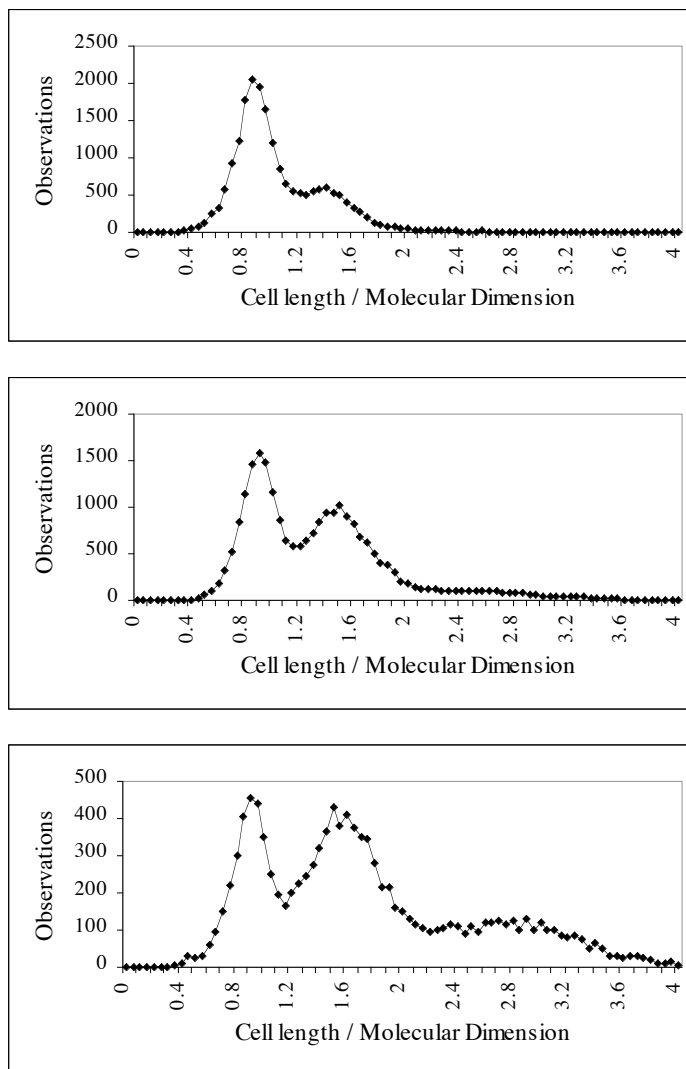
Figure 1. Graphs of pattern coefficient (cell length/ molecular dimension) vs. observations calculated for structures belonging to $P2_1$ (a), $P2_1/c$ (b), and $C2/c$ (c).

4. THE BOX MODEL OF CRYSTAL PACKING

The graphs of **Figure 1** clearly show that the spatial arrangement of molecules in unit cells is ordered. However, a model is required that explains the number, the positioning and relative heights of the peaks observed. In the graph of structures belonging to P2$_1$, there are two peaks, the first peak at approximately 0.9 and the second peak at approximately 1.4. The height of the first peak is greater than the height of the second peak and hence it is more common for a cell length to be described by 0.9D$_{mol}$ than 1.4D$_{mol}$. A model, based on the close-packing of 3-dimensional objects, in this case, boxes, is proposed to provide a basis for understanding these observations [2,3]. For a given number of identical boxes, with three unequal dimensions, L, M and S where L>M>S, there are a limited number of ways of stacking the boxes with faces touching and edges aligned. For example, for two boxes there are 3 ways of stacking the boxes using the above criteria and these "packing patterns" are shown in **Figure 2**. The differences between the packing patterns, the different surface areas and overall dimensions of the arrangements are determined by which faces of the boxes are in contact. Each packing pattern for 2 boxes can be said to belong to the 112 family where the integers are the pattern coefficients, analogous to the situation described for molecular crystal structures. Thus, the overall dimensions of an array of two boxes are given by 1x, 1x and 2x a box dimension. To encapsulate this information in the packing pattern name, we adopted the method of placing the unique pattern coefficient last, with the box dimension to which it relates. Thus the packing patterns shown in **Figure 2** are named (from left to right) 112L, 112M and 112S.
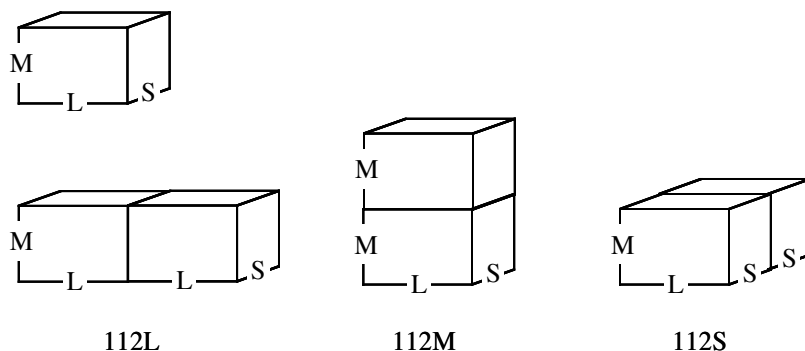
112L   112M   112S

Figure 2. The three possible packing patterns for 2 boxes (dimensions L, M and S where L>M>S), named (from left to right) 112L, 112M and 112S.

Using the same method as above, 2 families of packing patterns are generated for 4 boxes, those of the 221 packing pattern family (221L, 221M and 221S) and the 114 packing pattern family (114L, 114M and 114S). For eight boxes, two packing pattern families are possible; the 421 (6 members) family and the 222 (1 member) family.

Plotting the pattern coefficient vs. occurrence, for a given number of boxes, produces histograms which model the graphs of **Figure 1**. For 2 boxes, regardless of whether the packing pattern is 112L, 112M or 112S, the pattern coefficients (ratios of overall dimensions to box dimensions) are 1,1,2 and so the peak at a pattern coefficient value of 1 is twice has high as the peak at the pattern coefficient value of 2. The histograms for 2, 4 and 8 boxes are shown in **Figure 3**. A comparison of **Figure 1** and **Figure 3** indicates that the box model reproduces the form of the graphs shown in **Figure 1**. Certainly, in terms of the number of peaks and the positioning of the peaks, the box model is a viable description of the experimental data. The heights of the peaks in **Figure 1** are determined by the number of contributing structures to each packing pattern. In the histograms of **Figure 3** it is assumed that there are equal numbers of each packing pattern present hence an exact correspondence between the peak heights of **Figures 1** and **3** is not expected.
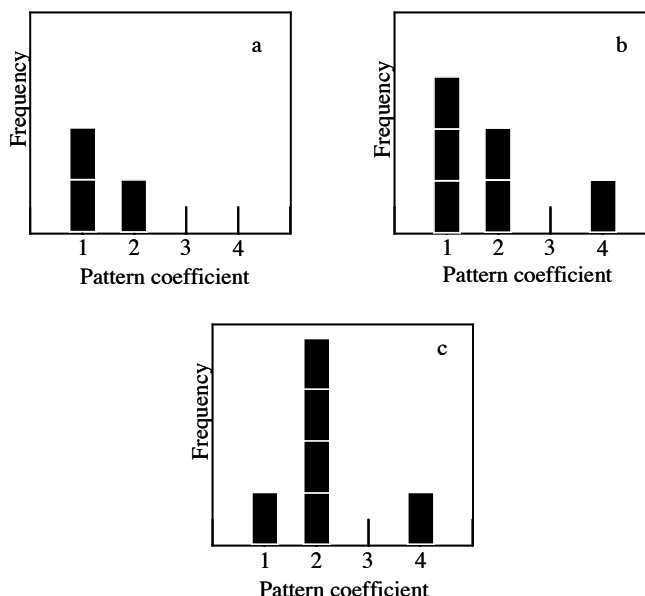
Figure 3. Histograms of pattern coefficient vs. frequency of occurrence for packing patterns for a) two, b) four and c) eight boxes. The histograms for both 4 and 8 boxes represent peak heights obtained for equal occupancy of each packing pattern family. Thus for four boxes, the histogram represents the pattern coefficient counts from a 221 packing pattern and a 114 packing pattern and for eight boxes the histogram represents the pattern coefficient counts from a 421 and 222 packing pattern.

5. PACKING PATTERNS AND CRYSTAL STRUCTURES

The structure observed in the graphs of **Figure 1** indicates that molecular packing is very regular and unit cell axes are related to molecular dimensions in a systematic way. The conceptually simple box model of crystal packing reproduces key features of the experimental graphs of **Figure 1**, notably the number and position of the peaks observed. The relative heights of the peaks (or more accurately the areas of the peaks) are determined by the number of contributing structures but the trends observed are consistent with the box model of crystal packing. Hence, thousands of experimental structures belonging to space groups $P2_1/c$, $P\text{-}1$, $P2_1$, $P2_12_12_1$ and $C2/c$ have been assigned to a packing pattern by measuring the goodness of fit between the experimental pattern coefficients and "ideal" pattern coefficients[3]. Datasets of structures belonging to the same packing patterns and space group have been collated and analysed. A number of interesting observations are presented below.

5.1 Position of Molecular Centres and Packing Patterns
It was found that not all orientations of packing pattern in the unit cell were equally popular, for example, for structures belonging to $P2_1/c$, the "1-direction" of a packing pattern (i.e the "1" of the 221 or 114 packing pattern families) was most commonly found aligned with the unit cell **a** axis and the unit cell **c** axis most commonly accommodated multiple molecular centres. This observation indicated there were correlations between the symmetry operators of a space group and the packing pattern of the structure. Hence, the positions, x_c, y_c and z_c in fractional coordinates of molecular centres for structures assigned to particular packing patterns were surveyed [6]. Scatterplots of the positions of molecular centres (projected on to a plane) for structures belonging to $P2_1/c$ are shown in **Figure 4**. For structures belonging to a 221 packing pattern family where the 1-direction of the packing pattern is aligned with the unit cell **a** axis, the position of the molecular centre on cell axis **a** (x_c) appears unconstrained. The symmetry operators in the **b** and **c** directions, which explicitly include translations of 1/2 are capable of accommodating the 2-directions of the packing pattern **(Figure 4, a)**. However, if the 1-direction of structures belonging to the 221 packing pattern family is aligned with the **b** or the **c** axis, and hence the **a** axis is required to accommodate 2 molecules, it can be seen that the molecular centre for these structures is found at $x_c = 1/4$. The symmetry operators of space group $P2_1/c$ transform x to 1-x only: from a starting position of 1/4, symmetry operators

generate a further position at 3/4, i.e. two positions evenly spaced along the **a** axis. The scatterplot of the distribution of molecular centres assigned to a 114 packing pattern is shown in **Figure 4, c**. It can be seen that positions corresponding to 1/8 on the **b** and **c** axes are favoured. Thus when four molecules are aligned with the **b** or **c** axis, the molecular centre is found at a position of 1/8 on the **b** or **c** axis, respectively. Inspection of the symmetry operators of P2_1/c reveals why this is so. From a starting point of y_c or z_c = 1/8, symmetry operators generate further positions at 3/8, 5/8 and 7/8, i.e. four positions evenly spaced along the cell axis. The **a** axis cannot accommodate four molecules as the symmetry operators (see above) only generate 2 positions. These scatterplots illustrate that there is a physical basis for the packing patterns. The packing patterns are due, at least in part, to the position the molecule adopts in unit cell, with respect to the symmetry operators [6].
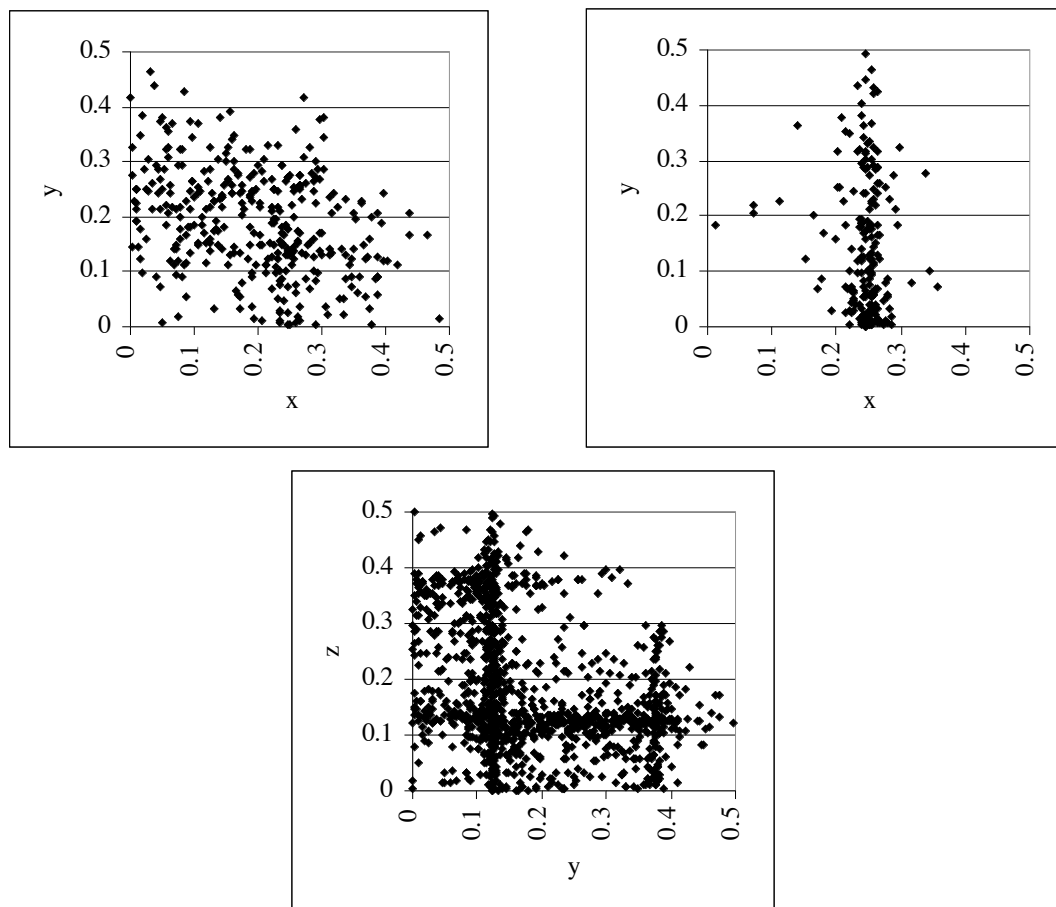
Figure 4. Scatterplot showing the distribution of molecular centres (in fractional coordinates) for structures belonging to P2_1/c (Z=4) and packing pattern 221L where 1L is aligned with the unit cell **a** axis (a), packing pattern 221L where 1L is aligned with the unit cell **b** axis (b), packing pattern 114S where the 4S direction is aligned with either the unit cell **b** or **c** axis (c).

5.2 Distribution of Experimental Structures Over Packing Patterns

A property of packing patterns constructed from the same number of boxes is that the volume of the total arrangement is the same. However, the total surface area of the arrangements is not the same. For example, in the packing pattern family 112, it can be seen **(Figure 2)** that the total surface area of the 112L arrangement, where the smallest faces of the boxes are touching, is greater than the surface area of the 112S packing pattern, where the largest faces of the boxes are touching. Similar arguments apply to the packing patterns constructed from 4 boxes, the 221 packing patterns have a lower surface area than the 114 packing patterns, the lowest surface area packing pattern being 221L and the highest surface area packing pattern being 114L. Thus, low surface area packing patterns are generated by minimising the repeats of L and maximising the repeats of S, in the packing pattern. As mentioned previously, thousands of experimental

crystal structures belonging to one of the top 5 space groups have been assigned to a packing pattern [3]. The packing patterns are not evenly populated by experimental structures and it was found that the packing patterns characterised by low surface area were populated to a greater extent. For example, for Z=2 structures belonging to space groups $P2_1$, P-1 or $P2_1/c$, 52 % of structures were assigned to the 112S packing pattern (6686/12863 structures) and only 16 % of structures were assigned to the 112L packing pattern [3]. Similar observations were made for Z = 4 structures: 43 % of structures assigned to one of the 221 packing patterns were assigned to 221L and only 26 % were assigned to 221S. The 114 packing pattern family (characterised by higher surface area than the 221 packing patterns) accounts for only 15 % of Z = 4 structures. Correlations between molecular shape and packing pattern have also been observed. For example, if a molecule has a shape classified as a disk or a rod then it is more likely to be found in a structure described by a low surface area packing pattern than its cubic counterparts. Molecules of an awkward shape can achieve better surface area for volume properties by aggregating in low surface area packing patterns [3].

5.3 Close-Packing Revealed

The similarity of the graphs in **Figure 1** to one another is remarkable and is in accord with the box model of crystal packing. Therefore beneath the intricacies of intermolecular interactions and symmetry operators is a regular structure that appears to be the foundation to thousands of experimental crystal structures. The form of the graphs in **Figure 1** have been analysed in some detail [7] and the results are summarised as follows. Gaussian fitting of the graphs has led to the parameterisation of the graphs, and the parameters, as expected, are remarkably similar. The peak broadening observed as the pattern coefficient increases has been explained in terms of perturbations to the box model caused by the orientation and overlap of the molecule within the unit cell. One significant conclusion obtained from the analysis of the graphs is that, in general, molecular packing mediated by symmetry operators is more efficient than molecular packing mediated by translation only. This conclusion was based upon the relative position of the first peak, the "translation peak" to the peaks centred at higher pattern coefficient values (the symmetry peaks). Thus cell axes which accommodate two (or four) molecules related by symmetry operators are shorter than the distance required by the equivalent number of molecules related by translation [7].

Coupling this result with the previous finding of preference for low surface area packing patterns yields an intriguing view of molecular crystal packing. As previously stated low surface area packing patterns require that the large faces of the boxes are touching, for example, in the 112S packing pattern, the LM faces of the boxes are in contact. The analysis of the graphs indicates that symmetry operators are more efficient at packing molecules than translational symmetry. Therefore, in molecular crystal structures, it is most common for the "large faces" of the molecule to be related by symmetry operators, the more efficient mode of packing, and the small faces of the molecule to be related via translation [7]

6. APPLICATIONS

The simple model of crystal packing presented in the earlier sections has practical applications. In polymorphism studies, the ability to classify polymorphs into structural types is desirable to aid the discussion of the similarities and differences between polymorphic structures. A brief survey of polymorphs found in the CSD indicates that polymorphs often belong to different packing patterns [3]. The packing pattern name encapsulates information regarding the spatial arrangement of molecules with respect to one another and the overall shape of the unit cell and thus represents a simple but useful means of classification.

In terms of the box model of crystal packing there are "natural" polymorphs. For example a "natural" polymorph of a 112S structure is a structure belonging to 221L, 221M or 114S, since the packing patterns 221L, 221M and 114S can be built from the addition of two 112S units. Thus if a favourable interaction between symmetry related molecules is present in the 112S structure, a "natural" polymorph would preserve the interaction. A survey of the occurrence of "natural" polymorphism is in progress.

Crystal Structure Prediction (CSP) may be assisted by the packing pattern results outlined above. In principle we can use the broad packing pattern statistics to reduce the search space for CSP trials or to provide a means of filtering the results of CSP trials. A limited number of CSP trials were performed on C-H only containing molecules using estimated ranges for cell dimensions, calculated from the molecular dimensions and pattern coefficients [3]. An increase of 50 % in the rate of successful prediction (correct solution at lowest energy) was observed when estimated cell ranges were used, instead of the more usual 30 x 30 x 30 Å cell, but the trial was not large enough to draw firm conclusions.

Indexing of powder patterns is another application of the relationship between molecular dimensions and cell dimensions. Similarly to crystal structure prediction, the estimated cell ranges can be used to narrow the search space or can be used to sort results of powder pattern indexing for the most likely solution. This is an, as yet, untested application of the box model.

7. CONCLUSIONS

The box model of crystal packing represents a unified description of thousands of experimental crystal structures. The uniform nature of the graphs presented in **Figure 1** indicates that at a fundamental level, crystal structures are very similar. The spatial arrangement of molecules in structures is regular, and the space group, Z, type of molecule, nature of intermolecular interactions do not appear to have a significant impact on the fundamental rules governing crystal packing. However, there is plenty more work to be done. Although unit cell dimensions can be estimated from molecular dimensions, and probabilities can be attached to the likelihood of certain packing patterns arising in particular orientations in the unit cell, we still do not know why a specific molecule adopts a particular structure, or packing pattern. This type of detail may of course be beyond this empirical approach. However, we believe that the study, in the context of the packing patterns, of molecular shape, polymorphism and intermolecular interactions will prove fruitful.

8. REFERENCES

[1]   A.I. Kitaigorodskii, *Organic Chemical Crystallography* (Consultants Bureau, New York, 1961)

[2]   E. Pidcock and W.D.S. Motherwell, *Chem. Commun*. (2003), 3028

[3]   E. Pidcock and W.D.S. Motherwell, *Cryst. Growth. Des*. **4** (2004), 611

[4]   F.H. Allen, *Acta Cryst*. **B58** (2002), 380

[5]   I.J. Bruno, J.C. Cole, P.R. Edgington, M. Kessler, C.F. Macrae, P. McCabe, J. Pearson and R. Taylor. *Acta Cryst*. **B58** (2002), 389

[6]   E. Pidcock and W.D.S. Motherwell, *Acta Cryst*. **B60** (2004), 539

[7]   E. Pidcock and W.D.S. Motherwell, *Acta Cryst*. **B60** (2004) 725

SYMMETRY AND CRYSTAL DESIGN

Joseph W. Lauher

Dept. of Chemistry, State Univ. of New York, Stony Brook, NY 11794

1. ABSTRACT

This paper presents a short discussion of how symmetry can be used to analyze the molecular assemblies that are found within molecular crystals. Discrete molecular assemblies have no translational symmetry and can be described by their point group symmetry. One-dimensional α-networks have one dimension of translational symmetry and are described by their rod group symmetry. Two-dimensional β-networks have two dimensions of translational symmetry and are described by their layer group symmetry. Three-dimensional γ-networks have three dimensions of translational symmetry and are described by their space group symmetry. The recent publication of the *International Tables for Crystallography*, *Volume E Subperiodic Groups* gives us the first official definition of the rod and layer groups, making this sort of analysis more practical for the average crystallographer.

2. INTRODUCTION

In the year 2002, a new volume of the *International Tables for Crystallography*, *Volume E Subperiodic Groups* was published [1]. This wonderful book, edited by V. Kopsky and D. B. Litvin, has yet to make the New York Times bestseller list, but it should nevertheless find its place on the desk of every crystal engineer or supramolecular chemist. Why? Because the subperiodic groups describe many of the things we make.

Supramolecular chemistry is all about assemblies of molecules. Many such molecular assemblies ultimately yield a molecular crystal. Crystals embody the idea of infinite order, order described by space group symmetry. Indeed any crystallographer knows that to fully investigate or report the structure of a molecular crystal it is essential to establish the space group symmetry of the crystal.

Yet, the concept of space group symmetry is usually far from the mind of a supramolecular chemist, who typically starts with a single molecular compound (or perhaps two in a binary system) and tries to predict how the molecules will assemble. The possible point group symmetry of a single molecule is usually apparent, but the space group of a molecular crystal is usually far from obvious at the early design stage. One knows that the properties of the eventual molecular crystal do depend upon the space group. Optical and magnetic properties are symmetry dependent. Chiral molecules will assemble with different space group symmetries than will achiral molecules or racemates. Yet how does one begin to predict the space group at an early design stage? Should one even care about crystallographic symmetry at the supramolecular design stage?

I believe that a supramolecular chemist should care. If a molecular assembly is going to yield a crystal then symmetry relationships between the molecules will ultimately determine the structure. Molecular assemblies incompatible with crystallographic symmetry will simply not form in most cases. However, it is not true that one must worry about the final space group. Often it doesn't really matter. What matters is the symmetry of the targeted molecular assembly.

3. MOLECULAR ASSEMBLIES

Molecular assemblies are groups of molecules that associate in some form, via hydrogen bonds, π-π stacking, metal-coordination or some other form of intermolecular bond. In terms of symmetry there are four fundamental types of molecular assemblies based upon the dimensionality of their periodicity, Table 1. [2]

Discrete Assemblies contain a finite number of molecules. Perhaps a dimer, a trimer, or a hexamer, if the molecules are alike; perhaps a host-guest complex, if the molecules are different. Discrete assemblies have no periodicity so their symmetry properties can be defined by their point group symmetry. If a discrete assembly is found in a crystal its point group must be one of the 32 allowed crystallographic point groups. The particular point group must be a subgroup of the space group of the entire crystal.

α-**Networks** are assemblies of molecules with one dimension of translational symmetry. The addition of one direction of translational symmetry requires a new type of subperiodic group symmetry, the rod group. There are 75 crystallographic rod groups. Standard international (Hermann-Mauguin) symbols for the rod groups have now been defined by Kopsky and Litvin [1] in the new *International Tables for Crystallography*, *Volume E.* In general the symbols are similar to the well know space group symbols.

All rod groups are primitive so each rod group symbol begins with a lower case script letter *p*. Either one or three entries follow designating the symmetry elements corresponding to the three crystallographic directions. The one periodic direction is assigned to be in the *z* direction. If one knows the standard space group symbols the rod group symbols are equally easy to interpret. The rod group *p*112 describes has a single two-fold along the *c* translational axis. Conversely the rod group *p*211 has a periodic array of two-fold axes perpendicular to the *c* axis.

The rod group of an α-network must be a subgroup of the space group of the entire crystal and a supergroup of the point group of any molecule or molecular assembly contained within the network.

β-**Networks** are assemblies of molecules with two dimensions of translational symmetry. The addition of two directions of translational symmetry also requires a new type of subperiodic group symmetry, the layer group. There are 80 crystallographic layer groups. Like the rod groups, standard international (Hermann-Mauguin) symbols for the layer groups have now been defined [1].

Each layer group symbol begins with a lower case italic letter *p* for the primitive groups or a lower case italic letter *c* for the centered groups. Again the z direction is designated at the unique direction meaning that *a* and *b* are the axes of translation. For example layer group *p*2_1/*b*11 has a two fold screw axis along the *a* axis with a perpendicular *b* glide plane.

The layer group of a β-network must be a subgroup of the space group of the entire crystal and a supergroup of the point group of any molecule or molecular assemblies or the rod group of any α-network contained within the network.

γ-**Networks** are assemblies of molecules with three dimensions of translational symmetry. Since they are periodic in three directions their symmetry will be designated by one of the 230 standard space groups. The space group of a γ-network does not have to be the same as the space group of the crystal, but the space group of the network must be at least a subgroup of the space group of the crystal. The point group of any molecule or molecular assembly, the rod group of any α-network, or the layer group of any β-network contained within the γ-network must be a subgroup of the space group of the γ-network.

Table 1
Four Fundamental Supramolecular Structures

Structure Type	No translations	Group Symmetry
Discrete assembly	Translation in one direction	Point group symmetry
α-Network	Translations in one direction	Rod group symmetry
β-Network	Translations in two directions	Layer group symmetry
γ-Network	Translations in three directions	Space group symmetry
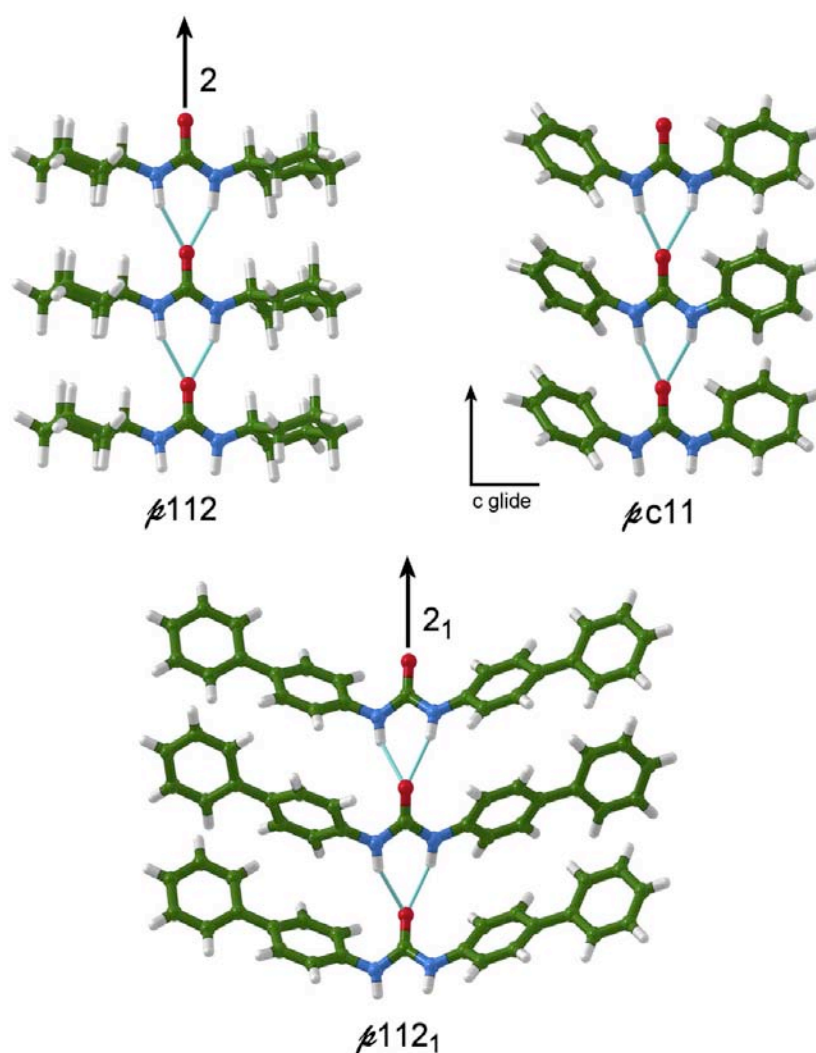
Figure 1. At the upper left, the molecule dicyclohexylurea [3] forms an α-network with p112 rod symmetry. On the upper right the molecule diphenyl urea [4] forms an α-network with pc11 rod symmetry. On the bottom the biphenyl urea [5] derivative has p112$_1$ rod symmetry.

The molecular assemblies or networks that make up a given crystal are sometimes obvious, but to a certain extent they are in the eye of the beholder. Two supramolecular chemists looking at the same crystal structure may define the networks differently, because they may choose to focus on different intermolecular interactions. However in principle the process of assigning networks can be quantified by using the energies of intermolecular interactions as a guide.

In any molecular crystal each molecule will be surrounded by others and there must be a net favorable intermolecular energy of interaction. Usually one particular intermolecular interaction and its symmetry related equivalents can be identified as the single most favorable interaction. Some other intermolecular interaction can be viewed as the second most favorable and so forth. The most important intermolecular interaction will define a molecular assembly of some order, perhaps a discrete molecular assembly or an α-network. Adding the second intermolecular interaction will often lead to a higher order network.

Crystal design can thus follow a simple thought process. A molecule is designed to form intermolecular bonds with one or more other molecules. The symmetries of the resulting intermolecular bonds determine the group symmetry and translation dimensionality of the molecular assemblies. The molecular assemblies in turn self-assemble to give more complex structures of higher order symmetry, ultimately leading to a crystal.

4. EXAMPLES

To illustrate how one uses the subperiodic groups to analyze structures let us engage in some *ex post facto* crystal design and take apart some known structures. We will focus on the urea and oxalamide molecular functionalities since they have played a very important part in our research program.

4.1 Ureas
The N,N'-disubstituted ureas are excellent molecules for designing supramolecular structures, because their paired hydrogen bonds are very dependable. The two hydrogen atoms of one urea chelate the oxygen atom of its neighbor. Symmetrical ureas with no steric problem very commonly retain their molecular two-fold axis within a crystal. The common molecular assembly of a N,N'-disubstituted urea is thus a α-network of $\textit{p}112$ rod symmetry**, Figure 1**. If the substituent is large other symmetries are found, such as $\textit{p}\textbf{c}11$ rod symmetry for diphenyl urea or $\textit{p}112_1$ for the biphenyl derivative.

Of course other symmetries are possible for urea α-networks. The unsymmetrical urea [6] shown in **Figure 2** has an intramolecular hydrogen bond forces each urea molecule to twist by 90° relative to the neighboring molecules in the α-network. This forced 90° twist results in a 4_1 screw axis giving the α-network $\textit{p}\textbf{4}_1$ rod symmetry.
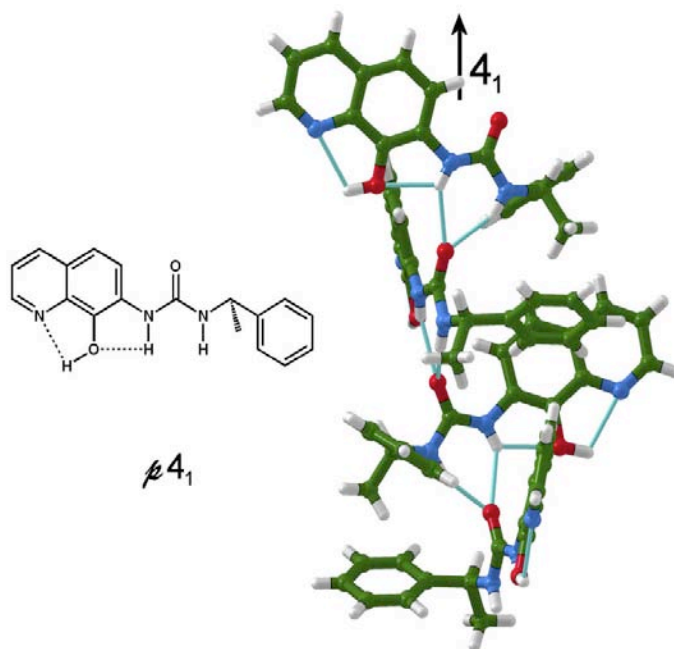
Figure 2. This asymmetric urea has an intramolecular hydrogen bond that forces each molecule to twist 90° with respect to its neighbors. The rod symmetry of the molecular assembly is $p4_1$.
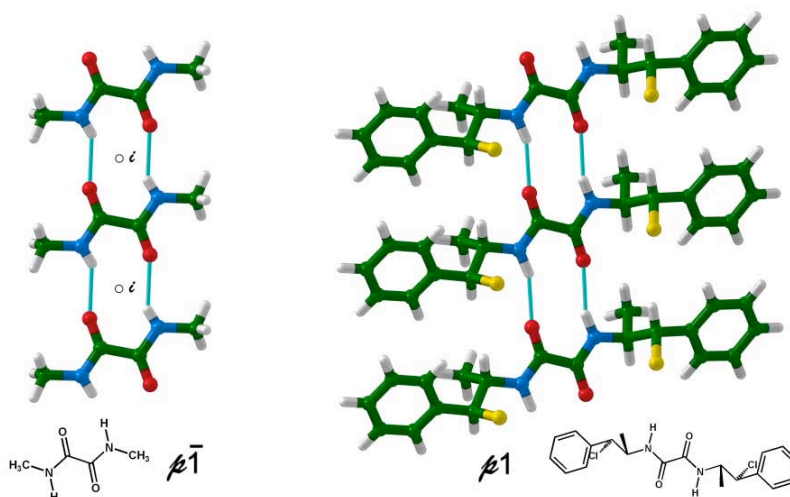
Figure 3. Dimethyloxalamide [10] is a typical centrosymmetric oxalamide. The molecule sits on an inversion center and the intermolecular hydrogen bond forms about an inversion center. The rod symmetry of the α-network is $p\bar{1}$ The oxalamide on the right is chiral [7]. A similar α-network forms, but without the inversion center, the molecules are related by simple translation. The rod symmetry of the α-network is $p1$.
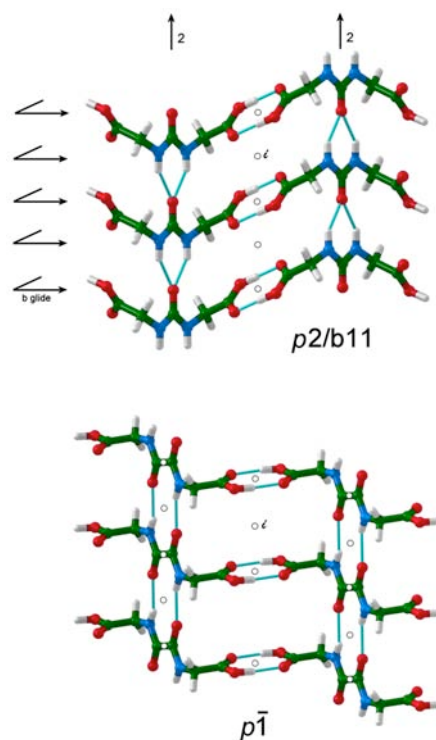
Figure 4. The top drawing shows the β-network formed by the urea of glycine [8]. The urea molecules form an α-network of ***p*112** rod symmetry. The carboxylic acid functionalities form a centrosymmetric dimer about an inversion center. Adding an adjacent inversion center to the ***p*112** rod group generates the ***p*2/b11** layer group. The bottom drawing shows the β-network formed by the oxalamide of glycine [9]. The oxalamide molecules form an α-network of ***p*$\overline{1}$** rod symmetry. The carboxylic acid functionalities form a centrosymmetric dimer about an inversion center. Adding an adjacent inversion center to the ***p*$\overline{1}$** rod group generates the ***p*$\overline{1}$** layer group.

4.2 Oxalamides

The oxalamides, diamides of oxalic acid, are an extraordinary group in terms of crystallographic symmetry. Like the urea functionality an oxalamide forms two hydrogen bonds. Symmetrical oxalamides have a molecular inversion center that is commonly preserved in crystals. Moreover, the intermolecular bond formed between two symmetrical oxalamides is also intrinsically centrosymmetric; see dimethyl oxalamide [10] in **Figure 3**. This means that the natural α-network favored for a symmetrical oxalamide has ***p*$\overline{1}$** rod symmetry.

If a symmetrical oxalamide is chiral, then inversion symmetry is prohibited. The symmetry of the resulting α-network cannot be ***p*$\overline{1}$** nor can it contain a glide plane. One would normally think of a two fold 2_1 screw axis, but in the case of an oxalamide a 2_1 screw axis is incompatible with the geometry of the paired hydrogen bonds. Thus one can predict that with some confidence that the α-network will have ***p*1** rod symmetry with neighboring oxalamides related by simple translation only.
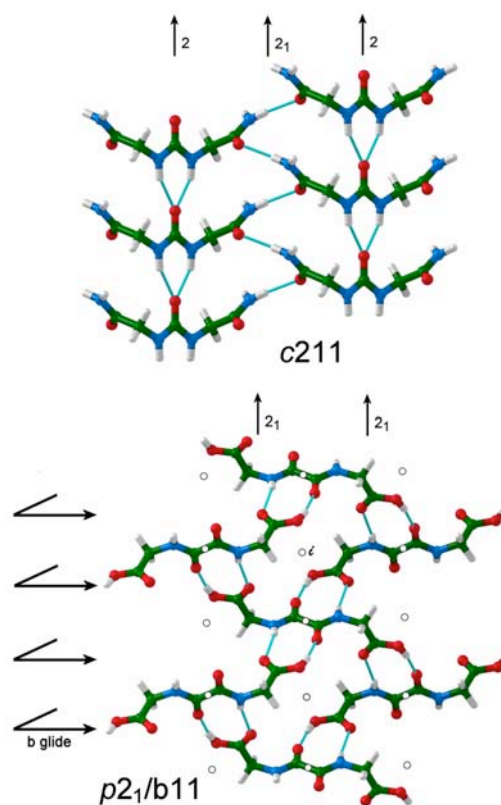
Figure 5. The top figure shows the β-network formed by the diamide of the urea of glycine [6]. The urea forms the usual $p112$ α-network. The α-networks in turn are linked together by helix of amide hydrogen bonds that from about a 2_1 screw axis. Adding a parallel screw axis to the $p112$ rod group generates the centered $c211$ layer group. The bottom figure shows a second polymorph of the oxalamide of glycine. Each centrosymmetric oxalamide forms carboxylic acid to amide hydrogen bonds to four neighboring molecules. The layer symmetry is $p2_1/b11$. There are no α-networks.

β-**Networks**. Adding an additional chemical functionality to a urea or oxalamide can bring about additional strong intermolecular interactions and thus a higher order network. Consider the urea and oxalamides derived from the simplest amino acid, glycine, **Figure 4**. Both of these groups form the expected primary α-networks, $p112$, for the urea and $p\bar{1}$ for the oxalamide. Each molecule has a carboxylic acid side group. Carboxylic acids are well known to form centrosymmetric dimers. That is the case here as well, in both cases an adjacent inversion center is added to the original α-network. Adding an inversion center to the rod group $p112$ generates the layer group $p2/b11$. Adding an inversion center to the rod group $p1$ generates the layer group $p\bar{1}$. These compound both form obvious layer structures with the hydrogen bonded β-networks defining the networks. In the case of the urea, the layers pack in an off set manner like a stack of logs. This generates a centering operation and the final space group of the resulting crystal is **C2/c**. The oxalamide layers pack via simple translation and the space group of the crystal is $p\bar{1}$.

The β-networks shown in **Figure 4** both contain two intersecting α-networks one based upon the urea or oxalamide hydrogen bonds and a second based upon the carboxylic acid hydrogen bonds. The rod symmetry of the carboxylic acid chains in the urea structure is $p2/c11$, the oxalamide carboxylic acid chains have $p\bar{1}$ rod symmetry. Many β-networks are formed by the intersection of two α-networks, but this is certainly not a requirement.

Consider the two β-networks shown in **Figure 5**. The diamide of the urea of glycine forms a conventional urea α-networks, which are in turn linked together via amide hydrogen bonds. There is no second α-network within the β-network shown. However, there is still an unused set of anti amide hydrogen atoms. These hydrogen atoms form additional hydrogen bonds to the amide oxygen atoms of neighboring layers. This unites the entire structure into a complex three-dimensional γ-network, which in this case is the entire crystal.

The oxalamide of urea forms a second $p2_1/c$ polymorph in addition to the $p\bar{1}$ polymorph shown in **Figure 4**. In the $p\bar{1}$ polymorph the hydrogen bonds were amide to amide and carboxylic acid to carboxylic acid. In the $p2_1/c$ polymorph the hydrogen bonds are like to unlike, amide to carboxylic acid. The resulting $p2_1/b11$ β-network has no α-sub-networks.

4.3 Complex Structures

The value of a proper symmetry treatment is that it becomes relatively easy to describe and to see relationships between relatively complex structures. The networks do not need to be based solely on hydrogen bonds. Consider the two coordination polymers shown in **Figure 6**. In both cases the symmetrical urea derived from 3-aminomethylpyridine is allowed to react with a transition metal salt.

The first structure is a copper nitrate derivative. The urea molecules form an α-network of $pc11$ rod symmetry with the two pyridine rings adopting different conformations. Each of the two pyridine nitrogen atoms is coordinated to a Cu^{+2} atom sitting an inversion center. The resulting square planar copper atom thus joins neighboring α-networks together to form a two-dimensional β-network. The symmetry of the β-network is $p2_1/b11$, the layer group generated when an adjacent inversion center is added to rod group $pc11$.

The second structure features the same ligand, but a different metal salt, silver tetrafluoroborate. In this case the urea preserves its twofold axis and the α-network has $p112$ rod symmetry. The four coordinate Ag^{+1} atoms adopt a tetrahedral, $\bar{4}$, geometry. Adding an external $\bar{4}$ center to the rod group $p112$ generates the space group $p4$ In this case there is no β-network.
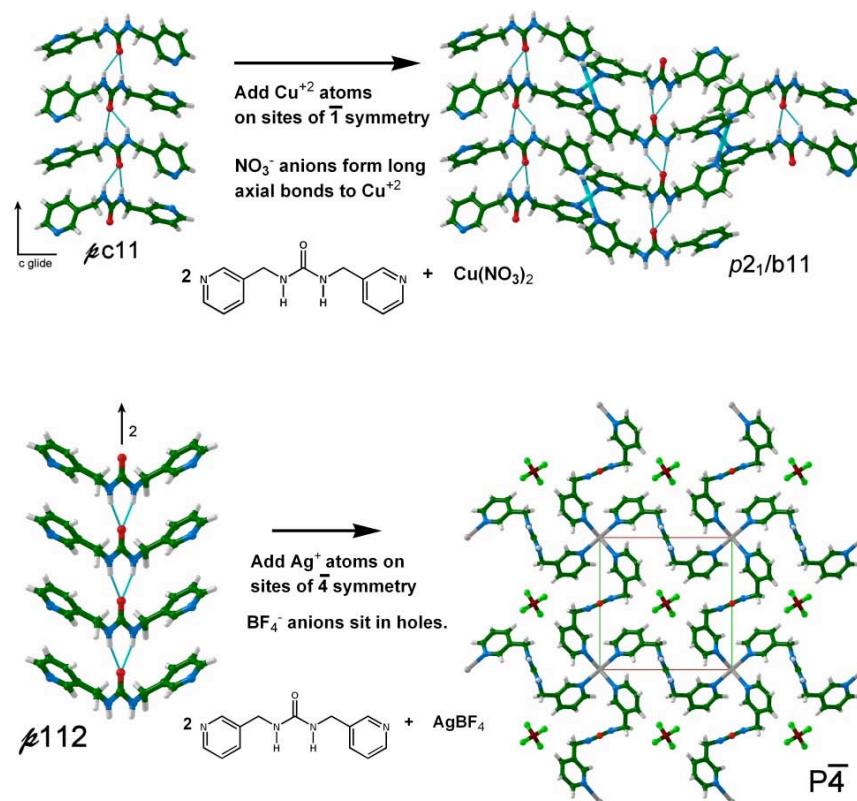
Figure 6. The top drawing shows a β-network formed by the reaction of $Cu(NO_3)_2$ with the urea of 3-aminopyridine [12]. The bottom drawing shows the γ-network formed by the reaction of $AgBF_4$ with the same ligand [13]. A top view of the γ-network is shown for the silver structure.

5. FINAL COMMENTS

The use of subperiodic groups to analyze supramolecular structures has been made much easier by the publication of the *International Tables for Crystallography*, *Volume E Subperiodic Groups*. The nomenclature for the rod and layer groups has now been standardized and is now readily available to all. The systematic evaluation of supramolecular structures in terms of symmetry is important because of the importance of intermolecular symmetry in crystallography.

In the common case of one molecule per asymmetric unit, crystallographic symmetry requires that each molecule within a crystal is related to every other molecule by some symmetry operation. This means that *every intermolecular interaction will correspond to a specific symmetry operation*. When designing a supramolecular structure one normally thinks of intermolecular interactions in terms of chemical forces, but should consider the *symmetry of the intermolecular bond*. Certain intermolecular bonds might be quite strong, but are simply not possible in a crystal. This will happen if there is no possible symmetry operator that can relate the two molecules.

Supramolecular chemistry and crystal design is not simple. The forces between molecules are weak and hard to predict. We need all tools and help that we can gather. A proper use of subperiodic symmetry is one useful tool that should not be overlooked.

6. ACKNOWLEDGMENTS

7. REFERENCES

[1]   V. Kopsky and D. B. Litvin, *International Tables for Crystallography*, *Volume E Subperiodic Groups*, (Kluwer Academic Publishers, Dordecht, 2002).

[2]   Y-L. Chang, M. A. West, F.W. Fowler, and J. W. Lauher. *J. Amer. Chem. Soc.* **115** (1993), 5991-6000.

[3]   V. M. Coiro, P. Griacomello, and E. Giglio. *Acta Crystallogr., Sect. B: Struct. Crystallograr. Chem.* **27** (1971), 2112.

[4]   W. Dannecker, J. Kopf, and H. Rust. *Cryst. Struct. Commun.* **8** (1979) 429.

[5]   S. George and A. Nangia. *Acta Crystallogr., Sect. E: Struc. Rep. Online.* **59** (2003) 901.

[6]   M. Albrecht, K. Witt, R. Frohlich, and O. Kataeva. *Tetrahedron* **59** (2002) 561.

[7]   A. Flores-Parra, P. Suarez-Moreno, S. A. Sanchez-Ruiz, M. Tlahuextl, J. Jaen-Gasper, H. Tlahuext, R. Salas-Coronado, A. Cruz, H. Noth, and R. Contreras. *Tetrahedron:Asymm.* **9** (1998) 1661.

[8]   X. Zhao, Y. –L. Chang, F. W. Fowler and J. W. Lauher. *J. Amer. Chem. Soc.* **112** (1990) 6627.

[9]   S. Coe, J. J. Kane, T. L. Nguyen, L. M. Toledo, E. Wininger, F. W. Fowler, and J. W. Lauher. *J. Amer. Chem. Soc.* **119** (1997) 86.

[10]   K. –H. Klaska, O. Jarchow, W. Scham. H. Widjaja, J. Voss, and H.W. Schmalle. *J. Chem. Res.* **104** (1980) 1643.

[11]   Y. –L. Chang. M. A. West, F. W. Fowler, and J. W. Lauher. *J. Amer. Chem. Soc.* **115** (1993) 5991.

[12]   M. J. Plater, B. M. de Silva, J. M. S. Skakle, R. A. Howie, A. Riffat, R. Gelbrich, and M. B. Hursthouse. *Inorg. Chim. Acta* **325** (2001) 141.

[13]   C. L. Schauer, E. Matwey, F. W. Fowler and J. W. Lauher. *J. Amer. Chem. Soc.* **119** (1997) 10245.

STUDIES OF PHASE RELATIONSHIPS IN COCRYSTAL SYSTEMS

Raymond E. Davis, Keith A. Lorimer[1], Matthew A. Wilkowski, and Joseph H. Rivers
Dept of Chemistry and Biochemistry, University of Texas at Austin, Austin, TX 78712

Kraig A. Wheeler and Jeffrey Bowers
Dept of Chemistry, Delaware State University, Dover, DE 19901

I. ABSTRACT

Thermomicroscopy is a technique with a broad range of applicability, and includes a number of microscopic methods used to observe phenomena at variable temperatures. The behavior of a sample observed through a temperature change can be used to decipher or estimate a variety of properties including purity, decomposition, crystal form, polymorphic forms, comparison of hydrate versus anhydrate forms, characteristics of binary mixtures, and many others. [1, 2, 3] These properties could sometimes be analyzed through other techniques and instruments that usually involve more time, effort, and starting material. Thermomicroscopic techniques require small quantities of material, often as little as a few crystals, and are often less time intensive than other methods by at least an order of magnitude.

A current focus of our research is to use thermomicroscopic methods to observe the main features of the temperature-composition melting point diagram for two-component systems and to determine whether cocrystalline phases are formed between the two components. Normally the determination of such a phase diagram would take many hours and a considerable amount of material, involving heating different mixtures of the components to determine the primary features of the diagram. Using the technique that was termed "mixed fusion" by Kofler and Kofler [4] and called "the contact method" by McCrone, [5] it is possible to determine the main features of the melting point diagram and the presence of newly formed compounds (i.e., cocrystalline phases) in a single experiment, in a much shorter time, and with only a few milligrams of material.

In this contribution, we first describe the technique and illustrate it with some previously known cocrystalline systems. Then we present some results obtained on some new quasiracemic systems. Finally, we present the results of some preliminary attempts to calculate the observed phase diagrams from thermodynamic data.

2. INTRODUCTION

The idea of using the microscope to determine chemical and physical properties of compounds arose in the nineteenth century. The earliest mixed fusion experiments using a microscope hot stage to elucidate cocrystal formation were carried out in 1877 by Lehmann. [6] Kofler and Kofler refined these methods over many years, and modern mixed fusion methods are based on their work. [4] They developed and polished techniques for compound identification, molecular weight determination, purity testing, polymeric analysis, and determination of composition diagrams. For controlled heating under the microscope, the Kofler Hot Stage was developed, and the Kofler approach is still the basis for other hot stage designs. Modern hot stage models are capable of reproducible temperature measurements to a few tenths of a degree, and the experiment is often carried out under computer control. Different designs and heating methods give different temperature ranges that the hot stage can accommodate accurately, and the choice is made based on the function desired for the particular experiment, and not on design aspects.

3. EXPERIMENTAL

The schematic design of the experiment is shown in **Figure 1**. In our laboratory setup, the hot stage, heating unit, and software were provided by Instec Inc., Boulder, Colorado. The heating unit is Instec model STC200D and

---

is controlled via a computer using the Instec program WinTemp. Observations were made through an Olympus BS41 polarizing microscope using a 10X objective and crossed polars. Images were first recorded with a Panasonic digital video recorder. Later this approach was superseded by the recording of individual frames using an Olympus C4040-Z digital camera controlled through the computer using another Instec program, WinDito.
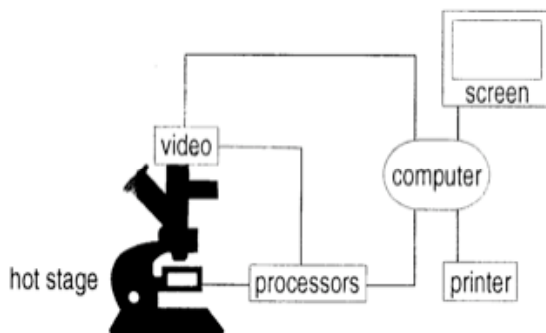
Figure 1. A schematic of computer-controlled thermomicroscopy apparatus. Various methods of recording images can be used, including video recording and sequential digital or analog photography.

The mixed fusion sample is prepared by first melting a small amount of the higher melting component at one edge of a cover slip on a microscope slide (**Figure 2**, point A). As the sample melts, it is drawn under the cover slip until it occupies about half the area of the cover slip. After this melt has cooled and solidified, the second (lower melting) component is placed at another edge of the cover slip, preferably near the other component (**Figure 2**, point B). As this lower-melting component is then melted, it is drawn under the coverslip and dissolves some of the first component at the boundary where they meet. This area is termed the mixing zone, and is the region of interest for these techniques. The sample is then allowed to cool. After the preparation has completely solidified, the mixing zone is observed under the microscope on a hot stage while the temperature is raised at a controlled rate.
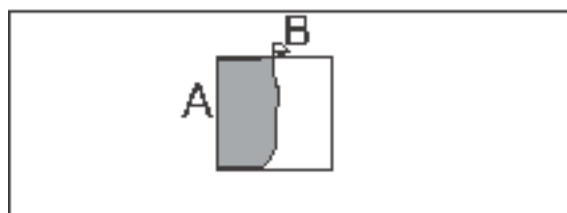
Figure 2. Preparation of the mixed fusion sample. The shaded region represents the solid phase of the higher melting component. The second (lower melting) component is introduced at point B.

4. RESULTS AND DISCUSSION

At some point in the mixing zone, there should be a 1:1 ratio of the two components. Moving from this point toward either pure component, the proportion of that component increases. Thus, a composition gradient exists across the mixing zone. It is in the mixing zone that there is a potential for new cocrystal structures to be formed. These cocrystals have different properties, in particular different melting behavior, from either of the pure components. When the sample is heated and observed under crossed polars, only solid phases will be visible, because they direct the polarized light so it is not blocked by the other polarizer. Liquid phases, on the other hand, allow the light to pass through unchanged, so no light reaches the microscope. Thus when a portion of the sample melts, it is quickly seen and easily recognized as a black line or region. Any new cocrystalline phases in the mixing

zone will be easily detectable under crossed polars during heating, due to the distinctive features of the melting point phase diagram.

Figure 3 shows the three fundamental types of mixtures formed from the mixed melting of two components A and B: (i) conglomerate, in which the two components each exist in separate crystalline regions, (ii) cocrystal or compound formation, in which a distinct crystalline region is formed with different properties than either component, and (iii) solid solution, in which the two components are miscible in the solid phase.
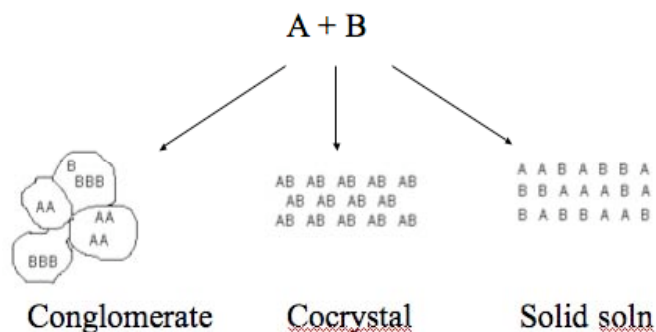
Figure 3. Three fundamental types of mixtures formed from the mixed melting of two components A and B.

These three situations can be distinguished experimentally by their binary melting point phase diagrams. For conglomerate crystallization **(Figure 4)**, the presence of each component lowers the melting point of the other one, so the melting point decreases from either side of the diagram. These curves eventually meet at some minimum melting point, termed a eutectic point. When a compound (cocrystalline phase) of stoichiometry AB is formed, the diagram has the general appearance shown in **Figure 5**, with three melting point maxima (pure A, pure B, and cocrystal AB) separated by two eutectics. When an ideal solid solution is formed, the melting point increases smoothly as shown in **Figure 6**. Nonideal solid solution diagrams can exhibit either a maximum or a minimum.
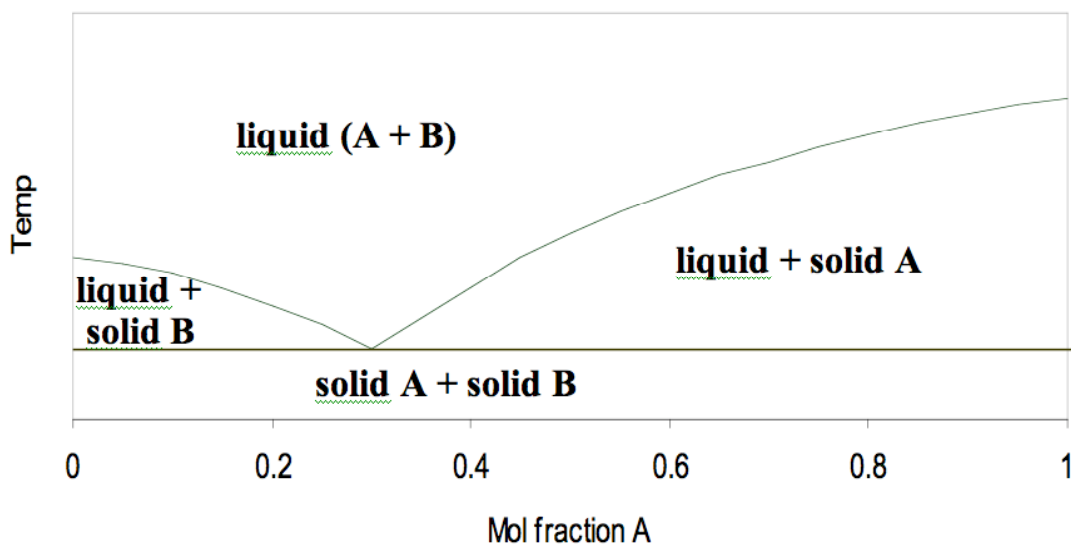
Figure 4. The binary melting point diagram for conglomerate crystallization of A and B.
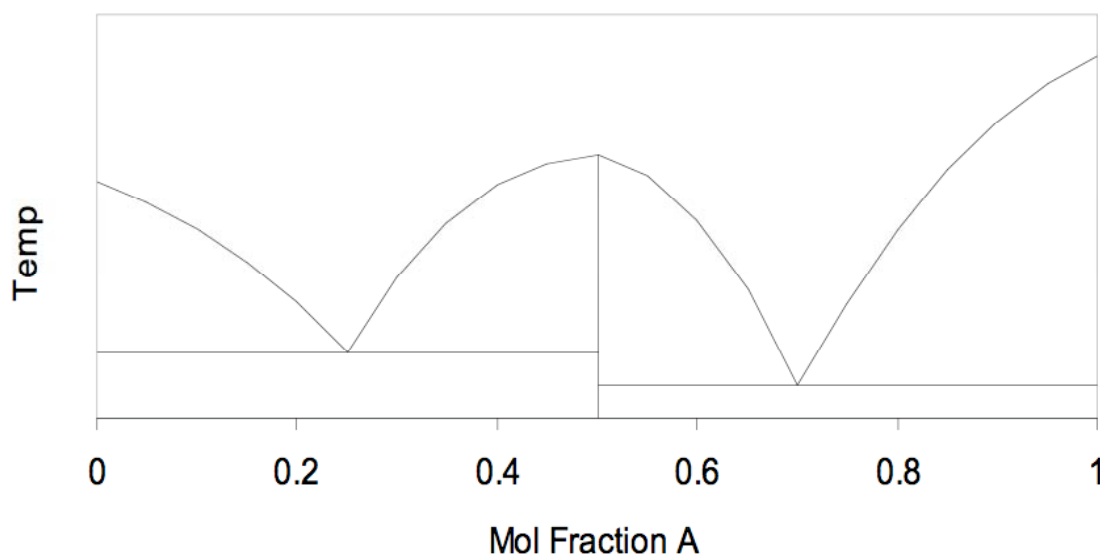
Figure 5. The binary melting point diagram for compound (cocrystal) formation with stoichiometry AB.
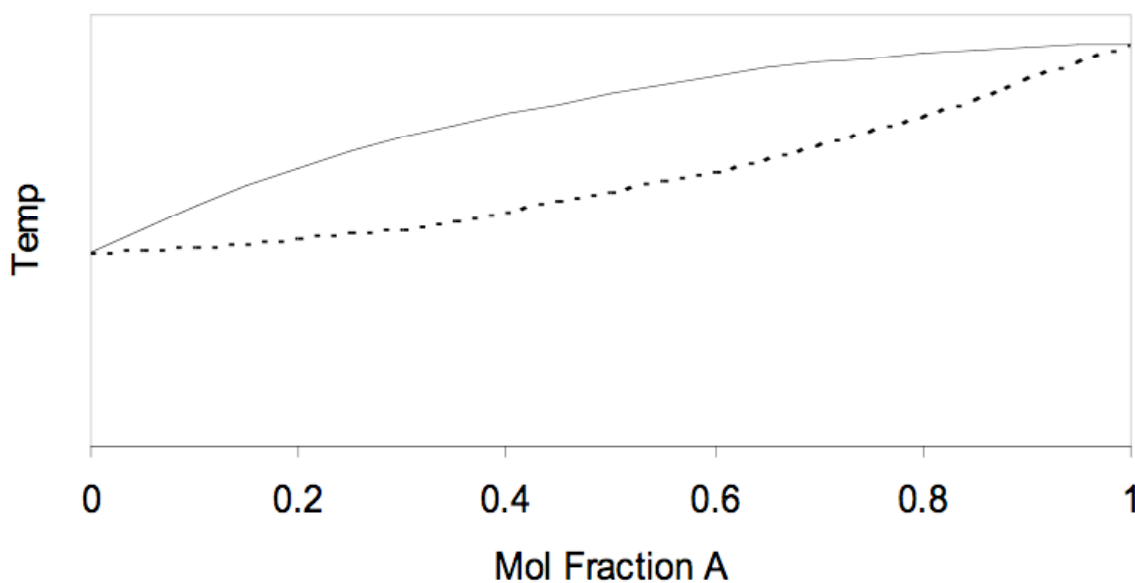
Figure 6. The binary phase diagram for an ideal solid solution of A and B.

If the two components simply recrystallize as separate microcrystals in the mixing zone (conglomerate crystallization), a melting point diagram with a single eutectic is expected, as in **Figure 4**. In the mixed fusion experiment, this would appear as a single black region of melt that gradually spreads as the temperature is raised. If, instead, a new cocrystalline phase is formed, the mixed fusion experiment would show two black regions (eutectics), perhaps at different temperatures, with the cocrystalline phase between them. These two situations are contrasted in **Figure 7**. The cocrystalline phase could have a higher or a lower melting point than either pure component, or it could be intermediate between the two (the case shown in **Figure 5**). If cocrystal structures with different stoichiometries are stable, there will be a corresponding number of eutectics (melt lines) that separate all the different crystalline phases.

(a)   (b)
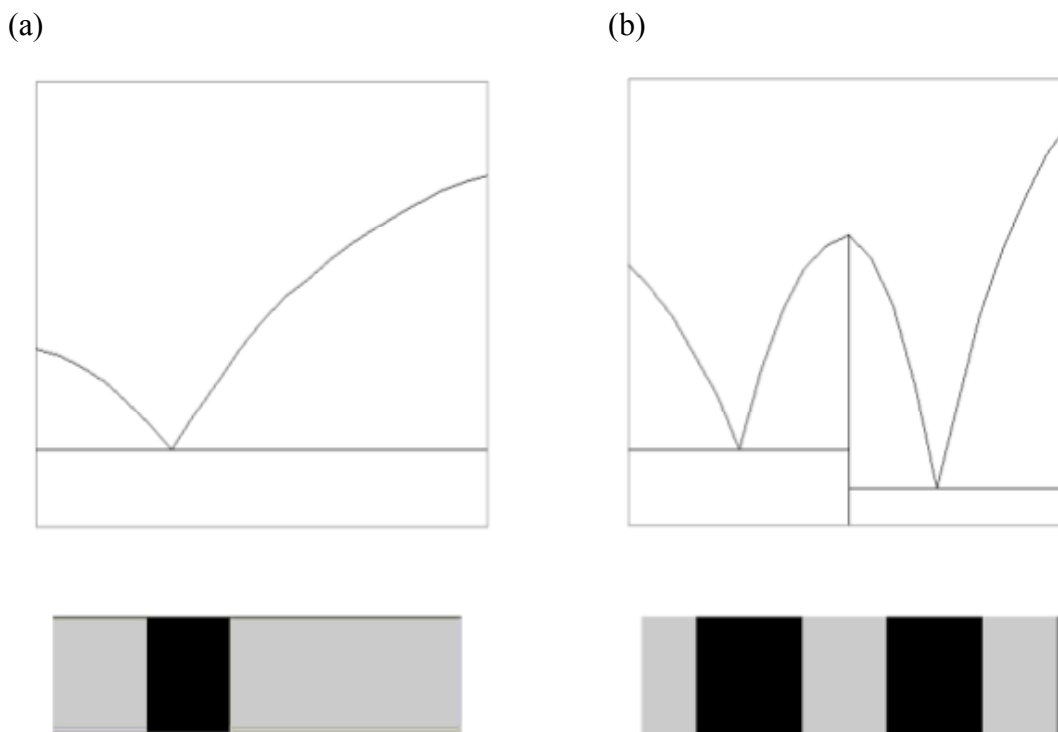
Figure 7. Schematic representations of the correspondence between melting point diagrams and the appearance of the mixed fusion samples. (a) Conglomerate sample, with a single eutectic, which appears as a single black region of melt in the mixed fusion experiment. (b) Cocrystal formation, which gives two eutectics that appear in the mixed fusion experiment as two black regions of melt flanking the solid cocrystalline phase.

The mixed fusion experiment can be illustrated with mixtures of (*R*)- and (*S*)-mandelic acid. In this experiment, the two components A and B are the two enantiomers of this chiral acid, and the "compound" that is formed is the stable racemic phase. Though the results of this mixed fusion experiment were recorded as a continuous video, they are illustrated here as individual snapshots at temperatures in **Figure 8**. At the temperature 105.1 °C, all phases are solid. By 107.5 °C, the two eutectics are just visible as narrow black stripes near the center of the diagram, with the racemic phase in between. In the next several shots, the melt broadens as the racemic phase melts by 109.0 °C. This series illustrates clearly the situation where the cocrystal (racemate in this case) melts at a lower temperature than either pure component (enantiomers in this case).

Mandelic acid 105.1 °C
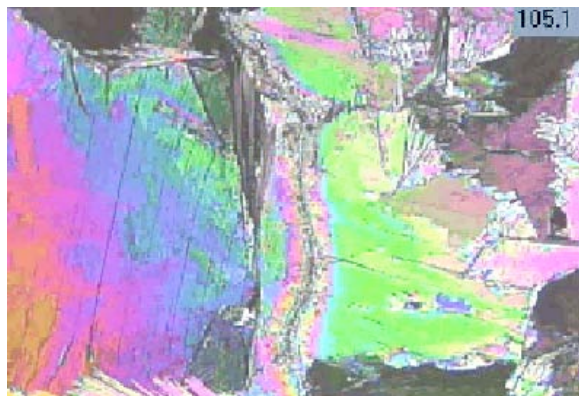
Mandelic acid 107.5 °C
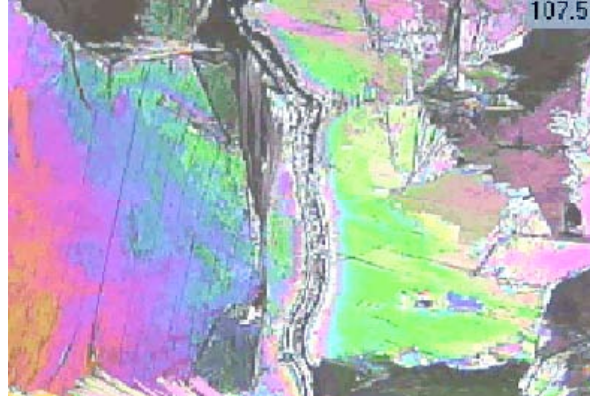
Mandelic acid 108.0 °C
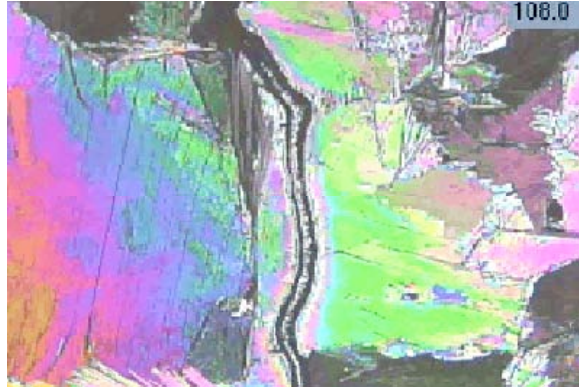
Mandelic acid 108.4 °C
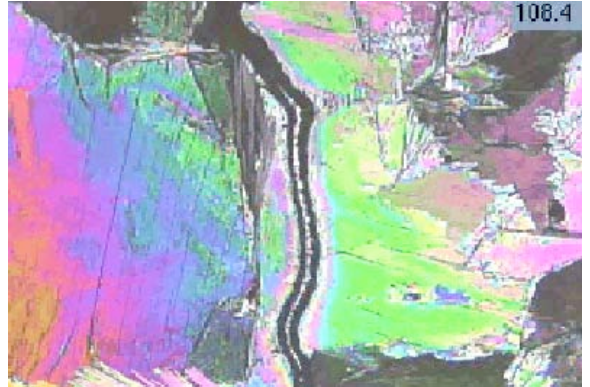
Mandelic acid 108.6 °C
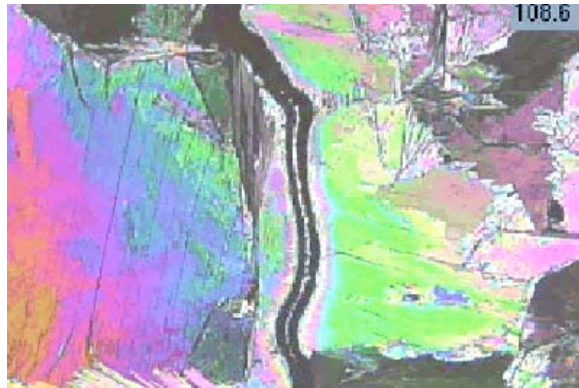
Mandelic acid 109.0 °C
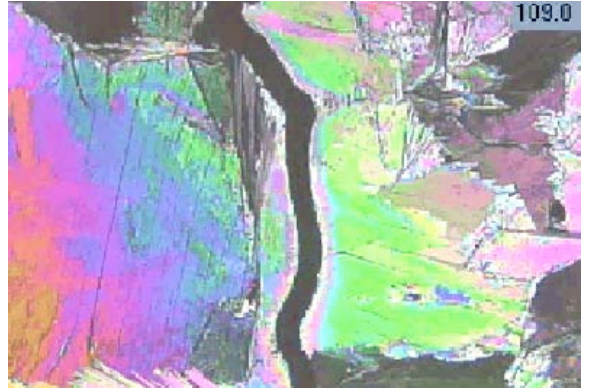
Figure 8. Some observations of the mixed fusion behavior of mandelic acid. The two sides of the sample are the two enantiomers of mandelic acid. The low melting cocrystalline phase is racemic mandelic acid.

By contrast, the melting points of the enantiomers of malic acid are lower than that of the racemate. This behavior is clearly seen in the series of observations in **Figure 9**. At 101.1 °C, all phases are solid. The eutectics then appear and melting occurs toward the pure component regions at increasing temperature, until the two pure (enantiomeric) phases are completely melted by 106.2 °C, at which point the racemate is still solid.

Malic acid 101.1 °C
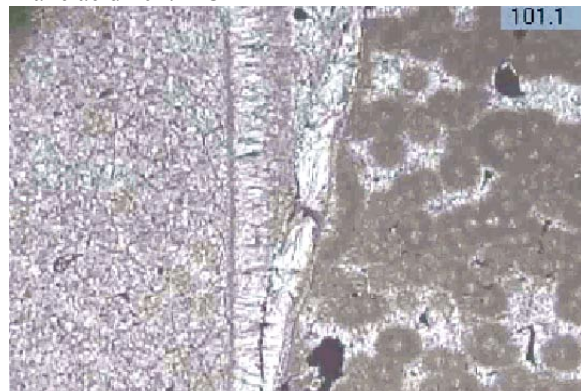
Malic acid 101.8°C
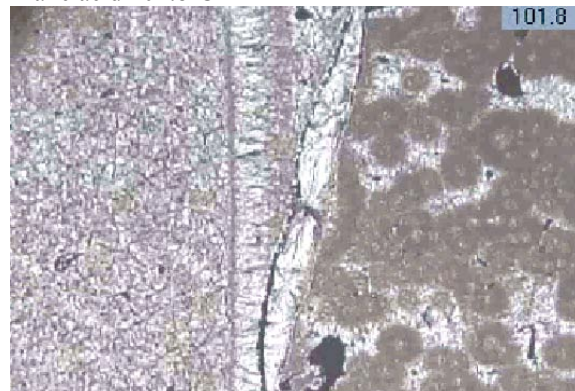
Malic acid 103.2 °C

Malic acid 104.4 °C
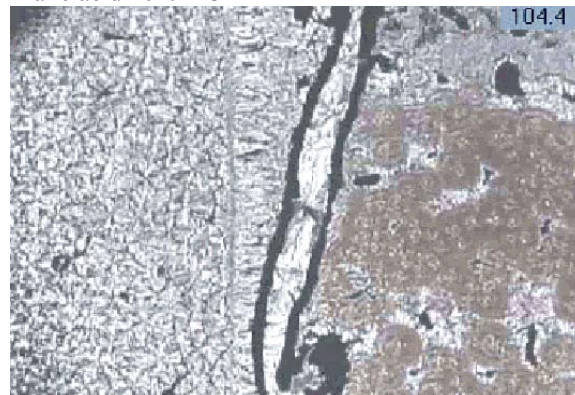
Malic acid 105.0 °C
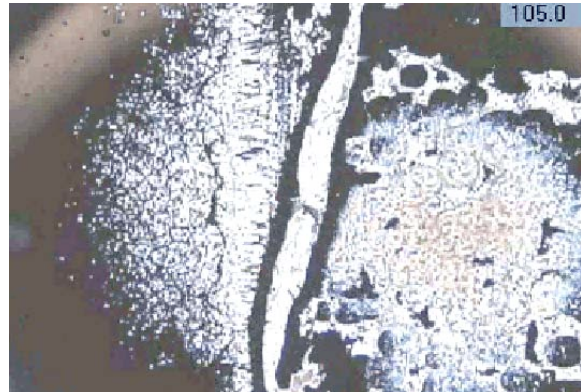
Malic acid 106.2 °C

Figure 9. Some observations of the mixed fusion behavior of malic acid. The two sides of the sample are the two enantiomers of malic acid. The high melting cocrystalline phase is racemic malic acid.

The catechol/*p*-phenylenediamine system is shown in the series of **Figure 10**. Now one component (catechol, on the left) has a lower melting point than the other (*p*-phenylenediamine, on the right). Through the first several frames shown, up to 113.2 $^{\circ}$C, one eutectic and then the other appear, flanking what seems to be one cocrystalline phase. But by 119.2 $^{\circ}$C, a third eutectic appears, clearly indicating the presence of two cocrystalline phases. Then the two cocrystalline phases melt at almost the same temperature.

Catechol/*p*-Phenylenediamine
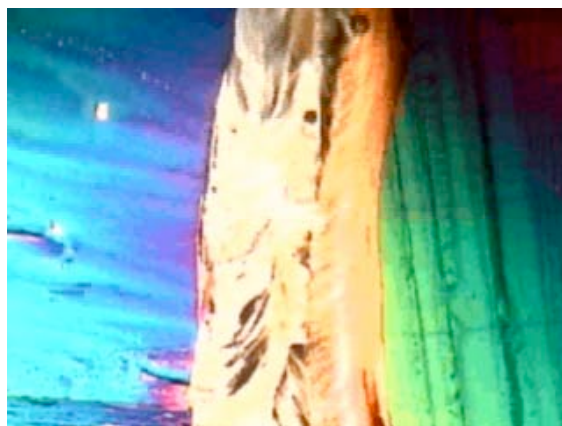
Catechol/*p*-Phenylenediamine
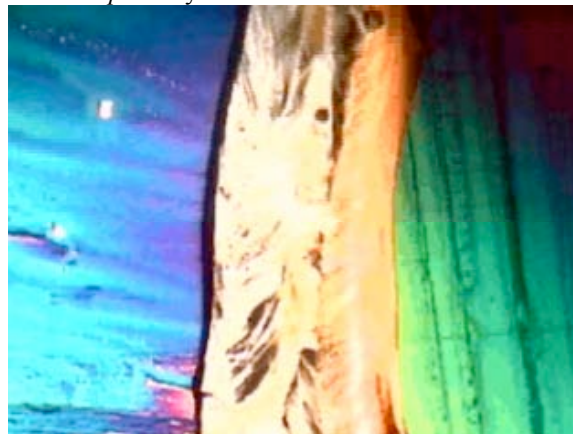
Catechol/*p*-Phenylenediamine

Catechol/*p*-Phenylenediamine 113.2 $^{\circ}$C
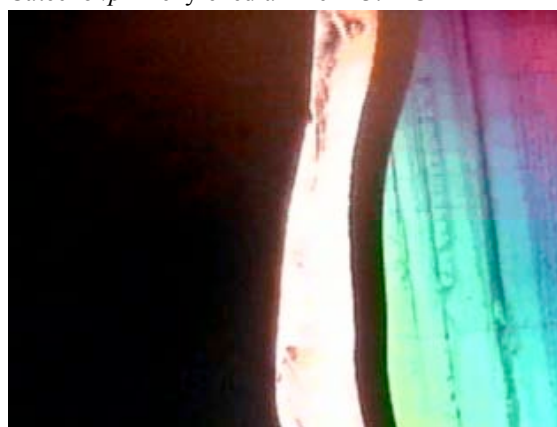
Catechol/*p*-Phenylenediamine 119.2 $^{\circ}$C

Catechol/*p*-Phenylenediamine
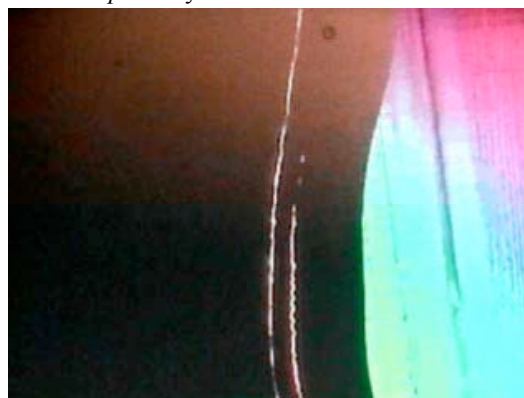
Figure 10. The mixed fusion behavior of the catechol (left) /*p*-phenylenediamine system.

Two experimental melting point phase diagrams for this catechol/*p*-phenylenediamine system have appeared in the literature, with different conclusions. Rai interpreted the diagram in **Figure 11** on the basis of a single 1:1 cocrystalline phase, [7] while Dhillon had already taken a nearly identical diagram **(Figure 12)** as evidence for a 2:1 catechol:*p*-phenylenediamine phase. [8] The mixed fusion experiment clearly shows the presence of both cocrystal phases, suggesting that the phase diagram should be more carefully drawn as in **Figure 13**.
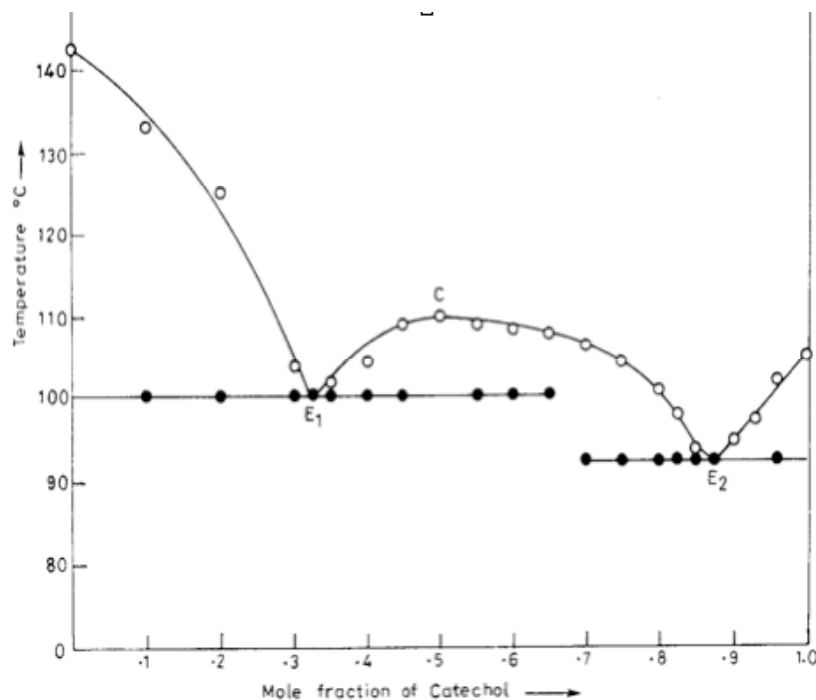
Figure 11. The catechol/*p*-phenylenediamine phase diagram as drawn by Rai. [7]
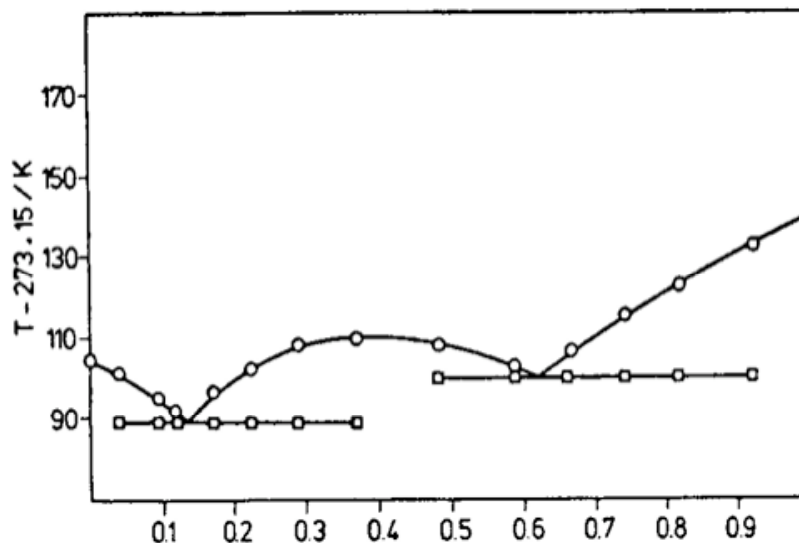
Figure 12. The catechol/*p*-phenylenediamine phase diagram as drawn by Dhillon. [8] Note that this diagram the mole fraction of catechol increases to the left.

Raymond E. Davis, Keith A. Lorimer, Matthew A. Wilkowski, Joseph H. Rivers, Kraig A. Wheeler and Jeffrey Bowers
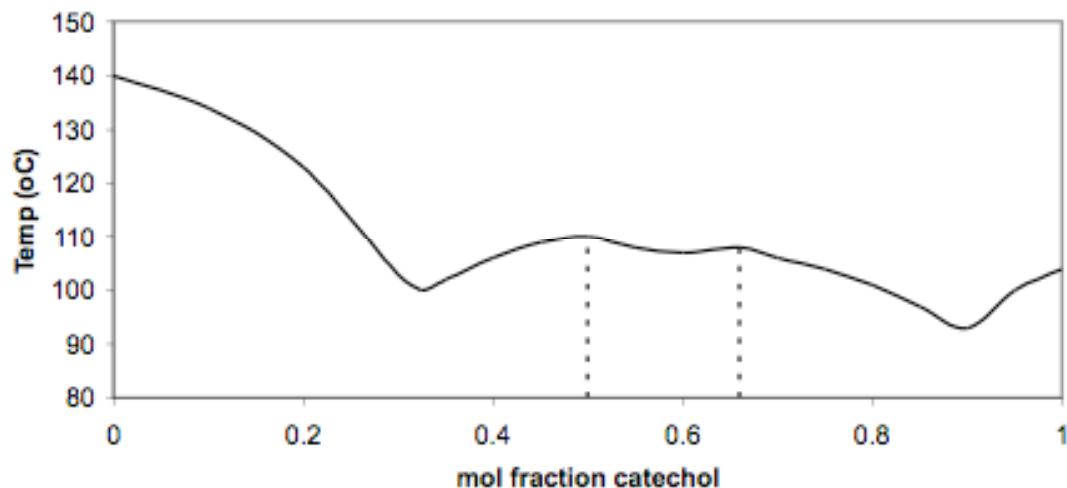
Figure 13. A suggested reinterpretation of the phase diagram of catechol/*p*-phenylenediamine showing both the 1:1 and 2:1 catechol:*p*-phenylenediamine phases indicated by the mixed fusion experiments.

We have determined the previously unreported crystal structure of the 1:1 phase, as shown in **Figure 14**. So far, we have not obtained suitable crystals of the 2:1 phase.
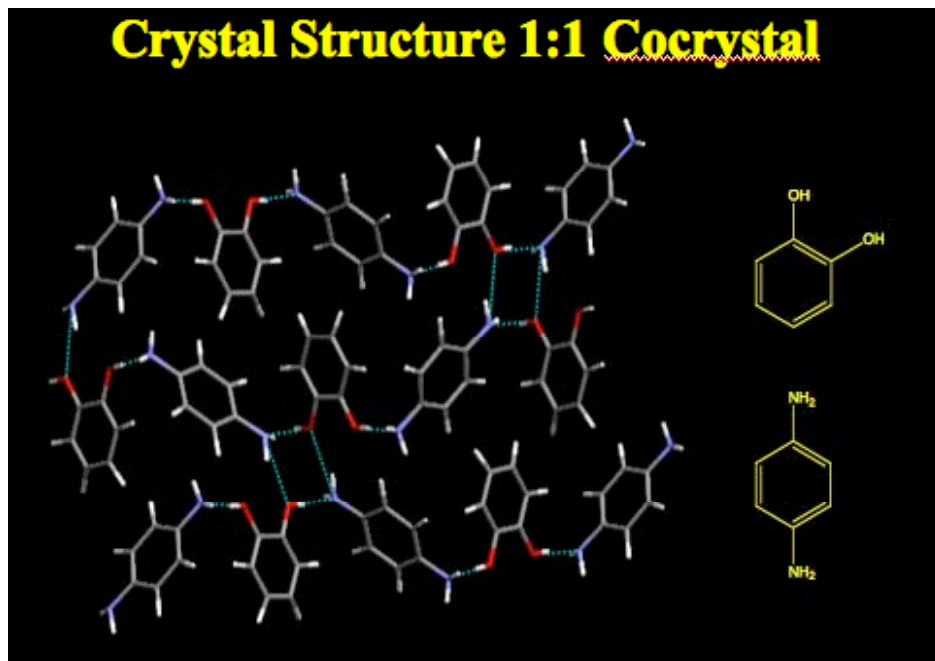
Figure 14. A drawing of the crystal structure of the 1:1 cocrystal of catechol/*p*-phenylenediamine.

Based on the phase diagram of **Figure 15**, Rai and Rai reported a 1:1 urea/resorcinol cocrystalline phase, [9] the structure of which **(Figure 16)** was reported by Pickering and Small. [10] Kofler and Kofler comment on the dimorphic phase change of this cocrystalline phase (at temperatures below the well-known resorcinol phase change). This change can be seen on careful inspection of the series in **Figure 17** (though it is much easier to see in the dynamic recording that, unfortunately, cannot be reproduced here).
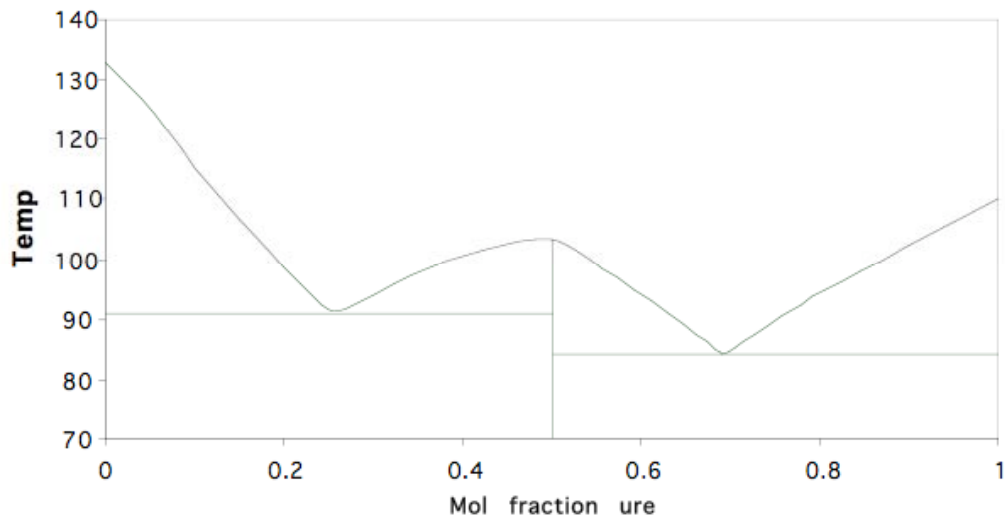
Figure 15. The melting point phase diagram for the urea/resorcinol system.
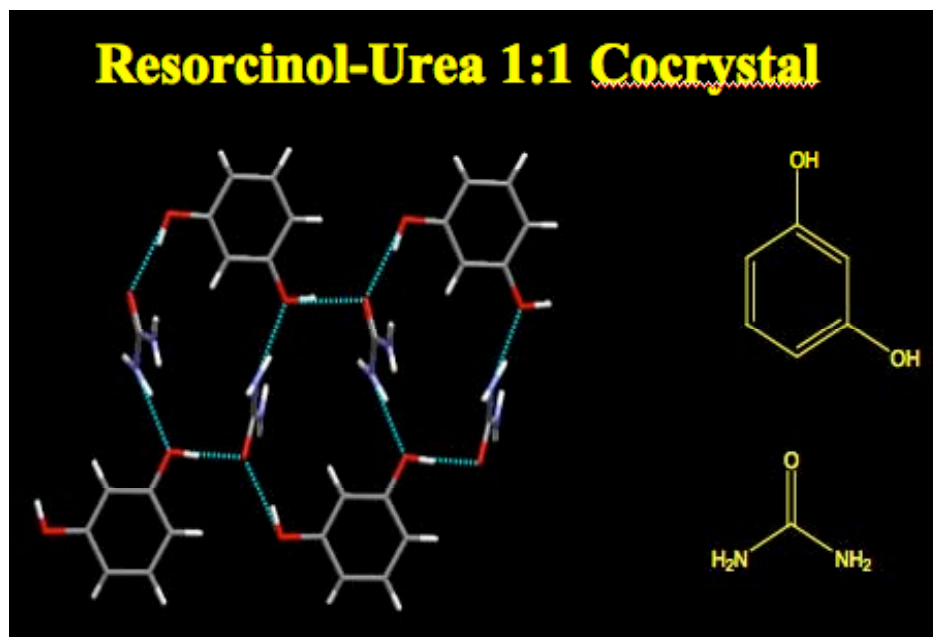
Figure 16. The crystal structure of the urea/resorcinol 1:1 cocrystal.
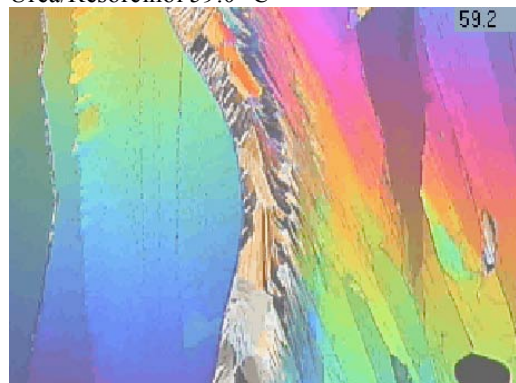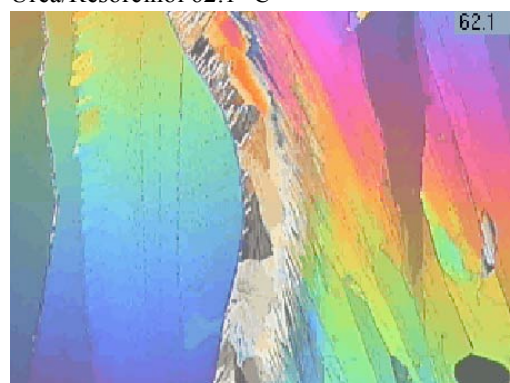
Urea/Resorcinol 54.0 °C
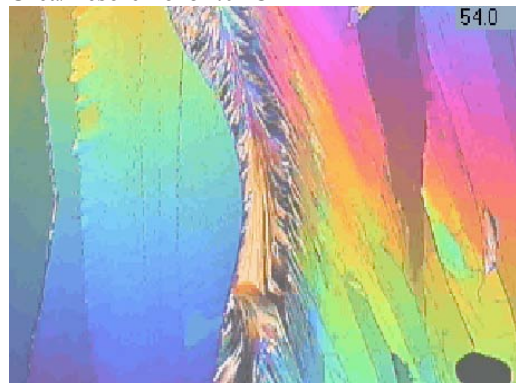
Urea/Resorcinol 57.2 °C
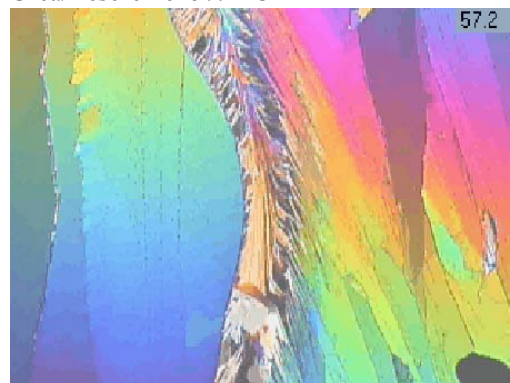
Urea/Resorcinol 59.0 °C

Urea/Resorcinol 62.1 °C

Figure 17. Mixed fusion behavior of the urea/resorcinol system, showing the solid-state phase change of the cocrystal, as evidenced by the changing appearance in the mixing zone.

We have made extensive studies [11] of a particular kind of cocrystals termed quasiracemates. [12] In quasiracemates, the shape similarity of two near-enantiomers facilitates formation of a structure that is nearly centrosymmetric. This packing arrangement can be achieved by cocrystallizing two components, (*R*)-X and (*S*)-X', where X and X' represent molecules that are sterically similar, though they might be electronically quite different. The strong preference for (near-)centrosymmetric packing can lead to an approximately centrosymmetric arrangement that sometimes mimics that of at least one of the corresponding racemates. One such system is the pair of substituted phenoxypropionic acids shown in **Figure 18**. [13]   In this system, the two enantiomers are isostructural, as are the two racemates, and the quasiracemate mimics the structure of the racemates, as suggested by comparison of the unit cell data and symmetries shown in **Figure 19**. We have determined crystal structures of both of these enantiomers **(Figure 20)**, both racemates **(Figure 21)**, and the quasiracemate **(Figure 22)**. (This is not invariably the case, however, as we have seen in some other such sets of compounds.) Excerpts from the mixed fusion experiment for these compounds appear in **Figure 23**.
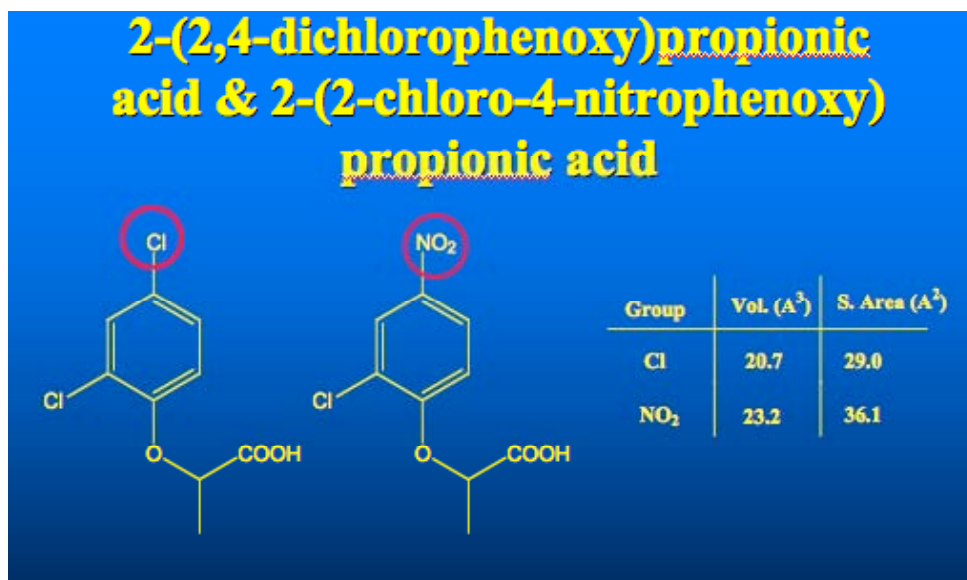
Figure 18. Two sterically similar phenoxypropionic acid derivatives that form quasiracemic cocrystals.
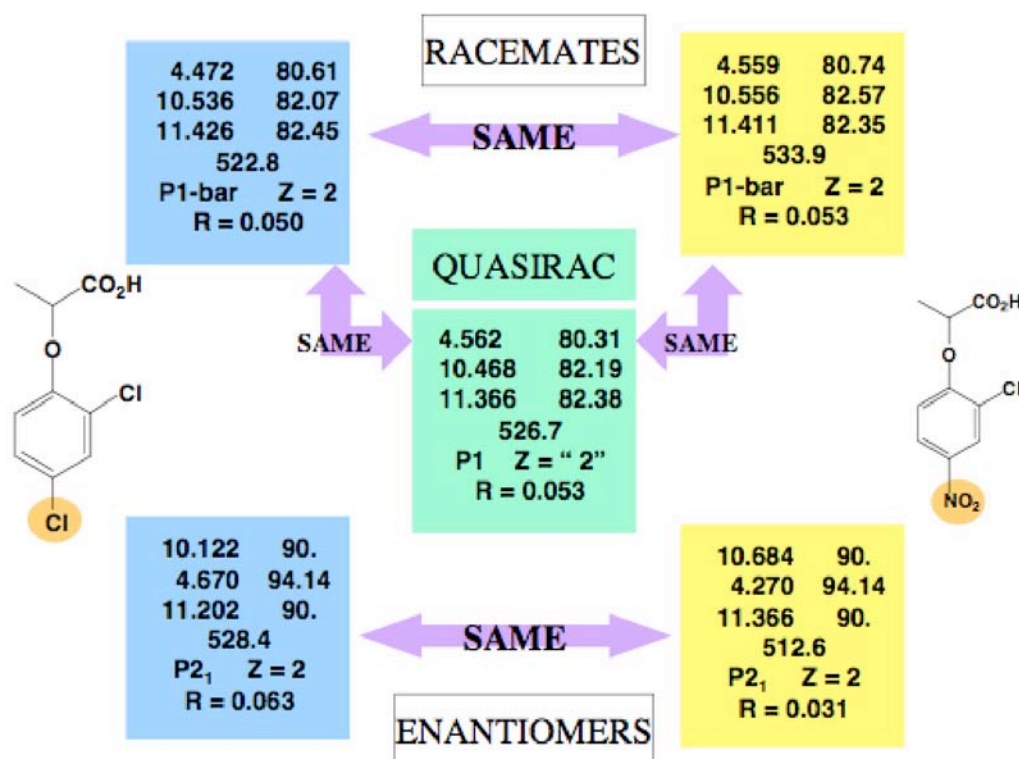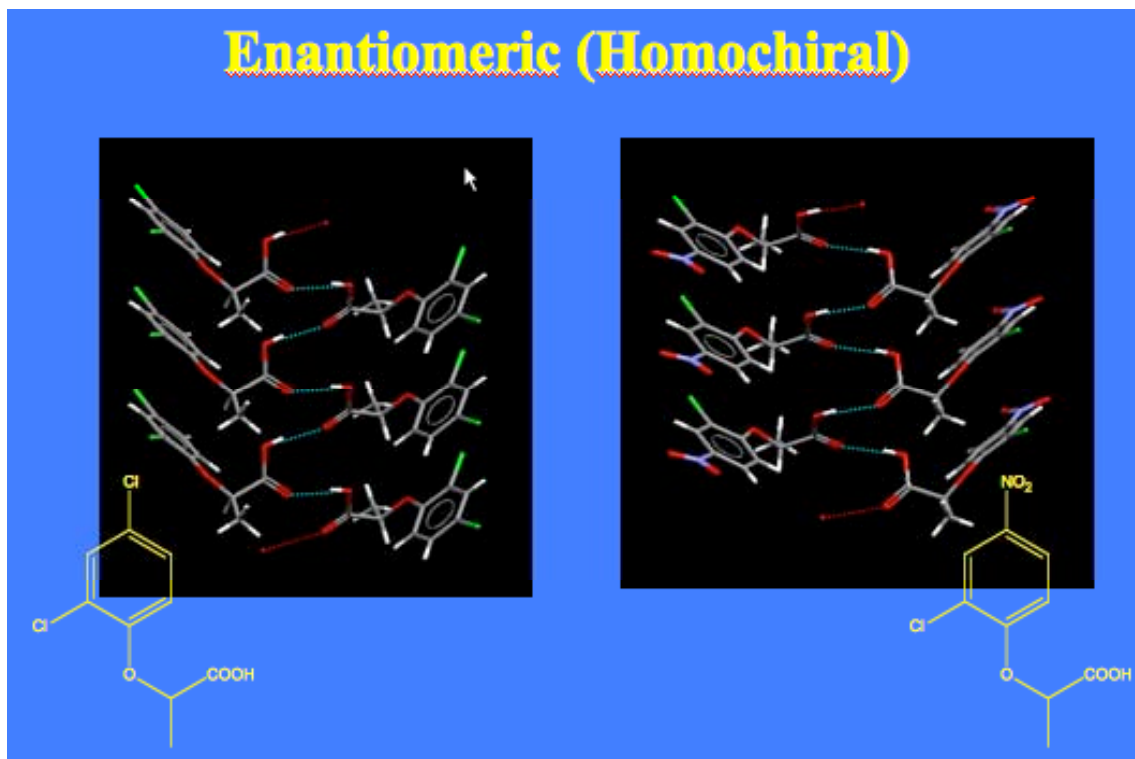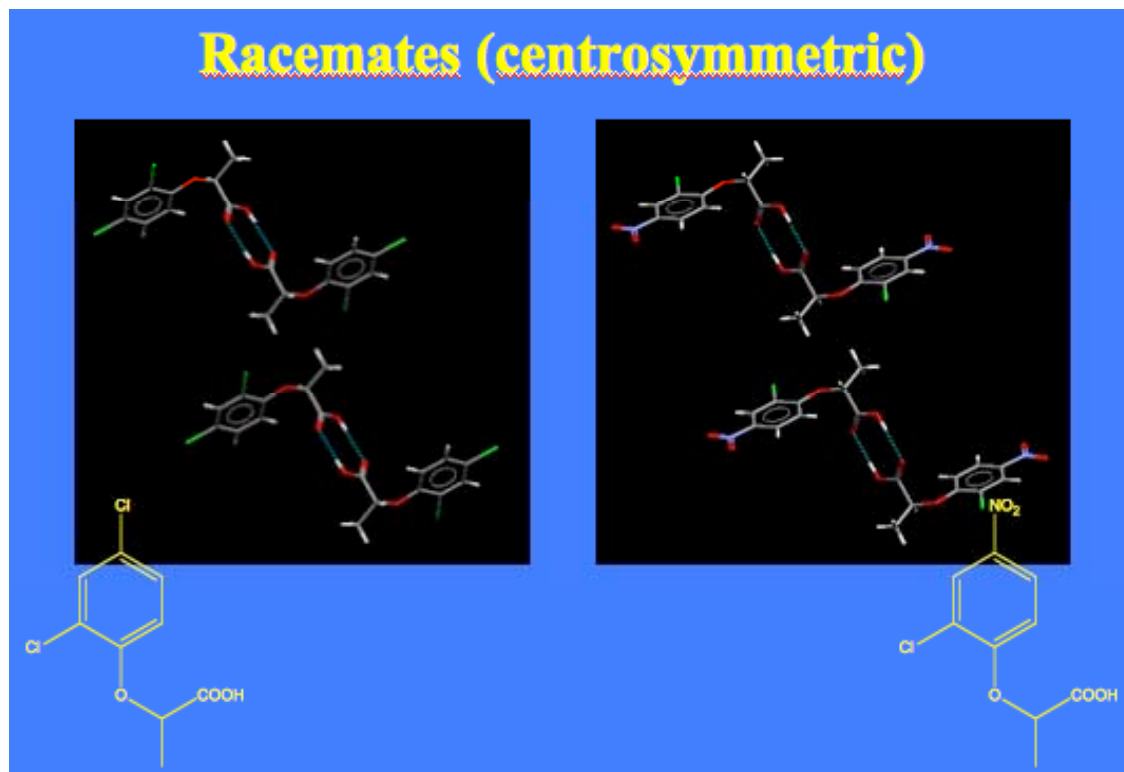

Figure 19. Relationships among the crystal structures of the two substituted phenoxypropionic acids shown in **Figure 18**.

Raymond E. Davis, Keith A. Lorimer, Matthew A. Wilkowski, Joseph H. Rivers, Kraig A. Wheeler and Jeffrey Bowers

Figure 20. Comparison of the crystal structures of the enantiomers of the two substituted phenoxypropionic acids shown in **Figure 18**.
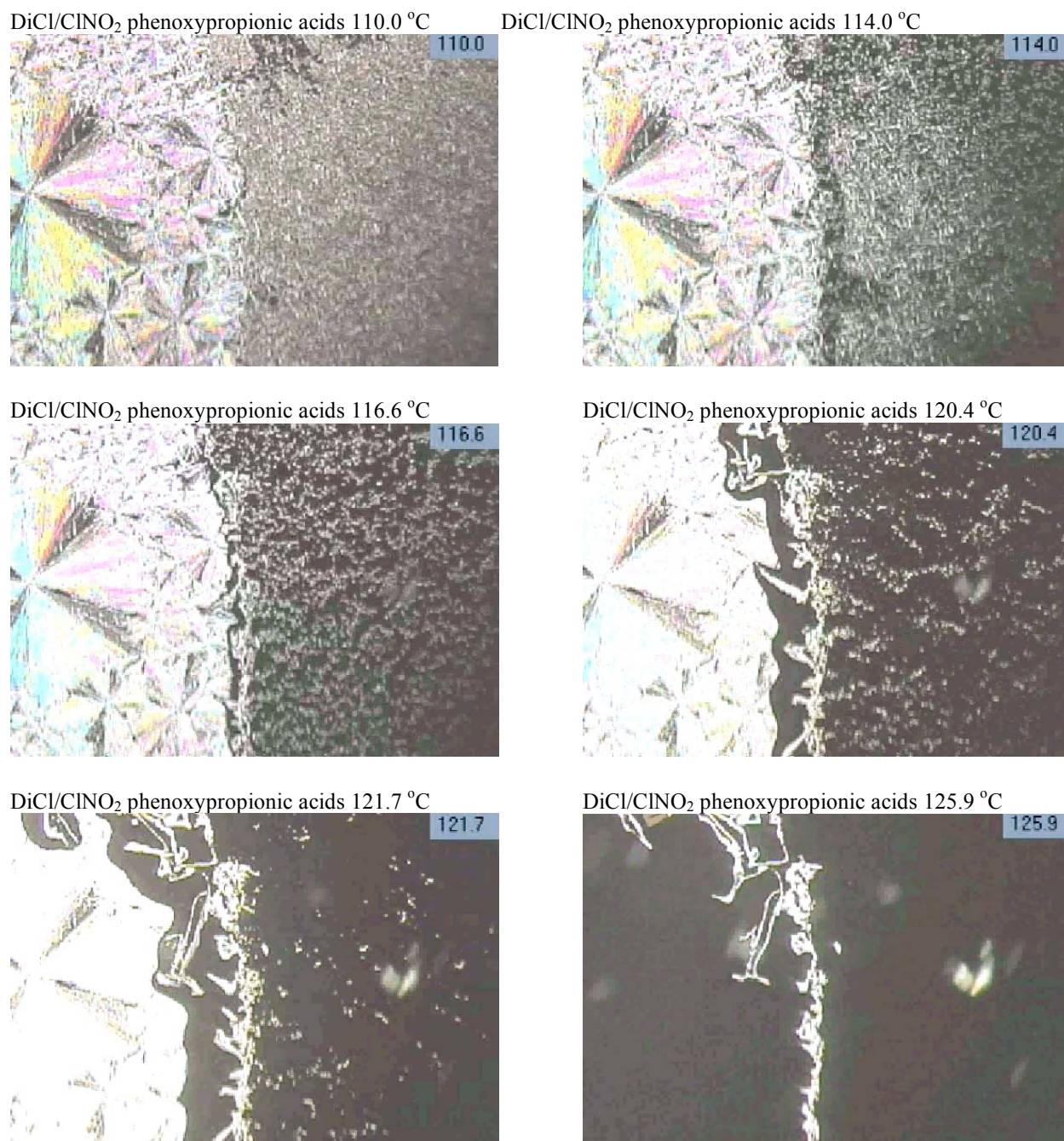

Figure 21. Comparison of the crystal structures of the racemates of the two substituted phenoxypropionic acids shown in **Figure 18**.
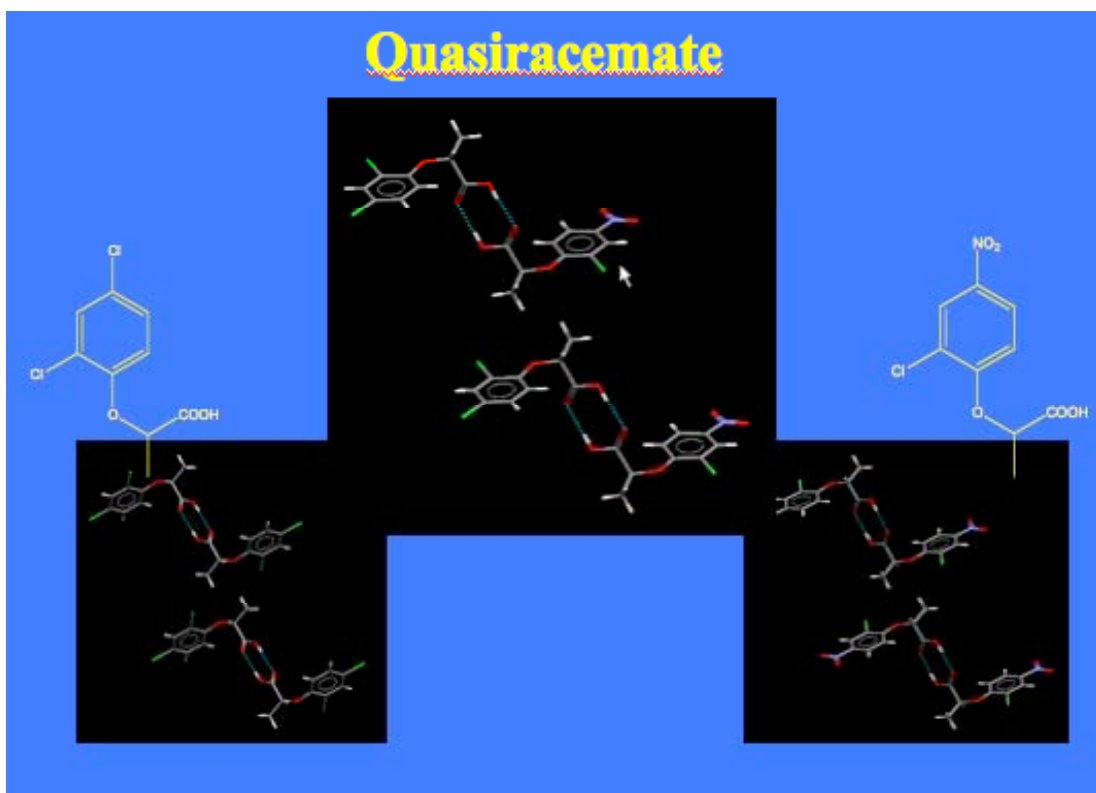
Figure 22. Comparison of the crystal structure of the quasiracemate of the two substituted phenoxypropionic acids shown in Figure 18 with those of the two pure racemates (bottom left, bottom right).

Raymond E. Davis, Keith A. Lorimer, Matthew A. Wilkowski, Joseph H. Rivers, Kraig A. Wheeler and Jeffrey Bowers

DiCl/ClNO$_2$ phenoxypropionic acids 110.0 ^{o}C

DiCl/ClNO$_2$ phenoxypropionic acids 114.0 ^{o}C

DiCl/ClNO$_2$ phenoxypropionic acids 116.6 ^{o}C

DiCl/ClNO$_2$ phenoxypropionic acids 120.4 ^{o}C

DiCl/ClNO$_2$ phenoxypropionic acids 121.7 ^{o}C

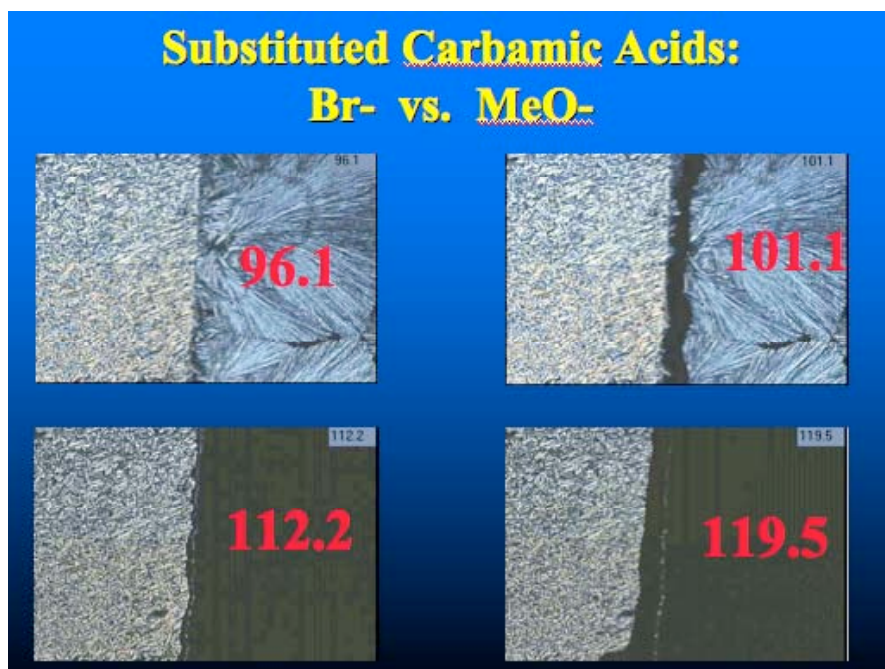DiCl/ClNO$_2$ phenoxypropionic acids 125.9 ^{o}C

Figure 23. Some results of the mixed fusion experiments for the substituted phenoxypropionic acids of Figure 18.

Some substituted carbamate compounds also form quasiracemates, for which the mixed fusion thermomicroscopic results are summarized in **Figures 24** and **25**.

Figure 24. Mixed fusion results for a pair of bromo- and methoxy- substituted carbamic acids.
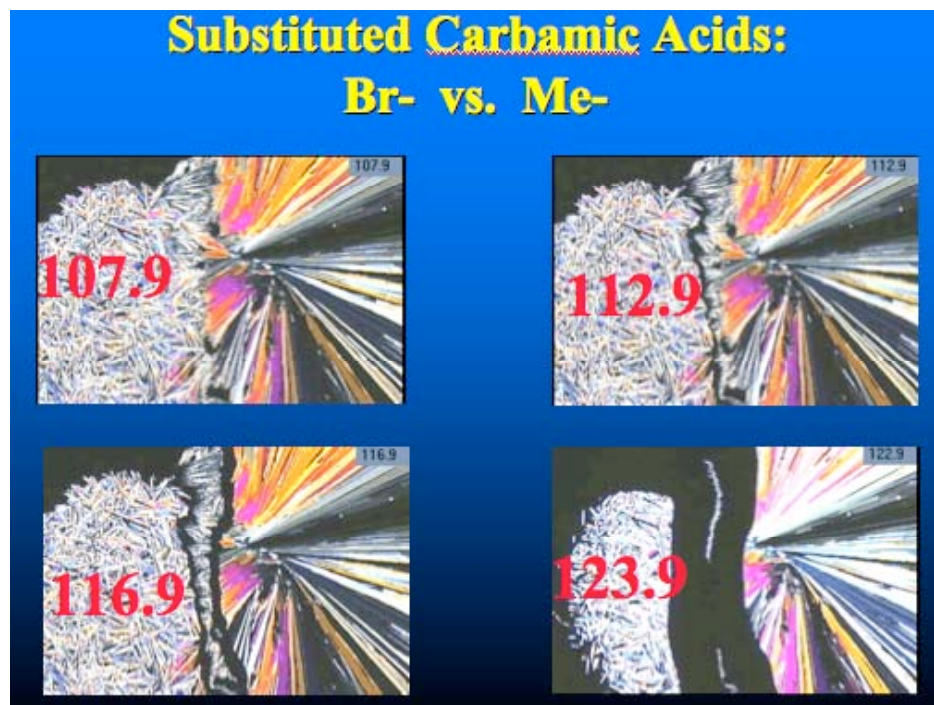
Figure 25. Mixed fusion results for a pair of bromo- and methyl- substituted carbamic acids.

The equations of Schroeder-Van Laar [14] and of Prigogine-Defay [15] have been used with reasonable success to simulate (or predict) the melting point diagrams of enantiomer/racemate systems from measured thermodynamic data of the pure phases. [16] These two equations (omitting usually negligible specific heat terms in the former) are shown in **Figures 26** and **27**, respectively.

$$\ln x = \frac{\Delta H^f_a}{R}\left(\frac{1}{T^f_a} - \frac{1}{T^f}\right)$$

- x = mol fraction of mixture
- ΔH^f_a = enthalpy of fusion of pure enantiomers
- R = molar gas constant
- T^f_a = melting point of pure enantiomers
- T^f = melting point of mixture

Figure 26. Simplified version of the Schroeder-Van Laar equation

$$\ln 4x(1-x) = \frac{\Delta H^f_{ab}}{R}\left(\frac{1}{T^f_{ab}} - \frac{1}{T^f}\right)$$

- x = mol fraction of mixture
- ΔH^f_{ab} = enthalpy of fusion of (quasi)racemate
- R = molar gas constant
- T^f_{ab} = melting point of (quasi)racemate
- T^f = melting point of mixture

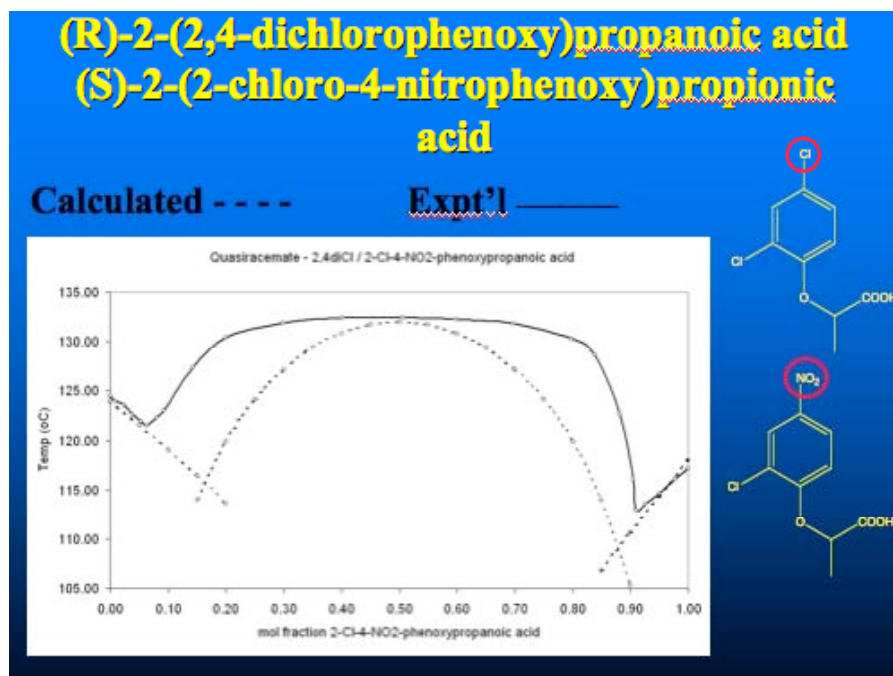**Figure 27.** The Prigogine-Defay equation

We have made some preliminary attempts to apply these equations to quasiracemate phase diagrams, with somewhat mixed results. The approach is summarized in **Figure 28**. For the system of trichloro-substituted propionic acid derivatives shown in **Figure 29**, the results are remarkably good. But for the set of dichloro/chloronitro-substituted propionic acids discussed earlier, the fit of calculated to experimental melting point curves in **Figure 30** is much less satisfactory. We presume that the poor fit in such cases is attributable to a significant lack of ideality of the melt that is in equilibrium with the solid phases.
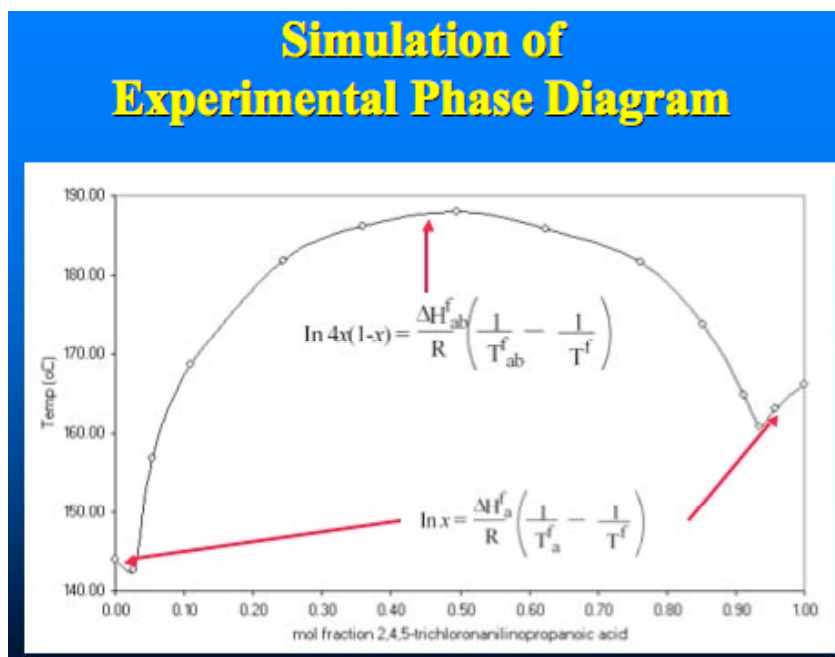
Figure 28. Application of the equations of Schroeder-Van Laar and of Prigogine-Defay to the simulation of melting point phase diagrams for quasiracemic systems.
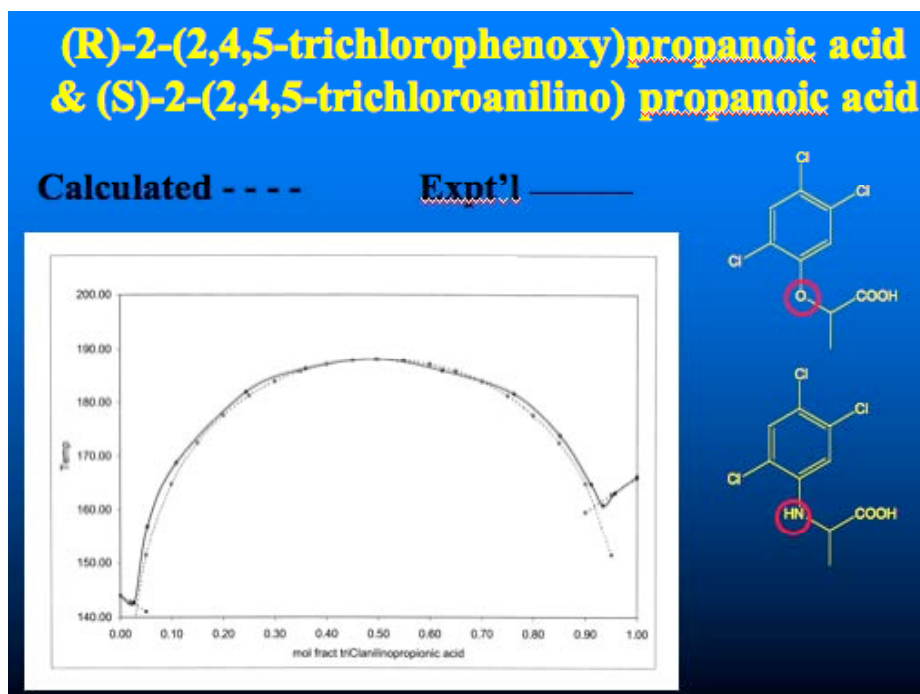
Figure 29. Comparison of melting point curves as calculated with the Schroeder-Van Laar and Prigogine-Defay equations with experimental curves for some trisubstituted propionic acid derivatives.

Raymond E. Davis, Keith A. Lorimer, Matthew A. Wilkowski, Joseph H. Rivers, Kraig A. Wheeler and Jeffrey Bowers

Figure 30. Comparison of melting point curves as calculated with the Schroeder-Van Laar and Prigogine-Defay equations with experimental curves for the quasiracemic system of **Figures 18-23**.

5. CONCLUSION

We have found the thermomicroscopic observation and recording of mixed fusion behavior to be quite convenient and useful in screening binary mixtures for possible cocrystal formation, and are currently extending our studies to include other types of systems.

6. ACKNOWLEDGEMENTS

7. REFERENCES

[1]   McCrone, W.C. *American Laboratory*, June (1996) 12-21.

[2]   Vitez, I.M. et al. *Thermochimica Acta*, 324 (1998) 187-196.

[3]   Wendlandt, W.W. *Thermal Analysis 3rd ed*, Wiley, NY 1986. 584-590.

[4]   Kofler, L., and Kofler, A. *Thermal Micromethods for the Study of Organic Compounds and Their Mixtures*, Wagner, Innsbruck (1952), translated by McCrone, W. C., McCrone Research Institute, Chicago (1980).

[5]   McCrone, W. C. *Fusion Methods in Chemical Microscopy*, Interscience Publishers, New York, (1957)

[6]   Lehmann, O. *Molecularphysik*, Engelmann, Leipzig (1888); see pp. 90-93 of ref 4.

[7]   Rai, U.S., *Thermichim. Acta*, (1989) 219.

[8]   Dhillon, M.S., *Z. Naturforsch.*, 32A (1977) 98.

[9]   Rai, U.S. and Rai, R.N., *Mol. Cryst. Liq.Cryst. Sci. Technol., Sect. C*, 9 (1998), 235.

[10]   Pickering, M. and Small, R., *Acta Crystallogr. B*, B38 (1982), 3161.

[11]   Some leading references are: (a) Davis, R. E., Whitesell, J. K., Wong, M.-S. and Chang, N.-L, in *The Crystal as a Supramolecular Entity*, G. R. Desiraju, Ed., John Wiley & Sons (1996), Chapter 3; (b) Davis,

R.E., Whitesell,, J.K., and Wheeler, K.A. in *Implications of Molecular and Materials Structure for New Technologies*, J.A.K. Howard et al, Ed., Kluwer Academic Publishers (1999), 263; (c) Fomulu, S., Hendi, M.S., Davis, R.E., Lynch, V.M., and Wheeler, K.A., *Cryst. Eng.*, 4 (2001) 11; (d) Fomulu, S., Hendi, M.S., Davis, R.E., and Wheeler, K.A., *Cryst. Growth Des.*, 2 (2002), 637; (e) Fomulu, S., Hendi, M.S., Davis, R.E., and Wheeler, K.A., *Cryst. Growth Des.*, 2 (2002) 645; (f) Hendi, M.S., Hooter, P., Davis, R.E., Lynch, V.M., and Wheeler, K.A., *Cryst. Growth Des.*, 4 (2004) 95.

[12] Fredga, A. *Ark Kemi*, 11 (1956), 23; Fredga, A. *Bull. Soc. Chim. Fr.*, 1 (1973), 173; and references therein.

[13] Reference 11(c).

[14] Schroeder, I. *Z. Phys. Chem.*, 11 (1893), 449; Van Laar, J.J., *Arch. Neerl. II*, 8 (1903), 264; LeChatelier, H., *C. R. Acad. Sci.,* 118 (1894), 638.

[15] Prigogine, I. and Defay, R., *Thermodynamique Chimique*, Desoer, Liege, Belgium (1950); English translation *Chemical Thermidynamics*, 4th edition, Longmans, London (1967).

[16] Jacques, J., Collet, A., and Wilen, S.H., *Enantiomers, Racemates and Resolutions*, Wiley-Interscience, New York (1981), Sections 2.2.3 and 2.3.2 (a,b).

LUMINESCENCE IMAGING OF GROWTH HILLOCKS IN POTASSIUM HYDROGEN PHTHALATE

T. Bullard, M. Kurimoto, S. Avagyan, S. H. Jang, and B. Kahr
Dept. of Chemistry, University of Washington, Box 351700, Seattle, WA 98195-1700, USA
kahr@chem.washington.edu

1. ABSTRACT

We present a method of labeling polygonal growth hillocks in crystals based on the luminescence of fluorophores that have become oriented and overgrown in selected vicinal slopes. Potassium hydrogen phthalate doped with triarylmethane dyes in the fast slopes of the (010) hillocks are well suited to this illustration. Confocal laser scanning microscopy is used to map the spatiotemporal distribution of screw dislocations throughout the crystal, and fractal analysis is used to characterize the distribution. This technique provides a relatively easy and efficient way to study the evolution of growth-active hillocks within as-grown crystals.

2. TRADITIONAL METHODS FOR IMAGING CRYSTAL GROWTH DEFECTS

Crystal growth from solution at low supersaturation often requires screw dislocations [1], displacements of adjacent crystal layers characterized by a Burgers vector with a component perpendicular to the crystal face. A step created in this way winds itself in a spiral around the dislocation core, sending out successive steps. This results in topographical features known as hillocks, shallow hills with persistent step edges. Real crystals often grow through the emergence, competition, and poisoning of many hillocks. The description of a crystal growth mechanism must incorporate this dynamic, which in turn requires the localization of screw dislocations in space and time.

A number of microscopies have been used to image screw dislocations and growth hillocks in crystals. Reflected light differential interference contrast (DIC) microscopy is one of the most common techniques for detecting hillocks on highly reflective surfaces [2]. Scanning tunneling microscopy (STM) [3] and atomic force microscopy (AFM) [4] have been used to image hillocks and other surface defects at high resolution, but they are restricted in their field of view ($\leq 100 \times 100 \ \mu m^2$). Real-time phase-shifting interferometry can reveal surface topography within a larger field ($2 \times 2 \ mm^2$), but with poorer resolution [5]. These techniques are limited to defects present on the surface during the analysis. X-ray topography [6] shows departures from the perfect crystal structure in the crystal *volume*, but all defects are projected onto a common plane. This method is good for recording long-range distortion and/or strain fields associated with macroscopic crystal deformation, however it does not give dynamic information and it often requires highly collimated synchrotron radiation in crystals of the highest quality [7]. Transmission electron microscopy (TEM) has similar limitations and sample preparation can be laborious [8]. Cathodal luminescence (CL), visible light emitted from a sample during electron bombardment, has been used by Reeder et al. to qualitatively image hillocks in minerals with transition metal inclusions that have undergone chemical zoning on the vicinal faces of growth hillocks [9]. It requires material properties and guest ions such that incident electrons can excite an electron into the conduction band, resulting in a hole. Light is produced upon recombination of the hole with a free electron. CL is restricted to surface layers and produces significant amounts of heat.

3. DYEING HILLOCKS

3.1 Dyeing Crystals
We have made a systematic study of the process of dyeing crystals [10], and have shown that simple molecular and ionic crystals including sulfates, phosphates, and carboxylates can orient and overgrow a

wide variety of colored or luminescent molecules during growth from solution. These dyed crystals, typically containing about 1 dye molecule per 10^4 - 10^6 host molecules, display both intersectoral and intrasectoral chemical zoning. *Inter*sectoral zoning occurs when impurities express different affinities for symmetry distinct growth sectors. For example, KH_2PO_4 shows a strong tendency to incorporate anionic dyes only on the {101} faces during growth [11]. *Intra*sectoral zoning may result from the selective interactions between the impurities and the distinct vicinal hillock slopes. This type of chemical zoning was additionally observed on the {101} surfaces of KH_2PO_4 by Zaitseva and co-workers [12], using the anionic dyes, amaranth and Chicago sky blue, that we had previously shown to have an exclusive affinity for these faces [11b]. The observation of intrasectoral zoning required the introduction of the dye during late growth, thereby coloring only a thin surface layer, so that the patterns of color were not confounded by the superposition of many colored hillocks throughout the growth sector. Amaranth was found to recognize two out of the three vicinal slopes, while Chicago sky blue preferred the remaining one.
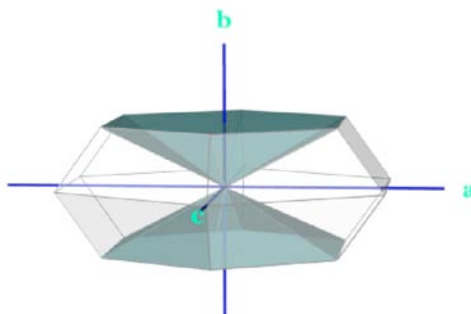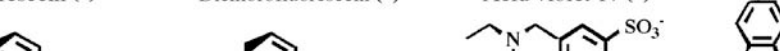

Figure 1. Representation of KAP habit with {010} growth sectors colored in green.

Luminescence labeling of hillocks with dyes was first seen in K_2SO_4 containing *o*-aminobenzenesulfonate [13]. This mixed crystal showed striking blue bands associated with the {021} faces when illuminated with ultraviolet light, due to recognition by the luminophore of the slowly advancing steps growing toward (001) but not the faster steps growing toward (010). Intrasectoral zoning was also observed in α-lactose monohydrate crystals grown in the presence of green fluorescent protein (GFP) [14]. The (010) sector of α-lactose monohydrate grows unidirectionally toward +*b* through a spiral dislocation mechanism, resulting in polygonal hillocks that partition the face into four vicinal regions that are pair-wise related by 2-fold symmetry [15]. GFP only recognizes the lateral slopes with the greatest step advancement velocity. Adenosine monophosphate and adenosine triphosphate were also found to recognize the slopes of KH_2PO_4 eschewed by amaranth [16].
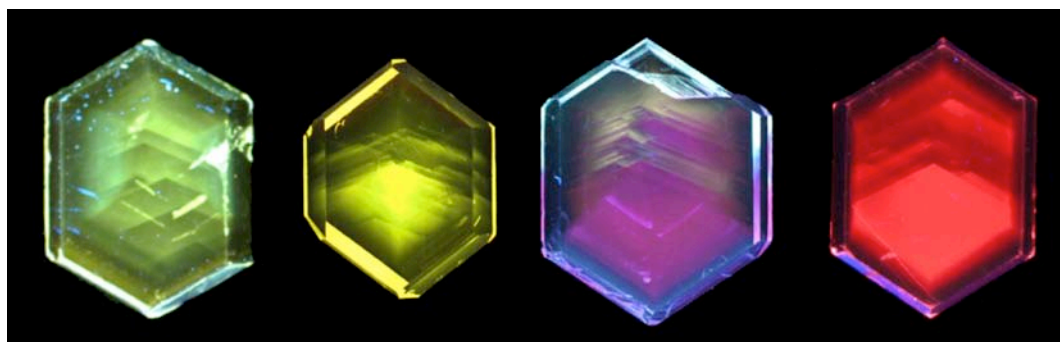
3.2 Dyeing Potassium Hydrogen Phthalate
One of the most remarkable crystals in its ability to orient and overgrow dye molecules is potassium hydrogen phthalate [17] (conventionally abbreviated KAP for <u>p</u>otassium <u>a</u>cid <u>p</u>hthalate, $C_6H_4 \cdot COOH \cdot COO^-$ K^+, space group $Pca2_1$) [18]. KAP is easily grown from aqueous solution as large {010} plates with well-defined growth hillocks and perfect (010) cleavage planes. **Figure 1** shows an idealized KAP crystal with the {010} growth sectors in green. Because the *c* direction is polar, the steps that propagate in the +*c* and −*c* directions are different in structure **(Figure 2a)** [19]. Differential recognition of additives for these steps leads to intrasectoral zoning on the *b*-face **(Figure 2b)**. We have observed intrasectoral zoning from over 25 different dyes in KAP, examples of which are shown in **Figure 3**. Luminescent labels that bind, say, to the "fast" steps **(Figure 3b-d)** that are widely spaced in preference to the "slow" steps that are closely spaced **(Figure 3a)** reveal themselves in patterns of light bounded by the perimeters of the fast slopes; the vertices of the colored chevrons mark the core of the screw dislocations. The correspondence between hillocks evidenced by DIC and by fluorescence microscopy is seen in **Figure 4**. **Figures 4a** and **b** show the DIC and fluorescence micrographs, respectively, of the triarylmethane dye acid violet 17 (**4**), within the fast slope of the KAP hillocks. In comparison, **Figures 4c** and **d** show KAP dyed with rhodamine labeled ribonuclease within the slow slope. KAP, with its largest expressed face growing through a screw dislocation that can be identified by intrasectoral zoning of luminophores, is an excellent model system for the optical investigation of hillock dynamics.

Figure 2. KAP Hillocks. (a) KAP crystal habit, viewed down *b*-axis, with (010) growth hillock and absolute indices. The orientation of the fast (-*c* direction) and slow (+*c* direction) moving slopes of a growth hillock is shown on (010) face. (b) Crystal of KAP with light green SF yellowish within the fast slopes of the (010) hillocks. Crystal size is 2 × 2.5 × 0.4 cm. (c) Triarylmethane dye, light green SF yellowish (LGSFY) [Colour Index #42095].

Figure 3. Intrasectoral zoning in the (010) growth hillocks of KAP. (a) Fluorescein [Colour Index #45350] recognizes the "slow" slope. (b) 2',7'-dichlorofluorescein, (c) acid violet 17 [Colour Index #42650], and (d) 1,1',3,3,3',3'-hexamethylindodicarbocyanine Iodide (HIDCI) recognize the "fast" slope, a far more common mode of adsorption. Average lateral crystal dimension is 6 mm.
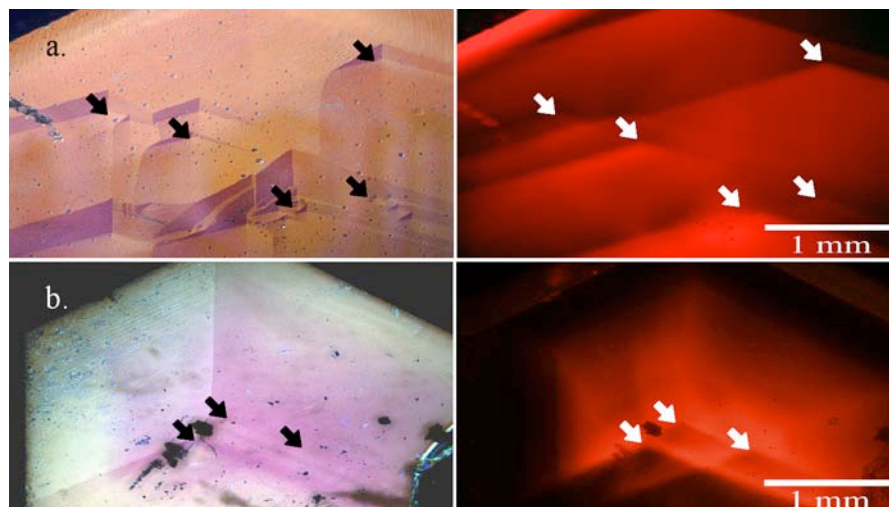
Figure 4. KAP hillocks imaged by reflected light DIC microscopy (left) and fluorescence microscopy (right) displaying (a) acid violet 17 (**4**) in the fast slopes and (b) rhodamine-labeled ribonuclease in the slow slopes. Arrows point to the screw dislocation cores of corresponding hillocks between left and right images.

Triarylmethane dyes tend to show an affinity for the fast slopes of the (010) KAP hillocks. Remarkably, these dyes have surprisingly little effect on the habit of the KAP crystal. However, even in cases where the polyhedral volume of the whole crystal is hardly perturbed, the hillock morphology may be substantially altered. **Figure 5a** displays the results from **4** interacting with the fast steps of the (010) hillock and strongly altering its morphology in the $-c$ direction; the steps are no longer straight. **Figure 5b** shows that **6** interacts with both the fast and the slow steps of the (010) hillocks, giving it a uniform color and altering the hillock morphology such that steps on both slopes are curved. The morphological changes shown in Figures 5a and b are very similar to those seen with other additives, such as tri-valent cations, that have been shown to dramatically alter the growth hillock morphology in KAP [20]. It is by no means obvious that two such closely related compounds would have such distinct effects on the color and hillock morphology of KAP crystals. Interpreting this behavior requires a deeper understanding of the recognition mechanisms.
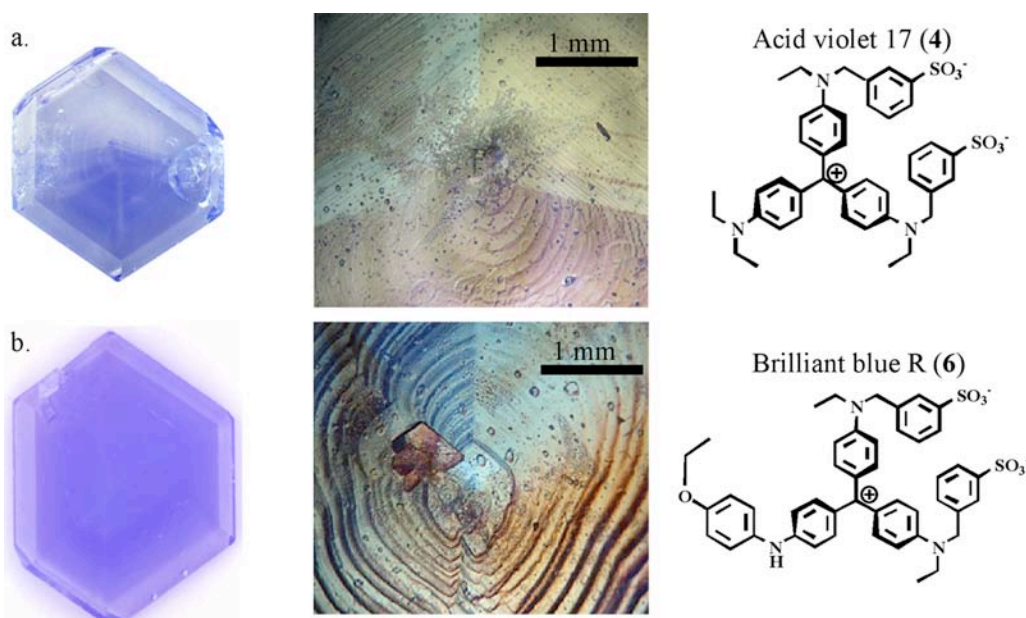

Figure 5. Triarylmethane dyes ($\sim 10^{-5}$ M) in KAP with corresponding DIC micrographs of hillock morphology. (a) Acid violet 17. (b) Brilliant blue R [Colour Index #42660]. Size of crystals is about $6 \times 8 \times 1.5$ mm.

3.3 ...With Light Green SF Yellowish

KAP crystals containing the triarylmethane dye **1** in the fast slopes of the (010) hillocks were selected for further analysis. Crystals were grown from aqueous solution in a 30°C water bath by slow evaporation. At typical dye concentrations (10^{-5} M), **1** has no observable effect on the hillock morphology. There is 1 dye molecule per 130,000 KAP molecules in whole crystals.

The dyed regions of these crystals appear green in white light and emit in the red upon excitation (630 nm). The linear dichroism (LD) is slight but greater anisotropy can be seen in the fast slopes that contain most of the dye **(Figure 6)**. The LD increases slightly, with the average dipole orientation aligning closer to the a-axis, for greater dye concentrations. LD was imaged by the rotating polarizer method in conjunction with a CCD camera [21].
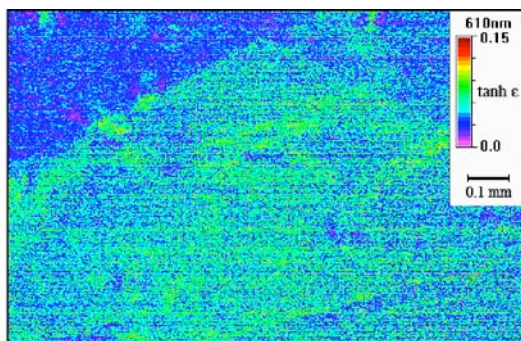

Figure 6. Linear Dichroism at 610 nm of **1** in fast slope of KAP (010) hillock. Image taken with MetriPol [21**Error! Bookmark not defined.**]. The parameter $\varepsilon = (a_x – a_y)/2$, where a_x and a_y are the absorption coefficients for orthogonal orientations.

4. CONFOCAL LASER SCANNING MICROSCOPY

In real crystals, screw dislocations can begin and end at any point, so they do not always make it to the surface to be observable in reflected light [22]. However, the fluorescent dyes are incorporated within the crystal throughout the growth process. Thus, even after subsequent overgrowth, the luminophores create a record of hillock evolution in patterns of light that can be revealed by successive cleavage or with a confocal luminescence microscope. Confocal laser scanning microscopy (CLSM) produces "optical sections" of the sample, with illumination and detection restricted to a single diffraction-limited point in the sample. The field-of-view and resolution are adjustable based on the objective and pinhole size used, with the capacity to achieve single molecule resolution at low dye concentrations. Likewise, the scan speed versus signal-to-noise ratio may be adjusted for the specific application (*in situ* or *ex situ*). Due to its ability to eliminate "out-of-focus" light, confocal microscopy can be used to image a "fossil record" of dyed hillocks throughout the crystal, even those that are no longer growth-active on the surface. Furthermore, by selecting an appropriate scanning step height for the *z*-series, it is possible to create a three-dimensional reconstruction of the dislocation patterns.

The KAP/**1** crystals were imaged using a Leica TCS SP/NT confocal microscope with 568 nm krypton ion laser excitation source [23]. By focusing from the crystal bottom through to the top, the number and position of the hillock dye patterns that formed throughout the (010) sector were recorded **(Figure 7)**. Each image represents a 20 μm thick optical section, which is thick enough such that the *z*-coordinate can roughly be taken as time of growth. The spatiotemporal distribution of all hillocks that occur throughout a crystal as it grows are then mapped out using ImageJ[TM] software by recording their positions in each optical section and comparing them to the positions from previous and subsequent sections. In the sample crystal shown in **Figure 7**, 61 growth active hillocks were found, of which 32 propagated through to the surface. The lifetimes of the growth hillocks varied from ~20 μm (seen in only one section) to ~320 μm (lasting through the entire crystal). The average hillock lifetime was ~140 μm. The average density for the whole *b*-face area was 3.2 dislocations/mm^2.
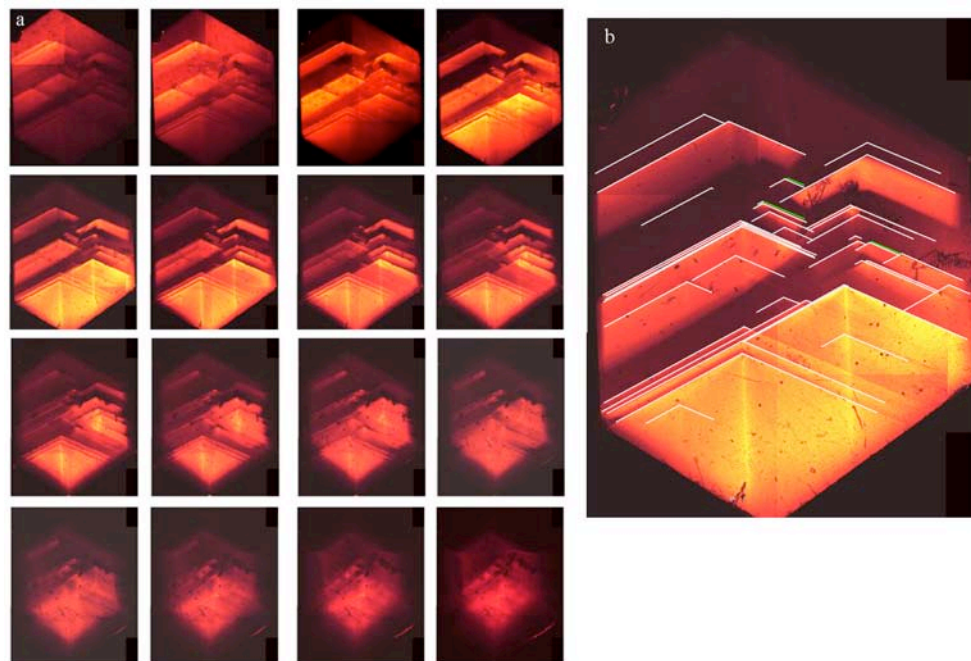
Figure 7. (a) Confocal slices of KAP/**1**. Images are read from the bottom (lower right) to the top of the crystal (upper left). Step size (image thickness) is 20 μm. Luminescence develops on the fast slopes of {010} growth hillocks, with vertices marking the dislocation core. Image size is 4 × 5.5 mm. (b) Slice 4 (top right optical section) in which the screw dislocations are found at the vertices formed by the overlaid white lines bounding the fast slopes of the hillocks.

4.1 Fractal Analysis

Fractal analysis can be used to determine whether the screw dislocation cores throughout the crystal are randomly distributed, fractal-like, or correlated with one another [24, 25]. There are a variety of methods for computing fractal dimensionality. Three of the most common methods include the box dimension or box counting, the information dimension, and the mass dimension. In general form, these methods are based on the power law $n(s) \sim s^d$, where $n(s)$ is a number and s is a size, both of which are specifically defined by the particular method used, and d is the fractal dimension. For example, the simplest algorithm for determining the fractal dimension of a system is to use "box counting", which consists of filling the plane with a grid of boxes of chosen size, s. After counting the number of boxes that enclose parts of the object, $n(s)$, the box size is reduced and the process is repeated. The results are plotted as the log[n(s)] versus log[1/s], and the fractal dimension is given by the slope of the line. An example of a plot from the box counting method is given in **Figure 8**, showing a comparison between the distribution of screw dislocation cores from the optical section featured in **Figure 7b**, on which 40 hillocks were found, and the corresponding distribution of randomly generated points. The box dimension calculated for the screw dislocation distribution is 1.09, while that of the random distribution is 1.32. **Figure 9** shows a plot of the box dimension results for all optical sections displayed in **Figure 7** as a function of height in the crystal *b*-face. As can be seen from this plot, the values for the fractal dimension converge to about 1.1 for the distribution of screw dislocation cores but rise to about 1.3 for the random point distributions, indicating that the dislocation distribution is non-random.
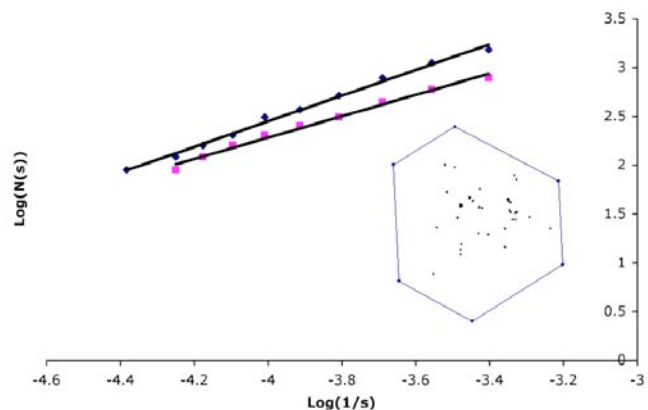
Figure 8. Box counting plot for distribution of screw dislocation cores from the optical slice shown in **Figure 7b**. Squares show data for the hillock pattern shown in the inset, while diamonds show the data that results from generating a random distribution of the same number of points.
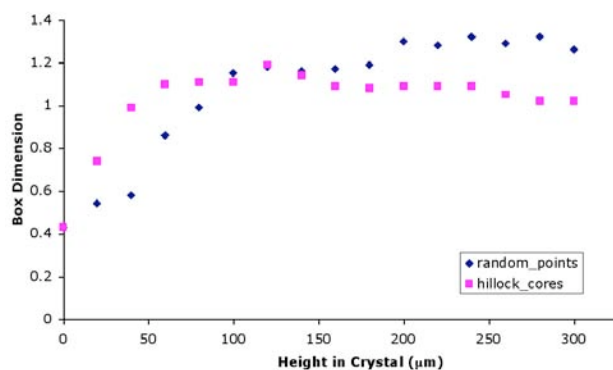

Figure 9. Results of box dimension calculations for all optical sections shown in **Figure 7**. Squares show hillock data, while diamonds show dimensions for an equal number of points randomly distributed.
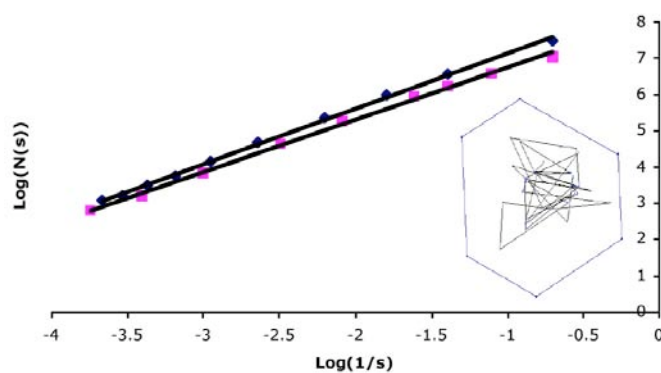
Figure 10. Box counting plot for the hillock growth sequence from the optical section shown in **Figure 7b**. Squares show data for the hillock pattern shown in the inset, while diamonds indicate the results from generating a random sequence of the same number of points.
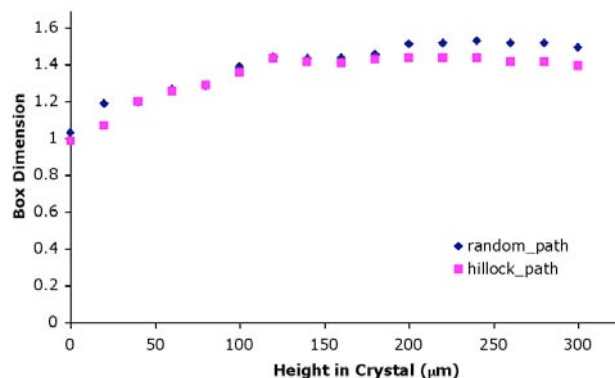
Figure 11. Resulting box dimensions for all optical section sequences. Squares show hillock data, while diamonds show dimensions for the paths resulting from randomly generated points.

This analysis can be taken a step further by looking at the sequence of hillock growth and evolution. New patterns are obtained by connecting the points, representing screw dislocation cores, according to the order in which each hillock appears in the confocal optical sections. These patterns can be compared to those of a random sequence generated within the boundaries of the crystal's *b*-face. **Figure 10** shows the box counting plot for the patterns corresponding to the optical section displayed in **Figure 7b**. The box dimension calculated for this hillock sequence pattern is 1.44, while that of the corresponding random walk is 1.53. When the results for all optical sections are plotted versus the height in the crystal *b*-face **(Figure 11)** it is seen that the fractal dimension for the hillock sequence converges to about 1.4, which is lower than the random walk dimension of 1.5, again indicating a non-random pattern.

Screw dislocation distributions can alternatively be characterized by calculating the 'mass dimension', $N(r)$. With this method, one counts the number of points that fall within the circle of a radius, r, from a point located near the center of the system, normalized by the total number of points in the system [24]. This relation only holds true for a certain range of *r*-values if the system has a finite boundary [25]. Doing this calculation for the optical section shown in **Figure 7b**, shows that the hillock distribution closer to the center of the *b*-face results in a mass dimension of 1.74, however in scanning out further from the center, approaching the boundaries of the *b*-face, the mass dimension drops to 0.26 **(Figure 12)**. This change in mass dimension indicates differing behavior at two length scales, with higher density of points at the small length scale and a smaller density at the large length scale. In other words, the screw dislocation cores tend to cluster, and they also accumulate more towards the center of the *b*-face than at the edges. Analyzing the hillock distribution from all optical sections projected into a single plane produces a similar behavior. The results are quite different, however, for the corresponding pattern of randomly generated points **(Figure 13)**. For the random distribution the mass dimension stays at a fairly constant value of 1.50 for all length scales, and it is less than that of the hillock distribution near the center of the *b*-face, indicating an even distribution with minimal clustering. All together, the fractal analysis shows that the screw dislocation distribution is not only non-random but tends to cluster, indicating a correlation between the positions of neighboring dislocations.
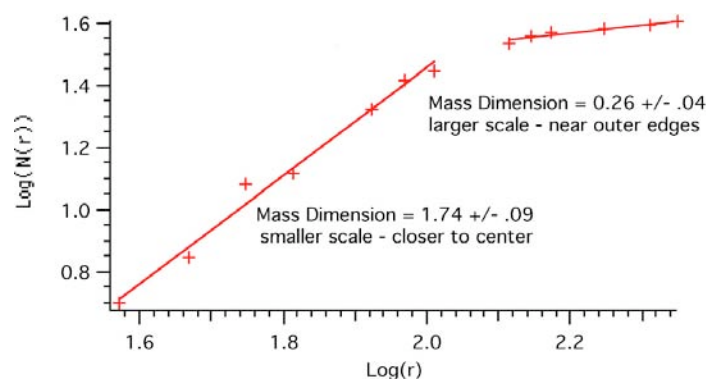
Figure 12. Mass dimension plot for the distribution of screw dislocation cores in the optical section shown in **Figure 7b**. Change in slope indicates different behavior at two length scales, as well as an aversion to the *b*-face edges.
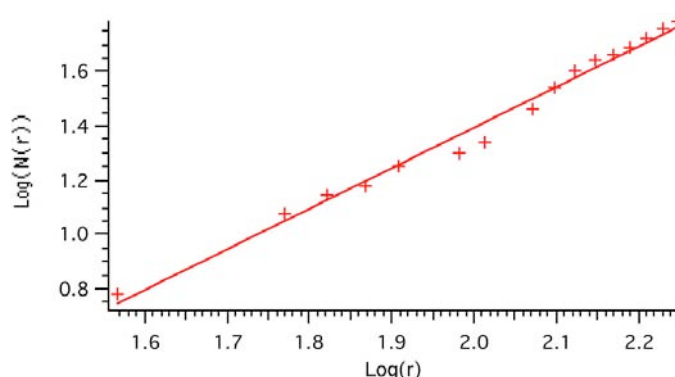
Figure 13. Mass dimension plot for the distribution of random points. Constant slope shows all length scales have the same mass dimension of 1.50.

6. CONCLUSION

Crystals of potassium hydrogen phthalate (KAP) with luminescent dyes intrasectorally zoned in the (010) vicinal hillock slopes provides an excellent model system for the optical investigation of hillock dynamics and crystal growth through the screw dislocation mechanism first proposed by Frank [26]. The family of triarylmethane dyes show an affinity for the fast slopes of the (010) KAP hillocks. Confocal imaging of luminescently labeled hillocks in crystals offers a new and relatively easy method for investigating the distribution and evolution of screw dislocations. Unlike most surface probes, this technique fixes when and where hillocks arise during crystal growth, thus extracting temporal information from as-grown crystals. Yet, CLSM may also be used *in situ* if desired. In contrast to other bulk probes, the confocal images are restricted to specific focal planes, minimizing background from out-of-focus light. Single crystals of KAP dyed with triarylmethane dye, light green SF yellowish (10^{-5} M), in the fast slopes of the (010) hillocks were imaged using a confocal microscope. Fractal analysis of the screw dislocation patterns indicates a non-random distribution and a tendency to cluster, alluding to a possible correlation mechanism between neighboring screw dislocations during crystal growth. CLSM is commonly used in the biological fields to study samples labeled with luminescent probes [27], but to the best of our knowledge, this has not heretofore been used to study growth mechanisms in luminescently labeled crystals.

7. ACKNOWLEDGEMENTS

use of his program WinMorph that was used to prepare **Figure 1**, as well as the W. M. Keck Center for Advanced Studies in Neural Signaling for use of the confocal microscope that was used to prepare **Figure 7**.

8. REFERENCES

[1]   W. K. Burton, N. Cabrera, and F. C. Frank, *R. Soc. London. Philos. Trans. A*, **243** (1951), 299-358.

[2]   M. Pluta, in: *Advanced Light Microscopy*, **2**, 146-196 (Elsevier, New York, 1989).

[3]   W. N. Unertl, in *Scanning Probe Microscopy and Spectroscopy: Theory, Techniques, and Applications*, 113-154, eds. D. Bonnell (Wiley-VCH, New York, 2001).

[4]   G. T. R. Palmore, T. J. Luo, T. L. Martin, M. T. McBride-Wieser, N. T. Voong, T. A. Land, and J. J. De Yoreo, *Transactions ACA*, **33** (1998), 45-57; J. J. De Yoreo, C. A. Orme, and T. A. Land, in: *Advances in Crystal Growth Research*, eds. K. Sato, Y. Furukawa, and K. Nakajima (Elsevier Science B. V., Amsterdam, Neth, 2001).

[5]   (a) N. A. Booth, B. Stanojev, A. A. Chernov, P. G. Vekilov, *Rev. Sci. Instrum.* **73** (2002), 3540; (b) N. A. Booth, A. A. Chernov, P. G. Vekilov, *J. Mater. Res.* **17** (2002), 2059-2065.

[6]   (a) X. Ma, M. Dudley, W. Vetter, and T. Sudarshan, *Jpn. J. Appl. Phys.* **42** (2003), 1077-1079; (b) M. Dudley, *Mat. Res. Soc. Symp. Proc.* **307** (1993), 213-224. (c) H. Klapper, *Mat. Sci. Forum*, **276-277** (1998), 291-306.

[7]   W. M. Vetter, H. Totsuka, M. Dudley, and B. Kahr, *J. Cryst. Growth.* **241** (2002), 498-506.

[8]   L. Reimer, in: *Transmission Electron Microscopy: Physics of Image Formation and Microanalysis*, 344-354, eds. P. W. Hawkes, A. L. Schawlow, A. E. Siegman, K. Shimoda, T. Tamir, H. K. V. Lotsch (Springer-Verlag, New York, 1993).

[9]   (a) J. Paquette and R. J. Reeder, *Geology,* **18** (1990), 1244-1247; (b) J. Paquette and R. J. Reeder, *Geochim. Cosmochim. Acta,* **59** (1994), 735-749; (c) N. G. Hemming, R. J. Reeder, and S. R. Hart, *Geochim. Cosmochim. Acta* **62** (1998), 2915-2922; (d) E. J. Elzinga and R. J. Reeder, *Geochim. Cosmochim. Acta,* **66** (2002), 3943-3954.

[10]   B. Kahr and R. W. Gurney, *Chem. Rev.* **101** (2001), 893-951.

[11]   (a) B. Kahr, S.-H. Jang, J. A. Subramony, M. P. Kelley, and L. Bastin, *Adv. Mater.* **8** (1996), 941-944; (b) J. A. Subramony, S.-H. Jang, and B. Kahr, *Ferroelectrics*, **191** (1997), 292-300.

[12]   N. Zaitseva, L. Carman, I. Smolsky, R. Torres, and M. J. Yan, *J. Cryst. Growth*, **204** (1999), 512-524.

[13]   (a) R. W. Gurney, C. A. Mitchell, S. Ham, L. D. Bastin, and B. Kahr, *J. Phys. Chem. B*, **104** (2000), 878-892; (b) R. W. Gurney, M. Kurimoto, J. A. Subramony, L. D. Bastin, and B. Kahr, in: *Anisotropic Organic Materials: Am. Chem. Soc. Symp. Ser.* eds. R. Glaser and P. Kaszynsky (American Chemical Society, Washington, DC, 2001).

[14]   M. Kurimoto, P. Subramony, R. W. Gurney, S. Lovell, J. Chmielewski, and B. Kahr, *J. Am. Chem. Soc.* **121** (1999), 6952-6953.

[15]   (a) R. A. Visser, *Neth. Milk Diary J.* **36** (1982), 167-193; (b) T. D. Dincer, G. M. Parkinson, A. L. Rohl, and M. I. Ogden, in: *Crystal. Growth Org. Mater. 4th International Workshop*, **4**, 25-32, eds. J. Ulrich (Shaker Verlag, Aachen, Germany, 1997); (c) T. D. Dincer, G. M. Parkinson, A. L. Rohl, and M. I. Ogden, *J. Cryst. Growth*, **205** (1999), 368-374.

[16]   M. Kurimoto, L. D. Bastin, D. Fredrickson, P. N. Gustafson, S.-H. Jang, W. Kaminsky, S. Lovell, C. A. Mitchell, J. Chmielewski, and B. Kahr, *Mat. Res. Soc. Symp.* **620** (2000), M9.8.1-M9.8.10.

[17]   J. B. Benedict, P. M. Wallace, P. J. Reid, S.-H. Jang, and B. Kahr, *Adv. Mater.* **15** (2003), 1068-1070.

[18]   (a) Y. Okaya, *Acta Cryst.* **19** (1965), 879; (b) L. A. M. J. Jetten, B. van der Hoek, and W. J. P. van Enckevort, *J. Cryst. Growth*, **62** (1983), 603.

[19]   W. J. P. van Enckevort and L. A. M. J. Jetten, *J. Cryst. Growth*, **60** (1982), 275-285.

[20]   (a) M. H. J. Hottenhuis and C. B. Lucasius, *J. Cryst. Growth,* **78** (1986), 379–388; (b) M. H. J. Hottenhuis and A. Oudenampsen, *J. Cryst. Growth*, **92** (1988), 513–529.

[21]   (a) A. M. Glazer, J. G. Lewis, and W. Kaminsky, *Proc. R. Soc. Lond. A*, **452** (1996), 2751-2765; (b) M. A. Geday, W. Kaminsky, J. G. Lewis, and M Glazer, *J. Microscopy*, **198** (2000), 1-9.

[22]   (a) V. I. Bredikhin, G. L. Galushkina, A. A. Kulagin, S. P. Kuznetsov, and O. A. Malshakova, *J. Cryst. Growth*, **259** (2003), 309-320; (b) V. I. Bredikhin, G. L. Galushkina, and S. P. Kuznetsov, *J. Cryst. Growth*, **219** (2000), 83-90; (c) O. Contreras, F. A. Ponce, J. Christen, A. Dadgar, and A. Krost, *App. Phys. Let.* **81** (2002), 4712-4714.

[23]   Leica TCS SP/NT on a DMIRBE incident-light inverted microscope through a 5x objective, pinhole width of 1 Airy unit, and with 568 nm excitation light from a 25mW krypton ion laser at the University of Washington W. M. KECK Center for Advanced Studies in Neural Signaling. http://depts.washington.edu/keck/

[24]   B. B. Mandelbrot, *The Fractal Geometry of Nature*, (W. H. Freeman and Company, New York, 1977).

[25]   (a) B. H. Kaye, *A Random Walk Through Fractal Dimensions*, (VCH Publishers, New York, 1989). (b) D. Avnir, O. Malcai, D. A. Lidar, and O. Biham, *Phys. Rev. E*, 56 (1997), 2817-2828.

[26]   F. C. Frank, *Disc. Faraday Soc.*, **5** (1949), 48, 67.

[27]   See for example, American Physiological Society, *Methods in cellular imaging*, eds. A. Periasamy, (Oxford University Press, Oxford, 2001).

IN SITU AFM STUDIES ON THE GROWTH OF CRYSTALS OF BIS(IMIDAZOLIUM 2,6-DICARBOXYLATEPYRIDINE) CU(II) DIHYDRATE

Tzy-Jiun Mark Luo[1], John C. MacDonald[2], and G. Tayhas R. Palmore[1,3]
[1]Division of Engineering, Brown Univ., Providence, RI
[2]Dept. of Chemistry and Biochemistry, WPI, Worcester, MA
[3]Division of Biology and Medicine, Brown Univ., Providence, RI

1. ABSTRACT

The kinetics of growth at the (100) face and the (0-11) of crystals of bis(imidazolium 2,6-dicarboxylatepyridine)Cu(II) dihydrate (**1-Cu**) were compared using atomic force microscopy. The rate at which the (011) step riser advanced across the (0-11) face was found to be consistently faster than that at the (100) face. This difference in kinetics of growth is attributed to the different chemistry exposed at these two surfaces and the manner in which these surfaces assemble.

2. INTRODUCTION

Molecular crystals are pursued widely for use in optical, electronic, and magnetic applications.[1-5] Such applications require careful control over the interface between a crystal and other surfaces.[6-11] The bulk properties of molecular crystals, intrinsically inherited from functional groups, rely on the packing arrangement of individual molecules. The crystal facets that develop during growth determine the surface properties of molecular crystals by reflecting the orientation of molecules exposed at a specific surface.

Atomic force microscopy (AFM) has been an important tool for investigating the rate at which a crystal facet forms and the mechanisms of assembly involved.[12-14] Several crystalline systems have been studied including inorganic solids such as calcite[15] and potassium dihydrogen phosphate (KDP),[16,17] proteins such as lysozyme,[18] canavalin,[19,20] catalase,[21] and insulin,[22] and molecular solids such as diketopiperizines.[13,23] An important finding of these latter studies was that all mechanisms of growth were similar to those described for inorganic crystals and independent of the size or complexity of the growth unit. In addition, studies of crystal surfaces that are anisotropic have provided information about the kinetics of growth and contributing energetic factors.[24] Such information is important for controlling the morphology of crystals as well as controlling the growth of epitaxial layers via solvent-mediated self-assembly.[25]

Despite years of investigation, significant questions remain concerning fundamental aspects of crystal growth from solution. Of particular interest is the pathway by which growth units leave a supersaturated solution to become incorporated in the crystalline solid. This pathway is described as either direct incorporation or surface diffusion of growth units.[26-29] The direct incorporation model is considered appropriate for crystals grown from solution because of the large supply of ions to its surface. Furthermore, the energy of dissolution is small relative to that of evaporation for vapor-phase growth and the diffusion coefficient of growth units in solution is large relative the diffusion coefficient of growth units across a surface. Nevertheless, the surface diffusion model has been demonstrated in crystals grown from solution.[20]

The purpose of this study is to examine the effect of surface chemistry and molecular packing on the kinetics of assembly of a crystal grown from solution regardless of whether growth occurs by direct incorporation or surface diffusion. Crystals of bis(imidazolium 2,6-dicarboxylatepyridine) Cu(II) dihydrate (**1-Cu**) were used for this study.[30,31] These crystals belong to a unique family of crystals in which the crystal structure is nearly invariant regardless of metal ion present (i.e., M (II) = Cu, Ni, Co, Mn, or Zn), making it an ideal crystal system for studying epitaxial growth via solvent mediated self assembly.[25] The rates at which the (011) step riser advanced across the (100) face (a surface consisting of either a pure layer

of imidazolium cations or Cu (II) complex anions) and the (0-11) faces (surfaces consisting of both imidazolium cations and Cu (II) complex anions) of (**1-Cu**) were measured using atomic force microscopy (AFM).[18, 32] The kinetics of growth at the (0-11) surface was found to be faster than that at the (100) face and becomes increasingly so with increase in supersaturation. This difference in kinetics of growth can be attributed to the different moieties exposed at these two surfaces and the manner in which these surfaces assemble.

3. RESULTS AND DISCUSSION

3.1 Preparation of Crystals of Bis(imidazolium 2,6-dicarboxylatepyridine) Cu(II) Dihydrate (1-Cu)

The preparation of **1-Cu** is shown in **Figure 1**. Typically, an aqueous dimethyl sulfoxide solution containing a 1:4 mixture of metal (II) ion and 2,6-dicarboxypyridine (**DCP**) is mixed with an aqueous dimethyl sulfoxide solution containing imidazole (**Im**) at a concentration equal to that of **DCP**. After leaving the mixture undisturbed for several hours at room temperature, seed crystals in the shape of flat rhombohedrons can be harvested (**Figure 2**, upper inset). Large single crystals subsequently are grown from a seed crystal using a microcrystallizer, which consists of a water-jacketed flask (100 ml) equipped with a rotary stirrer and temperature-controlled water circulator (**Figure 2**). The general procedure for growing crystals in the microcrystallizer is as follows. First, 40 ml of a stock growth solution (e.g., 1:4:4 solution of Cu(II):**Im**:**DCP**) is added to the water-jacketed flask and equilibrated to a desired temperature by the water circulator. Two seed crystals are mounted on top of the crystal stage using silicone grease (**Figure 2**, lower inset). The crystal stage is attached to the end of a stirring rod connected to a motor that reverses the direction of stirring at a controlled rate and duration. Finally, the mounted crystal is placed in the middle of the water-jacketed flask to initiate new growth. Using the microcrystallizer, single crystals with millimeter to centimeter dimensions can be grown for subsequent *in situ* AFM measurements.
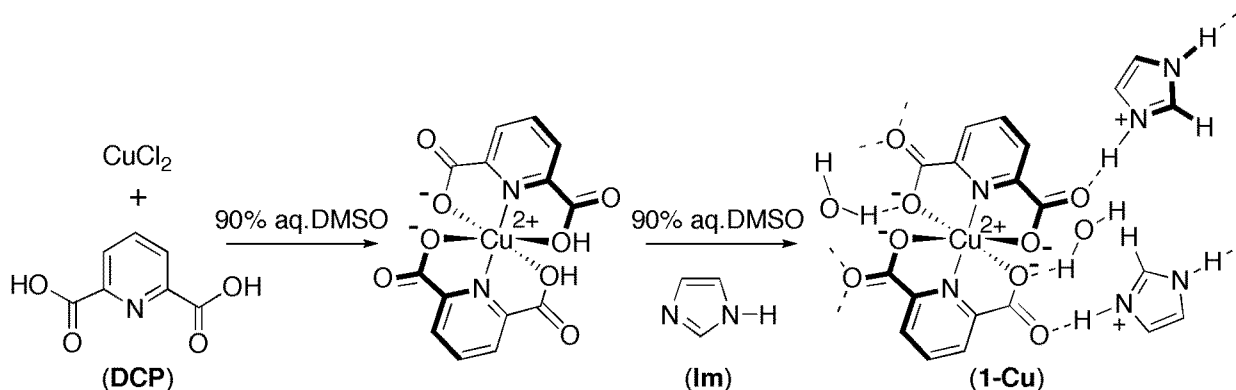
Figure 1. Preparation of bis(imidazolium 2,6-dicarboxypyridine) Cu(II) dihydrate (**1-Cu**) from one equivalent of CuCl₂ and two equivalents each of 2,6-dicarboxypyridine (**DCP**) and imidazole (**Im**).
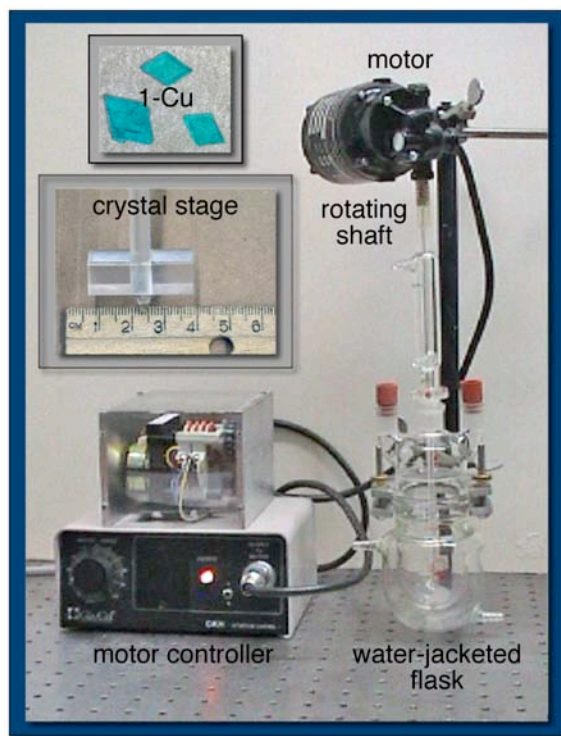
Figure 2. Microcrystallizer used to grow millimeter-sized crystals of **1-Cu**. The upper inset shows three rhombohedral-shaped crystals of **1-Cu**, which were grown from a 1:4:4 solution of Cu(II):**Im**:**DCP**. The lower inset shows the crystal stage upon which seed crystals are mounted on either side of the shaft. The direction of rotation and rate of rotation of the stage is set by the motor controller.

3.2 Changing the Size of (011) and (0-11) Facets Relative to the Size of the (100) Facet in Crystals of 1-Cu

Crystals of **1-Cu** are rhombohedral in shape when grown from a 1:4:4 solution of Cu(II):**Im**:**DCP**. The largest surface or most dominant facet in these crystals is the (100) facet. The sides of the rhombohedral-shaped crystals are defined by {011} and {0-11}, which are considerably smaller in size than the (100) facet. To compare the kinetics of step advancement across the (0-11) face to that of the (100) face using *in situ* AFM, it is convenient to work with a crystal with similar sized (100) and (0-11) facets. Because the crystal stage in the microcrystallizer alternates between clockwise and counterclockwise directions of rotation, diffusion of growth units perpendicular to the axis of rotation is enhanced relative to any other direction. Thus, by mounting seed crystals of **1-Cu** with either their (011) or (0-11) faces in contact with the surface of the crystal stage, the size of the (100) face relative to that of the (011) and (0-11) facets can be decreased.

To illustrate, shown in **Figure 3** is a comparison of the aspect ratio of two crystals grown from seed crystals of **1-Cu** mounted with either the (-100) face **(Figure 3a)** or the (0-11) face **(Figure 3b)** in contact with the surface of the crystal stage shown in the lower inset of **Figure 2**. When the seed crystal is mounted with the (-100) face in contact with the crystal stage, diffusion of growth units (green arrows in **Figure 3**) to (011) and (0-11) faces is enhanced by the rotation of the crystal stage. Thus, the (100) face remains the largest (slowest growing) facet in this crystal and the morphology of the crystal is a thin rhombohedron. In contrast, when the seed crystal is mounted with either the (011) face or (0-11) face in contact with the crystal stage, the enhanced diffusion of growth units to the (100) and (-100) faces generated by the rotation of the crystal stage results in a crystal with (011) and (0-11) facets similar in size to the (100) facet. The morphology of the crystal is a thick rhombohedron.
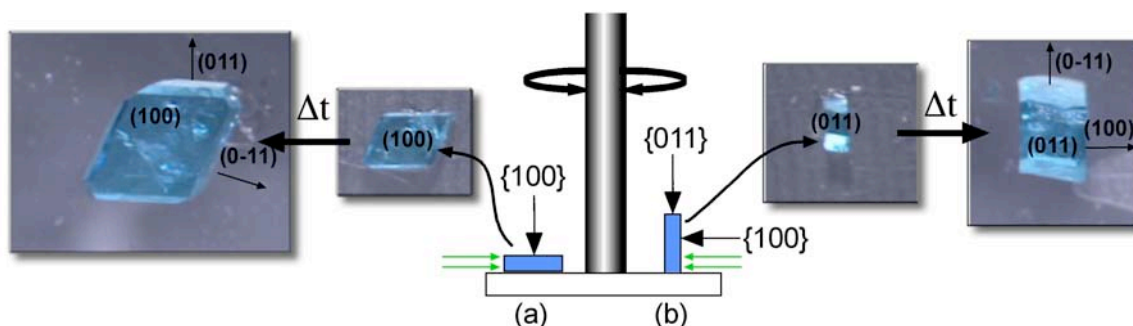
Figure 3. Illustration of seed crystals of **1-Cu** mounted with the (a) (-100) face or (b) (0-11) face in contact with the crystal stage of the microcrystallizer. The relative size of the (100) face to the (011) face of these crystals can be changed according to which surface of the crystal is in contact with the crystal stage. The green arrows indicate the direction in which the diffusion of growth units is enhanced by the rotation of the crystal stage.

### 3.3 Chemical Composition and Molecular Packing at the Surfaces of 1-Cu Studied By *in situ* AFM.

As stated previously, the dominant facet in crystals of **1-Cu** is the (100) face when grown from a 1:4:4 solution of Cu(II):**Im**:**DCP**.[25] The molecular components exposed at the (100) surface are shown in **Figure 4** and consists of either a pure layer of bis(2,6-dicarboxypyridine) Cu (II) anions **(Figure 4a)** or a pure layer of imidazolium cations **(Figure 4b)**.[30,31] In contrast, the molecular components exposed at the (0-11) and (011) surfaces shown in **Figure 4c** and **4d**, respectively, consist of a mixture of both anions and cations with similar patterns of packing. Thus, based solely on the chemical composition and molecular packing at these surfaces, the kinetics of growth at a surface that consists of pure layers of anions or cations (i.e., (100) face) is expected to be different from that at a surface that consists of a mixture of anions and cations [i.e., (0-11) and (011) faces]. The morphology of crystals of **1-Cu** (thin rhombohedrons with a (100) dominant facet) confirms this expectation and *in situ* AFM studies can be used to quantify the difference in rates of growth.
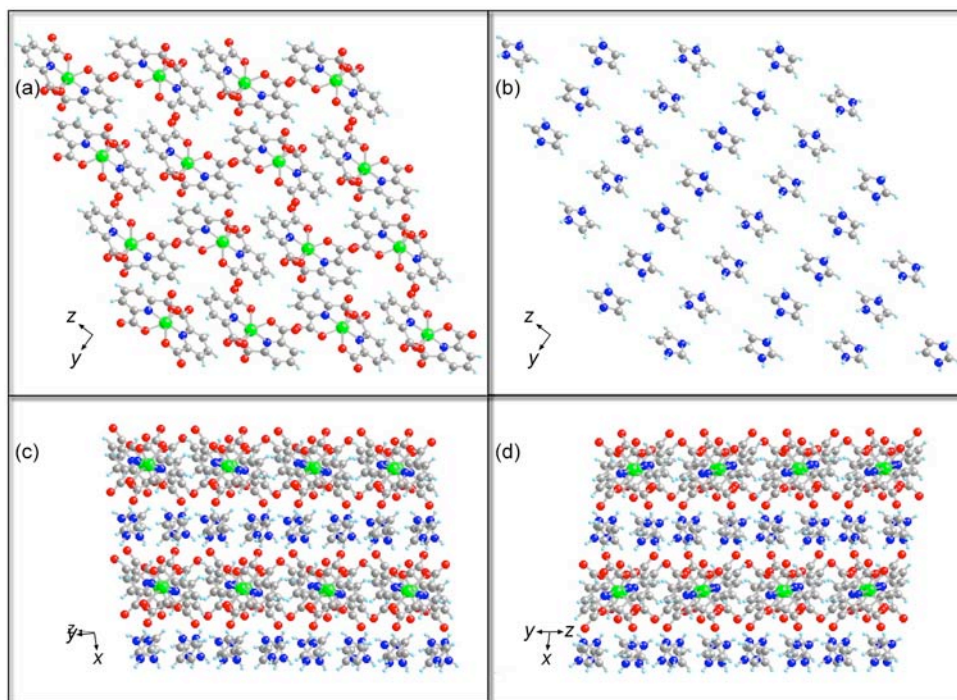

Figure 4. The crystal structure of **1-Cu** viewed perpendicular to three different surfaces. Shown in (a) and (b) is the (100) face, which reveals that either a layer of pure anions or pure cations, respectively, are exposed at this surface. Shown in (c) and (d) is the (0-11) face and (011) face, respectively, revealing that a mixture of anions and cations are exposed at these surfaces.

3.4 Measuring the Kinetics of Growth of Crystals With the AFM
The AFM is a tool with which to image nanoscale features on a surface. In the context of crystals, we have used the AFM to image features that span in size from the nano- to microscale such as the lattice spacing of molecules at the surface of a crystal, molecular steps, dislocations and surface nuclei **(Figure 5)**. [13,23, 25] During imaging, the AFM tip is rastered across the surface of a crystal. Rastering occurs in both a net downward direction (i.e., beginning in the upper left corner and ending in the lower right corner of the area to be imaged) and a net upward direction (i.e., beginning in the lower left corner and ending in the upper right corner of the area to be imaged). Under static conditions, features do not move while the surface is being imaged. Consequently, the same image is generated regardless of whether the tip is rastering the surface in the downward or upward direction. Under dynamic conditions (i.e., growing crystals), however, features are moving while the surface is being imaged. Consequently, the images generated by the downward and upward scans are different because of the time-lag between the rastering tip and the dynamic processes (i.e., step advancement) occurring at the surface.[32] This time-lag is illustrated in **Figure 6**.
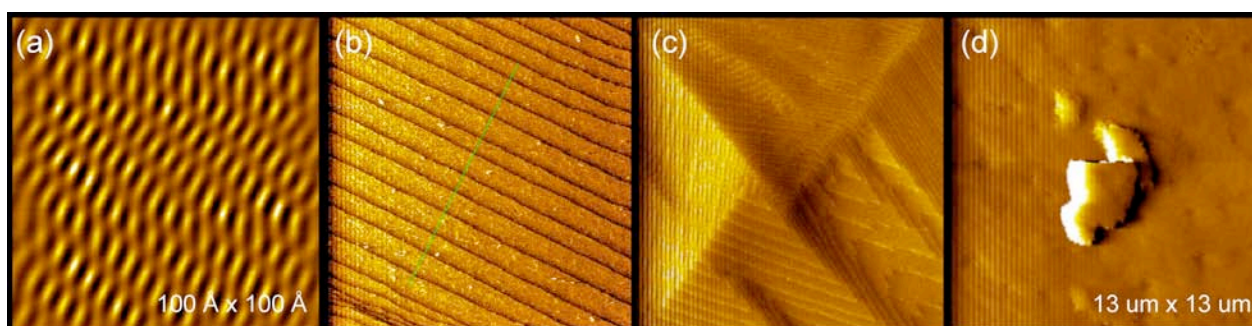
Figure 5. AFM images of the surface of a molecular crystal that reveal (a) lattice spacing, (b) step width, (c) screw dislocation, and (d) surface nuclei.
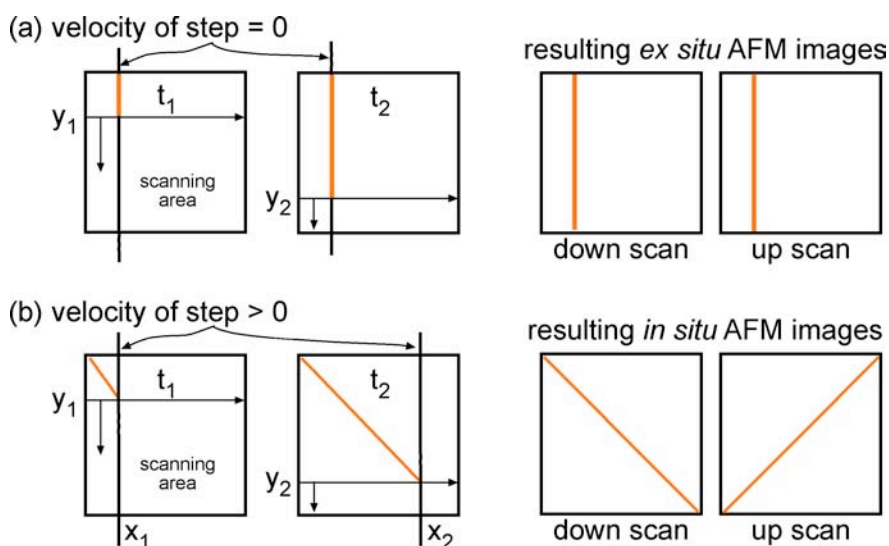

Figure 6. Illustration of what occurs when a static (a) or dynamic (b) surface is imaged with the AFM. For a static surface (*ex situ*), identical images are obtained regardless of the direction of rastering. For a dynamic surface (*in situ*), such as advancing steps in a growing crystal, the downward and upward scans generate different images.

To measure the rate at which a step advances across the surface of a crystal, the surface is imaged while the crystal is immersed in a growth solution of known concentration. Sequential downward and upward scans are collected and a line is drawn parallel to the edge of the advancing steps in both images **(Figure 7)**. Using these two images the velocity of step advancement (V) in units of nm s^{-1} is determined by measuring the angle (θ) between the line drawn in an image and a horizontal line drawn across the image for two consecutive images (i.e., θ_d for the downward scan and θ_u for the upward scan). The two values are then substituted into the equation

$$V = \frac{SR}{N} \frac{\cot(q_u) + \cot(q_d)}{\sqrt{\left(\cot(q_u) - \cot(q_d)\right)^2 + 4}} \qquad (1)$$

where S is the scan size (nm), R is scan rate (line s^{-1}), N is number of raster lines in each image. We have observed that the intrinsic error of this equation is avoided if the angle between the step-edges in the downward scan (θ_d) and upward scan (θ_u) is greater than 20º.
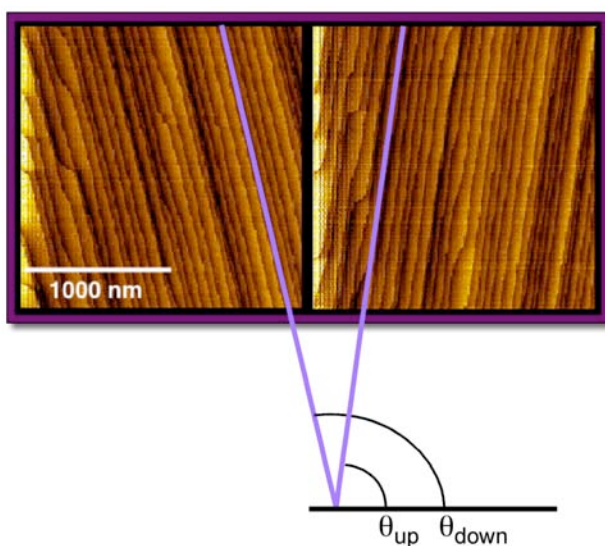

Figure 7. Two consecutive images of the (100) surface of a crystal of **1-Cu** from which θ$_{down}$ and θ$_{up}$ are measured for calculating the rate of step advancement.

3.5 Comparison of the Kinetics of Step Advancement Across the (100) Face and the (0-11) Face of Crystals of 1-Cu

Because the chemical composition and molecular packing exposed at the (100) surface is different than that of the (0-11) surface (cf., **Figure 4**), the rate of advancement of (011) step riser across these two surfaces is expected to be different **(Figure 8)**. To quantify this difference, the kinetics of growth at these two surfaces was studied *in situ* using atomic force microscopy. Experiments to measure the kinetics of crystal growth were performed in saturated solutions containing an equal volume of each stock solution described above to produce a solution that contained a 1:4:4 ratio of Cu(II):**Im**:**DCP**. When the level of supersaturation is such that the crystal is barely growing (i.e., [Cu^{2+}] = 30 mM, [**Im**] and [**DCP**] are each = 120 mM), the average rate at which the (011) riser advances across the (100) face is 7 nm s^{-1}. The average rate at which the (011) riser advances across the (0-11) face is over three times faster at 23 nm s^{-1}. When the concentration of Cu^{2+} ion is increased to 32 mM (and [**Im**] and [**DCP**] are each = 128 mM), the average rate at which the (011) riser advances across (100) and (0-11) is 23 nm s^{-1} and 37 nm s^{-1}, respectively. At the highest concentration of Cu^{2+} ion used in our kinetic measurements (i.e., 42 mM and [**Im**] and [**DCP**] are each = 168 mM), the average rate at which the (011) riser advances across (100) and (0-11) is 122 nm

s⁻¹ and 153 nm s⁻¹, respectively. Typical AFM images of steps advancing across (100) and (0-11) faces at high supersaturation are shown in **Figure 9**.
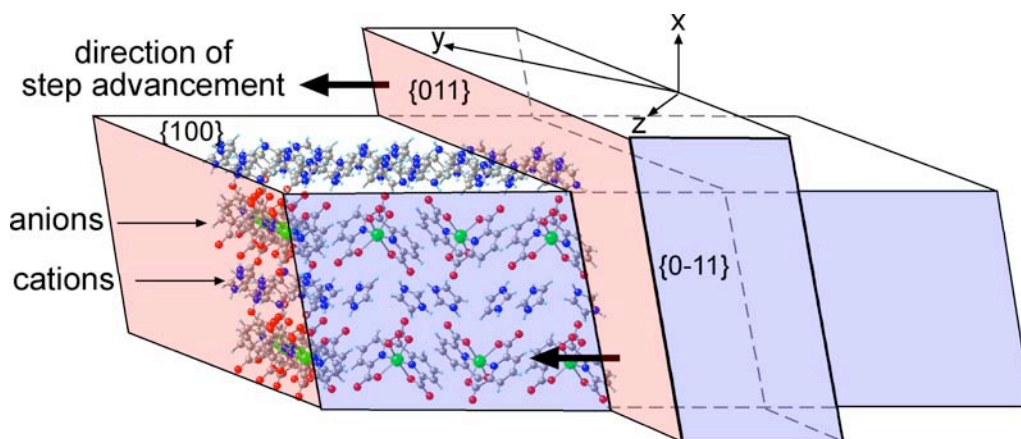
Figure 8. (a) Packing diagram that shows the (011) step riser relative to (100) face and (0-11) face of **1-Cu**.
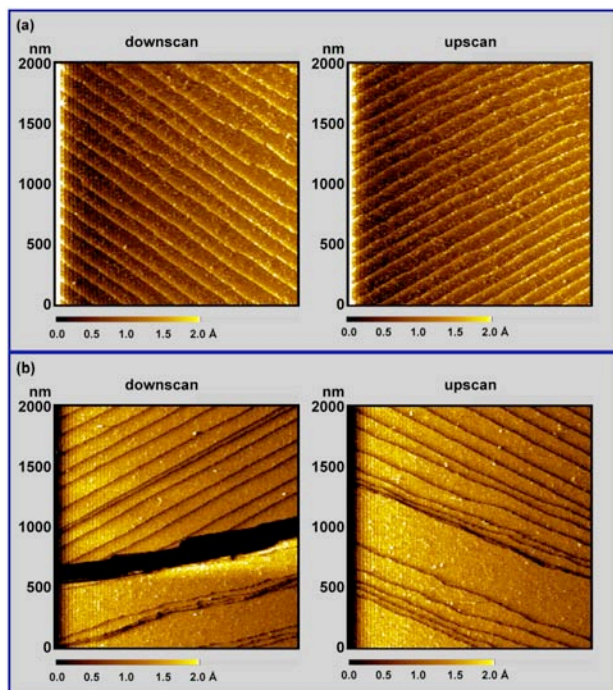

Figure 9. Typical AFM image of steps advancing *in situ* across the (a) (100) and the (b) (0-11) surfaces of **1-Cu** at high supersaturation.

3.6 Why Does the (011) Step-Riser Advance Faster Across the (0-11) Face than the (100) Face?
Figure 10 provides a graphical explanation of the differences in rate at which the (011) step-riser advances across (100) and (0-11) faces. Recall that the (100) surface consists of either a pure layer of anions or a pure layer of cations and the (0-11) surface consists of a mixture of anions and cations that are organized in parallel rows (cf. **Figure 4**). For the (100) face shown in **Figure 10a**, any anion resting on an underlying (100) surface of pure anions will inhibit the attachment and surface diffusion of incoming cations. Consequently, the inhibitory anion, located in a kink site that should be occupied by a cation, must diffuse

out of the kink site to another surface site (a temporary placement) and ultimately dissolve to make the kink site available for incoming cations. This mechanism (i.e., surface diffusion followed by dissolution) enables the incorporation of an incoming cation into the kink site and the resulting advancement of a step-edge. In contrast, a kink site on the (0-11) surface that is occupied incorrectly only requires the inhibitory cation (shown) or anion to diffuse out of the kink site to another surface site to make the kink site available for new growth. Eventually, the inhibitory cation (or anion) will diffuse to a correct surface site and once attached, add to the advancing step-edge.

The observation that the kinetics of growth at the two different faces diverges with increasing supersaturation can be explained by the fact that increasing the supersaturation results in a higher concentration of inhibitors on the surface and in kink sites. For the (100) surface, only dissolution of inhibitors ultimately clears the inhibited kink sites for subsequent growth. Dissolution, however, becomes increasingly difficult with increasing supersaturation. For the (0-11) surface, only surface diffusion is required to clear the inhibited kink sites for subsequent growth. Because the rate of surface diffusion is independent of supersaturation, the inhibitory effect of increasing supersaturation is lower at the (0-11) surface than at the (100) surface, which results in faster kinetics of growth at the (0-11) surface at all levels of supersaturation.
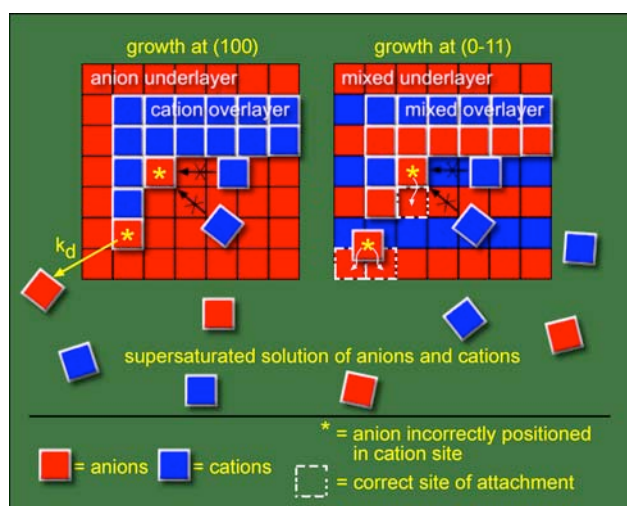
Figure 10. Cartoon illustrating advancement of steps across (a) (100) and (b) (0-11) surfaces of **1-Cu** at high supersaturation. An anion incorrectly positioned in a kink site (*) will either diffuse across the surface or dissolve (k_d) to make the kink site available to an incoming cation. At the (100) surface, both surface diffusion and dissolution are required whereas at the (0-11) surface, only surface diffusion is required.

4. CONCLUSION

We have shown that the AFM can be used to compare the rates at which the same step riser advances across two different crystal surfaces. The effects that molecular packing and supersaturation have on crystal growth kinetics are revealed by this quantitative comparison. Based on these experiments, we conclude that crystal growth is faster when molecular packing at a crystal surface is similar to that of the step-riser (e.g., in this case, both consisting of a mixture of anions and cations) as compared to when the same step-riser advances across a crystal surface with different molecular packing (e.g., in this case, one consisting of a mixture of anions and cations, the other consisting of a pure layer of either anions or cations). The significance of this conclusion is that small changes in supersaturation can lead to significant changes in the kinetics of growth at different crystal surfaces and these changes can be exploited to vary the shape of a crystal, an important capability in the context of batch processing of industrial solids such as pharmaceuticals. Future studies will be directed at exploiting this capability to fabricate complex crystalline solids with varied morphology and composition.

5. ACKNOWLEDGEMENTS

6. REFERENCES

[1]   Ashwell, G. J., *Molecular Electronics* Wiley: New York, 1992; 362.

[2]   Bosshard, C.; Sutter, K.; Prêtre, P.; Hulliger, J.; Flörsheimer, M.; Kaatz, P.; Günter, P., *Organic Nonlinear Optical Materials* Gordon and Breach Science Publishers, Switzerland: Postfach, 1995; Vol. 1.

[3]   Gatteschi, D., *Magnetic Molecular Materials* Kluwer Academic Publishers: Lucca, Italy, 1991; 411.

[4]   Fraxedas, J. *Adv. Mater.* **2002**, 14, 1603.

[5]   Vallee, R.; Damman, P.; Dosiere, M.; Toussaere, E.; Zyss, J. *J. Am. Chem. Soc.* **2000**, 122, 6701.

[6]   Hooks, D. E.; Fritz, T.; Ward, M. D. *Adv. Mater.* **2001**, 12, 228.

[7]   Hillier, A. C.; Ward, M. D. *Phys. Rev. B* **1996**, 54, 14037.

[8]   Carter, P. W.; Frostman, L. M.; Hillier, A. C.; Ward, M. D. In *Nucleation and Growth of Molecular-Crystals on Molecular Interfaces - Role of Chemical Functionality and Topography*, ACS Symposium Series, 1994; 186.

[9]   Davey, R. J. *J. Chem. Soc., Faraday Trans.* **1991**, 87, 3409.

[10]   Davey, R. J.; Black, S. N.; Bromley, L. A.; Cottier, D.; Dobbs, B.; Route, J. E. *Nature* **1991**, 353, 549.

[11]   Sarma, K. R.; Shlichta, P. J.; Wilcox, W. R.; Lefever, R. A. *Journal of Crystal Growth* **1997**, 174, 487.

[12]   Ward, M. D. *Chem. Rev.* **2001**, 101, 1697.

[13]   Palmore, G. T. R.; Luo, T. J.; Martin, T. L.; McBride-Wieser, M. T.; Voong, N. T.; Land, T. A.; De Yoreo, J. J. *Trans. ACA* **1998**, 33, 45.

[14]   Binnig, G.; Quate, C. F.; Gerber, C. *Physical Review Letters* **1986**, 56, 930.

[15]   Hillner, P. E.; Gratz, A. J.; Manne, S.; Hansma, P. K. *Geology* **1992**, 20, 359.

[16]   De Vries, S. A.; Goedtkindt, P.; Bennett, S. L.; Huisman, W. J.; Zwanenburg, M. J.; Smilgies, D. M.; De Yoreo, J. J.; Van Enckevort, W. J. P.; Bennema, P.; Vlieg, E. *Phys. Rev. Lett.* **1998**, 80, 2229.

[17]   De Yoreo, J. J.; Land, T. A.; Rashkovich, L. N.; Onischenko, T. A.; Lee, J. D.; Monovskii, O. V.; Zaitseva, N. P. *J. Cryst. Growth* **1997**, 182, 442.

[18]   Durbin, S. D.; Carlson, W. E.; Saros, M. T. *J. Phys. D-Appl. Phys.* **1993**, 26, B128.

[19]   Land, T. A.; Malkin, A. J.; Kuznetsov, Y. G.; McPherson, A.; De Yoreo, J. J. *Physical Review Letters* **1995**, 75, 2774.

[20]   Land, T. A.; De Yoreo, J. J.; Lee, J. D. *Surface Science* **1997**, 384, 136.

[21]   Malkin, A. J.; Kuznetsov, Y. G.; McPherson, A. *Surface Science* **1997**, 393, 95.

[22]   Yip, C. M.; Brader, M. L.; Defelippis, M. R.; Ward, M. D. *Biophysical Journal* **1998**, 74, 2199.

[23]   Luo, T.-J.; Palmore, G. T. R. *J. Phys. Org. Chem.* **2000**, 13, 870.

[24]   Teng, H. H.; Dove, P. M.; Orme, C. A.; De Yoreo, J. J. *Science* **1998**, 282, 724.

[25] Luo, T.-J. M.; MacDonald, J. C.; Palmore, G. T. R. *Chem. Mater*. **2004**, 16, 4916.

[26] Bennema, P. *J. Crystal Growth* **1969**, 5, 29.

[27] Bennema, P. *J. Crystal Growth* **1967**, 1, 278.

[28] Vekilov, P. G.; Kuznetsov, Y. G.; Chernov, A. A. *J. Crystal Growth* **1992**, 121, 643.

[29] Vekilov, P. G.; Alexander, J. I.; Rosenberger, F. *Phys. Rev. E* **1996**, 54, 1.

[30] MacDonald, J. C.; Dorrestein, P. C. *Trans*. *ACA* **1998**, 33, 121.

[31] MacDonald, J. C.; Dorrestein, P. C.; Pilley, M. M.; Foote, M. M.; Lundburg, J. L.; Henning, R. W.; Schutlz, A. J.; Manson, J. L. *J. Am*. *Chem*. *Soc*. **2000**, 122, 11692.

[32] Gratz, A. J.; Manne, S.; Hansma, P. K. *Science* **1991**, 251, 1343.

THE RELATIONSHIP BETWEEN URIC ACID CRYSTALS AND KIDNEY STONE DISEASE

Ryan E. Sours and Jennifer A. Swift
Georgetown Univ., 37th and O Streets NW, Washington, DC 20057, USA

1. ABSTRACT

Uric acid ($C_5H_4N_4O_3$) is one of the final products of protein metabolism in humans. Its concentration balance is maintained in the kidneys, but compromised kidney function can result in its crystallization, either in the renal tract where it can contribute to kidney stone formation and/or in the interstitial fluid of joints of those afflicted with gout. In low pH physiological environments, crystalline uric acid is most frequently found as either an anhydrous (**UA**) or dihydrate (**UAD**) phase. Developing a fundamental understanding of the crystal nucleation and growth mechanisms of these uric acid phases at the molecular-level may help to elucidate new strategies for the treatment or prevention of its precipitation *in vivo*. The history, macroscopic crystal growth, and characterization of **UA** and **UAD** crystals is described herein.

2. INTRODUCTION

Human kidneys have two basic functions – to excrete metabolic waste products and other foreign chemicals, and to regulate fluid volume, osmolarity, acidity and mineral composition in order to maintain normal concentrations in the extracellular fluid. Impaired kidney function can lead to the deposition of a number of different precipitates throughout the renal tract as well as contribute to kidney stone formation. When this occurs, the functioning of the kidneys is further compromised, and severe blockages may even lead to renal failure in some cases. Although the development of a kidney and/or urinary stone is very rarely fatal, severe pain is associated with the dislodging and passing of a renal stone. In the United States, it is estimated that 10-15% of the population will develop a kidney stone during their lifetime. [1,2] The costs associated with the evaluation and treatment of kidney stone disease were estimated at $1.83 billion per year in 1993. [3] When adjusted for inflation, keeping all other factors constant, this equates to nearly $2.4 billion dollars per year in 2004.

Kidney stones are aggregates of crystals held together by an organic matrix. They can consist of principally one crystalline component, or as mixture of two or more components present in significant quantities. Several different urinary components are capable of precipitating in the renal tract and serving as the building blocks of kidney stones. The chemical analysis of the principal stone constituent(s) is clinically valuable, since stones of different composition can sometimes indicate different medical conditions. The most common mineral species identified in renal deposits include calcium oxalates (whewellite, weddelite), calcium phosphates (hydroxyapatite, brushite, octacalcium phosphate, whitlockite) and magnesium phosphates (struvite, newberyite). The most common organic materials found in urinary stones are uric acid and cysteine. The composition of kidney stones shows a geographic dependence, with significant variation between countries around the world. This is most likely due to a combination of local genetics, diet, climate, and customs.

The focus of this manuscript is on the building blocks of uric acid kidney stones, the prevalence of which varies considerably among developed nations. Studies on kidney stone compositions have found different frequencies for uric acid stone occurrence internationally: 4% in Sweden [4], 5.3% in Belgium [5], 5.6% in Australia [6], 6.6% in Great Britain [7], 8.6-16.5% in the United States [8,9], 23.3% in France [10], 17-25% in Germany [11,12], and 39.5% in Israel [13]. Two large-scale studies describing the statistical analysis of over 10,000+ stones from the United States revealed a significant increase in the incidence of uric acid stones over a period of two decades. A 1962 study by Herring [8] reported an 8.6% occurrence for uric acid stones, while a 1989 study by Mandel and Mandel [9] cited a 16.5% occurrence. The exact reasons for the large discrepancy in the two US studies are not certain, as the composition of kidney stones is determined by a variety of factors. Some of the factors that increase the likelihood of uric acid stone

formation include richer diets (and hence the need to process more wastes), increased cell turnover rates (e.g. during chemotherapy) [14], chronic dehydration, and/or other metabolic uric acid regulation problems.

Of the known risk factors, diet and lifestyle have perhaps changed the most significantly in the last century. Uric acid is a waste product of protein metabolism in humans, and two studies have tested the relationship between dietary protein intake and uric acid excretion. [15,16] Fellström, et al. divided patients into two groups, which were fed low protein and high protein diets, respectively. After two weeks on each diet, the urine pH and uric acid concentration of each group were measured. The urine of subjects on the high protein diet was more acidic (by 0.9 pH units) and showed a 90% increase in uric acid concentration. The second study compared the diets of uric acid stone formers and non-stone formers. Coe, et al. found that those patients who had developed uric acid kidney stones consumed 66% more protein than those without stones. Therefore, both studies suggest that increased protein consumption increases the risk for uric acid stone formation. This relationship is especially significant given the current popularity of "low-carb" diets (e.g. Atkins [17], South Beach [18]), which are based on replacing most of the daily carbohydrate intake with protein. This suggests that the incidence rates of uric acid kidney stones may continue to increase in the future unless dietary trends are reversed.

3. STRUCTURE

Investigations into the molecular structure of uric acid date back as far as 1776, when Karl Wilhelm Scheele first isolated a substance from urinary calculi, which he originally named lithic acid. [19] Ten years later, he demonstrated that it was a normal constituent of human urine. George Pearson later renamed the compound uric acid in 1798. [20] The first correct molecular structure of uric acid was put forth by Ludwig Medicus in 1875, although even he lacked definitive evidence at the time. [21] Emil Fischer (Nobel, 1902) provided the first rational synthesis of uric acid twenty years later, proving that the Medicus structure was indeed correct (**Figure 1**). [22-24]
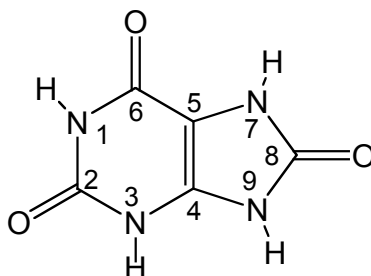

Figure 1. Molecular structure of uric acid with ring atoms numbered according to Fischer.

Under low pH conditions, uric acid is known to crystallize from aqueous solutions in either an anhydrous form (**UA**) or as a less stable dihydrate (**UAD**). Both **UA** and **UAD** phases are found in kidney stones, although the anhydrous form is more common. **UAD** is almost always found in association with the anhydrous phase, in part because the dihydrate phase can transform to the anhydrous phase in solution, presumably through a dissolution-recrystallization mechanism. In neutral or basic pH solutions, uric acid (pK_a = 5.4) exists predominantly as urate by deprotonation of the nitrogen at position 3. [25] Urate is significantly more soluble than uric acid, however, a number of different urate salts are also known to crystallize in physiologic environments. The two forms most frequently observed in pathological human deposits are monosodium urate monohydrate and ammonium acid urate. Monosodium urate monohydrate crystal precipitates in the interstitial fluid of joints are also the classic clinical symptom of gouty arthritis.

Although the optical properties of uric acid crystals were investigated at the end of the 19th century, [26-28] the first crystal structure of **UA,** solved by Hans Ringertz, did not appear until 1966. [29] **UA** crystals are monoclinic, with a space group of $P2_1/a$ and four molecules per unit cell. The unit cell dimensions are a = 14.464(3), b = 7.403(2), c = 6.208(1) Å, and β = 65.10(5)°. Uric acid packs in a layered motif, with

adjacent layers spaced 6.56 Å apart along a^* (see **Figure 2**). Each layer consists of parallel ribbons of uric acid molecules hydrogen-bonded head-to-head ($O_2 \cdots H\text{-}N_1$: 1.826 Å, 175.0°) and tail-to-tail ($O_8 \cdots H\text{-}N_7$: 1.734 Å, 155.8°), with the ribbon plane perpendicular to the $b\text{-}c$ plane. There is no hydrogen-bonding between ribbons within a layer, although ribbons in adjacent layers are hydrogen-bonded to one another and offset by ~ 62°.

The crystal structure of **UAD** continued to remain elusive for thirty more years. The primary obstacle in the structure determination of **UAD** was its ready dehydration in air, and the long data collection times required for small crystals on serial diffractometers. Initial diffraction studies of **UAD** were carried out by Artoli et al. [30] on natural crystal samples (bird droppings found on rock surfaces), which dehydrated less quickly but whose small size prohibited a full data collection. Using a crystal derived from human urinary sediments, the same group later reported the first full structure of **UAD** in 1997. [31] They assigned the crystal to the orthorhombic space group *Pnab,* and refined the structure with a 50:50 disorder of molecules about two positions, although a number of weak reflections violated systematic absences for the space group setting. Parkin and Hope revisited the structure determination of **UAD** a year later, this time using synthetic crystals. The structure was assigned to the monoclinic space group $P2_1/c$ with $a = 7.237(3)$, $b = 6.363(4)$, $c = 17.449(11)$, and $\beta = 90.51(1)°$, based on data collected at 120 K. [32] The monoclinic model was refined with both twinning and disorder, and showed no diffraction peak violations. Side by side analysis of the orthorhombic and monoclinic **UAD** structures shows them to be more or less identical, though the latter is arguably more crystallographically correct. Comparison of the **UAD** and **UA** structures shows their ribbon and layer motifs to be quite similar. The distance and registry between adjacent layers in **UAD** and **UA** are necessarily different, owing to the addition of a 2-dimensional hydrogen-bonded water layer in **UAD**. The interlayer distance in **UAD** is 8.73 Å.
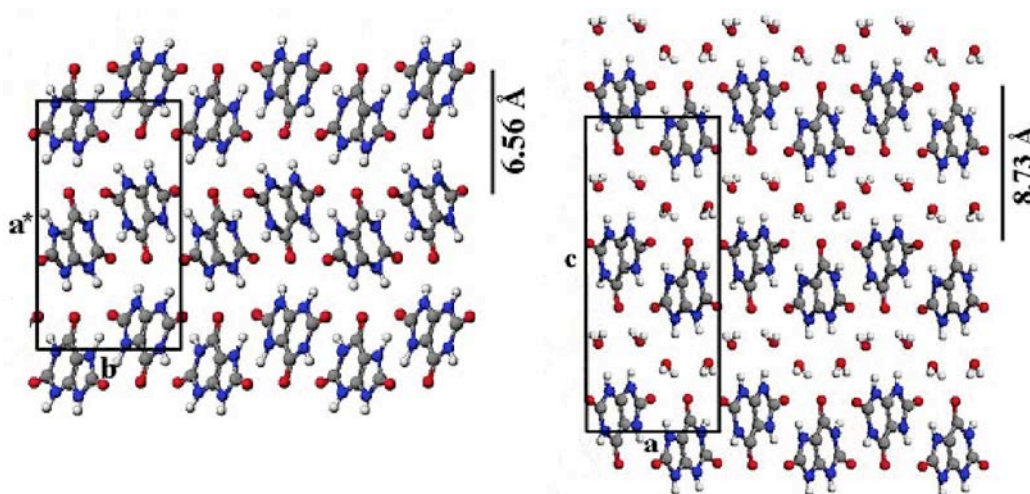

Figure 2. Crystal Structures of uric acid (left) and uric acid dihydrate (right) based on fractional coordinates provided in references [29] and [32], respectively.

4. CRYSTAL GROWTHS AND CHARACTERIZATION

While both **UA** and **UAD** phases grow in biological environments at physiologic temperature, **UA** and **UAD** phases can be grown selectively in a laboratory environment according to the following procedure. Supersaturated uric acid solutions were prepared by dissolving 15-20 mg of uric acid (Aldrich, 99+%) in 100 mL of boiling deionized water. Water was purified by passage through two Barnstead deionizing cartridges followed by distillation. Pure synthetic single crystals (200-300 μm in the largest dimension) of uric acid dihydrate (**UAD**) and uric acid (**UA**) were grown upon standing at ambient ($24 \pm 1°C$) and physiologic ($37 \pm 0.1°C$) temperatures, respectively. While pH can be an important factor in uric acid crystal growth, solutions prepared under the specified conditions were of pH = 4-5 and no further pH adjustment was made. Crystals of **UA** deposit as clear, colorless rectangular plates with large (100) faces bounded by (210), (201), (001), and sometimes (121) faces. [33] **UAD** also crystallizes as clear colorless

rectangular plates with large (001) faces bounded by (011) and (102) and infrequently (210) faces. Optical micrographs of **UA** and **UAD** crystals with their Miller indexes labeled are provided in **Figure 3**. In related crystal growth studies, we have also observed that the presence of known quantities of some synthetic dyes in the uric acid growth solutions can lead to alternative **UA** and **UAD** crystal habits. Details on the selective recognition of synthetic dye probes and habit modification of **UA** and **UAD** are elaborated in references 33–35.
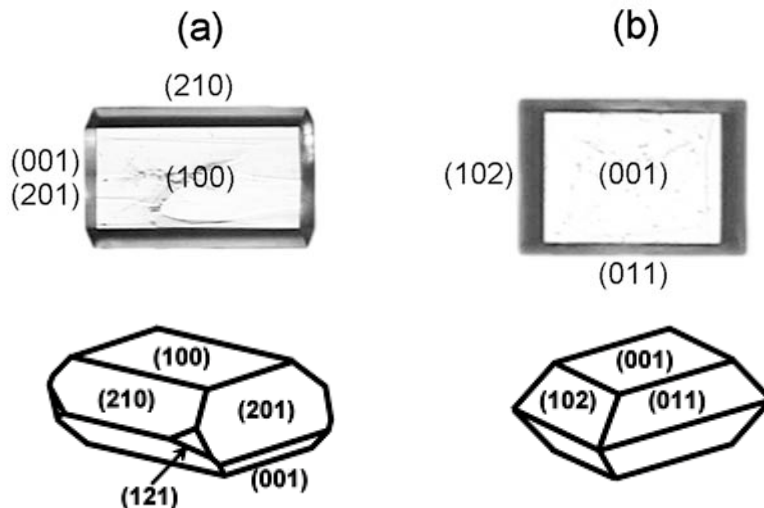
Figure 3. (a) Anhydrous uric acid (**UA**) and (b) uric acid dihydrate (**UAD**) crystals grown from aqueous solutions. Crystals are typically ~ 200-300 μm in their largest dimension.

Though both **UA** and **UAD** have similar structural features and general plate-like morphologies, differentiating between the two forms is relatively straightforward. The most obvious method for unambiguously determining the crystal form (besides X-ray diffraction) is infrared spectroscopy. The FTIR-ATR spectra of **UAD** exhibits a strong water absorption band at ~3440 cm^{-1} which is absent in **UA**. The main drawback of using this technique for routine characterization is that the crystals are frequently destroyed in the ATR press. An alternative and non-destructive method uses conoscopic light interference patterns. [36] Anhydrous uric acid crystals are biaxial positive, while dihydrate crystals are biaxial negative. [28] For monoclinic crystals, the refractive indexes do not all necessarily lie along crystallographic directions. This is true for **UA**, in which n_α (1.588) lies along b, while n_β (1.739) and n_γ (1.898) are offset by 45.6° from a^* and c. The refractive indices for **UAD** are more straightforward, as n_α (1.508) lies along a, n_β (1.691) along c, and n_γ (1.728) along b. [28,37] Therefore, the optic plane for **UA** is tilted 45.6° from the large (100) plate face, whereas the optic plane for **UAD** is perpendicular to the large (001) plate face.

Conoscopic interference patterns were obtained using an Olympus BX-50 polarizing microscope and a 505 nm interference filter **(Figure 4)**. The optic plane is perpendicular to (001) for **UAD**, although the melatopes (the points of emergence of the optic axes) are spaced too far apart to be observed by our objective lens (N.A. = 0.80, $2V_o = 140°$). The optic plane in **UA** is inclined relative to (100), as indicated by the asymmetry of the interference pattern. The inclination combined with the large angle between the optic axes also made it impossible for us to observe the melatopes for **UA** ($2V_a = 84°$). In any case, the difference between **UA** and **UAD** patterns is unmistakable **(Figure 4)**, and this method proved to be the easiest for rapidly distinguishing the two phases.
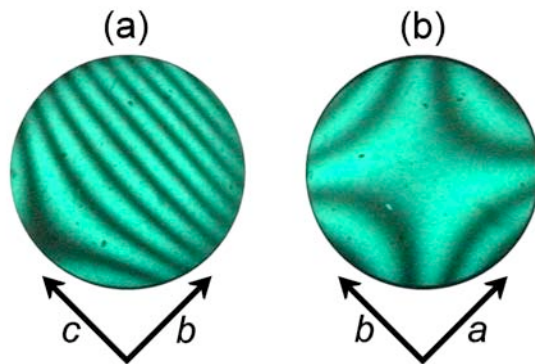
Figure 4. Conoscopic interference patterns obtained on the large plate faces of (a) **UA** and (b) **UAD** with crystallographic directions indicated.

5. EPITAXIAL GROWTH

The common coexistence of these uric acid phases and their frequent association with assorted mineral species in kidney stone deposits led Lonsdale [38] in 1968 to suggest that epitaxial relationships between biological crystalline phases may be an important factor contributing to their pathological formation. Epitaxy is defined as the growth of one crystal on the substrate of another, such that there is at least one preferred orientation and a near geometrical fit between the contacting surface lattices. When seed crystals with geometrically matched surface lattices are present in solution, the barrier to nucleation can be significantly reduced, such that crystallization occurs in environments that have otherwise not met critical supersaturation conditions. A seed crystal of the same material is usually regarded as the best-matched epitaxial surface, though surfaces of two different crystalline materials may also be related by epitaxy if their 2D surface lattice spacings are similar. A geometric lattice-matching protocol, EpiCalc [39], was used as a screening tool to identify all possible epitaxial interfaces between surfaces of **UA** and **UAD**. [40] The program rotates an overlayer (with lattice parameters b_1, b_2, and β) with respect to a substrate (with lattice parameters a_1, a_2, and α), through a series of azimuthal angles (θ). Because overlayer structures are particularly sensitive to competition between energy lowering interfacial interactions and energetic penalties associated with even minor reconstruction, geometric calculations allowed for the overlayer lattice parameters to be systematically varied by up to ± 5.0% of the unit cell dimensions. This screening method is mechanistically different from previous epitaxy searches, which typically examine the percentage of misfit (up to 15%) of various interfacial lattice alignments. [38,41]

When all possible pairs of the various natural faces of **UA** and **UAD** were subjected to EpiCalc screening, ten epitaxial relationships were identified. The best match between the plate faces of the two materials, **UAD** (001) / **UA** (100) ($\theta = 0°$), can be considered a near perfect commensurate relationship. The nine other matches identified were related by coincident epitaxy. Coincident matches include **UAD** (001) / **UA** (201) ($\theta = 0°$), **UAD** (001) / **UA** (210) ($\theta = 0°$), **UAD** (001) / **UA** (121) ($\theta = 0°$, 55°), **UAD** (001) / **UA** (001) ($\theta = 27°$), **UAD** (011) / **UA** (201) ($\theta = 1°$), **UAD** (011) / **UA** (210) ($\theta = 0°$), **UAD** (102) / **UA** (201) ($\theta = 25°$), **UAD** (102) / **UA** (210) ($\theta = 4°$). In our laboratory and also in others [42], the epitaxial growth of **UA** (100) on **UAD** (100) has been frequently observed **(Figure 5)** at the commensurate angle predicted by lattice-matching calculations. Crystals of **UAD** can also be grown on **UA** substrates with the same interfacial orientation. During the epitaxial growth of **UA** on **UAD**, which can occur over a period of days to weeks, the **UAD** substrate slowly becomes pitted or opaque. However, the exact molecular-level mechanism of this epitaxial growth process is not well understood at this time and requires further elucidation.
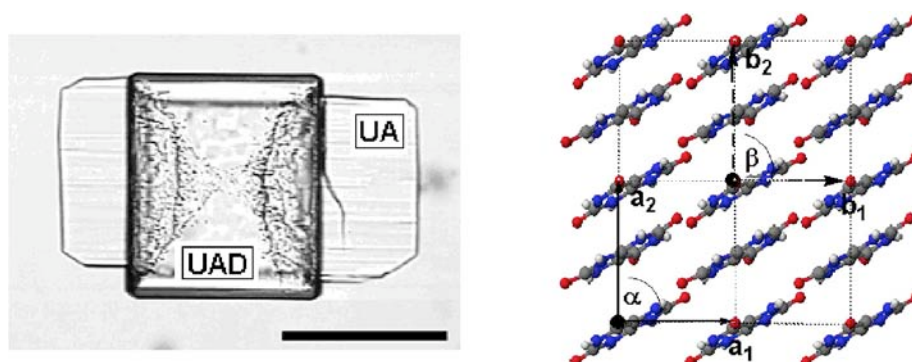
Figure 5. (left) Photomicrograph showing the epitaxial growth of **UA** (100) on a **UAD** (001) substrate. Scale bar = 100 μm. (right) Epitaxial relationship between the same **UAD** substrate (a1, a2, α) and **UA** overlayer (b1, b2, β).

The same EpiCalc screening procedure was applied to uric acid surfaces and the natural surfaces of minerals found in kidney stones. [40] Several potential coincident and commensurate epitaxial matches were also identified for these different uric acid / mineral interfaces. Ongoing experimental studies seek to establish epitaxy between these phases as a potential factor in pathological stone formation.

6. ACKNOWLEDGEMENTS

7. REFERENCES

[1]   Johnson, C.M., D.M. Wilson, W.M. O'Fallon, et. al., *Kidney Int.* **16** (1979) 624.

[2]   Sierakowski, R., B. Finlayson, R.R. Landes, et. al., *Invest. Urol.* **15** (1978) 438.

[3]   Clark, J.Y., I.M. Thomson, and S.A. Optenberg, *J. Urol.* **154** (1995) 2020.

[4]   Grenabo, L., H. Hedelin, and S. Pettersson, *Scand. J. Urol.* **19** (1985) 285.

[5]   Fuss, M., J. Simon, D. Verbeelen, et. al., *Eur. Urol.* **4** (1978) 90.

[6]   Wardlaw, H.S.H., *Med. J. Australia* **1** (1952) 180.

[7]   Sutor, D.J., S.E. Wooley, and J.J. Illingworth, *Br. J. Urol.* **46** (1974) 275.

[8]   Herring, L., *J. Urol.* **88** (1962) 545.

[9]   Mandel, N.S. and G.S. Mandel, *J. Urol.* **142** (1989) 1516.

[10]   Cottet, J. and A. Weber, *Pathol. Biol.* **7** (1959) 1975.

[11]   Scholz, D., P.O. Schwille, D. Ulbrich, et. al., *Urol. Res.* **7** (1979) 161.

[12]   Hesse, A., H.-J. Schneider, W. Berg, et. al., *Invest. Urol.* **12** (1975) 405.

[13]   Atsmon, A., A. de Vries, and M. Frank, *Uric Acid Lithiasis,* (Elsevier, Amsterdam, 1963)

[14]   Rieselbach, R.E. and M.B. Garnick, *Cancer and the Kidney*, (Lea & Febiger, Philadelphia, 1982)

[15]   Fellström, B., B.G. Danielson, B. Karlstrom, et. al., *Clin. Sci.* **64** (1983) 399.

[16]   Coe, F.L., E. Moran, and A.G. Kavalich, *J. Chronic Dis.* **29** (1976) 793.

[17]   Atkins, R.C., *Dr. Atkins' New Diet Revolution; 3rd ed,* (M. Evans and Co., New York, 2002)

[18]   Agatston, A., *The South Beach Diet: The Delicious, Doctor-Designed, Foolproof Plan for Fast and Healthy Weight Loss*, (Rodale, New York, 2003)

[19]   Scheele, K.W., *Opuscula* **2** (1776) 73.

[20]   Pearson, G., *Philos. Trans. R. Soc. London* **88** (1798) 15.

[21]   Medicus, L., *Justus Liebigs Ann. Chem.* **175** (1875) 230.

[22]   Fischer, E. and L. Ach*, Ber. Dtsch. Chem. Ges.* **28** (1895) 2473.

[23]   Fischer, E.*, Ber. Dtsch. Chem. Ges.* **30** (1897) 549.

[24]   Fischer, E.*, Ber. Dtsch. Chem. Ges.* **32** (1899) 435.

[25]   Mandel, N.S. and G.S. Mandel, *J. Am. Chem. Soc.* **98** (1976) 2319.

[26]   Brun, A., *Arch. Sci. Phys. Nat.* **7** (1899) 284.

[27]   Winchell, A.N., *The Optical Properties of Organic Compounds. 2nd ed.,* (Academic Press, New York, 1954)

[28]   Ringertz, H., *Acta. Cryst.* **19** (1965) 286.

[29]   Ringertz, H., *Acta. Cryst.* **20** (1966) 397.

[30]   Artoli, G., E. Galli, and M. Ferrari, *Riv. Mineral. Ital.* **2** (1993) 91.

[31]   Artioli, G., N. Masciocchi, and E. Galli, *Acta. Cryst.* **B53** (1997) 498.

[32]   Parkin, S. and H. Hope, *Acta. Cryst.* **B54** (1998) 339.

[33]   Sours, R.E., D.A. Fink, and J.A. Swift, *J. Am. Chem. Soc.* **124** (2002) 8630.

[34]   Fink, D.A., R.E. Sours, and J.A. Swift, *Chem. Mater.* **15** (2003) 2718.

[35]   Sours, R.E., D.A. Fink, K.A. Cox, and J.A. Swift, *Mol. Cryst. Liq. Cryst.* **440** (2005) 187.

[36]   Wood, E.A., *Crystals and Light, 2nd ed.*, (Dover, New York, 1977)

[37]   Shirley, R., *Science* **152** (1966) 1512.

[38]   Lonsdale, K., *Nature* **217** (1968) 56.

[39]   Hillier, A. and M.D. Ward, *Phys. Rev. B* **54** (1996) 14037.

[40]   Frincu, M.C., C.E. Fogarty, and J.A. Swift, *Langmuir,* **20** (2004) 6524.

[41]   Mandel, N.S. and G.S. Mandel, in: *Urolithiasis: Clinical and Basic Research,* eds. L.H. Smith, W.G. Robertson, and B. Finlayson (Plenum Press, New York, 1981), p. 469.

[42]   Boistelle, R. and C. Rinaudo, *J. Cryst. Growth* **53** (1981) 1.

DESIGNING MOLECULAR INTERFACES

Colin C. Seaton and Nicholas Blagden
Drug Delivery Group, Inst of Pharmaceutical Innovation
School of Pharmacy, Univ. of Bradford, Bradford BD7 1DP, UK

1. ABSTRACT

A key aim of crystal engineering is the design and synthesis of new materials with defined functionality through the control of intermolecular interactions. The formation of composite materials, created from two separate crystalline components bound through some epitaxial interface, are of interest since the properties can be controlled through selection of components. To gain an understanding of the intermolecular interactions occurring across the boundary, the differential evolution (DE) algorithm was applied to problem of optimising the position and orientation of two crystal blocks together. An investigation in the effect of the limited number of control parameters highlights the fact that a small range of values is required for optimal performance of the method. A test system of benzoic acid and benzamide was investigated and the computational results indicate the formation of hydrogen bonding between the {100} face of benzoic acid with the {010} face of benzamide.

2. INTRODUCTION

Composite materials play an increasingly important part in contemporary life with their properties inevitably being determined by their component materials and inherent interfacial characteristics. For example: concrete, polymers, paper and paint all depend on the integrity of solid/solid interfaces for their mechanical strength, while anti-corrosive treatments and adhesives depend on their integrity with a substrate for successful application [1,2]. Recently there has been increased emphasis on the development of sophisticated products and processes in which the design of multi-component systems is essential. Examples include; herbicides, fungicides and pharmaceutical drug delivery systems [3,4], all of which rely on multi-components to give optimum efficacy and controlled release. However, manipulation of epitaxy without mechanical processing of the host substrate remains an unresolved challenge.

Developments in the field of crystal engineering have highlighted the role that molecular recognition plays in the process of crystal growth [5,6] and imply the possibility of engineering epitaxial relationships between materials through purely molecular means. The understanding of molecular processes and structural nature of interactions at the interface has been boosted by the application of the vast accumulation of structural data that exists for molecular materials. These studies have been directed to a molecular level understanding of such processes as nucleation [7], growth of twinned crystals [8], polymorphism in crystals [9], formation of solid solutions [10,11], and the nature of the inorganic-organic interface in biominerals [12]. This understanding has lead to a tremendous progress in the ability to manipulate crystal properties such as morphology, structure and extent of crystal aggregation and the orientation of nuclei [13].

2.1 Interfaces And Epitaxy

At the interface between two materials both the composition and the arrangement of molecules or ions change from that corresponding to one pure phase to that of a second. When the structural registry (geometric and stereochemical) between the two phases lies within a narrow limit, the materials are said to display an epitaxial relationship to each other. In this configuration of the interface, stress is minimised and intermolecular/interionic attractive interactions are maximised, leading to optimum stability, strength and chemical integrity across the interface. Historically epitaxy was widely reported as occurring in mineral samples [14], for example rutile on hematite, marcasite on pyrite and staurtite on kainite [15,16]. The role of lattice match between the host substrate and the guest overlayer as a contributing factor to epitaxy was experimental verified by the study of a series of inorganic systems [17] and relating the occurrence of epitaxy to the degree of lattice mismatch. These system included sliver and gold deposition on calcite, mica and sodium chloride [18], urea on ammonia chloride [17]. Further studies have identified that the interfacial mixing relies not only on a lattice match at the interface [19] but also on the lattice relaxation away from the surfaces, which governs the azumathal alignment achieved [20-22].

Currently the study of epitaxy relies on macroscopic analysis of the phenomena [23] with nucleation described in terms of heterogeneous nucleation [24] modified by terms that account for a contribution from surface wetting [25] and the free energy of the guest host interaction [26-28]. Generally a mechanically cleaved surface is used to support the epitaxy and molecular organisation, for example in selection of polymorphs by molecular solids [29,30] and investigations into the role that the molecular topography and chemical functionality of the substrate plays in the deposition of molecular solids [31].

As noted above, historically epitaxy has been investigated with respect to inorganic systems and little work has focused on the epitaxial growth of organic molecular materials onto an organic molecular substrate or the understanding of the intermolecular interactions within these interfaces. Much of this work focuses on the problem of twinning, the situation where two or more individual single crystals are joined in a single particle such that the components are related by a symmetry element that does not exist in the single crystal [32], which can be considered as the epitaxy of one material with itself. Though an understanding of the symmetry relationships between the component parts of the twinned crystal can generally be obtained, exact understanding of the molecular relationship and intermolecular interactions between the components is often harder to obtain. In the case of saccharin [32], the application of energy calculations to a series of molecular juxtapositions about the known twin plane allowed the determination of a feasible molecular configuration.

Another area of interest is the selective growth of polymorphs upon a molecular solid [29,30]. Here a mechanically cleaved surface of a selected compound acts as a nucleating point for a secondary material, if this secondary material is polymorphic then the polymorph with the more favourable lattice match will grow. This work shows that the crystalline and intermolecular relationships between the substrate and overlayer must be fully understood if a substrate is to be designed to selectively grow a chosen polymorph.

To fully develop a method of molecular based epitaxy, a full understanding of both the lattice matching and potential molecular recognition of the substrate and the overlayer must be achieved. Computational modelling of the structural registry is required to give an insight into the interactions occurring between the interfacing components.

3. MODELLING THE INTERFACE

As a first step to model the creation of an interface between two organic crystal systems on an atomic scale, it was assumed that the known crystal structure sufficiently represented the system and that there was no molecular relaxation and negligible strain at the molecular interface. Therefore the substrate and overlayer crystal blocks are generated from the known crystal structures by combining a fixed number of unit cells in each direction.

For any face {hkl} of the substrate system, a vector system may be defined such that the mutually perpendicular unit vectors **u, v**, lie in the plane of the substrate face and a unit vector, **w**, is perpendicular to the face. The position of the overlayer crystal block may then be defined by reference to this coordinate system *(u, v, w)*. The orientation of the overlayer crystal block is defined by three angles *(θ, ϕ, γ)*, which allows the positioning of any crystal face onto the interface and reduces the number of assumptions about the nature of the interface **(Figure 1)**. Once the overlayer is positioned and rotated, the energy between the components may then be calculated by use of a force field. Since the interactions between molecules in the same crystal block are independent of the position of the two components, they will be constant for all potential crystal packings. Thus, for computational efficiency, only those interactions between separate crystal blocks are considered in the calculation of the system energy.

Thus, the system is modelled by nine problem parameters *(h, k, l, u, v, w, θ, ϕ, γ)* and for a given set of parameters the energy is calculated. The location of the global minima for the nine dimensional hypersurface should correspond with the feasible interactions across the interface, which may be located by use of a global optimisation algorithm. This optimisation problem may also be simplified by noting that the number of potential faces for growth will be very limited and so running a separate search for face pairs based on crystal criteria will be more efficient than searching over a large number of unfeasible faces, thus reducing the dimensionally of the optimisation problem. The potential faces for growth may be selected initially through consideration of experimental details (crystal morphology, habit modification studies) or by computation of the crystal morphology by habit prediction methods.
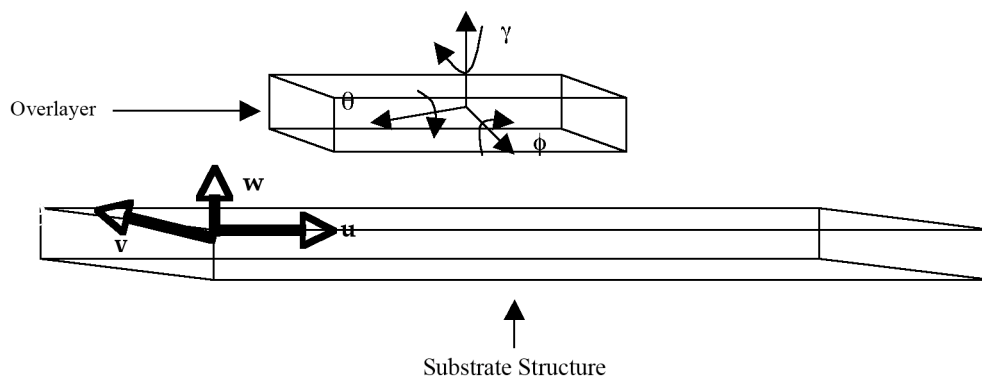
Figure 1. Representation of the formation of an interface between a substrate and an overlayer. The problem parameters (**u, v, w**, θ, ϕ, γ) are shown.

A number of global optimisation algorithms have been developed to solve a range of problem such as evolutionary algorithms, simulated annealing, tabu search and particle swarm [33-37]. Since the size of the optimisation problem prohibits the use of a systematic grid search of the hypersurface, the differential evolution algorithm was selected as the searching method for this work.

4. DIFFERENTIAL EVOLUTION

Differential Evolution (DE) is a recently developed evolutionary algorithm for the optimisation of real-valued problems. It was developed initially to solve the Chebychev polynomial fitting problem [38], though it has since been adapted to a broader range of optimisation problems; including digital filter design [39], modelling of disordered materials [40] and structure solution from powder X-ray diffraction data [41,42].

As with other evolutionary algorithms, DE operates on a population of trial solutions with new solutions being created through recombination and mutation. Each trial structure represents a potential solution to the problem to be solved and is represented as a vector of real numbers. Unlike traditional genetic algorithms the recombination and mutation steps are combined into a single step in the DE methodology. Initial implementations utilised a *uniform crossover* with fixed mutation (a) [38] however, due to problems with correlations between the control parameters [43], a modification based on *arithmetic crossover* was introduced (b). This arithmetic crossover form was utilised throughout the work reported here.

(a) Uniform Crossover

$$k = \text{int}(random(0,1) * D)$$

$$t_{i,k} = \begin{cases} P_{r_3,k} + F(P_{r_2,k} - P_{r_1,k}) \; if \; random(0,1) < C_R \, or \, j = k \\ P_{i,j} \qquad\qquad\qquad\qquad\qquad otherwise \end{cases}$$

$$k = (k+1) \bmod D$$

(b) Arithmetic Crossover

$$t_{i,j} = P_{i,j} + K(P_{r_3,j} - P_{i,j}) + F(P_{r_2,j} - P_{r_1,j})$$

where
N = population size,
D = Number of parameters to solve,
C_R = crossover probability
t_i=i^{th} trial structure to be generated

$r_1 \neq r_2 \neq r_3 \neq random(0,1)*N \neq i$
P_i = i^{th} member of DE population.
$i = 1 \ldots N, j = 1 \ldots D$

The DE operation is applied to each member of the DE population to create a new trial solution, which replaces the

parent in the population if it is a better solution than its parent. This process is repeated until a fixed number of generations have been processed or until the population converges upon a single solution. The DE algorithm is summarised below.

> Create a random initial population of size N
> Evaluate initial population
> Until G_{max} generations or convergence
>> For each member of population ($\underline{P_i}$)
>>> Generate a trial structure ($\underline{T_i}$)
>>> Check boundary conditions - adjust if necessary
>>> Evaluate trial solution (trial E)
>>> If trial $E \leq$ parent E
>>>> Replace $\underline{P_i}$ by $\underline{T_i}$

With a simplified method of creating trial structures and the use of a deterministic selection for the new population ensures that the DE method is simpler to implement than many traditional genetic algorithms, where a number of recombination and mutation steps are performed on randomly selected members of the population before the new population is probabilistically selected [44,45]. This simplification also results in fewer user-defined control parameters (population size N, maximum number of generations G_{max}, K and F) compared to other evolutionary algorithms and so greater understanding of the role each control parameter plays in controlling the dynamics of the search may be achieved. To this end a systematic study on these control parameters was performed.

An initial test system of benzamide as a substrate and benzoic acid as the overlayer was selected; since the crystal structures are very similar for both systems (**Figure 2** and Table 1). The similarities of the crystal structures is the basis for habit modification of benzamide by benzoic acid [46], which is a result of the benzoic acid blocking growth along the [010] axis of the benzamide. Consequently this face was selected as the initial face for these computational studies. A block of 3x3x1 unit cells of benzamide was generated as the substrate, while a single unit cell of benzoic acid was used as the overlayer. The force field detailed in No *et al* [47] was used to calculate the lattice energy of the generated structures with the partial charges calculated in Gaussian [48] at the HF3-21G level and a cut off value of 15Å.

Table 1
Unit cell parameters for benzoic acid and benzamide

Compound	a/Å	b/Å	c/Å	β/°	Volume/Å^3	Space Group
Benzoic Acid	5.4996	5.1283	21.95	97.37	613.95	P2$_1$/c
Benzamide	5.5657	5.0353	21.698	90.39	608.07	P2$_1$/c
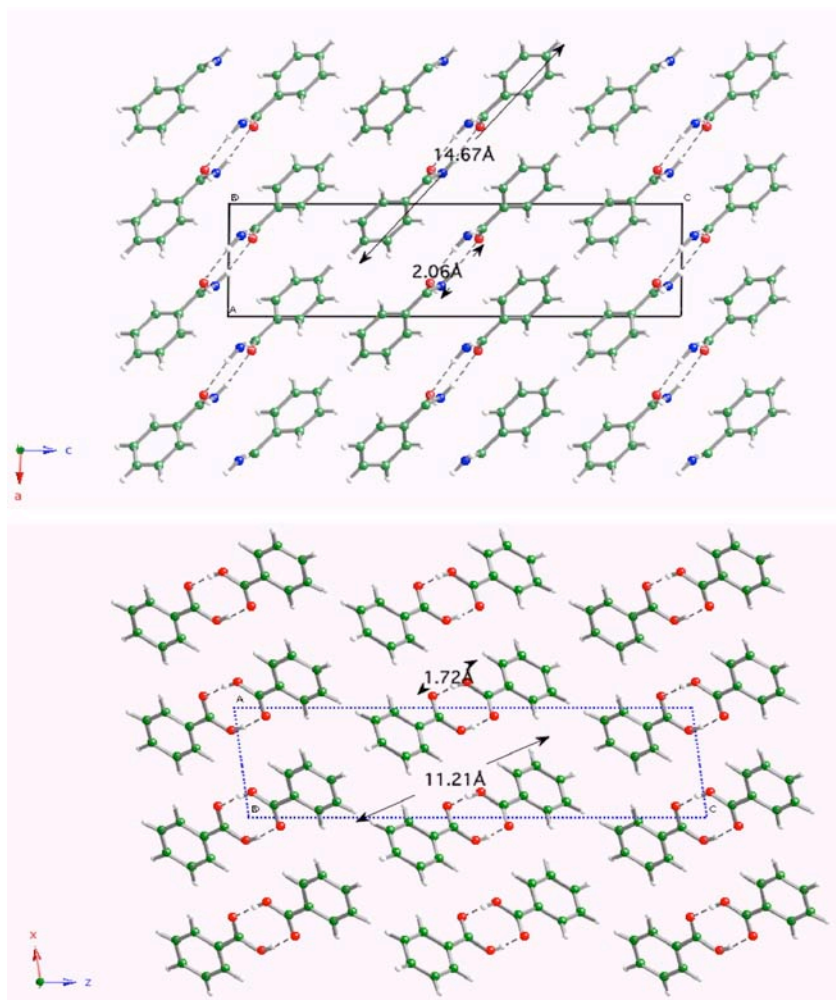
Figure 2. Crystal Packing for (a) benzamide (b) benzoic acid. Both systems are viewed along the b-axis and the lengths of the dimer unit and O…H hydrogen bond are indicated. C atoms are shown as green, N as blue, O as red and H as light grey.

The DE parameters K, F were varied from 0.1 to 1.0 in steps of 0.1 for population sizes $N = 30, 60$. Each of the DE calculations were performed for a maximum of 500 generations or until the difference between the mean energy and the best solution energy was less than 1×10^{-5} kcal mol^{-1} and convergence was assumed to have occurred. Ten individual DE calculations were performed for each set of parameters. The boundaries for each variable were [0, 360°] for θ, ϕ, γ, [7, -7Å] for u, v and [0, 360Å] for w. Generated values that exceeded a boundary were replaced by the median point between the parent and the exceeded boundary.

The mean energy located for each parameter set is shown in **Figure 3** for both population sizes. Similar features are shown in the surface for both experiments; a broad minima in the region bounded by 0.6, 1.0 for K and 0.5, 0.8 for F, a large maxima for high values of K with low values of F, while the rest of the surface is generally flat. A local maximum is also evident in the region bounded by 0.5 to 0.8 for K and 0.8 to 0.9 for F, which is greatly reduced by increasing the population size. Subsequent increases of the population size also leads to an increase in the size of the minima and reduction in the range of energies located.

Consequently, an effective search by the DE algorithm relies on balancing the convergence from the deterministic selection and the recombination with exploration by mutation through selection of K and F. These results show, for this problem, that small values of F with large values of K cannot balance the inward selection pressure and the population converges quickly into local minima, which is supported by consideration of the number of generations required for each DE calculation **(Figure 4)**. The majority of calculations ran until the maximum limit was reached

though a minima closely related to the maxima in the solution plot can clearly be seen. The lack of convergence is either due to very slow convergence or stagnation in the DE population. Stagnation is when the DE population, despite having diversity within the population, is unable to create any new trial structures that are superior to the old population. Small values of both K and F generally result in slow convergence, shown by the evolutionary progress plot (EPP) for K and F equal to 0.1 **(Figure 5a)**. In this case the DE performs as a population of random searches in the neighbourhood of each member of the initial population. The convergence properties for large values of K appear to form a similar pattern **(Figures 5b** and **5c)** with the value of F controlling the rate of convergence and so small values of F results in premature convergence while the large F values generally locate the global minima. The final case of median values for both K and F appear to result in stagnation **(Figure 5d)**, though often the population has predominately converged upon a solution and only a small percentage remain unique.

The process of stagnation, slow convergence and premature convergence all inhibit the ability of the DE calculation to perform successfully and so a further investigation into the dynamics of the DE population was undertaken, as this may help to optimise the selection of control parameters to the problem. To ensure effective searching, diversity must be maintained within the DE population during the search. To quantify this concept the population entropy as defined by Bessaou and Siarry [49] was evaluated for each population during each DE calculation. This measure is also an indicator of population stagnation, as these cases would exhibit a large stationary value for the population entropy, while the best and mean energies would remain constant.

The entropy (S_j^g) for the jth parameter in generation g is defined by equation 1.

$$S_j^g = \sum_{i=1}^{N} \sum_{k=i+1}^{N} -P_{i,k} \log(P_{i,k}) \tag{1}$$

$$P_{ik} = 1 - \frac{\left| x_{i,j}^g - x_{k,j}^g \right|}{Hi_j - Lo_j}$$

Where Hi_j = upper bound on the jth parameter
Lo_j = lower bound on the jth parameter.
$x_{i,j}$ = value of the jth parameter of the ith member of the population.

Thus, entropy is defined to be large when the values for the parameter differ widely and tends to zero as the values converge upon a single value. The mean entropy for the population can be determined by averaging over the entropies for each parameter. The entropies for four selected systems are included in the evolutionary progress plots given in **Figure 5**. Note that the entropy, unlike the best and mean energy, can increase during a DE calculation, indicating that the diversity of the population is increasing. Consideration of the entropy change during the DE calculation can therefore be used as an indicator of the variation of diversity within the population and so the rate of convergence, therefore it could be used to control the selection of K and F during the DE calculation, thus optimising the DE performance.
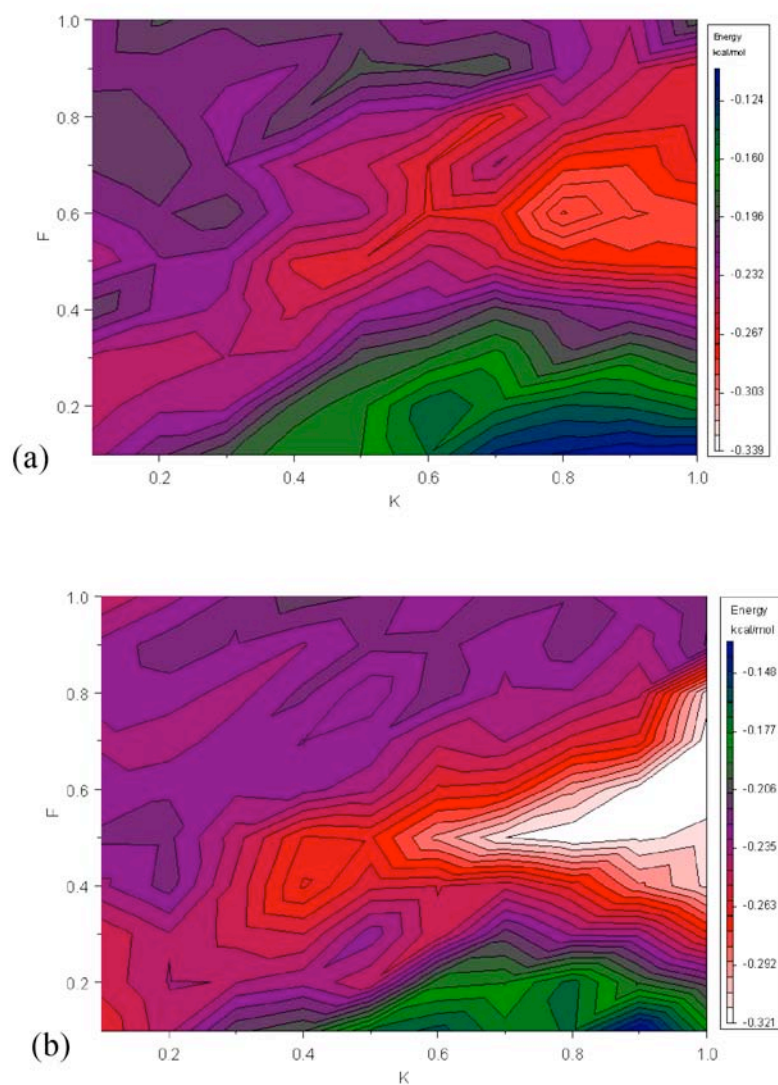
Figure 3. Contour Plots of the mean energy located by a given set of K, F over 10 DE calculations. (a) Calculation with N = 30 (b) Calculation with N = 60.
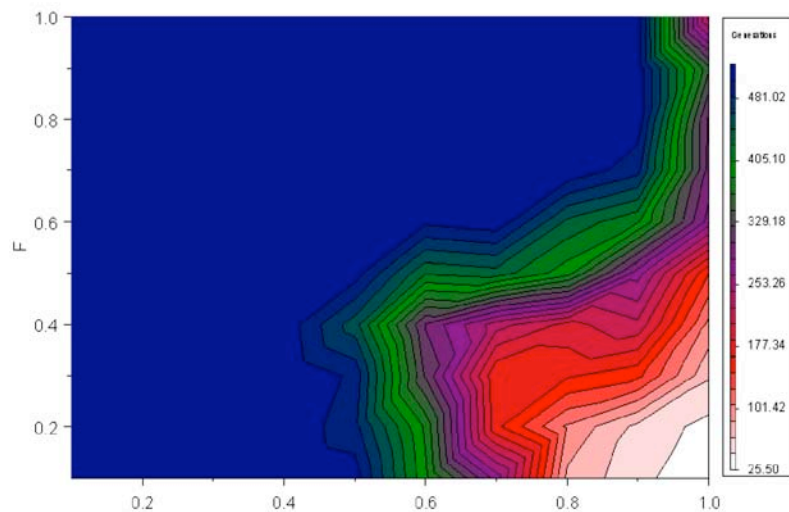
Figure 4. The mean number of generations performed for each set of K and F for population size 30.
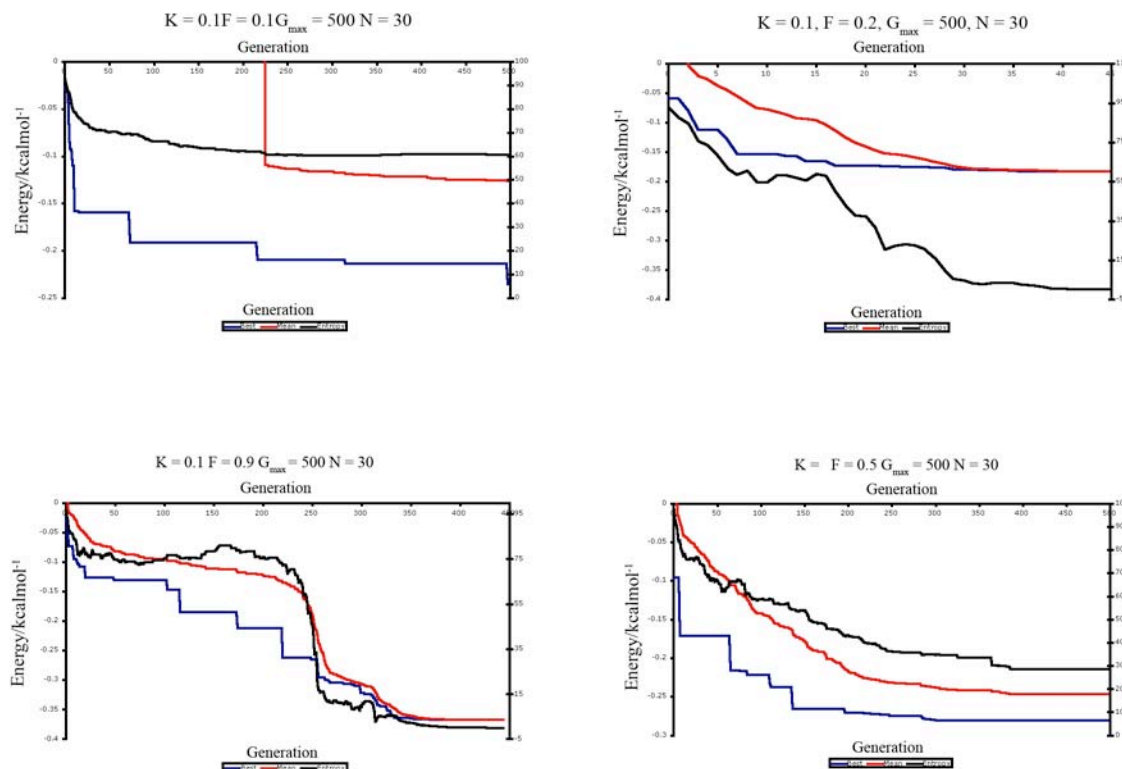
Figure 5. Evolutionary progress plots for four randomly selected DE calculations. In all cases $G_{max} = 500$ and N = 30. For (a) K = 0.1, F = 0.1 (b) K = 1.0, F = 0.2, (c) K = 1.0, F = 0.9, (d) K = 0.5, F = 0.5 The blue line is the energy of the lowest structure in the population, the red line the mean energy of population and the black line the entropy of the population.

Another problem with identifying stagnation is that the selection of population members for mutation and recombination are randomly selected and so a favourable selection may not have been made in the time the DE was run. To ensure that the DE calculations were allowed sufficient time to search, an investigation in the effect of increasing the value of G_{max} to 5000 was undertaken with the parameters: K equal to 1.0, F varied from 0.1 to 1.0 and N set to 30, 60 and 90. Ten DE calculations for each parameter set were performed and the mean number of generations required to converge calculated **(Figure 6)**. This shows that longer convergence times are achieved with both larger populations and larger values of F, except in the case of K = F where convergence is enhanced. This can be explained by consideration of the DE method of generating trial structure, when K = F this can be rearranged to be

$$t_{i,j} = (1-K)P_{i,j} + K(P_{r_3,j} + P_{r_2,j} - P_{r_1,j})$$
(2)

so the values of r_2 and r_3 are interchangeable, therefore the number of potential new trial structures is reduced. This is highlighted by performing the same DE calculations with K set to 0.99 **(Figure 7)**, again there is a drop in number of generations required when F is 1.0 but it is much smaller than when K is also 1.
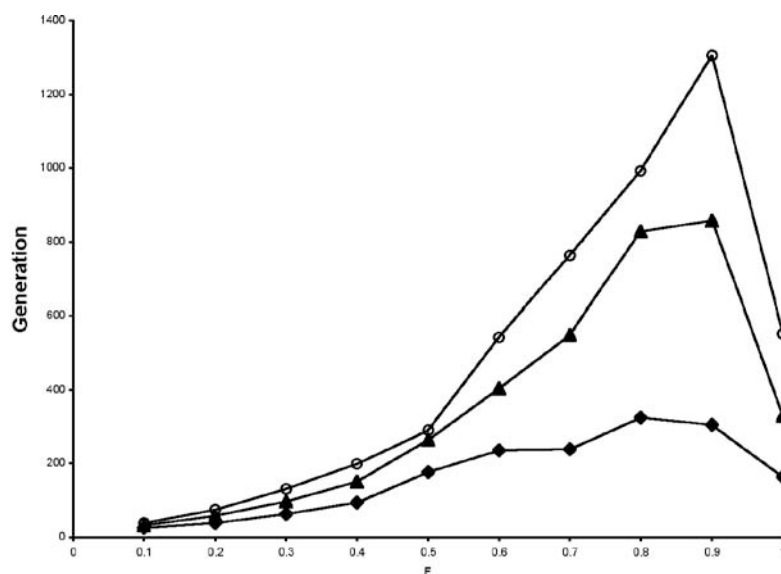
Figure 6. The mean number of generations required for convergence for increasing population sizes, 30 (diamonds), 60 (triangles), 90 (open circles). The DE parameters are $K = 1.0$, $G_{max} = 5000$.
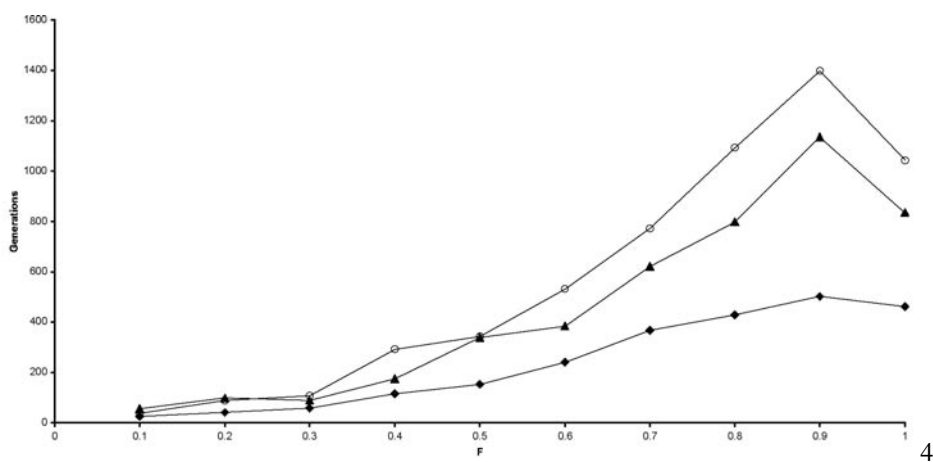
Figure 7. The mean number of generations required for convergence for increasing population sizes, 30 (diamonds), 60 (triangles), 90 (open circles). The DE parameters are $K = 0.99$, $G_{max} = 5000$.

5. COMPUTATIONAL CRYSTAL PACKINGS

The interface packings obtained from the DE calculations show a number of similarities within a small range of energies (Appendix 1), though due to the distance cut off in the energy calculation many of the lowest energy structures favoured overlayers positioned at the edges of the substrate **(Figure 8a)**. This is also enhanced by the boundary reset function used, which asymptotically approaches the boundary values during the calculation. Initial investigations into the application of a periodic boundary reset results in a lower mean energy located but with more of the solutions located over the substrate (Appendix 2). Analysis of the crystal packings for the remaining low energy solutions **(Figure 8b)** with the crystal faces of the component systems shows that the {100} benzoic acid face is interacting the {010} face of the benzamide and clearly shows a hydrogen boding interaction between the two components of the system. The crystal structures and composite packings were visualised using Cerius^2 and CrystalMaker [50,51].
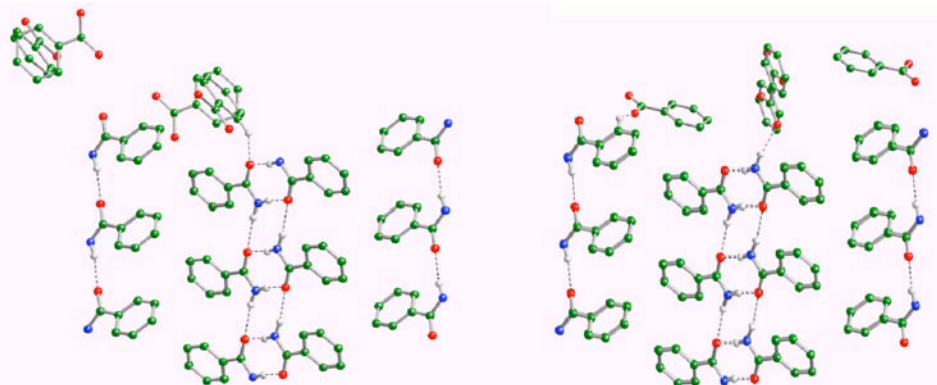
Figure 8. Crystal packings for a low energy solutions of the DE calculation. (a) The lowest energy solution located (E = -0.4182 kcalmol^{-1}). (b) A solution of low energy (E = -0.372 kcalmol^{-1}). C atoms are shown as green, N as blue, O as red and H as light grey. Only those Hs involved in Hydrogen bonding are shown.

6. EXPERIMENTAL RESULTS

The synthesis of composite benzoic acid and benzamide crystal was undertaken. Both samples were purchased from Aldrich. Seed crystals of benzoic acid were obtained through slow cooling of a saturated aqueous solution, which resulted in thin white plate-like crystals [52]. The seed crystals were then suspended into a saturated aqueous solution of benzoic acid and benzamide, which was slowly cooled. After three days the seed crystals were removed and inspected by polarizing optical microscopy, which indicated the existence of interfacial layer **(Figure 9)**. The expected binding face from the computational studies, {100}, exists as a small facet on the side of the crystal and so the potential level of binding may be small. Initial Raman spectroscopy studies, appear to suggest this since similar spectrums are obtained either side of the interface, though if only low levels of benzamide exist then the signal may be too weak to be seen. Therefore further work is required to fully characterise and validate the computational results, and further investigation into the manipulation of the crystal growth conditions to improve the quality of the material obtained is also required, for example habit modification of the seed crystals to enlarge the binding faces, variation of the temperature, rate of cooling and pH of the solutions during crystal growth.
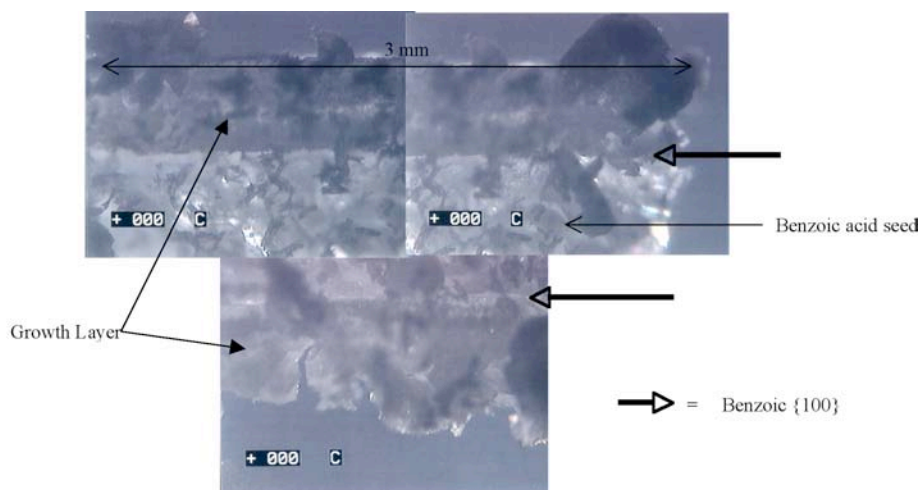
Figure 9. Cross-polarized microscopy image of the grown composite crystal.

7. CONCLUSIONS

In this paper we have demonstrated the application of global optimisation methods to the problem of designing composite molecular materials. The differential evolution algorithm has been shown to offer robust searching of minima, yet relatively simple to implement. The reduced number of control parameters associated with the method, means that optimisation of the search process is computational feasible. Initial investigation in the role of the control parameters K and F appears to show that a relatively small of values is required for optimal performance and these values are independent of the population size selected. Further investigations into the remaining parameters, population size (N) and the number of generation the calculation is run (G_{max}), need to be undertaken. The concept of the entropy of DE population offers a valuable tool in the understanding of the dynamics of the DE performance and consideration of the level of entropy during the calculation will improve the performance of the DE algorithm. Further experimental work is required to fully validate the computational results obtained and number of potential optimisations of the experimental set up are to be undertaken.

8. ACKNOWLEDGEMENTS

9. REFERENCES

[1]   P. Somasundaran & A. Hubbard (Eds.), *Encyclopedia of Surface and Colloid Science*, (Dekker, 2002)

[2]   W. Jones & C. N. R. Rao (Eds.), *Supramolecular Organization and Materials Design*, (Cambridge University Press, 2001).

[3]   C. T. Vogelson, *Modern Drug Delivery*, **4**, (2001), 49.

[4]   J. Yang, J. M. F. Ferreira, S. Mei, W. Weng, *Composite Fine Particles* in *Encyclopedia of Surface and Colloid Science*, Eds, P. Somasundaran & A. Hubbard, (Dekker, 2002).

[5]   J.M. Lehn, *Angew. Chem. Int. Ed.*, **27**, (1988), 89.

[6]   A.D. Burrows, C-W. Chen, M. Chewophry, J.E. McGrady, D. Micheal, P. Mingos, *Chemical Reviews*, **24**, (1995), 329.

[7]   L. Leiserowitz, *Industrial Crystallization*, (Elsevier, 1991).

[8]   R.J. Davey, L. Williams-Seton, H. F. Lieberman, N. Blagden, *Nature*, 402, (1999), 797.

[9]   N. Blagden, R.J. Davey, *Chemistry in Britain*, March, (1999), 44.

[10]   L. Leiserowitz, L.J.W. Shimon, M. Vaide, F. Frolow, M. Lahav, *Faraday Dis.*, 95, (1993), 307.

[11]   L. Leiserowitz in: *The Lock and Key Principle*, ed. J.P. Behr, (Wiley, 1994).

[12]   B.R. Heywood and S. Mann, *J. Am. Chem. Soc.*, **114**, (1992), 4681.

[13]   R.J. Davey, B.R. Heywood, *Particle Tech. Forum, A.M.I. Ch Eng*, **1**, (1994), 362.

[14]   M. Gebhart, *Crystal Growth: An Introduction*, (Wiley, 1973).

[15]   H. E. Buckley, *Crystal Growth*, (Wiley, 1951).

[16]   T. V. Barker, *Trans. Chem. Soc. London*, **89** (1906), 1120.

[17]   C.W. Bunn, *Proceedings of the Royal Society,* **141**, (1933), 567.

[18]   O. Rudgiger, *Ann. Physik,* **30,** (1937), 505.

[19]   G.H. van der Merve, *Surf. Sc.*, **31**, (1972), 1988.

[20]   M. J. Stowell, *Thin Films*, **1**, (1968), 55.

[21]   R. Kern, *Current Topics in Material Science*, **12**, (1985), 81.

[22]   R. Kern, *NATO ASI series B, Physics*, **201**, (1987), 143.

[23]   G. B. Stringfellow, *Advanced Crystal Growth*, (Elsevier, 1988).

[24]   W.K. Burton, N. Cabera, F. C. Frank, *Trans. Roy. Soc*, **A243**, (1951), 299.

[25]   J. Otsaki, T. Oga, S-H. Lee, *Chem. Comm.*, **21**, (1995), 2193.

[26]   N. Aleksandra in*: Epitaxi-Endotaxi*, ed., H.G. Scheider, (VEB, 1968)

[27]   E. Bauer, *Z. Krist.,* **110**, (1958), 372.

[28]   S. Feng, T. Bein, *Science*, **256**, (1994), 1839.

[29]   S. J. Bonafede, M.D. Ward, *J. Am. Chem. Soc*, **117**, (1995), 7853.

[30]   C. A. Mitchell, L. Yu, M.D. Ward, *J. Am. Chem. Soc.*, **123**, (2001), 10830.

[31]   D.E. Hookes, T. Fritz, M.D. Ward, *Adv. Mater.*, **13**, (2001), 227.

[32]   H.F. Lieberman, L. Williams, R.J. Davey, R.G. Pritchard, *J. Am. Chem. Soc*, **120**, (1998), 686.

[33]   A. P. Engelbrecht, *Computational Intelligence: An Introduction*, (Wiley, 2002)

[34]   S. Kirkpatrick, C.D. Gelatt, H. P. Vecchi, *Science*, **220**, (1983), 671.

[35]   J. H. Holland, *Adaptation in Natural and Artificial Systems*, (University of Michigan Press, 1975)

[36]   F. Glover, *ORSA Journal of Computing*, **1**, (1989), 190.

[37]   J. Kennedy and R. C. Eberhart in: *New Ideas in Optimisation*, eds. D. Corne, M. Dorigo and F. Glover (McGraw-Hill, 1999), p 379.

[38]   R. Storn and P. V. Price, *Journal of Global Optimisation*, **11** (1997), 341.

[39]   R. Storn in: *New Ideas in Optimisation*, eds. D. Corne, M. Dorigo and F. Glover (McGraw-Hill, 1999), p 108.

[40]   T. Weber, H-B. Bürgi, *Acta Cryst.*, **A58**, (2002), 536.

[41]   C.C. Seaton and M. Tremayne, *Chem. Comm.*, **8**, (2002), 880.

[42]   M. Tremayne, C.C. Seaton, C. Glidewell, *Acta Cryst.*, **B58**, (2002), 823.

[43]   P. V. Price in: *New Ideas in Optimisation*, eds. D. Corne, M. Dorigo and F. Glover (McGraw-Hill, 1999), 80.

[44]   D. L. Goldberg, *Genetic Algorithms in Search, Optimization and Machine Learning,* (Addison-Wesley, 1989).

[45]   T. Bäck, D.B. Fogel, T. Michalewicz (Ed.), *Evolutionary Computation 1: Basic Algorithms and Operators*, (Institute of Physics Publishing, 2000).

[46]   F. Vögtle, *Supramolecular Chemistry*, (Wiley, 1991).

[47]   K. T. No, O. Y. Kwon, S. Y. Kim, K. H. Cho, C. N. Yoon, Y. K. Kang, K. D. Gibson, M. S. Jhon, H. A. Scheraga, *J. Phys. Chem.*, **99**, (1995), 13019.

   [48]   M. J. Frisch, G. W. Trucks, H. B. Schlegel, G. E. Scuseria, M. A. Robb, J. R. Cheeseman, J. A. Montgomery, Jr., T. Vreven, K. N. Kudin, J. C. Burant, J. M. Millam, S. S. Iyengar, J. Tomasi, V. Barone, B. Mennucci, M. Cossi, G. Scalmani, N. Rega, G. A. Petersson, H. Nakatsuji, M. Hada, M. Ehara, K. Toyota, R. Fukuda, J. Hasegawa, M. Ishida, T. Nakajima, Y. Honda, O. Kitao, H. Nakai, M. Klene, X. Li, J. E. Knox, H. P. Hratchian, J. B. Cross, C. Adamo, J. Jaramillo, R. Gomperts, R. E. Stratmann, O. Yazyev, A. J. Austin, R. Cammi, C. Pomelli, J. W. Ochterski, P. Y. Ayala, K. Morokuma, G. A. Voth, P. Salvador, J. J. Dannenberg, V. G. Zakrzewski, S. Dapprich, A. D. Daniels, M. C. Strain, O. Farkas, D. K. Malick, A. D. Rabuck, K. Raghavachari, J. B. Foresman, J. V. Ortiz, Q. Cui, A. G. Baboul, S. Clifford, J. Cioslowski, B. B. Stefanov, G. Liu, A. Liashenko, P. Piskorz, I. Komaromi, R. L. Martin, D. J. Fox, T. Keith, M. A. Al-Laham, C. Y. Peng, A. Nanayakkara, M. Challacombe, P. M. W. Gill, B. Johnson, W. Chen, M. W. Wong, C. Gonzalez, and J. A. Pople, *Gaussian 03, Revision 6.0*, (Gaussian, Inc., Pittsburgh PA, 2003).

[49]   M. Bessaou and P. Siarry, *Adv. Eng. Soft.*, **32** (2001), 363.

[50]   *Cerius², Version 4.6*, (Accelrys Inc., Cambridge, UK,)

[51]   D. Palmer, *CrystalMaker, Version 6.3.6*, (CrystalMaker Software, Oxford, UK, 2003)

[52]   X. Holmbäck and Å.C. Ramuson, *J. Cryst. Grow.*, **198/199**, (1999), 780.

10. APPENDIX 1

The energies and model parameters of the fifteen lowest energy solutions located by the DE calculations with control parameters: $G_{max} = 500$, $N = 30$ using the asymmetric boundary reset.

θ	φ	γ	u	v	w	Energy	K	F
43.1139	181.4188	124.2822	6.9983	-6.9988	8.4653	-0.4182	0.7	0.8
223.3406	0.0278	303.0045	6.9729	-6.9755	8.4996	-0.4132	0.8	0.6
224.0255	0.4766	302.5999	6.9763	-6.9823	8.5321	-0.4113	1	0.6
222.2705	0.1511	302.0412	6.9751	-6.9939	8.3633	-0.4068	0.9	0.7
338.2288	346.7209	69.844	-3.7514	3.0639	8.3048	-0.3723	0.9	0.6
140.8144	200.8251	242.1966	-1.9241	-2.2341	8.2951	-0.3668	1	0.9
181.0654	185.089	251.1345	-3.2224	4.7522	8.3529	-0.3652	0.9	0.7
317.1483	358.9626	76.5565	-0.7146	-2.2112	8.9263	-0.361	1	0.7
157.8049	190.9717	252.6098	-3.653	3.2946	8.4341	-0.3589	0.5	0.7
183.9766	183.7777	248.8152	-3.0094	4.5959	8.5406	-0.3579	0.7	0.7
61.633	197.9187	130.1989	5.6925	-3.3446	9.3372	-0.3579	1	0.9
219.8356	2.4319	300.8803	6.7132	-6.9462	8.5025	-0.3557	0.6	0.7
316.5667	1.156	78.1893	-0.4703	-2.1489	8.9979	-0.354	0.9	0.5
357.5303	351.2201	79.4851	-3.3438	5.3436	8.2397	-0.3535	0.6	0.7
61.4582	196.6407	130.8331	5.7922	-3.2436	9.475	-0.3535	0.9	0.9

11. APPENDIX 2

The energies and model parameters of the fifteen lowest energy solutions located by the DE calculations with control parameters: $G_{max} = 1000$, $N = 30$ using a periodic boundary reset.

θ	φ	γ	u	v	w	Energy	K	F
158.238	193.2731	249.8365	-3.7512	3.0644	8.3049	-0.3723	0.9	0.8
186.0786	182.1966	239.7925	-2.8189	4.1042	8.5862	-0.3562	0.8	0.5
178.1329	188.4357	258.1398	-3.2619	5.4611	8.0162	-0.3482	0.9	0.9
139.9251	176.6658	257.9797	-0.9926	-2.3955	9.1961	-0.3412	0.4	0.5
222.8271	161.9671	51.6002	1.9904	-0.0225	9.4944	-0.3315	0.9	0.7
42.4558	18.5218	230.9883	1.9809	-0.0441	9.5115	-0.3307	0.9	0.6
141.3574	174.3229	259.808	-1.0084	-2.5184	9.3674	-0.3299	0.5	0.1
223.2379	161.4847	51.674	2.0183	0.0224	9.5293	-0.3295	0.9	0.5
212.5143	7.1264	300.1183	6.9599	-6.5524	8.7754	-0.3293	0.9	0.9
160.4309	194.811	257.4507	-3.8274	3.6735	8.599	-0.3287	0.6	0.6
222.5658	162.295	49.9119	1.961	-0.1307	9.6029	-0.3275	0.9	0.7
223.5758	162.3078	50.956	2.0199	-0.0594	9.6096	-0.3271	0.9	0.7
141.1663	177.8432	255.4193	-1.3296	-2.6766	9.3917	-0.3238	0.4	0.5
138.9523	182.8565	253.7138	-1.0847	-2.6969	9.2414	-0.3227	0.2	0.4
167.7148	194.7255	259.3945	-4.0432	4.5612	8.6741	-0.3197	0.4	0.6

MOLECULAR TECTONICS: DESIGN OF 1-D COORDINATION NETWORKS BASED ON RIGID METACYCLOPHANE BACKBONE

Cédric Klein, Ernest Graf, Mir Wais Hosseini and Nathalie Kyritsakas-Gruber
Laboratoire de Chimie de Coordination Organique, UMR-CNRS 7140 (Tectonique Moléculaire du Solide), University Louis Pasteur, Inst Le Bel, 4, rue Blaise Pascal, 67000 Strasbourg France
hosseini@chimie.u-strasbg.fr

1. ABSTRACT

Upon combining the rigid bis monodentate organic tectons **2** and **3** based on the [1.1.1.1] paracyclophane backbone and possessing a « V-type » shape with silver cation and mercury chloride, 1-D coordination networks were generated and structurally characterized by X-ray diffraction methods on single crystals. Whereas the tecton **2** leads in the presence of $HgCl_2$ to the formation of a 1-D network with « zigzag » geometry, the combination of the tecton **3** with Ag^+ generates a 1-D network which may be described as fused metallamacrocycles.

2. INTRODUCTION

Molecular tectonics [1-3] deals with the generation of molecular networks in the solid state. This approach is based on iterative molecular recognition processes [4] using molecular building block called tectons [2]. Molecular networks are in principle infinite structures obtained upon self-assembly of complementary tectons capable of mutual recognition. These types of molecular architectures possess translational symmetry and are defined by their dimensionality, their geometry and the nature of interactions involved in the recognition event. The dimensionality of molecular networks is defined by the number of translations operating on the recognition patterns formed between complementary or self-complementary tectons. Thus, 1-, 2- and 3-D networks are generated upon one, two and three translations of recognition patterns respectively. Within each dimensional category, molecular networks may be further described by their geometry. For 1-D networks one may define different geometries such as linear, stair type, "zigzag" type and helical. 2-D networks may be of the flat or puckered type. Finally, 3-D networks may be of the cubic or diamondoid or gyroid type. Dealing with the nature of interactions involved in the molecular recognition processes, in principle any type of reversible intermolecular interactions may be used. In particular, inclusion molecular networks based mainly on Van der Waals interactions [5], H-bonded molecular networks based on H-bonds [6] or a combination of H-bonds and charge-charge electrostatic interactions (charge-assisted H-bond) [7] and finally coordination networks based on coordination bonds between organic and metallic tectons [8] have been reported.

In this contribution, we will focus on the design of rigid organic coordinating tectons and on the formation of coordination networks upon their combination with metallic tectons.

3. RATIONAL

3.1 Design of Organic Tectons

Coordination networks or polymers are infinite molecular assemblies generated upon mutual bridging between organic coordinating tectons and metallic centers. Continuing our effort in this area [9], we designed the rigid tectons 2 and 3 that are of the bis monodentate type (Scheme 1) [10]. Both tectons 2 and 3 are based on the [1.1.1.1]metacyclophane backbone 1 [11] which adopts the 1,3-alternate conformation over a wide range of temperature (Scheme 2 A) [12]. A further interesting feature associated with this backbone is its rigidity which allows to set-up 1-4 coordinating sites upon further functionalization [13]. Both tectons **2** and **3** [10] bearing two coordination sites as well as tectons **4** and **5** [14] bearing four coordination sites have been designed and prepared previously. Two other tectons based on the

metacyclophane backbone bearing two chelating units such as quinoline or 2,2'-bipyridine have been also reported [15].
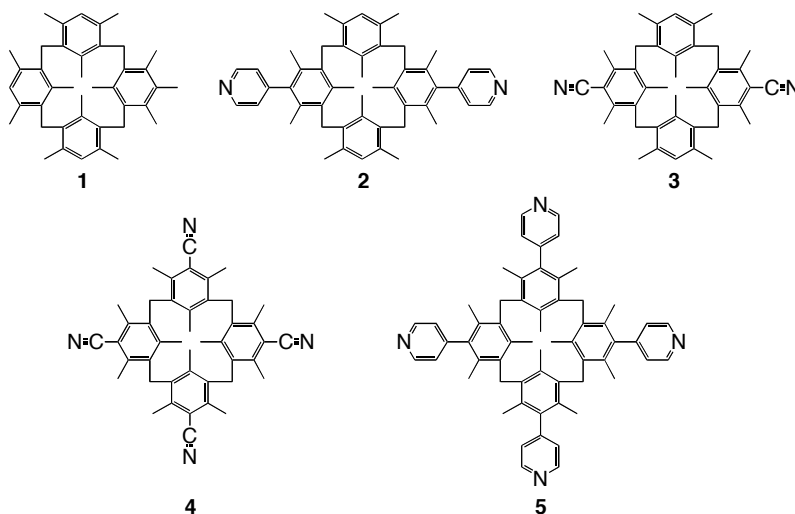

Scheme 1.
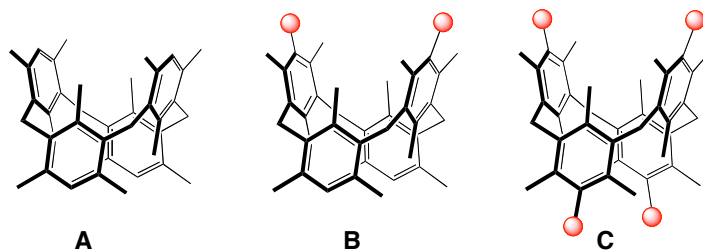
Scheme 2.

Whereas for both tectons **2** and **3** the two coordination sites (nitrile for **2** and pyridyle for **3**) are located at the extremities of a "V" **(Scheme 2 B)**, for the other two tetra functionalized tectons **4** and **5**, the coordinating site occupy the apices of a tetrahedron **(Scheme 2 C)**. We have previously demonstrated that the compounds **4** and **5** may behave as tetrakis monodentate tectons. Indeed, whereas a combination of **4** with silver cation leads to the formation of a 1-D tubular coordination network [16], the combination of **5** again with silver cation generates a doubly interpenetrated 3-D diamandoid type coordination network [17]. For both tectons **2** and **3**, depending on the nature of the metal centre used, one may expect either discrete entities such as metallamacrocycles **(Figure 1a)** or infinite coordination networks (**Figure 1b** and **c**). We have previously shown that the compound **2** in the presence of zinc halides, a neutral metallatecton posessing a tetrahedral coordination geometry and offering two free coordination sites, behaves as a bis monodentate ligand and forms metallamacrocycles of the type shown on **Figure 1a** [18]. Dealing with the infinite 1-D networks, one may envisage the formation of two types of connectivity. Whereas in the case of metallatectons offering two available coordination sites, one would expect the formation of 1-D networks of the type b **(Figure 1)**, for metallatectons offering four free coordination sites, one would envisage the formation of networks of the type c **(Figure 1)**. The latter case may be regarded as fused metallamacrocycles.
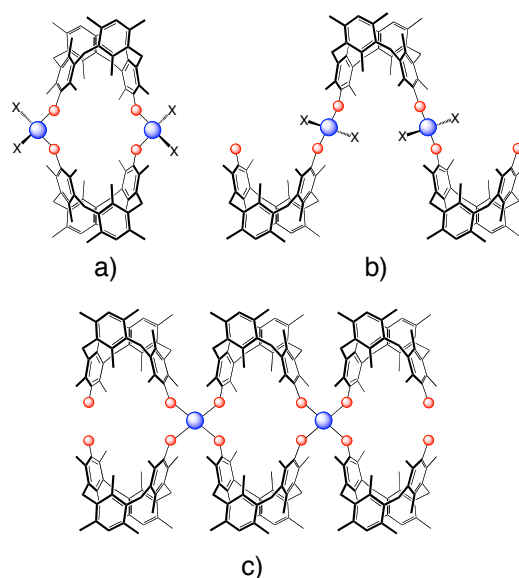
Figure 1. Schematic representation of combinations of a bis-monodentate organic tecton possessing a V-shape such as compounds **2** and **3** with metallic centers with coordination number 4 and adopting tetrahedral coordination geometry. A) discrete metallamacrocycle, b) and c) infinite 1-D coordination networks.

3.2 Choice of Metallic Tectons

As stated above, coordination networks are generated upon combining organic tectons with metallic centers. Thus, for their design, the nature of the metal complex used is of prime importance. First of all, since coordination networks are formed under self-assembly conditions, the interaction between the metal and the coordinating sites of the organic tecton must be reversible. For the choice of the metal cation, one may either use weakly coordinating anions such as SbF_6, PF_6 etc. or strongly coordinating anionic ligands such as halides. Whereas for the first case, all coordination sites of the metal would be available for the generation of the network, in the second case, some of the coordination sites will be occupied by the anionic ligands and thus only a restricted number of coordination sites may be available for the formation of the network. Silver cation is certainly one of the most used metal cation for the formation of coordination networks. The reason for that is related to his rather loose coordination geometry (linear, trigonal, T type, tetrahedral) and coordination number (2, 3, 4) requirements. For the same reasons, mercury dication is another interesting candidate. In particular, mercury halides may be used as neutral metallatectons. We have previously demonstrated the ability of mercury halides to generate discrete metallamacrocycles [19] as well as 1-D helical [20-21], linear [22-23] as well as 2-D [23] coordination networks.

4. EXPERIMENTAL

4.1 Synthesis and Crystallization

[**2** • $HgCl_2$]$_n$: Suitable colorless crystals for X-ray diffraction analysis on single crystal were obtained after 7 days in the dark and at room temperature in a crystallizing tube (L = 15 cm, Ø = 0.4 cm) upon slow diffusion of a EtOH solution (1.5 ml) of $HgCl_2$ (5 mg, 0.018 mmol) into a 1,1,2,2-tetrachloroethane solution (0.5 ml) of compound **2** (5 mg, 0.0073 mmol).

[**3** • $AgSbF_6$]$_n$: Suitable colorless crystals for X-ray diffraction analysis on single crystal were obtained after 4 days in the dark and at room temperature in a crystallizing tube (L = 15 cm, Ø = 0.4 cm) upon slow diffusion of a EtOH solution (1.5 ml) of $AgSbF_6$ (3 mg, 0.0087 mmol) into a chlorobenzene solution (0.5 ml) of compound **3** (3 mg, 0.0052 mmol).

5. X-RAY CRYSTALLOGRAPHY

X-ray diffraction data collection was carried out on a Kappa CCD diffractometer equipped with an Oxford Cryosystem liquid N_2 device, using graphite-monochromated Mo-Kα radiation. For all structures, diffraction data were corrected for absorption and analyzed using OpenMolen package [24]. All non-H atoms were refined anisotropically. CCDC 245945 and 245946 contains the supplementary crystallographic data for this paper. These data can be obtained free of charge at www.ccdc.cam.ac.uk/conts/retrieving.html or from the Cambridge Crystallographic data Center, 12 Union Road, Cambridge CB2 1EZ, UK; Fax: (Internat.) +44-1223/336-033; E-mail: deposit@ccdc.cam.ac.uk.

Crystallographic data for (**2**-HgCl$_2$)$_n$: (colorless crystals, 173 K): $C_{50}H_{54}N_2Hg$ $Cl_2 \cdot C_2H_2Cl_4$ $M = 1122.35$, monoclinic, $a = 18.0016(4)$, $b = 20.6568(5)$, $c = 13.0728(4)$ Å, $\beta = 109.488(5)$, $U = 4582.7(2)$ Å^3, space group $C2/c$, $Z = 4$, $Dc = 1.63$ g cm^{-3}; $\mu = 3.748$ mm^{-1}, 3341 data with I > 3σ(I), $R = 0.038$, $Rw = 0.074$.

Crystallographic data for (**3**-AgSbF$_6$)$_n$: (colourless crystals, 173 K): $C_{84}H_{92}N_4Ag \cdot SbF_6 \cdot 2H_2O \cdot C_2H_5OH$, $M = 1583.41$, monoclinic, $a = 26.1634(4)$, $b = 22.3454(4)$, $c = 16.7789(3)$ Å, $\beta = 120.396(5)$, $U = 8461.2(2)$ Å^3, space group $C2/c$, $Z = 4$, $Dc = 1.24$ g cm^{-3}; $\mu = 0.611$ mm^{-1}, 4810 data with I > 3σ(I), $R = 0.086$, $Rw = 0.118$.

6. RESULTS AND DISCUSSION

Upon slow diffusion, in the dark and at room temperature, of an EtOH solution of HgCl$_2$ into a 1,1,2,2-tetrachloroethane solution containing the tecton **2**, colorless crystals were obtained after several days. Structural analysis by X-Ray diffraction on single crystals (monoclinic, space group C 2/c) revealed that the solid was composed of the tecton **2**, HgCl$_2$ and 1 molecule of 1,1,2,2-tetrachloroethane.

As expected from the design, the combination of neutral tecton **2** and neutral HgCl$_2$ complex leads to the formation of a neutral "zigzag" type 1-D coordination network of the type b **(Figure 1b)**. The network is generated by mutual bridging between the organic tectons **2** and the metallatectons HgCl$_2$ **(Figure 2a)**.

a)   b)
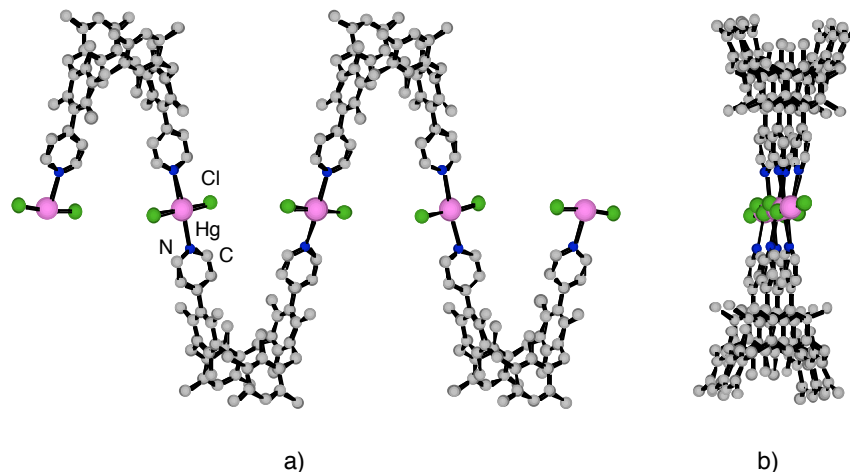
Figure 2. A portion of the X-ray structure showing the cationic coordination network formed between **2** and HgCl$_2$. a) View perpendicular to the axis of the network. b) View along the axis of the network. For clarity, H atoms and solvent molecules (1,1,2,2-tetrachloroethane) are omitted.

The organic tecton adopts the expected 1,3-alternate conformation imposing thus the localization of the two coordinating pyridyl groups on the same face of the backbone and affording a bis monodentate ligand possessing a "V-shape". The two pyridine units are tilted with respect to the phenyle moieties of **2** (CCCC dihedral angles of -89.0° and -90.3°). For the mercury (II) centers the coordination number is four and the

coordination sphere is composed of two Cl$^-$ anions (d$_{Hg-Cl}$ = 2.327 Å) and two N atoms of two pyridine units belonging to two consecutive tectons **2** (d$_{Hg-Cl}$= 2.606 Å). The coordination geometry around the metal centre is square planar (both ClHgCl and NHgN angles are 180°). The network may be regarded as an aligned arrangement of mercury cations with 9.19 Å distance between consecutive metal centers interconnected by tectons **2 (Figure 2b)**. The packing of the 1-D networks leads to the presence of cavities which are occupied by solvent molecules with no specific interactions with the networks.

Upon slow diffusion, in the dark and at room temperature, of an EtOH solution of Ag(SbF$_6$) into a chlorobenzene solution containing the tecton **3**, colorless crystalline material was obtained after few days. X-Ray diffraction on single crystals (monoclinic, space group C 2/c) revealed that in addition to **3**, Ag$^+$, and SbF$_6^-$ anions, 2 molecules of H$_6$O and 1 molecule of EtOH are present in the lattice.
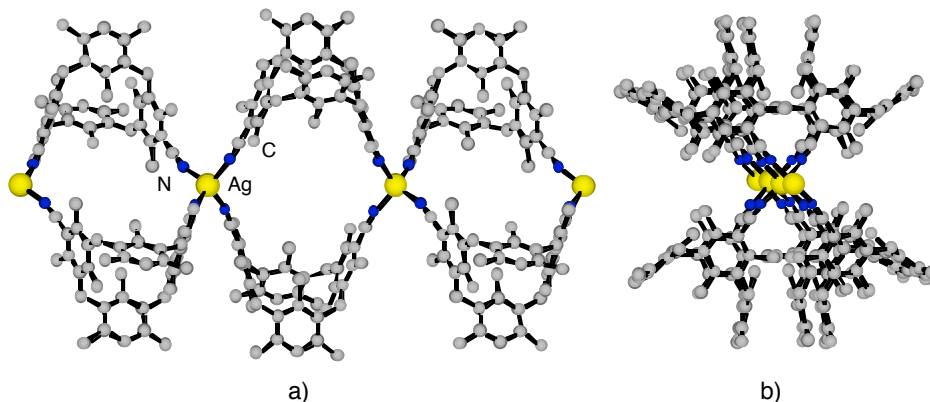
Figure 3. A portion of the X-ray structure showing the cationic coordination network formed between **3** and silver cations. a) View perpendicular to the axis of the network. b) View along the axis of the network. For clarity, H atoms, solvent molecules (chlorobenzene, ethanol) and SbF$_6^-$ anions are omitted.

As expected from the design, the organic tecton **3** indeed adopts the V-shape conformation thus leading to the localization of the two nitrile groups (dC-N = 1.15 and 1.16 Å) on the same face of the molecule. Tectons **3** are bridged by silver cations leading thus to a cationic 1-D coordination network **(Figure 3)**. The Ag$^+$ cation is surrounded by four nitrogen atoms belonging to four different tectons **3** (d$_{Ag-N}$) varying between 2.18 Å and 2.24 Å) and adopts a distorted tetrahedral coordination geometry with and NAgN angle varying between 104.4° and 115.0° **(Figure 3a)**. Within the 1-D network, the cations are arranged in a linear fashion **(Figure 3b)** with a distance of 11.42 Å between consecutive silver cations. The parallel packing of consecutive networks generates space which are occupied by anions (SbF$_6^-$) and solvent molecules (H$_2$O and EtOH). No specific interactions between the cationic networks and anions or solvent molecules can be spotted.

The 1-D network formed between **3** and Ag$^+$ cation may be described as fused metallamacrocycles **(Figure 1 c)**.

7. CONCLUSIONS

The combination of the rigid bis monodentate tectons **2** and **3** possessing a "V-shape" with metal centers leads as expected to the formation of 1-D coordination networks. The type of network generated depends on the nature of the metal centre used to bridge consecutive organic tectons. Whereas the use of neutral mercury chloride complex offering two free coordination sites leads to the formation of a neutral "zigzag" type 1-D network in the presence of tecton **2** bearing two pyridine units as coordinating sites, the combination of silver cation with the tecton **3** bearing two nitrile groups generates a cationic 1-D network which may be described as an array of fused metallamacrocycles. We are currently investigating the ability

of tectons **2** and **3** as well as other derivatives bearing other coordinating sites such as thiols, thioethers, phosphines and phine oxide [10] to form coordination networks with a variety of metal centers.

8. ACKNOWLEDGEMENTS

9. REFERENCES

[1]   S. Mann. *Nature*, 365 (1993),499.

[2]   M. Simard, D. Su, J. D. Wuest, *J. Amer. Chem. Soc.*, **113** (1991), 4696.

[3]   M. W. Hosseini, Cryst. Eng. Comm., **2004**, *6*, 318; G. Brand, M. W. Hosseini, O. Félix, P. Schaeffer, R. Ruppert, *in NATO ASI Series*, O. Kahn, Ed, Serie c, Kluwer, Dordrecht, **484** (1995), 129; M. W. Hosseini *in NATO ASI Series*, G. Tsoucaris, Ed, Serie c, Kluwer, Dordrecht, **518** (1998), 209; M. W. Hosseini, *in NATO ASI Series*, Eds. D. Braga, F. Grepioni, G. Orpen, Serie c, Kluwer, Dordrecht, Netherlands, **538** (1999), 181.

[4]   J.-M. Lehn, *Supramolecular Chemistry, Concepts and Perspectives,* VCH, Weinheim, **1995**.

[5]   M. W. Hosseini, A. De Cian, *Chem. Comm.*, (1998), 727; J. Martz, E. Graf, A. DE Cian, M. W. Hosseini, in *Perspectives in Supramolecular Chemistry, Ed. G. Desiraju, Wiley*, (2003), 177.

[6]   M.C. Etter, *Acc. Chem. Res.*, **23** (1990), 120; G. D. Desiraju, *Crystal Engineering: The Design of Organic Solids*, Elsevier, New York, **1989**; G. M. Whitesides, J. P. Mathias, T. Seto, *Science*, **254** (1991), 1312; C. B. Aakeröy, K. R. Seddon, *Chem. Soc. Rev.*, 22 (1993), 397; S. Subramanian, M. J. Zaworotko, *Coord. Chem. Rev.*, **137** (1994), 357; D. S. Lawrence, T. Jiang, M. Levett, *Chem. Rev.*, **95** (1995), 2229; J. F. Stoddart, D. Philip, *Angew. Chem. Int. Ed. Engl.*, **35** (1996), 1155.

[7]   M.D. Ward, P.J. Fagan, J.C. Calabrese, D.C. Johnson, *J. Am. Chem. Soc.*, **111** (1989), 1719; E. Fan, J. Yang, S. J. Geib, T. C. Stoner, M. D. Hopkins, A. D. Hamilton, *Chem. Commun.*, (1995), 1251; K. E. Schwiebert, D. N. Chin, J. C. MacDonald, G. M. Whitesides, *J. Am. Chem. Soc.*, **118** (1996), 4018; K. T. Holman, A. M. Pivovar, J. A. Swift, M. D. Ward, *Acc. Chem. Res.*, **34** (2001), 107; M. W. Hosseini, *Coord. Chem. Rev.*, **240** (2003), 157.

[8]   S. R. Batten, R. Robson, *Angew. Chem. Int. Ed.*, **37** (1998), 1460; A. J. Blake, N. R. Champness, P. Hubberstey, W.-S. Li, M. A. Withersby, M. Schröder, *Coord. Chem. Rev.*, **193** (1999), 117; M. Eddaoudi, D. B. Moler, H. Li, B. Chen, T. M. Reineke, M. O'Keeffe, O. M. Yaghi, *Acc. Chem. Res.*, **34** (2001), 319; B. Moulton, M. J. Zaworotko, *Chem. Rev.* **101** (2001), 1629.

[9]   C. Kaes, M. W. Hosseini, C. E. F. Rickard, B. W. Skelton, A. White, *Angew. Chem. Int. Ed. Engl.*, **37** (1998), 920; G. Mislin, E. Graf, M. W. Hosseini, A. De Cian, N. Kyritsakas, J. Fischer, *Chem. Comm.*, (1998), 2545; M. Loï, M. W. Hosseini, A. Jouaiti, A. De Cian, J. Fischer, *Eur. J. Inorg. Chem.*, (1999), 1981; M. Loï, E. Graf, M. W. Hosseini, A. De Cian, J. Fischer, *Chem. Comm.*, (1999), 603.; H. Akdas, E. Graf, M. W. Hosseini, A. De Cian, J. McB. Harrowfield, *Chem. Comm.*, (2000), 2219; A. Jouaiti, M. W. Hosseini, A. De Cian, *Chem. Comm.*, (2000), 1863; B. Schmaltz, A. Jouaiti, M. W. Hosseini, A. De Cian, *Chem. Comm.*, (2001), 1242; A. Jouaiti, V. Jullien, M. W. Hosseini J.-M. Planeix, A. De Cian, *Chem. Comm.*, (2001), 1114; S. Ferlay, S. Koenig, M. W. Hosseini, J. Pansanel, A. De Cian, N. Kyritsakas, *Chem. Comm*, (2002), 218; B. Zimmer, M. Hutin, V. Bulach, M. W. Hosseini, A. De Cian, N. Kyritsakas, *New. J. Chem*, 26 (2002), 26, 1532; A. Jouaiti, M. W. Hosseini, N. Kyritsakas, *Eur. J. Inorg. Chem.* 2002, 57; A. Jouaiti, M. W. Hosseini, N. Kyritsakas, *Chem. Comm*, (2002), 1898; B. Zimmer, V. Bulach, M. W. Hosseini, A. De Cian, N. Kyritsakas, *Eur. J. Inorg. Chem*, (2002), 3079; A. Jouaiti, M. W. Hosseini, N. Kyritsakas, *Chem. Comm*, (2003), 472; P. Grosshans, A. Jouaiti, M. W. Hosseini, N. Kyritsakas, *New. J. Chem.*, 27 (2003), 793.

[10]   C. Klein, E. Graf, M. W. Hosseini, A. De Cian, N. Kyritsakas-Gruber, *Eur. J. Org. Chem.* (2003), 395.

[11]   F. Bottino, G. Montaudo, P. Maravigna, *Ann. Chimica*, **57** (1967), 972.

[12]   S. Pappalardo, F. Bottino, *Phosphorus and Sulfur*, **19** (1984), 327.

[13]   S. Pappalardo, G. Ferguson, J. F. Gallagher, *J. Org. Chem.*, **57** (1992), 7102.

[14]   C. Klein, E. Graf, M. W. Hosseini, A. De Cian, N. Kyritsakas, *Eur. J. Org. Chem.*, (2002), 802.

[15]   C. Klein, E. Graf, M. W. Hosseini, G. Mislin, A. De Cian, *Tetrahedron Lett.* **41** (2000), 9043.

[16]   C. Klein, E. Graf, M. W. Hosseini, A. De Cian, J. Fischer, *Chem. Comm.*,(2000), 239.

[17]   C. Klein, E. Graf, M. W. Hosseini, A. De Cian, *N. J. Chem.* **25** (2001), 207.

[18]   C. Klein, E. Graf, M. W. Hosseini, A. De Cian, N. Kyritsakas-Gruber, *Eur. J. Inorg. Chem.* (2003), 1299.

[19]   P. Grosshans, A. Jouaiti, V . Bulach, J.-M. Planeix, M. W. Hosseini, N. Kyritsakas, *Eur. J. Inorg. Chem.*, (2004), 453.

[20]   P. Grosshans, A. Jouaiti, V . Bulach, J.-M. Planeix, M. W. Hosseini, J.-F. Nicoud, *Chem. Comm*, (2003), 1336.

[21]   Grosshans, A. Jouaiti, V. Bulach, J.-M. Planeix, M. W. Hosseini, J.-F. Nicoud, *C. R. Chimie*. **7** (2003), 189.

[22]   M. Henry, M. W. Hosseini, *New J. Chem.*, **28** (2004), 897.

[23]   P. Grosshans, A. Jouaiti, N. Kardouh, M. W. Hosseini, N. Kyritsakas, *New J. Chem., **27** (2003), 1806.

[24]   OpenMolen, Interactive Structure Solution, Nonius B.V., Delft, The Netherlands, **1997**.

AN INFINITE HYDROGEN-BONDED MOLECULAR ASSEMBLY BASED ON CATECHOL AND A BIFUNCTIONAL OLEFIN

Giannis S. Papaefstathiou,[†] Tomislav Friščić[†] and Leonard R. MacGillivray
Dept. of Chemistry, Univ. of Iowa, Iowa City, IA 52242, USA
len-macgillivray@uiowa.edu

1. ABSTRACT

Catechol (cat) and *trans*-1,2-bis(4-pyridyl)ethylene (4,4'-bpe) form a 1:1 co-crystal, of composition (cat)·(4,4'-bpe) 1, that consists of infinite one-dimensional (1D) undulating chains held together by O-H···N hydrogen bonds. The chains are based on an alternating sequence of five crystallographically independent molecules, two that involve cat and three that involve 4,4'-bpe, and an eight-component repeat unit. The cat molecules adopt an *anti-anti* conformation, while the olefins adopt either a co-planar or twisted conformation. The chains self-assemble *via* a combination of face-to-face π-π interactions, C-H···π forces, and C-H···O hydrogen bonds.

2. INTRODUCTION

The engineering of molecular crystalline solids with components assembled in predefined geometries and packing arrangements is a central goal of the crystal engineer.[1] Such control of geometry and packing, when combined with the myriad of chemical functionalities offered by a molecular approach, provides a means to design a vast array of solids with predictable and controllable properties (*e.g.* porosity, reactivity). This goal, however, is underscored by the fact that geometry and packing in the solid state are sensitive to subtle changes to molecular structure such that structurally similar molecules typically do not exhibit similar geometry and packing arrangements.[2] Thus, to confront such apparent disparity between molecular and solid-state structure, we,[3] and others,[1] are focused upon identifying geometries and packing patterns that may be used as synthons[4] to reliably control the organization of molecules in solids to achieve and control desired properties.

In this context, a property of the organic solid state that we aim to control is reactivity.[3] Specifically, we have revealed the ability of ditopic molecules, in the form of linear templates, to orient olefins in the solid state, *via* hydrogen bonds, in geometries suitable for single and multiple [2+2] photodimerizations.[2] Thus, co-crystallization of 1,3-benzenediol, or resorcinol (res), with *trans*-1,2-bis(4-pyridyl)ethylene (4,4'-bpe) produced a discrete four-component molecular assembly, 2(res)·2(4,4'-bpe),[5] held together by four O-H···N hydrogen bonds wherein two olefins were juxtaposed in a geometry suitable[2] for photoreaction. Ultraviolet (UV) irradiation of the crystalline solid produced *rctt*-tetrakis(4-pyridyl)cyclobutane in quantitative yield.[3] We have also demonstrated that the arrangement adopted by the templates and reactants is robust such that the geometry can be 'transferred' to additional solids to construct targets such as a [2.2]paracyclophane[6] and [*n*]-ladderanes (where *n* = 3 and 5).[7]

Having demonstrated the ability of res to force stacking of 4,4'-bpe in the solid state, we turn to structurally related 1,2-dihydroxybenzene, or catechol (cat). In particular, we wish to describe the formation of an infinite solid-state molecular assembly based on cat and 4,4'-bpe of composition (cat)·(4,4'-bpe).[8] Similar to resorcinol, cat can adopt more than one conformation based on the orientation of the two hydroxyl groups.[9] Specifically, two stable conformations can form: *anti-anti* and *syn-anti* (Scheme 1). In the former, the hydrogen atoms of the hydroxyl groups of the hydroxyl groups point away from each other, while in the latter one hydroxyl group participates in an intramolecular O-H···O hydrogen bond. *Ab initio* calculations indicate that the *syn-anti* conformation is more stable by approximately 5 kcal mol^{-1},[9]

---

† Authors contributed equally to the manuscript.

which suggested to us that cat may assemble with 4,4'-bpe in the solid state to produce, similar to 2(res)·(4,4'-bpe), a discrete hydrogen-bonded assembly that is photoactive.[10]


anti-anti   *syn-anti*
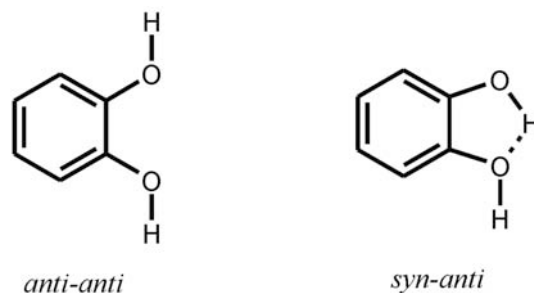
Scheme 1.

3. EXPERIMENTAL

Addition of cat (0.12 g, 1.1 mmol) to acetone (10 mL) in the presence of 4,4'-bpe (0.182 g, 1.0 mmol) yielded, upon standing for a period of approximately 2 days, yellow crystals of **1** (yield: 100%) suitable for X-ray analysis. The formulation of **1** was confirmed by ^{1}H NMR spectroscopy, as well as single-crystal X-ray diffraction.[11]

4. RESULTS AND DISCUSSION

The asymmetric unit of **1** consists of two full molecules of cat [based on O-atoms O1/O2 (cat$_A$) and O3/O4 (cat$_B$)], one full molecule of 4,4'-bpe [based on N-atoms N1/N2 (4,4'-bpe$_A$)], and two half-molecules of 4,4'-bpe [based on N-atoms N3/N3^i (4,4'-bpe$_B$) and N4/N4^{ii} (4,4'-bpe$_C$)] **(Fig. 1a)**. The components have assembled *via* O-H···N hydrogen bonds, in the sequence 4,4'-bpe$_C$···cat$_A$···4,4'-bpe$_A$···cat$_B$···4,4'-bpe$_B$ **(Fig. 1b)**, to form a one-dimensional (1D) chain based on alternating cat and 4,4'-bpe molecules.
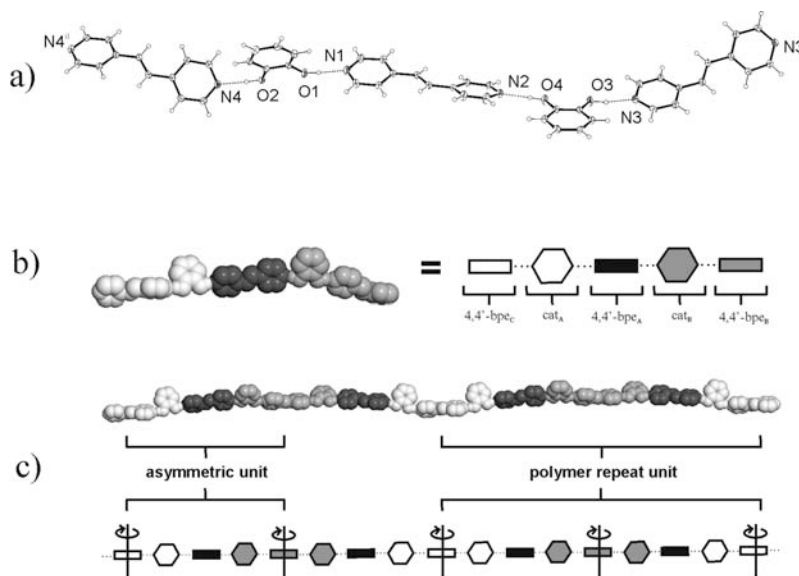
Figure 1. Perspectives of **1**: (a) ORTEP of the asymmetric unit (all non-hydrogen atoms at 30 % probability level), (b) space-filling model of the asymmetric unit along with a schematic representation, and (c) space-filling model of the eight-component repeat unit along with a schematic representation. Selected interatomic distances (Å) and angles (°): O1···N1 = 2.733(2), O1−H1O···N1 = 171.0(1), O2···N4 = 2.756(2), O2−H2O···N4 = 174.37(9); O3···N3 = 2.710(2), O3−H3O···N3 = 167.00(9); O4···N2 = 2.749(2), O4−H4O···N2 = 172.67(9). Symmetry operators: *i* = -*x*+3, *y*, -*z* + 3/2; *ii* = -*x*, *y*, -*z* + ½.

Each cat molecule adopts the *anti-anti* conformation, while the pyridyl groups of each 4,4'-bpe molecule deviate from co-planarity [pyridine···pyridine twist angles (°): 41 (4,4'-bpe$_B$); 39 (4,4'-bpe$_C$); 22.7(1) (4,4'-bpe$_A$)]. In this arrangement, the aromatic units of each hydrogen bond are either twisted or lie approximately co-planar, the twist angles involving cat$_A$ and cat$_B$ being 71° (4,4'-bpe$_A$) and 67° (4,4'-bpe$_C$), and 10° (4,4'-bpe$_A$) and 11° (4,4'-bpe$_B$), respectively. The components of the hydrogen-bonded sequence are propagated along the crystallographic [100] direction, *via* two-fold rotation axes, to give a polar, undulating chain (wavelength: 6.8 nm) based on the eight-component repeat unit 4,4'-bpe$_C$···cat$_A$···4,4'-bpe$_A$···cat$_B$···4,4'-bpe$_B$···cat$_B$···4,4'-bpe$_A$···cat$_A$ **(Figure 1c)**

The chains of **1** have self-assembled in the solid state to form centrosymmetric dimers **(Figure 2a)**. The dimers are held together by a combination of face-to-face π-π interactions, involving the pyridyl units and cat molecules, and C-H···π forces.[12] These interactions occur between peaks and troughs of adjacent polymers **(Figure 2b)**. Neighboring dimers interact *via* a combination of two-point C-H···O forces and face-to-face π-π interactions **(Figure 2c)** involving nearest-neighbor pyridyl units and cat molecules.[13] The shortest distance between neighboring carbon-carbon double bonds of **1** is 6.85 Å, involving molecules 4,4'-bpe$_A$ and 4,4'-bpe$_B$[iii] (symmetry operator *iii* = -*x*+2, -*y*+2, -*z*+1). This distance extends beyond the separation criteria of Schmidt for [2+2] photodimerization.[2] Moreover, the olefins of **1**, as determined by irradiating a powdered crystalline sample of **1** with UV-radiation (broadband Hg lamp), are photostable.
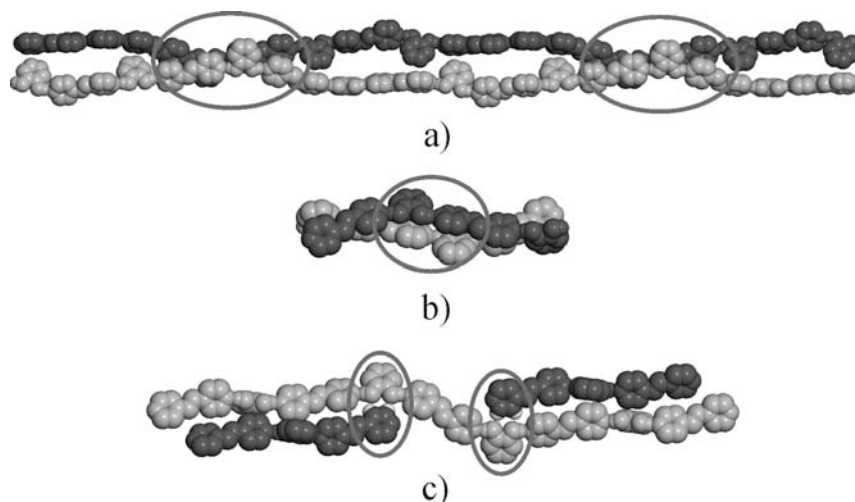
Figure 2. Space-filling views of: a) self-assembled chain dimers highlighting the peak and trough interaction, (b) interactions between the chains highlighting the π-π interactions in the central region of the fragment, and (c) interactions between the dimers highlighting the C-H···O forces (hydrogen atoms colored white).

5. CONCLUSION

In conclusion, we have revealed that cat assembles with 4,4'-bpe in the solid state to form a 1D hydrogen-bonded chain of composition (cat)·(4,4'-bpe) **1**. The cat molecules of the chain adopt the *anti-anti* conformation.[9] Efforts are currently underway to engineer cat derivatives[14] that may provide access to photoactive solids based on discrete hydrogen-bonded assemblies akin to 2(res)·2(4,4'-bpe).[15]

6. REFERENCES

[1]   Braga, D. *Chem. Comm.* **2003**, 2751; (b) Hosseini, M.W. *Coord. Chem. Rev.* **2003**, *240*, 157; (c) Hollingsworth, M.D. *Science* **2002**, *295*, 2410; (d) Holman, K.T.; Pivovar, A.M.; Swift, J.A.; Ward, M.D. *Acc. Chem. Res.* **2001**, *34*, 107; (e) Aakeröy, C.B.; Beatty, A.M. *Aust. J. Chem.* **2001**, *54*, 409; (f) Moulton, B.; Zaworotko, M.J. *Chem. Rev.* **2001**, *101*, 1629; (g) Blake, A.J.; Champness, N.R.; Hubberstey, P.; Li, W.-S.; Withersby, M.A. Schröder, M. *Coord. Chem. Rev.* **1999**, *183*, 117.

[2]   Schmidt, G.M.J. *Pure Appl. Chem.* **1971**, *27*, 647.

[3]   MacGillivray, L.R. *CrystEngComm*, **2002**, *4*, 37.

[4]   Desiraju, G.R. *J. Mol. Struc.* **2003**, *656*, 5.

[5]   MacGillivray, L.R.; Reid, J.L.; Ripmeester, J.A. *J. Am. Chem. Soc.* **2000**, *122*, 7817.

[6]   Friščić, T.; MacGillivray, L.R. *Chem. Commun.* **2003**, 1306.

[7]   Gao, X.; Friščić, T.; MacGillivray, L.R. *Angew. Chem. Int. Ed.* **2004**, *43*, 232.

[8]   St Pourçain, C.B. *J. Mater. Chem.* **1999**, *9*, 2727.

[9]   Puebla, C.; Ha, T.-K. *J. Mol. Struc. (Theochem)* **1990**, *204*, 337.

[10]   Such an assembly would involve a bifurcated interaction involving the hydroxyl group of cat that participates in the intramolecular O-H···O hydrogen bond such that cat serves as a ditopic U-shaped moiety.

[11]   Crystal data for **1**: monoclinic, *P*2/c (No. 13), $Z = 4$, $a = 23.927(2)$ Å, $b = 7.4219(7)$ Å, $c = 17.631(2)$ Å, $\beta = 109.006(5)^{\circ}$, $V = 2960.4(5)$ Å^3, 6729 unique reflections, $R = 0.0455$ [for 4512 reflections with $I \geq 2\sigma(I)$], $R = 0.0827$ (all data) and w$R^2 = 0.1627$ (all data). Crystallographic data has been deposited with the Cambridge Crystallographic Data Centre and has been allocated with deposition number CCDC 244922.

[12]   Jorgensen, W.L.; Severance, D.L. *J. Am. Chem. Soc.* **1990**, *112*, 4768.

[13]   The *anti-anti* conformation adopted by cat in **1** may be attributed to the intermolecular forces (*i.e.* face-to-face π···π stacking, C−H···π, and C−H···O hydrogen bonds) that occur between the chains.

[14]   Papaefstathiou, G.S.; Friščić, T.; MacGillivray, L.R. *J. Supramol. Chem.* **2003**, *2*, 227.

[15]   For a related strategy, see: Papaefstathiou, G. S.; MacGillivray, L. R. *Org. Lett.* **2001**, *3*, 3835.

COMPLEMENTARY FEATURES OF INORGANIC AND ORGANIC HALOGENS: APPLICATION TO CRYSTAL ENGINEERING

Lee Brammer, Fiorenzo Zordan, Guillermo Mínguez Espallargas, Stephen L. Purver, Luis Arroyo Marin
and Harry Adams
Dept. of Chemistry, Univ. of Sheffield, Brook Hill, Sheffield S3 7HF, UK
lee.brammer@sheffield.ac.uk

Paul Sherwood
*Computational Science and Engineering Dept., CLRC Daresbury Laboratory, Daresbury,
Warrington WA4 4AD, UK*

1. ABSTRACT

Inorganic (M–X) and suitably chosen organic (C–X) halogens exhibit anisotropic electrostatic potentials whose complementary aspects can be exploited to permit supramolecular assembly of molecules or ions based upon attractive M–X···X'–C interactions. Electrostatic potential calculations and crystal syntheses are presented to illustrate this approach to the design of crystalline materials.

2. INTRODUCTION

Halogens (X) are present at the periphery of a large number of organic and inorganic molecules. As such they provide a potential site for intermolecular interactions in condensed phases. In recent years we have examined the geometric aspects of intermolecular interactions involving halogens and sought to understand the electronic factors that govern the observed geometries and the interaction energies. In this article we examine the similarities and, particularly, the differences in the electronic nature of organic halogens (C–X) and inorganic halogens (M–X) and show how the complementary electronic features of halogens in these two environments can be harnessed to provide a class of non-covalent interactions of the type M–X···X'–C

3. GEOMETRIC AND ELECTROSTATIC MODELS

Examination of the electrostatic potential in the vicinity of organic and (terminal) inorganic halogens shows a marked anisotropy that is a manifestation of the charge density distribution about the halogens. Specifically halogens in both environments show far greater negative electrostatic potential in directions inclined at 90-130 º to the C–X or M–X bond relative the direction axial to the bond (180 º) [1]. **Figure 1** illustrates this point and highlights the far greater potential associated with the inorganic halogens, consistent with the M–X bond being the more polar of the two. It is also evident that as bond polarity decreases with decreasing electronegativity of the halogen (F > Cl > Br > I) then so does the magnitude of the negative electrostatic potential.

organic halogen   **inorganic halogen**
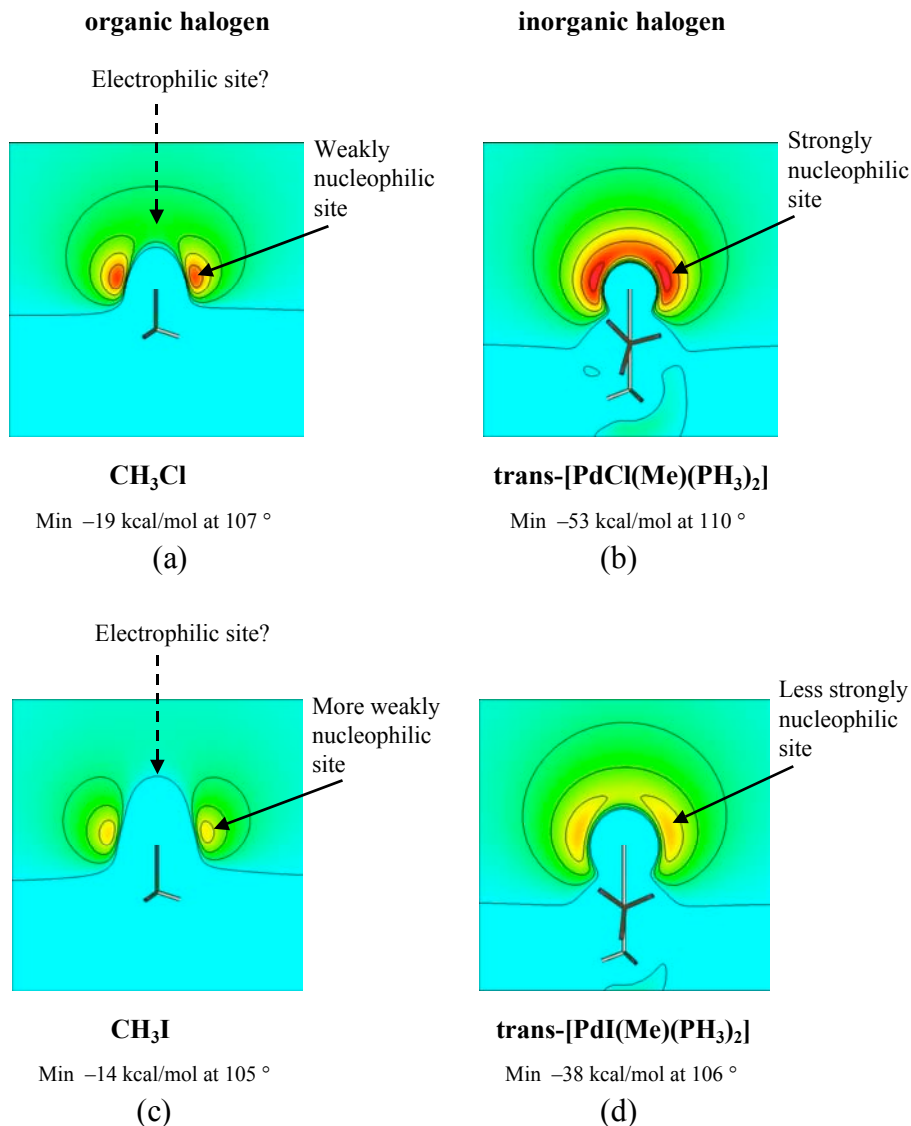
Figure 1. Calculated negative electrostatic potentials for model compounds (a) CH₃Cl, (b) *trans*-[PdCl(Me)(PH₃)₂], (c) CH₃I, (b) *trans*-[PdI(Me)(PH₃)₂], contoured at intervals of 4 kcal/mol for organic halogens and 10 kcal/mol for inorganic halogens. The calculations are presented and described in full in ref. 1. Figures are adapted from ref 1 with permission of the American Chemical Society.

3.1 Halogens As Nucleophiles

These electrostatic potential distributions provide a rationalization for the interaction of halogens with electrophiles such as hydrogen bond donors or metal ions. Thus, the negative potential at the halogen contributes to an attractive interaction with electrophiles. Furthermore, use of the Cambridge Structural Database [2] has shown that the geometric distribution of hydrogen bond donors in the vicinity of terminal halogens **(Figure 2)** is quite consistent with an electrostatic driving force for hydrogen bond formation since there is a significant preference for interactions occurring along the directions at which the halogen potential is most negative [1]. H···X distances are found to lengthen over the sequence F < Cl < Br < I and are typically longer for organic halogens (C–X) than for comparable inorganic (M–X) halogens (Table 1), again consistent with the importance of the importance of the electrostatic component in these hydrogen bonds.

Lee Brammer, Fiorenzo Zordan, Guillermo Mínguez Espallargas, Stephen L. Purver, Luis Arroyo Marin, Harry Adams and Paul Sherwood
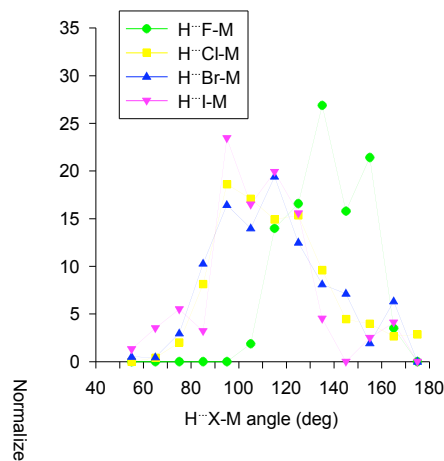
Figure 2. Normalized [3] angular distribution of N–H···X–M hydrogen bonds. Reproduced from ref 1 with permission of the American Chemical Society.

The directional preference of N–H···X–M hydrogen bonds has been used in design strategies for synthesis of hydrogen-bonded crystals of perhalometallate salts [4-8]. C–X hydrogen bond acceptors are generally considered too weak for use in a hydrogen bonding strategy for crystal synthesis, though the importance of such hydrogen bonds has been the subject of some recent attention [9-11].

Table 1

Mean normalized HX distances for N–H···X–M and N–H···X–C hydrogen bonds [1]

	L_nM-X	R_nC-X
Nucleophile (Lewis base)		
Electrophile (Lewis acid)	H–N	H–N

Mean normalized H···X distance, R_{HX}	R_{HX} [d(H···X)]		R_{HX} [d(H···X)]	
	0.776 [2.072 Å]	(X = F)	**0.923** [2.464 Å]	
$R_{HX} = d(H···X)/(r_{vdW}H + r_{vdW}X)$	**0.853** [2.516 Å]	(X = Cl)	**0.963** [2.841 Å]	
	0.879 [2.681 Å]	(X = Br)	**0.973** [2.968 Å]	
[using data for $R_{HX} < 1.05$]	**0.923** [2.917 Å]	(X = I)	*ca.* **0.99** [3.13 Å]	
	Stronger hydrogen bond		Very weak hydrogen bond	
	M–X bond very polar		C–X bond somewhat polar	

3.2 Organic Halogens As Electrophiles

Evidence from crystal structure data has clearly established that organic halogens (C–X) are involved in short contacts with nucleophiles such as oxygen and nitrogen bases via an axial approach geometry, i.e. approximately linear C–X···O/N geometries [12,13] **(Figure 3)**. *Ab initio* intermolecular perturbation theory (IMPT) calculations on model dimers by Lommesrse et al have permitted a detailed analysis of the contributions to the interaction energies of C–Cl···O interactions [13]. It is illustrative to consider their analyses of the chloromethane···formaldehyde (I) and chloro-cyanoacetylene···formaldehyde (II) systems **(Figure 4)**. For both I and II the geometry with the minimum energy involves a linear C–Cl···O arrangement. However, there is no net attractive interaction for I while the interaction in II is attractive. In

both systems the exchange repulsion is quite anisotropic and is at a minimum for a linear C–Cl···O arrangement. This is consistent with an earlier theoretical study on C–Cl···Cl–C interactions by Price [14] and has led to the suggestion that chlorine (and the heavier halogens) should be considered to have aspherical van der Waals radii [15].
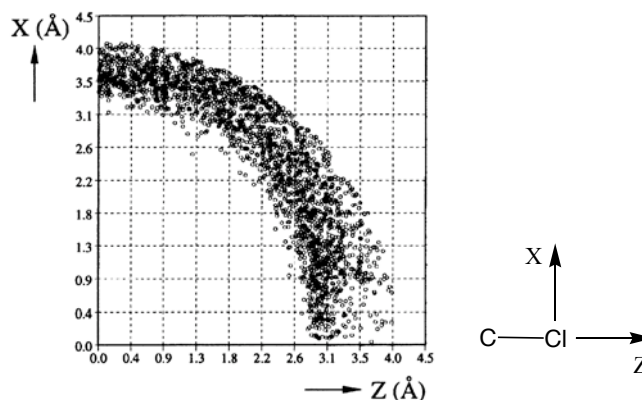
Figure 3. Plot of C–Cl···O contacts in crystal structures (Cl at origin) illustrating that the shortest interactions lie along the C–Cl bond axis. Adapted from ref .13 with permission of the American Chemical Society.
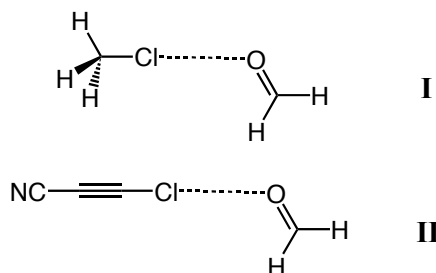
Figure 4. The chloromethane···formaldehyde (I) and chloro-cyanoacetylene···formaldehyde model systems for C–Cl···O interactions [13].

The electrostatic component of the interaction energy in **I** and **II** is also anisotropic, being most attractive (or least repulsive) for a linear C–Cl···O geometry. For **I** the electrostatic term is repulsive for all geometries, but least repulsive for the axial interaction, consistent with the small but negative electrostatic potential associated with an axial approach to CH_3Cl **(Figure 1a)**. However, the electrostatic contribution to the interaction energy in **II** is attractive for a linear C–Cl···O geometry. Here the electron distribution associated with the C–Cl group is influenced by the electron-withdrawing effect of the alkyne and nitrile groups, presumably diminishing the negative electrostatic potential associated with the chlorine atom (relative to that in CH_3Cl) and leading to a slightly positive potential in the direction of the axial approach. The charge transfer, polarization and dispersion energy terms are all attractive but small in comparison to the exchange repulsion and electrostatic contributions to the interaction energy. The situation regarding the contribution of the exchange repulsion, electrostatic and charge transfer components of the interaction energy are summarized in **Figure 5**. Lommerse et al. have also noted that (heavier) more polarizable halogens form stronger/shorter interactions with nucleophiles [13]. This arises primarily from an enhanced electrostatic term: I > Br > Cl [> F], though the (smaller) charge transfer energy term should also be significantly enhanced. Finally, it should be noted that in a CSD search C–F groups were found to exhibit very few short contacts with nucleophiles and to show no directional preferences within such interactions [13].

Lee Brammer, Fiorenzo Zordan, Guillermo Mínguez Espallargas, Stephen L. Purver, Luis Arroyo Marin, Harry Adams and Paul Sherwood
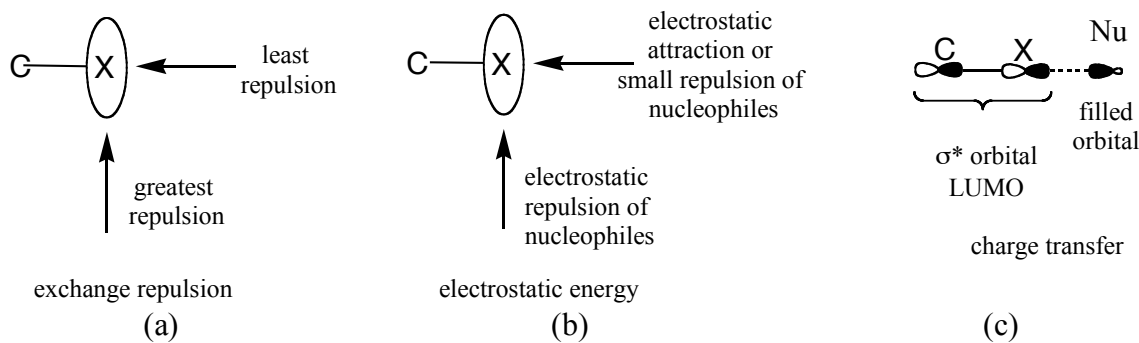
Figure 5. Schematic representation of the contributions to the C–X···O interaction energy from (a) exchange repulsion, (b) electrostatic energy and (c) charge transfer.

4. APPLICATION TO CRYSTAL DESIGN

4.1 Design Strategy Using M–X···X'–C Interactions As Synthons

The calculations summarized above, but those considering the electrostatic potential in particular, have led us to anticipate that inorganic halogens have electronic features complementary to suitably "activated" organic halogens such that interactions of the type M–X···X'–C should have an attractive electrostatic energy contribution and in all likelihood should be attractive interactions. It is on this basis that we have pursued a two-pronged approach to crystal synthesis based upon such intermolecular interactions as supramolecular synthons **(Scheme 1)**. Halopyridines have been chosen to include the organic halogen as part of a rigid and geometrically well-defined molecular component. The presence of ring nitrogen atom also exerts an electron withdrawing effect on the halogen substituent enhancing its electrophilicity. This effect has then been accentuated by either (i) protonation of the ring nitrogen atom or (ii) coordination through nitrogen to a metal center, and is expected to lead to a positive electrostatic potential along the axial approach to the C–X group, with the greatest effect being seen for the heavier halogens. In the first approach, the inorganic halogen with which the C–X group is intended to interact is provided by a perchlorometallate anion to accompany the halopyridinium cations. The second strategy allows coordinated chloride ligands to be present on the same (neutral) building blocks as the halopyridine ligand.
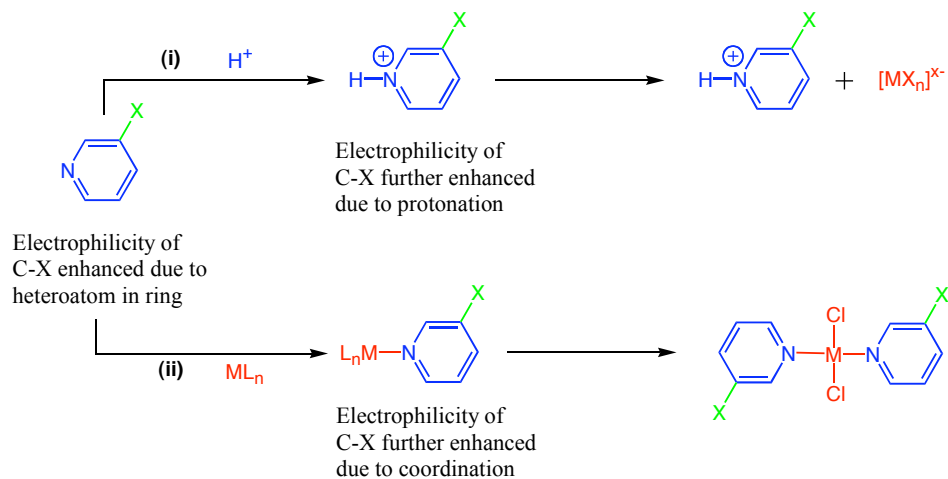
Scheme 1. Two approaches for combining nucleophilic inorganic halogens (M-X) with electrophilic organic halogens (C-X') for construction of network propagated via M–X···X'–C interactions. Reproduced from ref .20 with permission of the American Chemical Society.

A family of ionic compounds $[HpyX-3]_2[CoCl_4]$ (pyX-3 = 3-halopyridine, X = I, Br, Cl, F) have been prepared and crystallographically characterized [16] **(Figure 6)**. All exhibit N–H···Cl–Co hydrogen bonds

linking cations and anions. All but the fluoropyridinium salt also show Co–Cl⋯X–C interactions with geometries that are approaching linearity at the organic halogen, but markedly angular at the inorganic halogen. Analogous interactions have been observed for [HpyX-n]$_2$[CuX'$_4$] (X =Cl, Br; X' = Cl, Br; n = 2, 3, 4) [17]. The M–Cl⋯X–C interaction geometry is consistent with that anticipated from our analysis of the likely behavior of the inorganic and organic halogens used as nucleophiles and electrophiles, respectively and the interaction can be referred to as a halogen bond [18,19]. The absence of Co–Cl⋯F–C interactions in the crystal structure of [HpyF-3]$_2$[CoCl$_4$] suggests that such an interaction may be repulsive, probably due to a repulsive electrostatic component. This is consistent with the findings of Lommerse et al. regarding possible C–F⋯O interactions [13] and is confirmed by our own calculations on the electrostatic potential surrounding C–F groups [1,20].

(a)

(b)

(c)
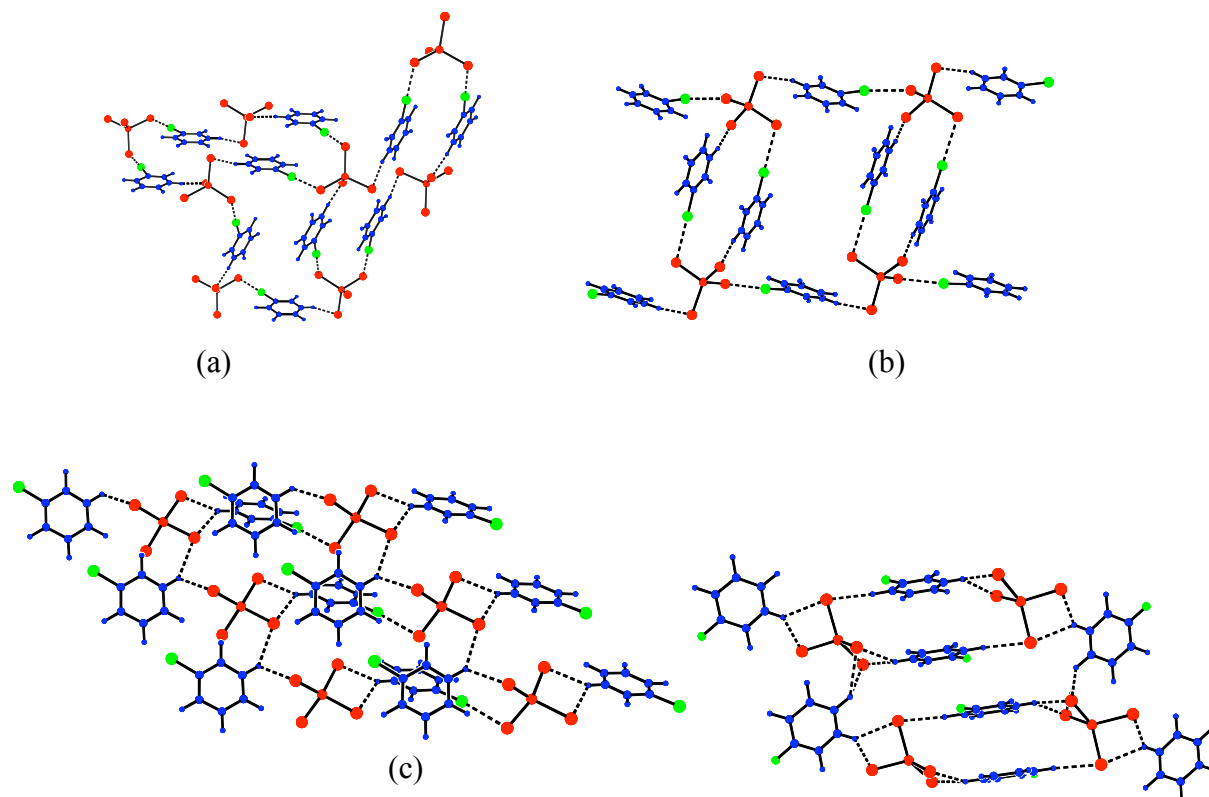
Figure 6. (a) A (4,4) grid network formed by [HpyI-3]$_2$[CoCl$_4$], (b) a ladder network formed by [HpyBr-3]$_2$[CoCl$_4$] and (c) a (4,4) grid network formed by [HpyCl-3]$_2$[CoCl$_4$], each involving N–H⋯Cl–Co hydrogen bonds and Co–Cl⋯X–C halogen bonds linking cations and anions. (d) Network formed by [HpyF-3]$_2$[CoCl$_4$] involving N–H⋯Cl–Co and C–H⋯Cl–Co hydrogen bonds, but no Co–Cl⋯F–C interactions. Color scheme: anions (red),cations (blue), organic halogen (green). Figures (a)-(c) reproduced from ref.16 with permission of the Royal Society of Chemistry.

In adopting the second strategy shown in Scheme 1, we have prepared a family of compounds *trans*-[MCl$_2$(pyX-3)$_2$] (M= Pd, Pt   X = I, Br, Cl, F) [20]. Like their ionic counterparts (vide supra) the crystal structures of these compounds (for X ≠ F) comprise networks based upon M–Cl⋯X–C interactions with geometries that are quite angular at inorganic halogen, but approaching linearity at the organic halogen. The structures fall into two main types, namely those in which the molecules are connected via M–Cl⋯X–C interactions to two neighbors and those in which such interactions provide links to four neighbors **(Figure 7)**. The fluoropyridine-containing compounds again do not form M–Cl⋯F–C interactions, and calculations on *trans*-[PdCl$_2$(pyF-3)$_2$] suggest that the electrostatic contribution to a putative M–Cl⋯F–C interaction would be repulsive. Rather, the *trans*-[MCl$_2$(pyF-3)$_2$] crystal structures are based predominantly upon C–H⋯Cl–M hydrogen bonds and π-stacking interactions between fluoropyridine rings.

Lee Brammer, Fiorenzo Zordan, Guillermo Mínguez Espallargas, Stephen L. Purver, Luis Arroyo Marin, Harry Adams and Paul Sherwood


(a)   (b)
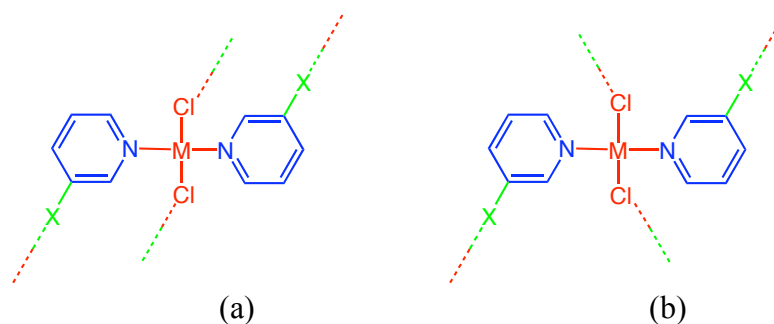
Figure 7. Two types of networks found for *trans*-[MCl$_2$(pyX-3)$_2$] compounds, involving (a) two M–Cl···X–C interactions to each of two neighbors and (b) one M–Cl···X–C interaction to each of four neighbors.

4.2 Resistance of M–X···X'–C Interactions To Water Molecule Insertion

A third set of compounds has allowed us to examine solvent incorporation in crystal growth, an almost universal issue in crystal engineering. Specifically we have examined the effect of water incorporation in the salts [HpyX-3]$_2$[PtCl$_6$] (X = I, Br), which in the absence of water would be expected to form networks based upon N–H···Cl–Pt hydrogen bonds and Pt–Cl···X–C halogen bonds by analogy to the perchlorocobaltate and perchlorocuprate systems previously mentioned [21]. In principle the water molecules have the necessary donor and acceptor functions to insert into either the hydrogen bonds or halogen bonds as shown in Scheme 8. In the three structures studied (including two polymorphs for [HpyI-3]$_2$[PtCl$_6$].2H$_2$O) insertion of water molecules occurs exclusively into the hydrogen bonds leaving the halogen bonds intact, as illustrated in **Figure 8** for [HpyBr-3]$_2$[PtCl$_6$].2H$_2$O.
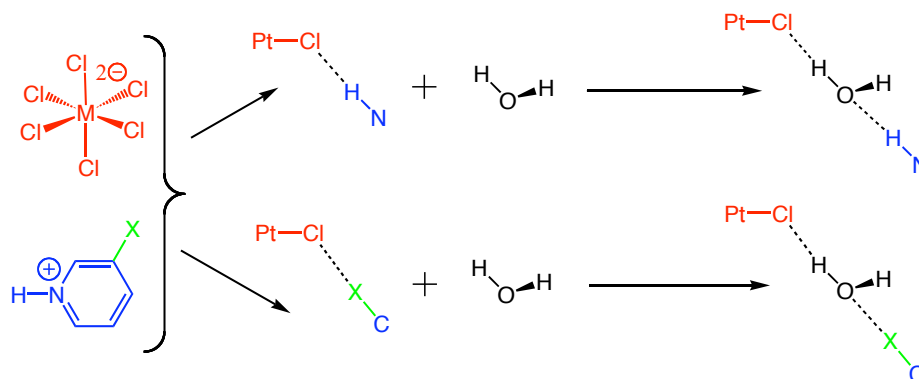
Scheme 2. The two types of interaction, N–H···Cl–Pt hydrogen bonds (top) and Pt–Cl···X–C halogen bonds (bottom) expected to be present in the crystal structures of [HpyX-3]$_2$[PtCl$_6$] (X = I, Br) and the possible means of insertion of a water molecule into each type of interaction.
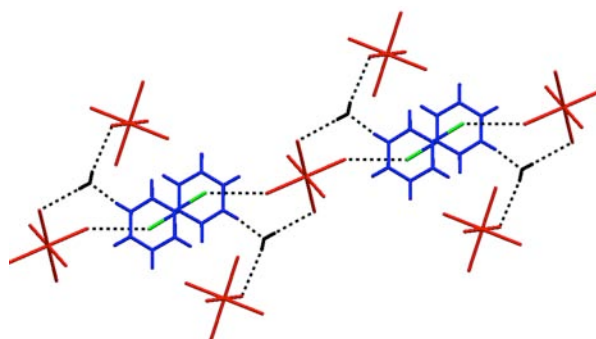
Figure 8. View of the crystal structure [HpyBr-3]$_2$[PtCl$_6$].2H$_2$O showing N–H···O and O–H···Cl–Pt hydrogen bonds along with Pt–Cl···Br–C interactions [21].

5. CONCLUSIONS

The anisotropic electron distributions around terminally bonded halogens manifest themselves in similarly anisotropic electrostatic potential distributions. While the potential is negative in all directions for inorganic halogens (M–X), the potential distribution can range from negative to positive for suitably chosen (or "activated") organic halogens (C–X). Thus, pairings of inorganic and organic halogens can be used in forming directional M–X···X'–C interactions (halogen bonds) for supramolecular assembly. We have developed such an approach and illustrated it herein with examples using neutral and ionic molecular units to construct crystals in which M–Cl···X–C halogen bonds play a structure directing role. In each case the organic halogen is part of a halopyridine moiety for which the halogen has been further activated towards halogen bond formation either by protonation of the pyridine or its coordination to a metal center. These studies also illustrate that M–Cl···F–C interactions are not formed in the corresponding fluoropyridine-containing compounds. Finally we refer to a study in which hydrates are formed for the salts [HpyX-3]$_2$[PtCl$_6$] (X = I, Br). While water molecule incorporation could in principle disrupt either the anticipated hydrogen bonds or halogen bonds it is only the latter that remain unaffected.

6. ACKNOWLEDGEMENTS

7. REFERENCES

[1]   L. Brammer, E.A. Bruton and P. Sherwood, *Cryst. Growth Des*. **1** (2001) 277.

[2]   F.H. Allen, *Acta Crystallogr.* **B58** (2002) 380.

[3]   A cone correction was applied. See J. Kroon and J.A. Kanters, *Nature* **248** (1974) 667.

[4]   L. Brammer, J.K. Swearingen, E.A. Bruton and P. Sherwood, *Proc. Nat. Acad. Sci.*, *USA* **99** (2002) 4956.

[5]   J.C. Mareque Rivas and L. Brammer, *Inorg. Chem.* **37** (1998) 4756.

[6]   G.R. Lewis, and A.G. Orpen, *Chem. Commun.* (1998) 1873.

[7]   A. Angeloni and A.G. Orpen, *Chem. Commun.* (2001) 343.

[8]   B. Dolling, A.L. Gillon, A.G. Orpen, J. Starbuck and X.-M Wang, *Chem. Commun.* (2001) 567.

[9]   M.T. McBride, T.-J.M. Luo and G.T. Palmore, *Cryst. Growth Des.* **1** (2001) 39.

[10]   T.-J.M. Luo and G.T. Palmore, *Cryst. Growth Des.* **2** (2002) 337.

[11]   R. Banerjee, G.R. Desiraju, R. Mondal and J.A.K. Howard, *Chem. Eur. J.* **10** (2004) 3373.

[12]   N. Ramasubbu, R. Parthasarathy and P. Murray-Rust *J. Am. Chem. Soc.* **108** (1986) 4308.

[13]   J. P.M. Lommerse, A.J. Stone, R. Taylor and F.H. Allen *J. Am. Chem. Soc.* **118** (1996) 3108.

[14]   S.L. Price, A.J. Stone, J. Lucas, R.S. Rowland, A.E. Thornley, *J. Am. Chem. Soc.* **116** (1994) 4910.

[15]   (a) S.C. Nyburg, W. Wong-Ng, *Proc. R. Soc. London* **A367** (1979) 29. (b) S.C. Nyburg, C.H. Faerman, *Acta Crystallogr.* **A41** (1985) 274.

[16]   L. Brammer, G. Mínguez Espallargas and H. Adams, *CrystEngComm* **5** (2003) 343.

[17]   R.D. Willett, F. Awwadi, R. Butcher, S. Haddad and B. Twamley, *Cryst. Growth Des.* **3** (2003) 301.

[18]   A.C. Legon, *Angew. Chem. Int. Ed.* **38** (1999) 2687.

[19]   E. Corradi, S.V. Meille, M.T. Messina, P. Metrangolo and G. Resnati, *Angew. Chem. Int. Ed.* **39** (2000) 1782.

[20]   F. Zordan, L. Brammer and P. Sherwood, *J. Am. Chem. Soc.* **127** (2005) 5979.

[21]   F. Zordan and L. Brammer, *Acta Crystallogr.* **B60** (2004) 512.

BORONIC ACIDS AS VERSATILE SUPRAMOLECULAR REAGENTS

Christer B. Aakeröy, John Desper, Brock Levin, and Debra J. Salmon
*Dept. of Chemistry, Kansas State Univ., Manhattan, KS, 66506, USA*
aakeroy@ksu.edu

1. ABSTRACT

Crystal engineering and supramolecular synthesis is governed by the structural consequences of intermolecular forces, and by the way in which such interactions are utilized for controlling the assembly of molecules into predictable structural motifs. A vital part of crystal engineering is thus dedicated to identifying robust intermolecular synthons that can be used as reliable connectors between molecules. In this paper we describe how the hydrogen-bond capabilities of boronic acids $R-B(OH)_2$ can be translated into versatile co-crystallizing tools capable of forming heteromeric structure-directing hydrogen-bond interactions with a variety of complementary structural partners e.g. 2-aminopyrimidine and 4,4'-bipyridine.

2. INTRODUCTION

The synthesis of supramolecular assemblies composed of several different molecular fragments [1] held together by non-covalent forces is still a relatively young discipline and our understanding of how groups of molecules communicate, bind, organize, and function, is still incomplete [2]. Despite recent advances in supramolecular synthesis, the detailed control over the assembly of molecules into ordered solids remains an elusive goal, and we are rarely able to predict the structure of a simple crystalline material. Much more work is required to increase the choice of reliable building blocks of low-dimensional architectures and, more importantly, to allow us to rationalize and predict structural arrangements of molecules within new crystalline materials. An enhanced understanding of intermolecular forces may also enable us to better address crucial questions about polymorphism and crystal morphology.

Boronic acids are receiving considerable attention from the synthetic community due to the fact that they are invaluable intermediates in very versatile and useful aryl-aryl cross-coupling reactions [3]. However, the same chemical functionalities have, by and large [4, 5], remained unexplored as supramolecular connectors despite the fact that aryl-boronic acids can produce hydrogen-bonded dimers and ladders akin to motifs observed in carboxylic acids and carboxamides, Scheme 1 [6].
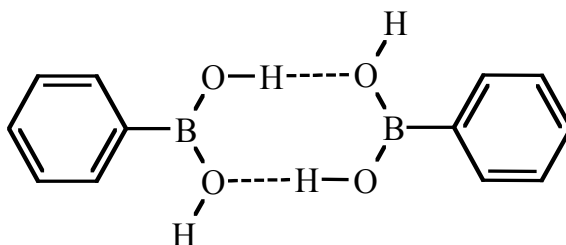
Scheme 1. Head-to-head hydrogen-bonded motif common among phenylboronic acids.

The boronic acid moiety may represent a potentially versatile supramolecular synthetic tool but there are still no systematic structural studies that have examined how this particular moiety competes or interacts with other hydrogen-bond functionalities e.g. carboxylic acids, carboxamides, oximes, 2-aminopyridines, *etc*.
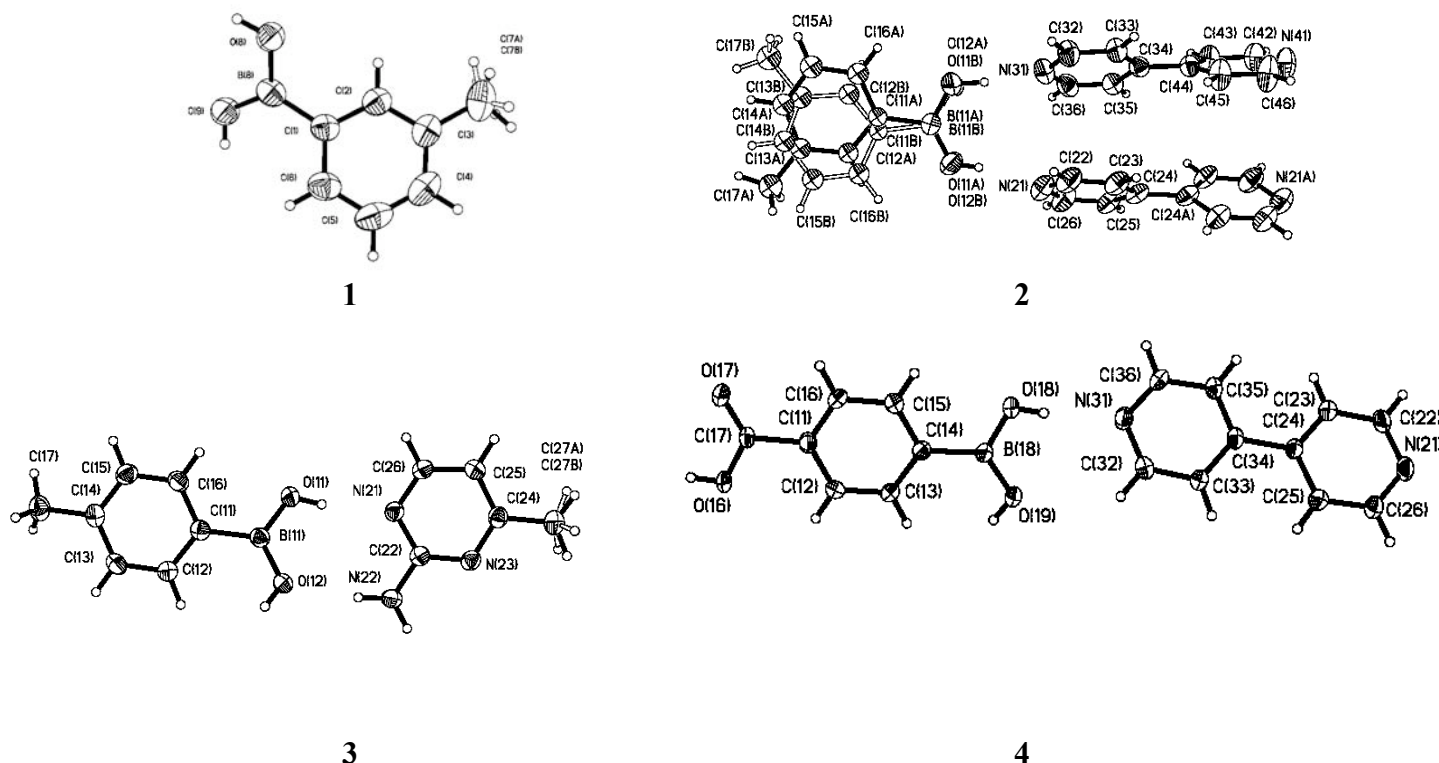
In this study we employ co-crystallization techniques as a way of probing the supramolecular behavior of boronic acids, and we demonstrate that they are capable of engaging in a variety of predictable structure-directing intermolecular interactions. These results indicate that boronic acids may become an important addition to the tools employed in hydrogen-bond based crystal engineering and supramolecular synthesis.

Here we present the crystal structures of 3-methylphenylboronic acid **1**, (4,4'-bipyridine)$_3$:(3-methylphenylboronic acid)$_2$ **2**, 2-amino-4-methylpyrimidine:(4-methylphenylboronic)$_2$ acid **3**, and 4,4'-bipyridine:4-carboxyphenyl boronic acid **4**, Table 1.

3. EXPERIMENTAL

3.1 Crystallography

X-ray data were collected on a Bruker SMART 1000 four-circle CCD diffractometer using a fine-focus molybdenum Kα tube. Data were collected using SMART [7]. Initial cell constants were found by small, widely separated "matrix" runs. Preliminary Laué symmetry was determined from axial images. Generally, an entire hemisphere of reciprocal space was collected regardless of Laué symmetry. Scan speed and scan width were chosen based on scattering power and peak rocking curves. Unless otherwise noted, 0.3 ° scans were used.

Unit cell constants and orientation matrices were improved by least-squares refinement of reflections thresholded from the entire dataset. Integration was performed with SAINT [8] using this improved unit cell as a starting point. Precise unit cell constants were calculated in SAINT from the final merged dataset. Lorenz and polarization corrections were applied, but data were not corrected for absorption. Laué symmetry, space group, and unit cell contents were found with XPREP. Data were reduced with SHELXTL [9]. The structures were solved in all cases by direct methods without incident. In general, hydrogen atoms were assigned to idealized positions and were allowed to ride. Unless otherwise noted, the coordinates of hydrogen atoms engaged in hydrogen-bonding were allowed to refine. Thermal ellipsoids and labeling schemes are shown in **Figure 1** a-d and the crystallographic data are listed in Table 1.

Figure 1.   Thermal ellipsoids and labeling schemes for **1-4**.

Table 1

Structure code	1	2	3	4
Systematic name	3-methylbenzene-boronic acid	(3-methylbenzene-boronic acid)$_2$, (4,4'-bipyridine)$_3$	2-amino-4-methyl-pyrimidine, 4-methylbenzene-boronic acid	4-carboxybenzene-boronic acid, 4,4'-bipyridyl
Formula moiety	$C_7 H_9 B O_2$	$(C_7 H_9 O_2 B)_2$ $(C_{10} H_8 N_2)_3$	$(C_5 H_7 N_3)$ $(C_7 H_9 B O_2)$	$(C_7 H_7 B O_4)$ $(C_{10} H_8 N_2)$
Empirical formula	$C_7 H_9 B O_2$	$C_{44} H_{42} B_2 N_6 O_4$	$C_{12} H_{16} B N_3 O_2$	$C_{17} H_{15} B N_2 O_4$
Molecular weight	135.95	740.46	245.09	322.12
Color, Habit	colorless prism	colorless prism	amber prism	colorless prism
Crystal system	Monoclinic	Monoclinic	Monoclinic	Triclinic
Space group, Z	P2(1)/c, 4	C2/c, 4	P2(1)/c, 4	P1, 1
a, Å	15.063(4)	20.2663(10)	9.5084(10)	3.9552(8)
b, Å	5.6710(17)	9.2707(5)	11.9386(12)	8.3612(16)
c, Å	9.101(3)	22.3043(11)	11.2657(12)	11.670(2)
a, °	90.00	90.00	90.00	101.613(3)
b, °	94.854(5)	113.787(2)	102.717(2)	98.910(4)
g, °	90.00	90.00	90.00	98.038(4)
Volume, Å^3	774.6(4)	3834.6(3)	1247.5(2)	367.59(13)
Density (g/cm^3)	1.166	1.283	1.305	1.455
Temperature (K)	203(2)	163(2)	203(2)	203(2)
X-ray wavelength	0.71073	0.71073	0.71073	0.71073
m, (mm^{-1})	0.081	0.083	0.089	0.104
Q_{min} (°)	2.71	2.00	2.20	1.81
Q_{max} (°)	27.45	28.26	28.28	28.23
Reflections				
collected	4389	13899	9199	2657
independent	1677	4428	2873	2225
observed	656	2332	2009	1860
Threshold expression	I >2s(I)	I >2s(I)	I >2s(I)	I >2s(I)
R_1 (observed)	0.0387	0.0514	0.0474	0.0446
wR_2 (all)	0.0997	0.1381	0.1407	0.1085

3.3 Synthesis

3-Methylphenylboronic acid was synthesized by adding the Grignard reagent of 3-bromotoluene to a THF solution of triisopropyl borate. The mixture was stirred at -78 ºC for one hour, whereupon the reaction was quenched with sulfuric acid and the desired product was subsequently extracted with ether and recrystallized from hot water to produce colorless needles; yield: 84%; mp: 160-163 ºC. 4-Methylphenylboronic was prepared in the same way; yield 83%; m.p. 244-246 ºC. 4-carboxyphenyl boronic acid was synthesized by oxidation with potassium permanganate of 4-methylphenyl boronic acid; yield 59%; m.p. 232-233 ºC.

The crystal structure determination of **1** shows that the two hydroxyl groups are arranged in a *syn* and *anti* manner, respectively. [10] The primary hydrogen-bond motif in this structure, Table 2, is a head-to-head dimeric interaction composed of two symmetry related O-H…O interactions (similar to a classic dimeric carboxylic acid motif**) Figure 2**.

Table 2.
Hydrogen-bond geometries for 1-4

	D–H	H…A	D…A	<(DHA)	Generator for A
1					
O8-H8…O9	0.922(19)	1.804(19)	2.7241(19)	175.5(18)	-x, -y, -z
O9-H9…O8	0.873(19)	1.848(19)	2.7024(19)	165.6(18)	X, -y-1/2, z-1/2
2					
O11A-H11C…N21	0.83(3	1.99(2)	2.80(2)	170(3)	
O12B-H12D…N21	0.86(4)	1.99(2)	2.83(3)	167(3)	
O11B-H11D…N31	0.92(4)	1.793(19)	2.70(3)	169(2)	
O12A-H12C…N31	0.98(3)	1.793(19)	2.76(2)	169.9(18)	
3					
O11-H11…N21	0.85(2)	1.93(2)	2.7719(16)	169.8(18)	
N22-H22A…O12	0.894(19)	2.131(19)	2.9987(17)	163.4(16)	
N22-H22B…O11	0.90(2)	2.19(2)	3.0003(18)	151.0(16)	x, -y-1/2, z-1/2'
O12-H12…N23	0.80(2)	2.03(2)	2.8094(17)	164.3(18)	-x, y+1/2, -z+1/2
4					
O16-H16…N21	0.82	1.85	2.667(3)	173.9	
O18-H18…N31	0.82	2.00	2.813(3)	173.0	
O19-H19…O17	0.82	2.11	2.839(2)	148.8	
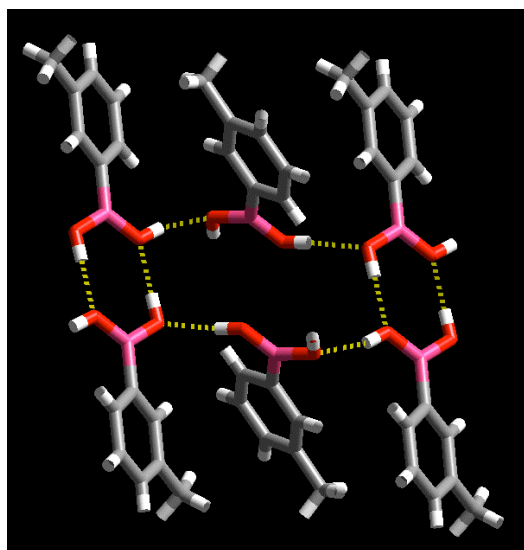
Figure 2. Head-to-head hydrogen-bonded dimers interconnected into an infinite ladder in the crystal structure of **1**.

The centrosymmetric dimers are further connected into a ladder like structure with the same connectivity as the motif commonly displayed by primary amides [11]. However, whereas the latter are often more or less planar, the boronic acid ladder is composed of dimers that are arranged in alternating perpendicular fashion along the ladder.

The crystal structure of **2** [12] demonstrates that a pyridyl moiety is capable of breaking the boronic acid dimer and replacing it with near-linear O-H···N hydrogen bonds (Table 2), which is similar to the well-known structure-directing COOH···py [13] and R-OH···py synthons, **Figure 3**[14].
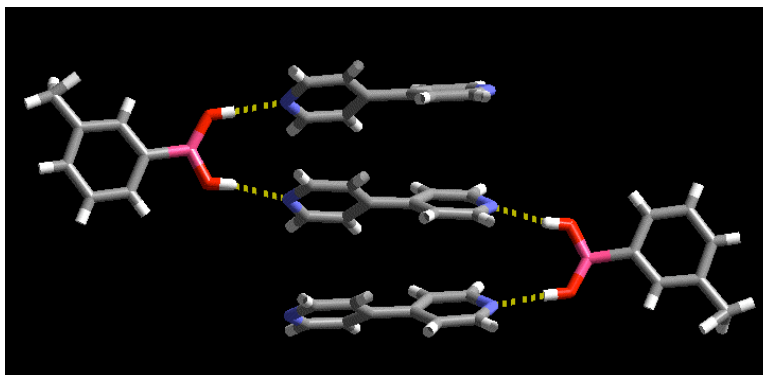
Figure 3. Discrete pentameric supermolecule in **2** assembled via four (two equivalent) O-H···N hydrogen-bond interactions.

One part of the hydrogen-bonded motif in **2** is akin to the interactions that commonly take place between resorcinol-based components and bipyridyl-type compounds [15]. However, the separation between OH groups in boronic acid is not sufficient to allow for the formation of a discrete tetramer as observed in resorcinol:4,4'-bipy [16]. The end result is a discrete pentameric supermolecule that leaves two terminal nitrogen atoms, N(41) without any strong hydrogen-bond interactions. There are also no C-H···N interactions involving this nitrogen atom (the shortest N(41)···C distance is over 3.4Å).
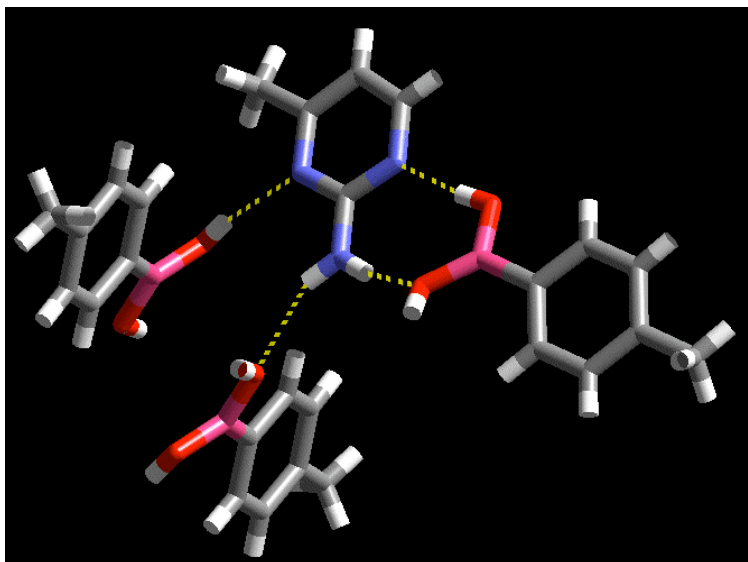
Figure 4. The complementarity of 2-aminopyrimidine:boronic acid drives the formation of the co-crystal in **3.** The additional proton on boronic acid provides a crosslink.

A paper by Etter *et al* [17] reporting the crystal structure of a carboxylic acid: 2-aminopyrimidine co-crystal provided a classic example of how heteromeric complementary hydrogen-bond interactions can be employed as the driving force for binary molecular solids. The crystal structure of **Figure 4** shows that the boronic acid moiety engages in an $R_2^2(8)$ motif with 2-aminopyrimidine (as do carboxylic acids), Table 2. However, the additional hydrogen-bond donor on boronic acid creates a more complex 3-D motif compared with the discrete 0-D motif (between 2-aminopyrimidine and monocarboxylic acids) or 1-D motif (in the case of 2-aminopyrimidine and dicarboxylic acids).

Finally, given the fact that both carboxylic acids and boronic acids are capable of forming strong and directional O-H⋯N hydrogen bonds to a pyridyl moiety, the crystal structure of **4** [18]**,** does not reveal any surprising primary intermolecular interactions, **Figure 5**. The primary interaction is likely to be the py⋯COOH hydrogen bond; a common supramolecular interaction that has been instrumental in the design of one- and two-dimensional supramolecular architectures, such as infinite chains, [19] honeycomb layers,[[20] and sheets,[21]. Since the reaction was carried out in a 1:1 ration, this leaves a good hydrogen-bond donating moiety, the $B(OH)_2$ group) and one good hydrogen-bond acceptor, the remaining pyridyl moiety. As demonstrated in previous studies [4, 5] the self-complementary boronic acid dimer can be broken in favor of a $B(OH)_2$⋯py interaction, which is exactly what happens in the crystal structure of **4**.
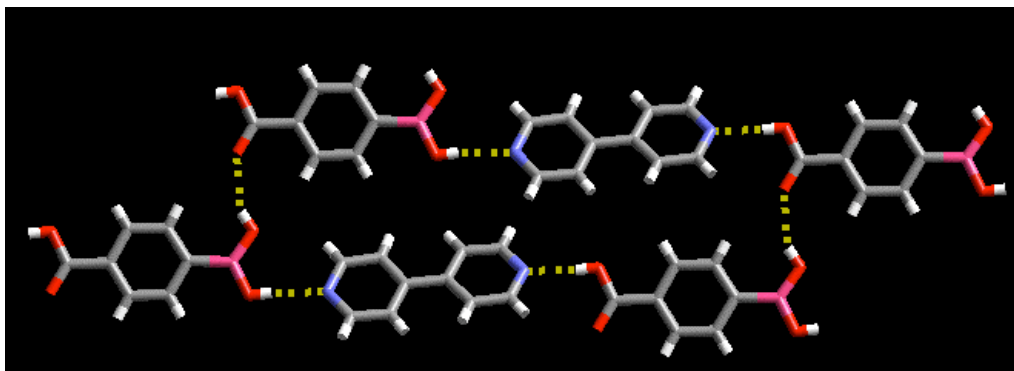
Figure 5. Horizontal infinite chains of bipy and 4-carboxyphenylboronic molecules in the crystal structure of **4** connected through O-H⋯N hydrogen bonds.

The combination of the acid⋯py, $B(OH)_2$⋯py, and $B(OH)_2$⋯acid hydrogen bonds leads to infinite chains of alternating bipy and 4-carboxyphenyl boronic acid held together via COOH⋯py and R-OH⋯py, which are cross-linked by O-H⋯O interactions (from boronic acid to carboxylic acid) resulting in a 2-D hydrogen-bonded sheet.. All primary hydrogen-bond donors and acceptors are satisfied and the main intermolecular interactions in **4** are readily rationalized based upon existing structural information.

This study has demonstrated that the boronic acid moiety may be incorporated into more complicated modular supramolecular synthetic strategies by virtue of its ability to form predictable hydrogen-bond interactions with a variety of well-known acceptor sites. It remains to be seen how reliable this moiety is, or how it can be made to fit in a hierarchical approach to the assembly of ternary and higher-order supermolecules and molecular solids. However, these results indicate that it can become a useful building block along the lines of carboxylic acids, carboxamides and oximes in the construction of robust and reliable extended architectures.

4. ACKNOWLEDGEMENTS

5. REFERENCES

[1] N. Miyaura and A. Suzuki, *Chem. Rev.* **95** (1995), 2457.
[2] C.B. Aakeröy, J. Desper, and B. Levin, *CrystEngComm.,* **7**, (2005), 102.

[3]   S.J. Rettig and J. Trotter, *Can. J. Chem*. **55** (1977), 3071.

[4]   SMART v5.060, © 1997 - 1999, Bruker Analytical X-ray Systems, Madison, WI.

[5]   SAINT v6.02, © 1997 - 1999, Bruker Analytical X-ray Systems, Madison, WI.

[6]   SHELXTL v5.10, © 1997, , Bruker Analytical X-ray Systems, Madison, WI.

[7]   Two –CH$_3$ rotamers were included in the structure model, with common carbon temperature factors and coordinates, and total occupancy constrained to 1.0.

[8]   L. Leiserowitz and F. Nader, *Acta Crystallogr. Sect. B*, **33** (1977), 2719.

[9]   Colourless needles, m.p. 62-65 ^{o}C, obtained via slow evaporation from 1:1 ethanol/water.

[10]   (a) C.B. Aakeroy, A.M. Beatty and B.A. Helfrich, *J. Am. Chem. Soc.* **124** (2002), 14425. (b) P. Vishweshwar, A. Nangia and V.M. Lynch, *Cryst. Growth Des*. **3** (2003), 783. (c) R. D. Bailey Walsh, M.W. Bradner, S. Fleischman, L.A. Morales, B. Moulton, N. Rodriguez-Hornedo and M.J. Zaworotko, *Chem. Commun*. **186** (2003) 186. (d) T. Nguyen, F.W. Fowler and J.W. Lauher, *J. Am. Chem. Soc.* **123** (2001), 11057.

[11]   Two superimposed boronic acid molecules were observed, occupying nearly the same volume but differing in the orientation of the *m*-CH$_3$ group. Thermal parameters for the two B(OH)$_2$ moieties were highly correlated and were therefore combined pairwise with free variables. Geometry for the two boronic acid molecules was constrained with a SHELXTL "SAME" command.

[12]   L.R. MacGillivray, J.L. Reid and J.A. Ripmeester, *J. Am. Chem. Soc*., **122** (2000), 7817.

[13]   The separation between hydroxylic protons in 1,3-resorcinol is 3.5 Å, which is ideally suited for bringing two aromatic systems together for a 2+2 photodimerization reaction.

[14]   M.C. Etter and D.A. Adsmond, *J. Chem. Soc., Chem. Commun*. (1990) 589.

[15]   The molecule lies on an approximate center of symmetry, with the boronic and carboxylic acid groups nearly superimposed. The structure refined poorly in the centrosymmetric space group P-1 and symmetry was decreased to P1 (Friedel coverage = 37%). Attempts to refine hydroxyl hydrogen atoms led to unreasonable bond distances; these hydrogen atoms were constrained to idealized positions with the SHELX "AFIX 83" constraint.

[16]   N. Shan, A.D. Bond, and W. Jones, *New J. Chem.* **2003**, *2*, 365; N. Shan, E. Batchelor, and W. Jones, *Tetrahedron Lett.* **2002**, *43*, 8721; R. Liu, S. Valiyaveettil, K.-F. Mok, J.J. Vittal, and A.K.M. Hoong, *CrystEngComm.* **2002**, *4*, 574.

[17]   C.V.K. Sharma and M.J. Zaworotko, *Chem. Commun.* (1996), 2655; B.R. Bhogala and A. Nangia, *Cryst. Growth Des*. **3**, (2003), 547; B.-Q. Ma and P. Coppens, *Chem. Commun.* (2003), 2290.

[18]   K.K. Arora and V.R. Pedireddi, *J. Org. Chem.* **68**, (2003), 9177; P. Vishweshwar, A. Nangia, and V.M. Lynch, *J. Org. Chem*. **67**, (2002), 556.

HYDROGEN-BONDED HOST FRAMEWORKS WITH TUNABLE CAVITIES: STRUCTURAL CHARACTERIZATION AND INCLUSION-BASED SEPARATIONS OF MOLECULAR ISOMERS

Matthew J. Horner, Sara Grabowski, Kevin Sandstrom, K. Travis Holman, Mamoun Bader
and Michael D. Ward
*Dept. of Chemical Engineering and Materials Science, Univ. of Minnesota, Amundson Hall, 421
Washington Ave SE, Minneapolis, MN, 55455, USA*
*wardx004@umn.edu*

Woo-Sik Kim
Dept. of Chemical Engineering, Kyung-Hee Univ. Kyungki-do 449-701, Korea

1. ABSTRACT

Single crystal X-ray diffraction reveals that inclusion compounds formed from **G$_2$MDS** and **G$_2$TMBDS** hosts (**MDS** = mesitylenedisulfonate; **TMBDS** = 2,4,5,6-tetramethylbenzenedisulfonate) and various isomeric methylated benzene guests crystallize in polar space groups with guests occupying one-dimensional channels between sheets of hydrogen-bonded guanidinium ions and sulfonate moieties. The inclusion selectivity for isomeric mixtures of trimethylbenzenes and tetramethylbenzene guests by these host frameworks has been examined. The organic residues of the **MDS** and **TMBDS** pillars mimic the isomeric trimethylbenzenes and tetramethylbenzenes, respectively, suggesting an avenue to a separations protocol based on molecular recognition during inclusion and subsequent crystallization. Pairwise competition experiments, in which inclusion compounds are crystallized from solutions containing a mixture of two molecular isomers, map the inclusion selectivity of a particular host as a function of guest content in solution. The single crystal structures suggest that guest inclusion selectivity is governed by the ability of a host to achieve efficient packing with the guest molecules and its ability to allow efficient guest-guest packing in the one-dimensional channels. Consequently, the more compliant **G$_2$MDS** host exhibits higher selectivities for guest inclusion. Overall, the selectivity patterns appear to reflect size and shape compatibility between the host and guest, suggesting opportunities for separations of isomers based on straightforward crystallization processes.

2. INTRODUCTION

Distillation, crystallization, and liquid-liquid extractions are commonly employed unit operations that isolate constituents of a mixture based on differences in volatility or solubility. If the components of a mixture have extremely similar properties, as is generally the case for molecular isomers, traditional separation methods can be unfeasible to the extent that less conventional approaches, such as selective sorption or inclusion within a host material, may be required. Whereas traditional porous materials, such as inorganic zeolites, have been studied extensively and have achieved considerable commercial success in this respect,[1] modern "designer" inclusion materials, such as molecule-based organic[1,2] and metal-organic[4] hosts, also hold considerable promise for selective inclusion. Unlike covalent host frameworks, which rely on selective sorption and diffusion through pre-existing pores, the "pores" in non-covalent frameworks are typically created during assembly of the crystalline inclusion compound and are generally only sustainable when occupied by guest molecules.[5] Nevertheless, if the host is selective, the preferentially included guest can be separated from a solution mixture by filtration of the crystallized inclusion compound. The guest can then be retrieved, for example by dissolution and extraction, under mild conditions and the host material can be recycled (Scheme 1).
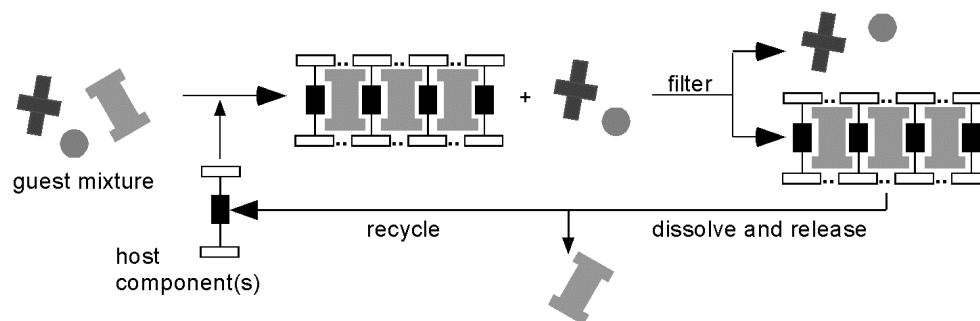
Scheme 1.

Organic or molecular hosts are particularly appealing candidates for selective inclusion because their general solubility allows for both effective retrieval of included guests and recycling of the host material. Serious limitations still exist, however, with respect to the design of an appropriate organic host for a particular separations application. For example, many traditional organic hosts, such as (thio)urea,[6] tri-*o*-thymotide,[7] Dainin's compound,[8] perhydrotriphenylene,[9] and cyclotriveratrylene,[10] cannot be chemically modified or tailored without the concomitant loss of the inclusion capabilities of the host. Although some molecular hosts, such as Werner complexes[11] and many diol hosts,[12,13] are amenable to chemical modification, such modifications rarely lead to *predictable* changes in the size or shape of the inclusion cavities. Therefore, even though numerous inclusion hosts are available and strategies for the *de novo* molecular-level design of hosts have been proposed,[3] a particular separation typically requires the design and testing of a variety of hosts, frequently with rather disparate compositions and architectures. In contrast, libraries of homologous inclusion hosts, in which the composition of the host is systematically adjusted but key architectural features are retained, may provide a route to effective and facile optimization of a particular separation.
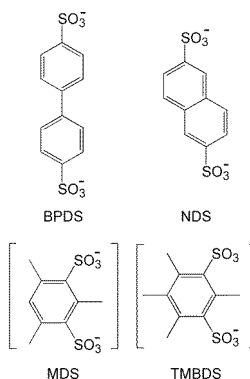
We have recently reported a family of homologous inclusion hosts that fulfill the above criteria.[14] Guanidinium (**G**) salts of organosulfonate anions (**S**) readily form lamellar motifs through hydrogen bonding between the N-H moieties of the **G** cations and the sulfonate moieties of the **S** anions.[14,15] The H-bonded **GS** lamellae adopt either a "quasi-hexagonal" arrangement **(Figure 1)** that reflects the complementary symmetries of the **G** ions (D_{3h}) and the sulfonate moieties (C_{3v}), or a closely related, albeit less common, "shifted-ribbon" motif (not shown). In either arrangement, the **GS** lamellae can be pillared in the third dimension by the readily modified organic residues of organo*di*sulfonate anions, thereby creating inclusion cavities between the sheets that are occupied by guest molecules during assembly of the **GS** host lattice. The lamellar character of the **GS** host framework persists for a diverse collection of pillars and guests, a feature that can be partially attributed to an inherent ability of the **GS** sheet to pucker about an axis of hydrogen bonds connecting adjacent rigid one-dimensional **GS** "ribbons, thus allowing the host to optimize packing of the pillars and guests. Furthermore, these hosts can adopt several architectures that differ with respect to the manner in which the pillars connect adjacent sheets.[16]

Matthew J. Horner, Sara Grabowski, K. Sandstrom, K. Travis Holman, M. Bader, M. D. Ward and Woo-Sik Kim

Our laboratory recently capitalized on the unique characteristics of these pillared hosts to separate molecular isomers of xylenes and dimethylnaphthalenes,[17] demonstrating that remarkable selectivities could be achieved by choosing hosts with inclusion cavity sizes that straddled the steric boundary between two host architectures –in this case the "discrete bilayer" and the "simple brick" forms - for a particular set of guest isomers **(Figure 1)**. This protocol relied on linear organodisulfonate pillars in which the sulfonate groups were strictly antiparallel, for example, 4,4'-biphenyldisulfonate (**BPDS**) and 2,6-naphthalenedisulfonate (**NDS**). Our laboratory, however, also has reported inclusion compounds based on "bent," or "banana-shaped," pillars, such as mesitylenedisulfonate (**MDS**) and 2,4,5,6-tetramethylbenzenedisulfonate (**TMBDS**). These inclusion compounds adopted layered orthorhombic and monoclinic brick architectures, with the **GS** sheets puckered as a consequence of the geometric constraints imposed by the pillar (rather than puckering driven by close-packing between pillars and guests for linear pillars).[18] Furthermore, the geometry of the bent pillar and the continuous architecture of the simple brick host enforce polar symmetry (*Imm*2 for the orthorhombic compounds). The guests in these compounds were confined to one-dimensional channels perpendicular to the pleats of the **GS** sheet **(Figure 2)**.
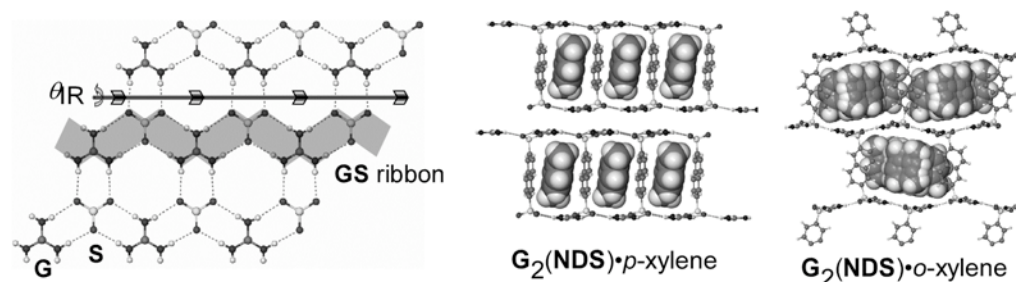
Figure 1. (left) Schematic representation of the **GS** sheet, illustrating the hydrogen-bonding "hinge" about which the sheet puckers to optimize host-guest packing when "straight" pillars are used. (right) The discrete bilayer and simple brick architectures observed for guanidinium-2,6-naphthalenedisulfonate with *p*-xylene and *o*-xylene guests, respectively.
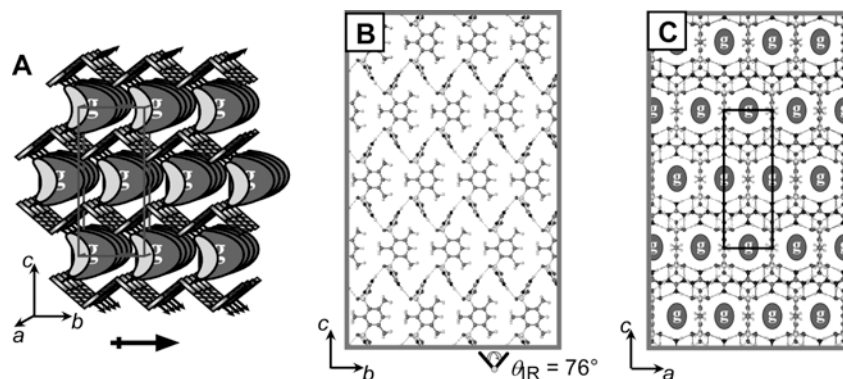
Figure 2. (A) Schematic representation of an inclusion compound prepared with a bent "banana-shaped" organodisulfonate and dipolar guest molecules. The host is inherently polar because the framework can only assemble with all the bent pillars oriented in the same direction. (B, C) Views of a typical inclusion compound, here illustrated by **G₂MDS•(nitrobenzene)**.

The organic residues of the **MDS** and **TMBDS** pillars mimic isomeric trimethylbenzenes (3MB) and tetramethylbenzenes (4MB), respectively, suggesting they may provide some degree of molecular recognition with these isomers, which is essential for the crystallization-based separations protocol. Furthermore, the size of the channels in these hosts is comparable to the dimensions of the 3MB and 4MB isomers, a characteristic that could yield selectivity due to subtle shape differences among the isomeric guests. We describe herein the crystal structures of several inclusion compounds based on these pillars and guests and the selectivity of guest inclusion by these hosts.

3. RESULTS AND DISCUSSION

3.1 Selectivity And Separations Protocol

Pairwise competition experiments, wherein inclusion compounds are grown from a series of solutions of known guest composition, can be used to determine the dependence of inclusion selectivity on the solution content of the two guests (A and B). The selective preference of a host (**H**) for one compound (A) from the mixture can be described by a *selectivity coefficient* ($K_{A:B}$), defined according to equation (1), where X_A and X_B represent the mole fractions of the two competing guests in the original solution and Y_A and Y_B represent the corresponding mole fractions of the same guests in the resulting inclusion compound. If the selectivity coefficient is constant over the entire range of X_A, the selectivity profile will be symmetrical about a line drawn from the lower right to the upper left corners (**Figure 3**, curves a-d). Symmetrical curves are common for host materials with pre-existing pores and host structures that are unchanged upon guest inclusion.[1a] The $K_{A:B}$ of molecular hosts, however, can be influenced by the relative concentrations of guests in the original solution mixture, affording less symmetrical curves such as that depicted in curve (e) of **Figure 3**.[8] Asymmetric curves also can reflect the formation of structurally dissimilar inclusion compounds for different guests.

$$K_{A:B} = (K_{B:A})^{-1} = Y_A/Y_B \cdot X_B/X_A \qquad\qquad (X_A + X_B = 1)$$

(1)
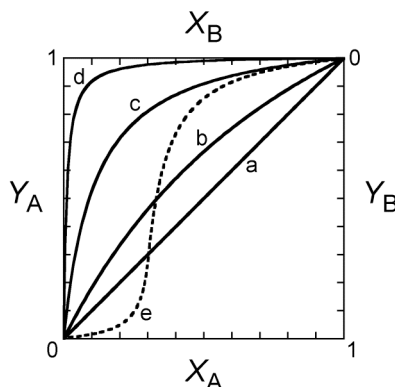
Figure 3. Pairwise competition experiments can be used to map the inclusion selectivity of one guest (A) relative to another (B). The mole fractions of guests in the inclusion compound (Y_A or Y_B) are plotted as a function of the mole fraction of guests in the original solution mixture (X_A or X_B). The selectivity coefficient, $K_{A:B}$ (or $K_{B:A}$) can be extracted from any point on the curve. Larger selectivity coefficients correspond to a greater enrichment of guest A in the inclusion compound. (a) $K_{A:B} = 1$ (no selectivity), (b) $K_{A:B} = (K_{B:A})^{-1} = 2$, (c) $K_{A:B} = (K_{B:A})^{-1} = 10$, (d) $K_{A:B} = (K_{B:A})^{-1} = 100$. (e) $K_{A:B}$ is concentration dependent. Under conditions of low X_A ($0 < X_A < 0.3$) guest B is preferentially included ($K_{A:B} < 1$). At larger X_A ($0.3 > X_A > 1$) the selectivity is inverted ($K_{A:B} > 1$) and guest A is included preferentially.

The inclusion selectivity of molecular isomers by the **GS** hosts with bent pillars was examined by pairwise competition experiments, wherein crystals of inclusion compounds were retrieved from methanolic solutions containing a particular **GS** host and a combined excess of guest isomers. The mole fractions of the two guests in solution were varied and their compositions in the crystallized inclusion compounds were determined by gas chromatography and plotted in a manner identical to **Figure 3**, with X_{guest} and Y_{guest} representing the mole fraction of one of the guests in the original solution and the inclusion compound, respectively.

3.2 Single Crystal Structures Of Inclusion Compounds

G_2MDS and G_2TMBDS readily form crystalline inclusion compounds with various trimethylbenzene (3MB) and tetramethylbenzene (4MB) isomers. Single crystal structures for G_2MDS·(1,2,4-3MB), G_2MDS·(1,3,5-3MB), G_2TMBDS·(1,2,3-3MB), G_2TMBDS·(1,3,5-3MB), and G_2TMBDS·(1,2,3,5-4MB) (Table 1) reveal the anticipated polar host architecture in which the GS sheet is highly puckered and the banana-shaped pillars are oriented along the polar *b* axis of the crystals. The guest molecules are confined within 1D corrugated channels, oriented along the *b* axis **(Figure 4)**. The guests are offset in the *b* direction with respect to the bent pillars such that they occupy inclusion cavities between "pinch-points" created by the pleats of GS sheets. For convenient comparison of these structures, which crystallize in orthorhombic or

Matthew J. Horner, Sara Grabowski, K. Sandstrom, K. Travis Holman, M. Bader, M. D. Ward and Woo-Sik Kim

monoclinic structures, the crystallographic lattice constants are rearranged at the bottom of Table 1 so that the polar axis is along *b* for all these compounds. The monoclinic structures deviate from the ideal *Imm2* space group symmetry due to a slight twist [19] of the disulfonates, which ranges from 11º for G_2TMBDS·(1,2,3-3MB) to 17º for G_2TMBDS·(1,3,5-3MB). This in turn induces a tilt of the guest molecules along the *a* direction, ranging from 13º to 18º with respect to the normal to the GS sheet. The guests in the G_2MDS·(1,2,4-3MB) and G_2TMBDS·(1,2,3-3MB) structures are disordered over multiple positions and orientations. For G_2TMBDS·(1,2,3-3MB) the guest molecules are disordered over a mirror plane located at the center of the channels parallel to the GS sheets. The guests in G_2MDS·(1,2,4-3MB) are disordered over four positions because they sit on mirror planes that intersect in the center of the guest channels.

Table 1

Crystallographic Data and Selected Structural Features for the Guanidinium Organodisulfonate Inclusion Compounds

compound	G_2**MDS**·(*1,2,4-3MB*)	G_2**MDS**·(*1,3,5-3MB*)	G_2**TMBDS**·(*1,2,3-3MB*	G_2**TMBDS**·(*1,3,5-3MB*)[18]	G_2**TMBDS**·(*1,2,3,5-4MB*)
formula	$C_{20}H_{34}N_6O_6S_2$	$C_{20}H_{34}N_6O_6S_2$	$C_{21}H_{36}N_6O_6S_2$	$C_{21}H_{36}N_6O_6S_2$	$C_{22}H_{38}N_6O_6S_2$
formula wt.	518.66	518.66	532.68	532.68	546.70
crystal system	orthorhombic	orthorhombic	monoclinic	monoclinic	monoclinic
space group	*Imm2*	*Imm2*	*C2*	*C2*	*C2*
color	colorless	colorless	colorless	colorless	colorless
a (Å)	19.246(3)	20.578(7)	20.061(3)	20.018(5)	19.929(4)
b (Å)	7.512(1)	7.386(2)	9.255(1)	9.211(2)	9.297(2)
c (Å)	9.219(2)	8.168(3)	7.555(1)	7.558(2)	7.581(2)
α (°)	90	90	90	90	90
β (°)	90	90	108.723(2)	107.459(4)	107.757(4)
γ (°)	90	90	90	90	90
V (Å^3)	1332.9(4)	1241.4(7)	1328.6(3)	1329.4(6)	1337.6(5)
temp. (K)	173(2)	173(2)	173(2)	173(2)	173(2)
Z	2	2	2	2	2
R_1 [$I > 2\sigma(I)$]	0.0703	0.0450	0.0389	0.0344	0.0270
wR_2 [$I > 2\sigma(I)$]	0.2064	0.1138	0.1079	0.0865	0.0721
G.O.F.	1.267	1.100	1.017	1.012	1.052
θ_{IR} (°)	96.2	80.5	97.4	96.6	98.0
Torsion[19] (°)	0.0	0.0	11.6	17.0	16.4
Guest Tilt (°)	0	0	13	18	17
Packing Fraction[20]	67.7	70.3	68.2	68.5	69.8

Rearranged lattice constants (*a*, *b*, *c*) for direct comparison of orthorhombic and monoclinic structures

|					
a (Å)	7.512(1)	7.386(2)	7.555(1)	7.558(2)	7.581(2)
b (Å)	9.219(2)	8.168(3)	9.255(1)	9.211(2)	9.297(2)
c (Å)	19.246(3)	20.578(7)	20.061(3)	20.018(5)	19.929(4)
α (°)	90	90	90	90	90
β (°)	90	90	108.723(2)	107.459(4)	107.757(4)
γ (°)	90	90	90	90	90

The inter-ribbon puckering angles (θ_{IR}) ranged from 80.5º to 98º, smaller than the value of 120º expected from the geometry of the pillars. These values reflect a contraction along the *b*-direction that supercedes the geometric enforcement of the pillars, which results in pillar-to-pillar distances ranging from 8.17 Å to 9.30 Å along *b*. For example, the inter-ribbon puckering angle for **G$_2$MDS**·(1,3,5-3MB) is noticeably lower (θ_{IR} = 80.5º) than **G$_2$MDS**·(1,2,4-3MB), as reflected by the smaller *b* value for **G$_2$MDS**·(1,3,5-3MB). This can be attributed to greater steric crowding between the methyl groups of the 1,2,4-3MB guest molecules along the channel direction (the *para* methyl substituents of the 1,2,4-3MB guest are oriented along the channel direction). The ability of the **G$_2$MDS** host to accommodate this steric crowding illustrates the compliant nature of this host, a property associated with the ease of puckering of the **GS** sheet. Furthermore, these structures reveal that the channel dimensions are dictated more by the guest-guest contacts than steric crowding between the **MDS** pillars. The effect of steric crowding between pillars, however, is evident from a comparison of **G$_2$MDS**·(1,3,5-3MB) and **G$_2$TMBDS**·(1,3,5-3MB), which have channel lattice constants of 8.168 Å and 9.211 Å, respectively, even though the guests are identical. Clearly, the fourth methyl group on the **TMBDS** pillar, which is pointing along the channel direction, forces expansion along the channel and a larger puckering angle. This steric crowding naturally makes the **G$_2$TMBDS** host less compliant, to the extent that is unable to shrink to dimensions that would optimize packing with the 1,3,5-3MB guest molecules. Notably, the packing fraction for **G$_2$MDS**·(1,3,5-3MB) is larger than that of **G$_2$TMBDS**·(1,3,5-3MB). It is not unreasonable to suggest that the compliance of the host would be an important factor in determining inclusion selectivity for guest isomers.
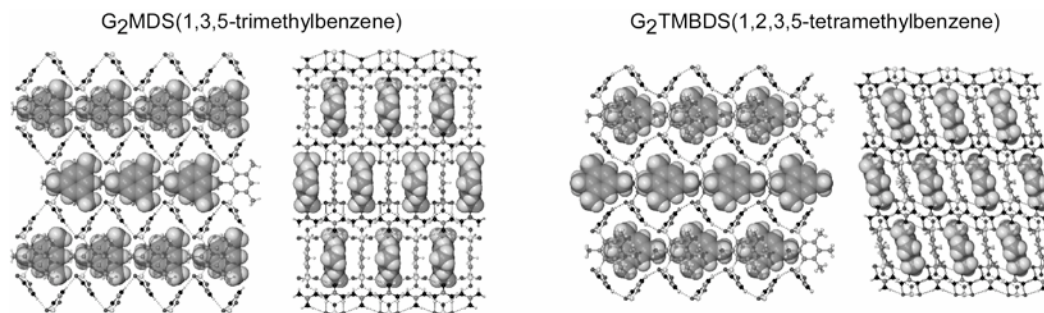
Figure 4. Representative structures of inclusion compounds obtained for the **G$_2$MDS** and **G$_2$TMBDS** hosts, here depicted with 1,3,5-trimethylbenzene (1,3,5-3MB) and 1,2,3,5-tetramethylbenzene (1,2,3,5-4MB) guests, respectively. The side views on the left reveal the puckering of the **GS** sheets enforced by the strict geometric constraints of the bent pillars. The views on the right depict the infinite channels running through the crystal, with the **G$_2$TMBDS** host exhibiting an unusual tilt of the pillars associated with a slight rotation of the sulfonates out of the plane of the **GS** ribbons.

3.3 Inclusion-Based Separations And Selectivity

Pairwise competition experiments were employed to determine the selectivity of the G$_2$MDS host towards different 3MB and 4MB isomers. The selectivity profiles, in which the mole fraction of a particular guest included in the host (*Y*) is plotted against the mole fraction of the same guest present in the initial crystallization medium (*X*), are depicted in **Figure 5**. Moderate selectivity is observed during separation of the 3MB isomers with the G$_2$MDS host, with the preference for inclusion decreasing in the order 1,3,5-3MB > 1,2,3-3MB > 1,2,4-3MB. The selectivity coefficients are $K_{1,3,5\text{-}3MB:1,2,4\text{-}3MB}$ = 9.2, however, $K_{1,3,5\text{-}3MB:1,2,3\text{-}3MB}$ = 1.8 and $K_{1,2,3\text{-}3MB:1,2,4\text{-}3MB}$ = 2.9. [21] The selectivity for the 4MB isomers with the G$_2$MDS host decreases in the order 1,2,3,5-4MB >> 1,2,4,5-4MB > 1,2,3,4-4MB, with 1,2,3,5-4MB included almost exclusively in pairwise competition with 1,2,4,5-4MB ($K_{1,2,3,5\text{-}4MB:1,2,4,5\text{-}4MB}$ = 32). This selectivity was observed when $0.3 < X_{1,2,3,5\text{-}4MB} < 1.0$, but fell steeply with decreasing $X_{1,2,3,5\text{-}4MB}$, becoming negligible at $X_{1,2,3,5\text{-}4MB}$ = 0.1. Similar behavior was observed for 1,2,3,4-4MB/1,2,4,5-4MB competition, with a selectivity coefficient of $K_{1,2,3,4\text{-}4MB:1,2,4,5\text{-}4MB}$ = 5.6, although the profile was more symmetrical. Negligible selectivity was observed for 1,2,3,5-4MB vs. 1,2,3,4-4MB ($K_{1,2,3,5\text{-}4MB:1,2,3,4\text{-}4MB}$ = 1.1).
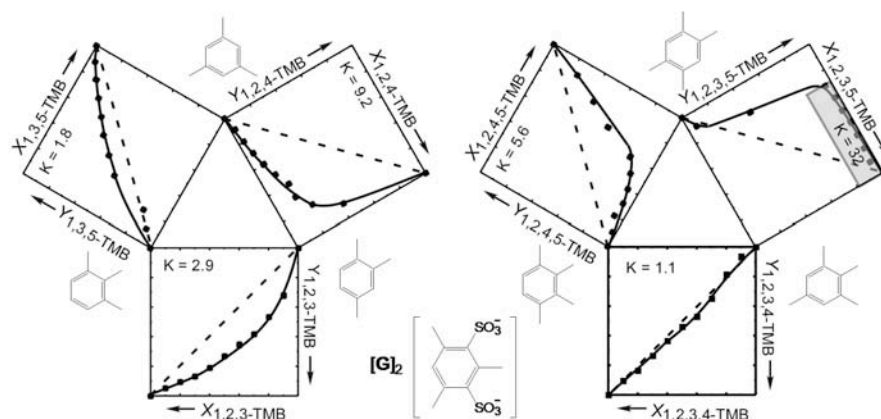
Figure 5. (left) Selectivity profiles for the inclusion of trimethylbenzene isomers by **G₂MDS**. The results of pairwise competition experiments are depicted as points on the plots at the periphery of the central triangle. The smooth curves represent average selectivity coefficients derived from the point data for pairwise competition. (right) Selectivity profiles for the inclusion of tetramethylbenzene isomers by **G₂MDS**. The smooth curves for 1,2,3,4-TMB/1,2,4,5-TMB and 1,2,3,4-TMB/1,2,4,5-TMB represents an average selectivity coefficients derived from the point data. The selectivity profile for 1,2,3,5-TMB/1,2,3,5-TMB competitions are highly concentration dependent, and the curves represent an arbitrary best fit of the data.

The selectivity profiles for inclusion of 3MB and 4MB isomers with **G₂TMBS** are depicted in **Figure 6**. Modest selectivities were observed for the 3MB isomers with the **G₂TMBS** host, decreasing in the order 1,2,4-3MB > 1,2,4-3MB > 1,2,3-3MB. The selectivity profiles are nearly symmetric, with $K_{1,3,5\text{-}3MB:1,2,3\text{-}3MB}$ = 3.4, $K_{1,3,5\text{-}3MB:1,2,4\text{-}3MB}$ = 2.0 and $K_{1,3,5\text{-}3MB:1,2,3\text{-}3MB}$ = 1.43. The selectivities for the 4MB isomers are also modest, with $K_{1,2,3,5\text{-}4MB:1,2,3,4\text{-}4MB}$ = 4.1, $K_{1,2,3,5\text{-}4MB:1,2,4,5\text{-}4MB}$ = 1.7 and $K_{1,2,3,5\text{-}4MB:1,2,4,5\text{-}4MB}$ = 1.1.
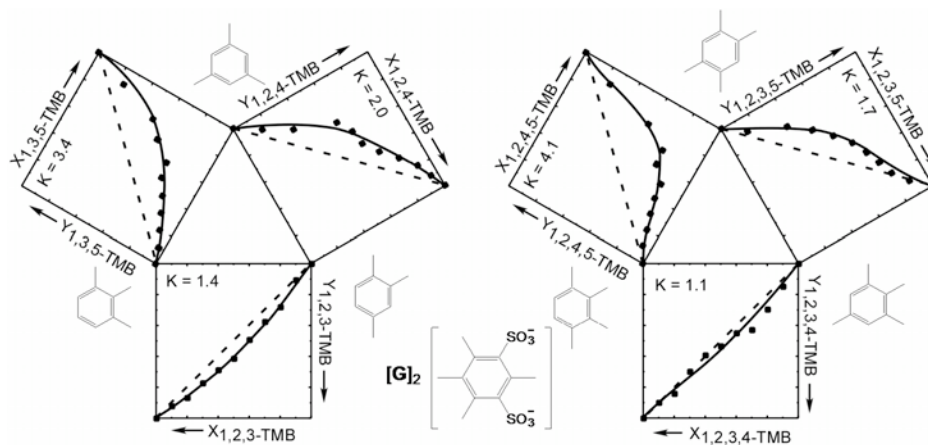
Figure 6. (left) Selectivity profiles for the inclusion of trimethylbenzene isomers by **G₂TMBDS**. The results of pairwise competition experiments are depicted as points on the plots at the periphery of the central triangle. The smooth curves represent average selectivity coefficients derived from the point data for pairwise competition. (right) Selectivity profiles for the inclusion of tetramethylbenzene isomers by **G₂TMBDS**.

4. CONCLUSION

The inclusion selectivity for trimethyl- and tetramethylbenzene isomers by the **G₂MDS** and **G₂TMBDS** hosts is moderate overall compared with the selectivities observed previously in our laboratory when architectural isomerism accompanied inclusion of different xylene and dimethylnaphthalene isomers by hosts with certain linear pillars. Instead, the selectivities observed here for the bent pillar host more closely resemble the behavior for the separation of xylenes with the **G₂BPDS** host, for which each xylene isomer was included in the bilayer architecture. Therefore, it is perhaps not surprising that bent-pillar hosts exhibit only marginal selectivities, simply because these hosts cannot adopt different architectures. Consequently,

effective isomer separation can only be achieved through some form of molecular recognition, most likely driven by differences in the compatibility of the shape of the host inclusion cavity and the included guest. Such an effect must be responsible for the rather high selectivity observed for **G$_2$MDS**·(1,2,3,5-4MB) and **G$_2$MDS**·(1,3,5-3MB). Notably, the selectivity coefficients generally are higher for the **G$_2$MDS** host. Inspection of the crystal structures of the **G$_2$MDS** and **G$_2$TMBDS** described above, as well as others reported previously, reveals that the former is more compliant and has the ability to achieve a smaller lattice constant along the channel direction. Consequently **G$_2$MDS** can achieve smaller inclusion cavity volumes that can better discriminate between guest isomers based on subtle shape differences. In contrast, the extra methyl group of the **TMBDS** pillar forces a larger separation between pillars and makes this host less compliant compared with **G$_2$MDS**. This in turn would create larger and more rigid inclusion cavities with reduced discriminating ability.

5. EXPERIMENTAL

5.1 Materials
Trimethylbenzenes and tetramethylbenzenes were used as received from either TCI America or Aldrich (Milwaukee, WI). Mesitylenedisulfonyl chloride and Tetramethylbenzenedisulfonyl chloride were purchased from TCI America. The disulfonic acids were prepared by hydrolysis of the corresponding disulfonyl chlorides by refluxing in dioxane/water overnight. The **G$_2$MDS** and **G$_2$TMBDS** hosts were prepared first as acetone clathrates by direct reaction of guanidinium tetrafluoroborate, prepared by neutralization of guanidinium carbonate with tetrafluoroboric acid, with the corresponding disulfonic acid in acetone. These compounds readily lose enclathrated acetone under ambient conditions to yield pure guanidinium organodisulfonate apohosts. Single crystals for X-ray diffraction were obtained from methanolic solutions containing the dissolved **GS** apohost and the corresponding guest where applicable. In addition to single crystal X-ray diffraction, the stoichiometry of guest inclusion was determined by ^{1}H NMR (Varian INOVA 200 MHz spectrometer) or thermal gravimetric analysis (Perkin Elmer TGA 7).

5.2 X-ray Crystallography
Single crystal structures of the inclusion compounds were determined at -100 ºC using either a Siemens or Bruker CCD platform diffractometer with graphite monochromated Mo-Kα radiation (λ= 0.71073 Å). The structures were solved by direct methods and refined with full-matrix least-squares/difference Fourier analysis using the SHELX-97-2 suite of software. [22] Where appropriate, all non-hydrogen atoms were refined with anisotropic displacement parameters and all hydrogen atoms were placed in calculated positions and refined with a riding model. Data were corrected for the effects of absorption using SADABS. Experimental details of the crystal structure determinations are compiled in Table 1. Single crystals of the inclusion compounds suitable for X-ray structure determination were prepared under ambient conditions by slow evaporation of methanolic solutions containing the appropriate host and guest components.

5.3 Inclusion Selectivity
A prepared isomeric mixture (with mole fractions ranging from 0.0 to 1.0) of two potential guests was added, in an approximate twenty-fold excess, to a methanolic solution of the guanidinium organodisulfonate host. Crystallization of the corresponding inclusion compounds commenced upon standing or after slow evaporation of some solvent. After approximately 25% of the total host material had precipitated from solution, the resulting crystals were harvested by filtration and washed briefly with cold methanol (to remove surface residue). The crystals were then dissolved in methanol and the solution was evaluated for isomer composition by gas chromatographic analysis. When the quality of the crystalline inclusion compounds permitted, the data obtained from batches of crystalline material were compared to data that could be obatined from what were seemingly individual single crystals. In all cases the results were essentially identical.

5.4 Gas Chromatography
Gas chromatographic analyses were performed with an HP 6890 series instrument using helium carrier gas and a flame ionization detector. The inlet and detector were held at constant temperatures of 200 °C and 250 °C, respectively, for all analyses. Complete resolution of trimethylbenzene and tetramethylbenzene

isomers was achieved with an All Tech Econocap capillary column (30m x 25mm diameter x 0.25μm stationary phase of EC-Wax) using a constant 1 ml/min flow rate and 150 °C.

6. ACKNOWLEDGEMENTS.

7. SUPPORTING INFORMATION

 CCDC 233456-233459 contains the supplementary crystallographic data for this paper. These data can be obtained free of charge via www.ccdc.cam.ac.uk/data_request /cif, by emailing data_request@ccdc.cam.ac.uk, or by contacting the Cambridge Crystallographic Data Centre, 12 Union Road, Cambridge CB2 1EZ, UK; fax: +44 1223 336033.

8. REFERENCES

[1]   (a) Q.-Q. Guo, H. Chen and Y.-C. Long, *Microporous Mesoporous Mater.* **39** (2000), 149. (b) J. Padin and R. T. Yang, *Chem. Eng. Sci.* **55** (2000), 2607. (c) H.-R. Lee and C.-S. Tan, *Ind. Eng. Chem. Res.* **39** (2000), 1035.

[2]   (a) J. L. Atwood, J. E. D. Davies, D. D. MacNicol (Eds) *Inclusion Compounds*, *Vol. 2* (*Structural Aspects of Inclusion Compounds Formed by Organic Host Lattices*) Academic Press: London, (1984). (b) E. Weber and H.-P. Josel, *J. Inclusion Phenom.* **1**, (1983), 79. (c) E. Weber, *Top. Cur. Chem.* **140** (1987), 1. (d) R. Bishop,. *Chem. Soc. Rev.* **25** (1996), 311. (e) Y. Aoyama, *Top. Curr. Chem.* **198** (1998), 131. (f) F. H. Herbstein, *Acta Chim.Hung.* **130** (1993), 377.

[3]   (a) E. Weber, *Top. Curr. Chem.* **149** (1988), 45. (b) E. Weber, in *Comprehensive Supramolecular Chemistry* (J. L. Atwood, J. E. D. Davies, D. D. MacNicol, F. Vögtle and K. S. Suslick, Eds.) **Vol. 6**, Elsevier: Oxford, (1996), 535. (c) O. Ermer and L. Lindenberg, *Helv. Chim. Acta* **74** (1991), 825. (d) R. K. R. Jetti, S. S. Kuduva, D. S. Reddy, F. Xue, T. C. W. Mak, A. Nangia and G. R. Desiraju, *Tetrahedron Lett.* **39** (1998), 913.

[4]   (a) M. J. Zaworotko, *Chem. Comm.* (2001), 1. (b) R. Robson, *Dalton* (2000), 3735. (c) P. J. Hagrman, D. Hagrman and J. Zubieta, *Angew. Chem. Int. Ed.* **38** (1999), 2639. (d) M. O'Keeffe, M. Eddaoudi, H. Li, T. Reineke and O. M. Yaghi, *J. Solid State Chem.* **152** (2000), 3. (e) S. R. Batten and R. Robson, *Angew. Chem. Int. Ed.* **37** (1998), 1461.

[5]   Some examples of molecule-based materials which maintain structural integrity upon guest removal have been recently reported: (a) M. Eddaoudi, D. B. Moler, H. Li, B. Chen, T. M. Reineke, M. O'Keeffe and O. M. Yaghi, *Acc. Chem. Res.* (2001), 34, 319. (b) P. Brunet, M. Simard and J. D Wuest,. *J. Am. Chem. Soc.* **119** (1997), 2737. (c) S.S.-Y. Chui, S.M.-F. Lo, J. P. H. Charmant, A. G. Orpen and I. D. Williams, *Science* **283** (1999), 1148. (d) S. Noro, S. Kitagawa, M. Kondo and K. Seki, *Angew. Chem. Int. Ed.* **39** (2000), 2082.

[6]   (a) K. D. M. Harris, *Chem. Soc. Rev.* **26** (1997), 279. (b) M. D. Hollingsworth and K. D. M. Harris, in *Comprehensive Supramolecular Chemistry Chemistry* (J. L. Atwood, J. E. D. Davies, D. D. MacNicol, F. Vögtle and K. S. Suslick, Eds.) **Vol. 6**, Elsevier: Oxford, (1996), 177.

[7]   (a) R. Gerdil, in *Comprehensive Supramolecular Chemistry Chemistry* (J. L. Atwood, J. E. D. Davies, D. D. MacNicol, F. Vögtle and K. S. Suslick, Eds.) **Vol. 6**, Elsevier: Oxford, (1996), 239. (b) R. Gerdil, *Top. Curr. Chem.* **140** (1987), 71.

[8]   D. D. MacNicol, in *Inclusion Compounds* (J. L. Atwood, J. E. D. Davies and D. D. MacNicol, Eds.) *Vol. 2*, Academic Press: London, (1984), 1.

[9]   (a) J. Hulliger, S. W. Roth, A. Quintel and H.Bebie, *J. Solid State Chem.* **152** (2000), 49. (b) M. Farina and S. G. P. Di Sozzani, in *Comprehensive Supramolecular Chemistry Chemistry* (J. L.

Atwood, J. E. D. Davies, D. D. MacNicol, F. Vögtle and K. S. Suslick, Eds.) **Vol. 6**, Elsevier: Oxford, (1996**)** 371. (c) M. Farina, in *Inclusion Compounds* (J. L. Atwood, J. E. D. Davies and D. D. MacNicol, Eds.) **Vol. 2**, Academic Press: London, (1984**)**, 69.

[10] (a) A. Collet, in *Comprehensive Supramolecular Chemistry Chemistry* (J. L. Atwood, J. E. D. Davies, D. D. MacNicol, F. Vögtle and K. S. Suslick, Eds.) **Vol. 6**, Elsevier: Oxford, (1996**)**, 281. (b) A. Collet, J.-P. Dutasta, B. Lozach and J. Canceill, *Top. Curr. Chem.* **165** (1993), 103. (c) A. Collet, *Tetrahedron* **43** (1987), 5725. (d) A. Collet, in *Inclusion Compounds* (J. L. Atwood, J. E. D. Davies and D. D. MacNicol, Eds.) **Vol. 2**, Academic Press: London, (1984**)**, 97.

[11] (a) W. D. Schaeffer, W. S. Dorsey, D. A. Skinner and C. G. Christian, *J. Am. Chem. Soc.* **79** (1957), 5870. (b) F. V. Williams, *J. Am. Chem. Soc.* **79** (1957), 5876. (c) J. Lipkowski, in *Comprehensive Supramolecular Chemistry Chemistry* (J. L. Atwood, J. E. D. Davies, D. D. MacNicol, F. Vögtle and K. S. Suslick, Eds.) **Vol. 6**, Elsevier: Oxford, (1996**)**, 691.

[12] (a) F. Toda, in *Comprehensive Supramolecular Chemistry Chemistry* (J. L. Atwood, J. E. D. Davies, D. D. MacNicol, F. Vögtle and K. S. Suslick, Eds.) **Vol. 6**, Elsevier: Oxford, (1996**)**, 465.

[13] (a) M. R. Caira, A. Horne, L. R. Nassimbeni and F. Toda, *J. Mater. Chem.* **7** (1997), 2145. (b) M. R. Caira, A. Horne, L. R. Nassimbeni and F. Toda, *J. Mater. Chem.* **8** (1998), 1481. (c) M. R. Caira, L. R. Nassimbeni, D. Vujovic and F.Toda, *J. Phys. Org. Chem*. **13** (2000), 75. (d) M. R. Caira, L. R. Nassimbeni, F. Toda and D. Vujovic, *J. Am. Chem. Soc.* **122** (2000), 9367. (e) J. Deng, Y. Chi, F. Fu, X. Cui, K. Yu, J. Zhu and Y. Jiang, *Tetrahedron: Asymmetry* **11** (2000), 1729. (f) K. Deketov, E. Weber, J. Seidel, K. Köhnke, K. Makhkamov and B. Ibragimov, *Chem. Comm.* (1999), 91.

[14] (a) J. A. Swift, A. M. Pivovar, A. M. Reynolds and M. D. Ward, *J. Am. Chem. Soc.* **120** (1998), 5887. (b) K. T. Holman, A. M. Pivovar, J. A. Swift and M. D. Ward, *Acc. Chem. Res.* **34** (2001), 107-118. (c) J. A. Swift, A. M. Reynolds and M. D. Ward*, Chem. Mater.* **10** (1998), 4159. (d) V. A. Russell, C. C. Evans, W. Li and M. D. Ward, *Science* **276** (1997), 575. (e) K. T. Holman and M. D. Ward, *Angew. Chem. Int. Ed.* **39** (2000), 1653. (f) C.C. Evans, L. Sukarto and M.D. Ward, *J. Am. Chem. Soc*. **121** (1999), 320. (g) J. A. Swift and M. D. Ward, *Chem. Mater*. **12** (2000), 150.

[15] (a) V. A. Russell, M. C. Etter and M. D. Ward, *J. Am. Chem. Soc.* **116** (1994), 1941. (b) V. A. Russell, M. C. Etter and M. D Ward,. *Chem. Mat.* **6** (1994), 1206. (c) V. A. Russell and M. D. Ward, *J. Mater. Chem.* **7** (1997), 1123.

[16] K. T, Holman, S. M. Martin, D. P. Parker and M. D. Ward, *J. Am. Chem. Soc*. **123** (2001), 4421.

[17] A. M. Pivovar, K. T. Holman and M. D. Ward, *Chem. Mater.*, **13** (2001), 3018.

[18] K. T. Holman, A. M. Pivovar and M. D. Ward, *Science* **294** (2001), 1907.

[19] The torsion angle is measured as the angular rotation along the bond between the sulfur atom and adjacent carbon atom containing the methyl group.

[20] Packing Fraction (PF) calculations were performed using MSI Cerius[2] v.4.2. PF values were obtained from the following relationship PF = ($V_{cell} - V_{available}$)/V_{cell}: where V_{cell} = Unit cell volume and $V_{available}$ is obtained by determing the "available volume" (probe radius = 0.5 Å, grid spacing of "fine").

[21] A selectivity coefficient, *K*, can be assigned for each data point on the respective competition plots. The values reported are averages of the selectivity coefficients obtained from the points in the regions of *X* specified. It should be noted that, owing to the limited amount of data, extremely small variation in the experimental values of *Y* lead to large differences in the calculated selectivity coefficients, consequently, the errors associated with *K* can be as large as ±60%

[22] *SHELX*-97, Sheldrick, G. M., University of Göttingen, (1997).

MAKING, USING, TRANSFORMING CRYSTALS: AN ORGANOMETALLIC HYDROGEN BONDED MATERIAL THAT REACTS WITH VAPOURS AND CRYSTALS

Dario Braga, Lucia Maini, Marco Polito, Stefano Giaffreda
Dipartimento di Chimica G. Ciamician, Univ. of Bologna, Via Selmi 2, 40126 Bologna, Italy
dario.braga@unibo.it

Katia Rubini
Centro CNR per la Fisica delle Macromolecole, c/o Dipartimento di Chimica G. Ciamician, Via Selmi 2, 40126 Bologna, Italy

Fabrizia Grepioni[†]
Dipartimento di Chimica, Univ. of Sassari, Via Vienna 2, 07100 Sassari, Italy
grepioni@ssmain.uniss.it

1. ABSTRACT

The organometallic zwitterion $[Co^{III}(\eta^5\text{-}C_5H_4COOH)(\eta^5\text{-}C_5H_4COO)]$ **1** reacts as a crystalline solid with both vapors and solids in solvent-free processes. When exposed to hydrated vapors of volatile acids (HCl, CF_3COOH, HBF_4, HCOOH) or bases (NH_3, NMe_3, NH_2Me) the corresponding salts or co-crystals are produced quantitatively. All these reactions are reversible, with the acid or base molecules being easily removed by thermal treatment under vacuum regenerating the starting material. The same compound reacts as a solid with crystalline alkali salts MX (M = K^+, Rb^+, Cs^+, NH_4^+; X = Cl^-, Br^-, I^-, PF_6^-, though not in all permutations of cations and anions). Manual co-grinding of the powdered materials generates supramolecular complexes of formula $[Co^{III}(\eta^5\text{-}C_5H_4COOH)(\eta^5\text{-}C_5H_4COO)]_2 \cdot M^+X^-$. In some cases the mechanochemical complexation requires *kneading* of the two solids with a catalytic amount of water. The robustness of the organometallic solid is due to the O-H···O hydrogen bond network joining carboxylic and carboxylate groups in molecular chains. Both solid-gas and solid-solid processes occur with profound transformations of the hydrogen bond networks. The solid-state structures of the novel compounds $[Co^{III}(\eta^5\text{-}C_5H_4COOH)(\eta^5\text{-}C_5H_4COO)] \cdot [Co^{III}(\eta^5\text{-}C_5H_4COOH)_2]^+I^-$ and $[C_6H_{12}N_2H_2]^{2+}[Co^{III}(\eta^5\text{-}C_5H_4COO)_2]_2^{2-} \cdot 1.5\ H_2O$ are also reported. The former has been obtained directly from solution crystallization while the latter has been obtained by mechanochemical treatment of the organometallic zwitterion **1** with the solid base 1,4-diazabicyclo[2.2.2]octane $[C_6H_{12}N_2]$.

2. INTRODUCTION

Crystal engineering is *making crystals by design* [1]. The paradigm is that of being able to assemble molecular or ionic components into a given target functional structure by controlling the periodical distribution of supramolecular interactions responsible for recognition, nucleation and growth of the crystalline material [2]. The deliberate construction of a molecular solid that can perform a desired function is conceptually related to the construction of a supermolecule [3]. In both cases, crystals and supermolecules, the collective properties depend on the aggregation via intermolecular bonds of two or more component units [4]. These interactions can be coordination bonds between ligands and metal centers and non-covalent bonds between neutral molecules or ions or – of course – any of their combinations.

A popular motivation for crystal engineering investigations and experiments is the design and preparation of nanoporous structures with voids and channels of controllable size that can be used for sensing, trapping, and storing small molecules [5]. Remarkable results have indeed been obtained [6]. An alternative to

---

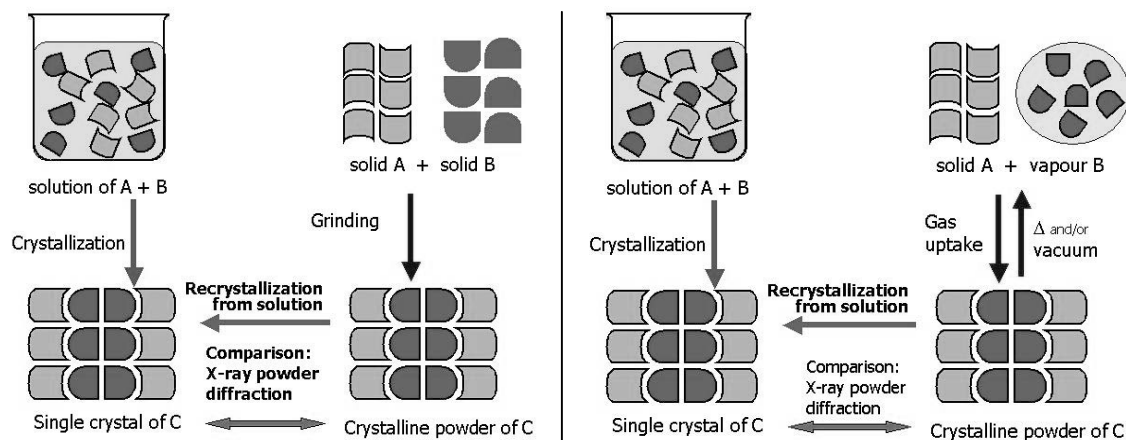[†] Present address: Dipartimento di Chimica, G. Ciamician, Univ. Bologna

nanoporosity is represented by *conventional* chemical reactivity. The controlled uptake and release of small molecules can be achieved by means of (possibly reversible) heterogeneous gas-solid reactions [7]. Solid-gas reactions of the type useful for gas uptake often imply profound transformations of the chemical and physical nature of the solid material and rarely are of practical use, unless fully reversible [8].

It is interesting to speculate on the analogy between the uptake of small molecules by a nanoporous material and the reaction between a molecular crystal and molecules to yield a co-crystal or a salt: both processes are *supramolecular reactions* whereby non-covalent interactions between guest and the host are broken and formed [9]. Solvent-free reactions between a molecular crystal and a gas or between two molecular crystals to yield molecular crystalline products are of interest in the quest for environmentally friendly processes (green chemistry) [10].

Here we report that the peculiar molecular and supramolecular features of the zwitterion sandwich complex $[Co^{III}(\eta^5-C_5H_4COOH)(\eta^5-C_5H_4COO)]$ [11], (**1**), permits both reversible gas-solid reactions with the hydrated vapors of a variety of acids (e.g. HCl, CF_3COOH, CCl_3COOH, CHF_2COOH, HBF_4 [12-14] but also weaker acids such as HCOOH [15]) and bases (e.g. NH_3, NMe_3, NH_2Me [12]) as well as solid-solid reactions with crystalline alkali salts. The reaction with crystalline alkali salts MX ($M = K^+$ [16a], Rb^+, Cs^+, NH_4^+; $X = Cl^-$, Br^-, I^-, PF_6^-, though not in all permutations of cations and anions) generates by means of mild manual co-grinding of the powdered materials supramolecular complex of formula $[Co^{III}(\eta^5-C_5H_4COOH)(\eta^5-C_5H_4COO)]_2 \cdot M^+X^-$ [16b]. Two new derivatives of **1** have also been obtained and are described herewith. Compound $[Co^{III}(\eta^5-C_5H_4COOH)(\eta^5-C_5H_4COO)] \cdot [Co^{III}(\eta^5-C_5H_4COOH)_2]^+I^-$ has been obtained directly from solution crystallization while $[C_6H_{12}N_2H_2]^{2+}[Co^{III}(\eta^5-C_5H_4COO)_2]_2^{2-} \cdot 1.5H_2O$ has been obtained by mechanochemical treatment of the organometallic zwitterion **1** with the solid base 1,4-diazabicyclo[2.2.2]octane $[C_6H_{12}N_2]$.

It is worth pointing out, before proceeding that both gas-solid and solid-solid reactions involving **1** yield powdered materials, which renders the determination of the solid-state structure rather complicated because of the lack of single-crystals. We have circumvented this problem by taking advantage of the *seeding* technique [17]. The use of pre-formed micro crystals of the desired phase can be exploited to *instruct* to generate the desired product [17].

Seeding procedures are commonly employed in pharmaceutical industries to make sure that the desired crystal form is always obtained from a preparative process [18]. The use of a *seeding* procedure often allows preparation of single crystals of suitable size, which, in turn, can be used to confirm *a posteriori* that the same phase obtained from solution crystallization and that yielded by solid-solid mixing processes has been obtained by comparing calculated and observed powder diffraction patterns [19]. The process described above, and used throughout this study, is pictured in **Scheme 1**.

Dario Braga, Lucia Maini, Marco Polito, Stefano Giaffreda, Katia Rubini and Fabrizia Grepioni

Scheme 1. Schematic representation of the procedure adopted to characterize products of mechanochemical treatments. The solid yielded by grinding reactants in a mortar is compared *via* X-ray powder diffraction with the solids obtained by crystallization *via* seeding of a solution of the ground powder of the adduct.

The zwitterion $[Co^{III}(\eta^5-C_5H_4COOH)(\eta^5-C_5H_4COO)]$ **1** can be quantitatively prepared from the corresponding dicarboxylic cationic acid $[Co^{III}(\eta^5-C_5H_4COOH)_2]^+$. The amphoteric behavior of the zwitterion depends on the presence of one -COOH group, which can react with bases, and one -COO$^{(-)}$ group, which can react with acids (see **Figure 1**). Incidentally, the organometallic zwitterion **1** is easy to handle and it is thermally stable up to a temperature of 506 K.
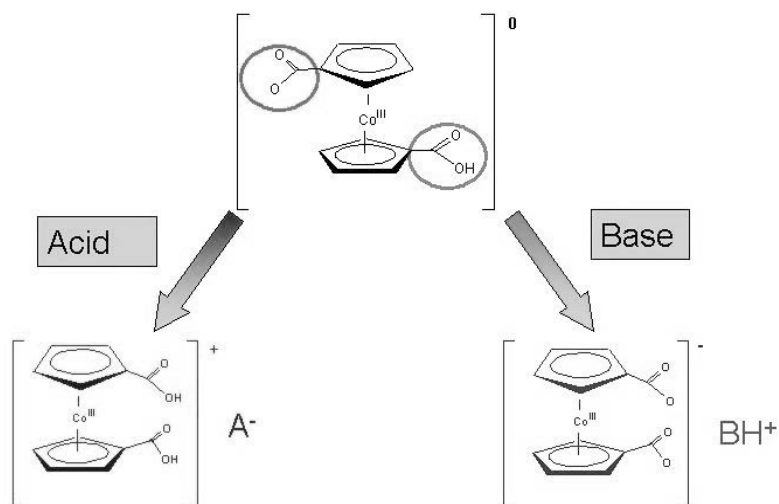
Figure 1. Compound $[Co^{III}(\eta^5-C_5H_4COOH)(\eta^5-C_5H_4COO)]$ **1** reacts with bases to yield the fully deprotonated form $[Co^{III}(\eta^5-C_5H_4COO)_2]^-$ and with acids to yield the fully protonated form $[Co^{III}(\eta^5-C_5H_4COOH)_2]^+$.

3. SOLID STATE REACTIVITY: GAS-SOLID REACTIONS AND SOLVATION PROCESSES

As mentioned above $[Co^{III}(\eta^5-C_5H_4COOH)(\eta^5-C_5H_4COO)]$ undergoes fully reversible heterogeneous reactions with the hydrated vapors of a variety of acids (e.g. HCl, CF_3COOH, CCl_3COOH, CHF_2COOH, HBF_4, and HCOOH) and bases (e.g. NH_3, NMe_3, NH_2Me), with formation of the corresponding salts.

For instance, complete conversion of the neutral crystalline zwitterion into the crystalline chloride salt is attained in 5 min of exposure to vapors of aqueous HCl 36%. Formation of the salt in the heterogeneous reaction is easily assessed by comparison of the observed X-ray powder diffraction pattern with that calculated on the basis of the single-crystal structure determined previously.

Crystalline $[Co^{III}(\eta^5-C_5H_4COOH)_2]Cl \cdot H_2O$ (see **Figure 2**) can be converted back to neutral $[Co^{III}(\eta^5-C_5H_4COOH)(\eta^5-C_5H_4COO)]$ by heating the sample for 1h at 440 K in an oil-bath under low pressure (10^{-2} mbar). Thermogravimetric analysis (TGA) demonstrates that the solid product releases one water molecule and one HCl molecule per molecular unit at 394 and 498 K, respectively. The powder diffractogram of the final product corresponds precisely to that of the anhydrous $[Co^{III}(\eta^5-C_5H_4COOH)(\eta^5-C_5H_4COO)]$ (see **Figure 2**). The formation of $[Co^{III}(\eta^5-C_5H_4COOH)_2]Cl \cdot H_2O$ from **1** requires that the O-H···O bonds involving the protonated -COOH group and the deprotonated -COO$^{(-)}$ of neighboring zwitterion molecules are replaced, upon absorption of HCl, by $^{(+)}$O-H···Cl$^{(-)}$ interactions between the -COOH groups on the fully protonated organometallic cation $[Co^{III}(\eta^5-C_5H_4COOH)_2]^+$ and the Cl$^{(-)}$ anions.
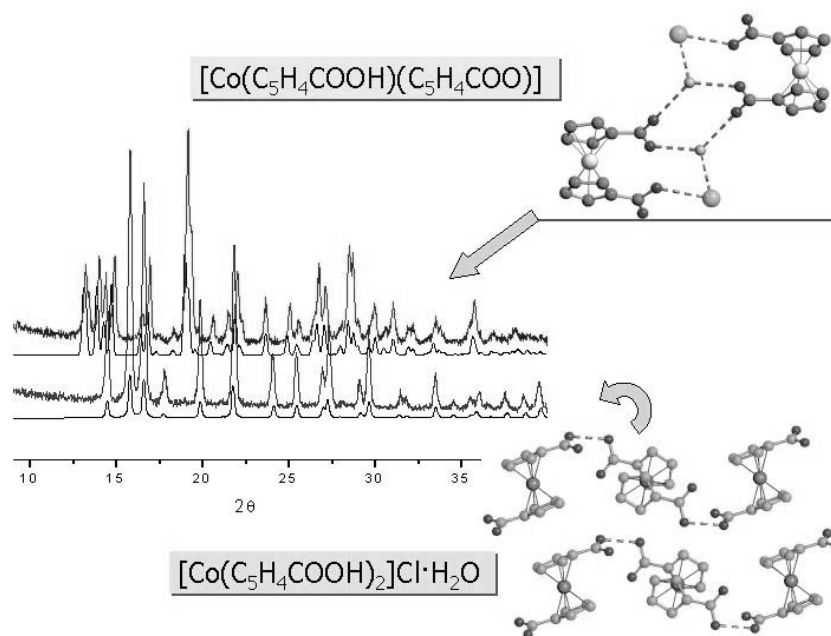
Figure 2. The solid state structures of $[Co^{III}(\eta^5-C_5H_4COOH)_2]Cl\cdot H_2O$ and $[Co^{III}(\eta^5-C_5H_4COOH)(\eta^5-C_5H_4COO)]$.and a comparison of calculated and measured powder diffractograms.

The behavior of the zwitterion towards NH_3 is similar to that towards HCl but obviously opposite in terms of proton exchange. Single crystals of the ammonium salt for X-ray structure determination can be obtained if the reaction of the zwitterion with ammonia is carried out in aqueous solution. 1-10 mg of the neutral system quantitatively transforms into the hydrated ammonium salt $[Co^{III}(\eta^5-C_5H_4COO)_2][NH_4]\cdot 3H_2O$ (see **Figure 3**) upon 5 min exposure to vapors of aqueous ammonia 30%. The structure is shown in Figure 3a. The salt is characterized by the presence of charge-assisted $^{(+)}N\text{-}H\cdots O^{(-)}$ interactions between the ammonium cation and the deprotonated $-COO^{(-)}$ groups on the organometallic anion.

As in the case of the chloride salt, formation of $[Co^{III}(\eta^5-C_5H_4COO)_2][NH_4]\cdot 3H_2O$ in the heterogeneous reaction is assessed by comparing observed and calculated X-ray powder patterns. Absorption of ammonia is also fully reversible: upon thermal treatment (1h at 373 K, ambient pressure) the salts converts quantitatively into the neutral zwitterion.
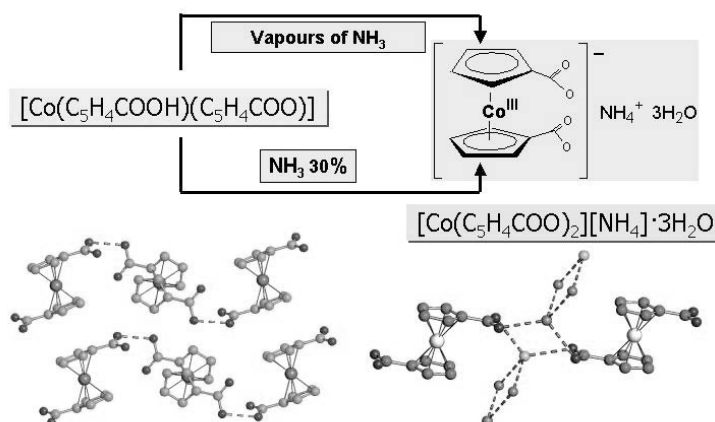
Figure 3. The structures of $[Co^{III}(\eta^5-C_5H_4COOH)(\eta^5-C_5H_4COO)]$ and of $[Co^{III}(\eta^5-C_5H_4COO)_2][NH_4]\cdot 3H_2O$ as obtained from solution and solid-gas reactions.

The two crystalline powders $[Co^{III}(\eta^5-C_5H_4COOH)_2]Cl \cdot H_2O$ and $[Co^{III}(\eta^5-C_5H_4COO)_2][NH_4] \cdot 3H_2O$ can be cycled through several absorption and release processes without decomposition or detectable formation of amorphous material. Infrared spectroscopy can also be utilized to quickly detect formation of the organometallic cation or anion upon reaction with volatile acids or bases.

3.1. Reactions With Other Acid Vapors

Exposure of solid **1** to vapors of CF_3COOH and HBF_4 quantitatively produces the corresponding salts of the cation $[Co^{III}(\eta^5-C_5H_4COOH)_2]^+$, viz. $[Co^{III}(\eta^5-C_5H_4COOH)_2][CF_3COO]$ (see **Figure 4**) and $[Co^{III}(\eta^5-C_5H_4COOH)_2][BF_4]$ (see **Figure 5**). As in the previous cases, all heterogeneous reactions are fully reversible and the acids can be removed by thermal treatment, which quantitatively regenerates the starting material.

In terms of crystal structure organization, formation of $[Co^{III}(\eta^5-C_5H_4COOH)_2][CF_3COO]$ (see **Figure 4**) and $[Co^{III}(\eta^5-C_5H_4COOH)_2][BF_4]$ (see Figure 5), beside leading from a formally neutral system to molecular salts, implies profound molecular rearrangements and breaking and forming of non-covalent interactions. From the analogy between gas-solid and solution reactions, one may thus suppose that the gas-solid reactions occur *via* a process of dissolution and recrystallization as the vapors are adsorbed by the crystalline powder. The reverse process, *i.e.* reconstruction of the zwitterion crystals, is more difficult to explain as it implies proton removal from the cationic acid.
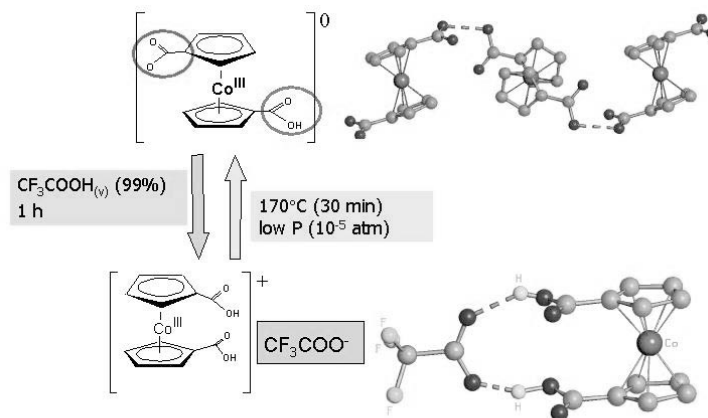
Figure 4. The reaction between **1** and CF_3COOH to yield $[(\eta^5-C_5H_4COOH)_2Co^{III}][CF_3COO]$ as obtained from solution and solid-gas reactions.
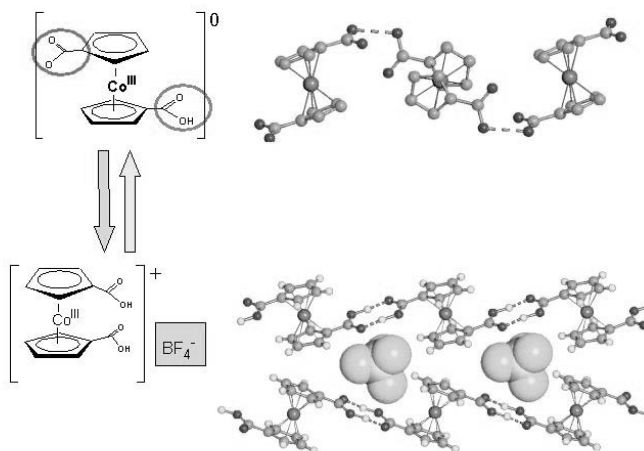
Figure 5. The reaction between **1** and HBF_4 structure to yield $[(\eta^5-C_5H_4COOH)_2Co^{III}][BF_4]$ as obtained from solution and solid-gas reactions.

Analogously to the reaction with CF_3COOH, exposure of the solid zwitterion to vapors of CHF_2COOH quantitatively produces the corresponding salt of the cation $[Co^{III}(\eta^5-C_5H_4COOH)_2][CHF_2COO]$. As in the cases discussed above the solid-gas reaction implies a profound rearrangement of the hydrogen bonding patterns (see **Figure 6**). In fact, the chain of zwitterions linked by O-H⋯O hydrogen bonds between the carboxylate and the carboxylic acid groups needs to be broken and each molecule is required to change conformation to yield the observed ionic pairs between organometallic and organic moieties.

The reaction with hydrated vapors of $CH_2ClCOOH$ produces the hydrated salt $[Co^{III}(\eta^5-C_5H_4COOH)_2][CH_2ClCOO]\cdot H_2O$. Crystalline **1** was also made to react in solution with CHF_2COOH and $CH_2ClCOOH$; single crystals of $[Co^{III}(\eta^5-C_5H_4COOH)_2][CHF_2COO]$ and anhydrous $[Co^{III}(\eta^5-C_5H_4COOH)_2][CH_2ClCOO]$ for X-ray diffraction were obtained from solution crystallization, allowing comparison between computed and measured powder diffraction patterns.

All compounds share the same feature, regardless of how they are obtained: formation of ion pairs (or adducts) between the two acids. What varies is the conformation of the cyclopentadienyl rings and the inter-acid hydrogen bonds as compared in **Figure 7**. In the case of $[Co^{III}(\eta^5-C_5H_4COOH)_2][CH_2ClCOO]$ there is evidence of formation of pseudo-polymorphic forms depending on the reaction condition (whether heterophase or solution). As in the cases discussed above, the heterogeneous reactions are fully reversible; the acids can be quantitatively removed by mild thermal treatment, which regenerates the starting material.
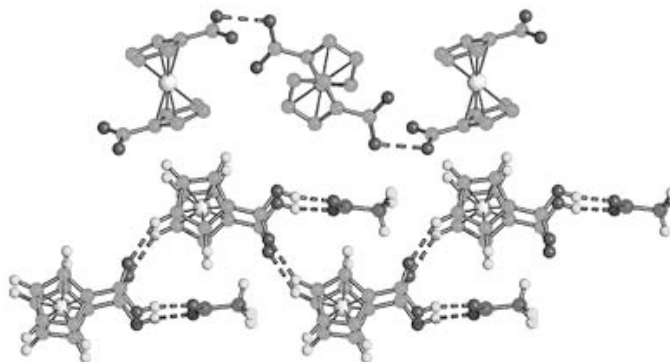
Figure 6. The "transition" from the zwitterionic chain present in crystalline $[(\eta^5-C_5H_4COOH)(\eta^5-C_5H_4COO)Co^{III}]$ **1** (top) and the packing in $[Co^{III}(\eta^5-C_5H_4COOH)_2][CHF_2COO]$ (bottom).
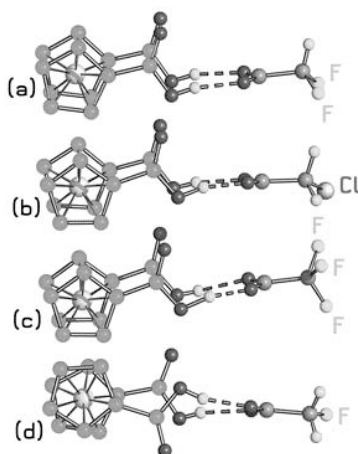
Figure 7. Ion pairs in the solid-state structure of $[Co^{III}(\eta^5-C_5H_4COOH)_2][CHF_2COO]$ and $[Co^{III}(\eta^5-C_5H_4COOH)_2][CH_2ClCOO]$, as obtained from single-crystal X-ray diffraction. The (a) $[CHF_2COO]^-$ and (b) $[CH_2ClCOO]^-$ anions "pinch" the two protonated COOH groups on the organometallic moiety. A similar arrangement is present in crystals of $[Co^{III}(\eta^5-C_5H_4COOH)_2][CF_3COO]$ (c) and in crystalline $[Co^{III}(\eta^5-C_5H_4COOH)_2][CH_2FCOO]$ (d).

Compound **1** also reversibly absorbs formic acid from humid vapors forming selectively a 1:1 co-crystal, $[Co^{III}(\eta^5\text{-}C_5H_4COOH)(\eta^5\text{-}C_5H_4COO)][HCOOH]$, from which **1** can be fully recovered by mild thermal treatment. Complete conversion of crystalline **1** (50 mg) into $[Co^{III}(\eta^5\text{-}C_5H_4COOH)(\eta^5\text{-}C_5H_4COO)][HCOOH]$ is attained in 4h of exposure to hydrated vapors of HCOOH.

It is worth noting that, contrary to the other compounds described above, no proton transfer from the adsorbed acid to the organometallic moiety is observed. Hence, the reaction between **1**(solid) and HCOOH(vapor) would be more appropriately described as a special kind of solvation rather than as a heterogeneous acid-base reaction.

As shown in **Figure 8**, crystalline $[Co^{III}(\eta^5\text{-}C_5H_4COOH)(\eta^5\text{-}C_5H_4COO)][HCOOH]$ is composed of pairs of zwitterion molecules linked by O-H···O bonds between the protonated -COOH and the deprotonated –COO⁻ groups [O···O separation 2.526(4) Å]. On the other hand, the C-O distances within the HCOOH moiety [C-O5 1.305(5), C-O6 1.199(5) Å] indicate that the formic acid molecule retains its acidic hydrogen. This is also confirmed by ^{13}C CPMAS NMR spectroscopy.
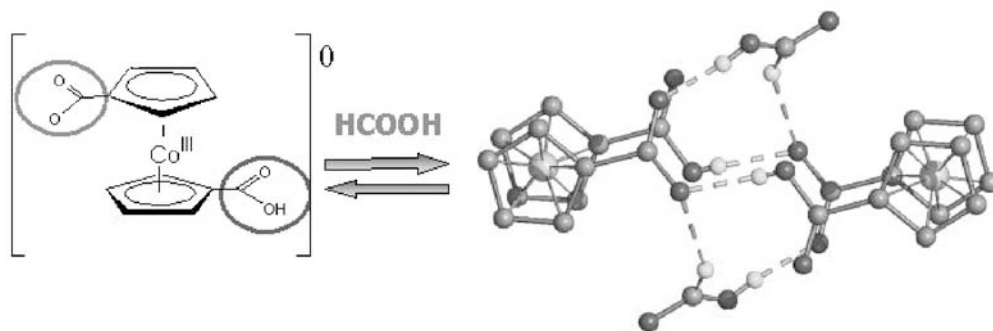

Figure 8. The reaction between **1** and HCOOH to yield $[Co^{III}(\eta^5\text{-}C_5H_4COOH)(\eta^5\text{-}C_5H_4COO)][HCOOH]$ as obtained by gas-phase or solution chemistry.

The product, as the others, can be converted back to **1** by leaving the sample at room temperature in the air for few days or by mild heating in a thermogravimetric experiment (stoichiometric loss of formic acid at 417 K). The powder diffractogram of the degassed product corresponds precisely to that of **1**, which can be cycled through several absorption and release processes without decomposition or detectable formation of amorphous material.

In a previous paper [20] we reported the synthesis of the iodide salt $[Co^{III}(\eta^5\text{-}C_5H_4COOH)_2]^+I^-$ obtained from 1-1'-dimethylcobalticinium and using the acid HI as a 54% aqueous solution. In the context of this work we were interested in the preparation of same salt *via* vapor uptake of HI from the zwitterion **1**. Unfortunately, no reaction was observed even after long exposure of the organometallic reagent to the hydrated acid vapors. The reaction was also conducted in solution, by reacting **1** directly with HI in a 1:1 molar ratio. The resulting compound, which we were able to characterize by single crystal X-ray diffraction, turned out to possess a different stoichiometry from the one already reported earlier since the cation $[Co^{III}(\eta^5\text{-}C_5H_4COOH)]_2^+$ co-crystallizes with one equivalent of the zwitterion $[Co^{III}(\eta^5\text{-}C_5H_4COOH)(\eta^5\text{-}C_5H_4COO)]$ **1** with formation of a salt of formula **1**·$[Co^{III}(\eta^5\text{-}C_5H_4COOH)]_2^+I^-$. In view of the structural relationship with the compounds described thus far, it is worth pointing out some essential structural features of this novel compound. (See **Figure 9**)

The two organonometallic moieties form a sort of hydrogen bonded dimeric unit linked by intermolecular hydrogen bonds. The hydrogen bonded system is, however, disordered because the two moieties are related by an inversion center. This crystallographic symmetry is very likely due to the fact that in the crystal the two sites of the sandwich compounds are occupied randomly by the neutral zwitterionic form and by the cations dicarboxylic acid with a total of three protons for six potential hydrogen bonds. One of the possible

combinations of hydrogen bonds compatible with this structure and with the site symmetry is shown. No H atoms have been located (see Experimental section).
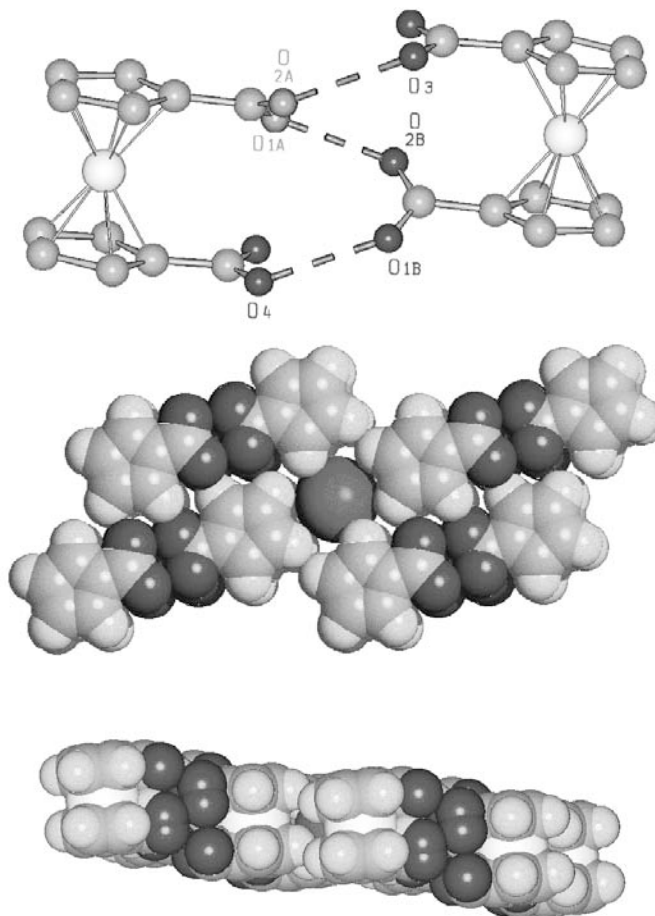
Figure 9. (Top) One of the possible structures of the "super"-cation $\mathbf{1}\cdot[Co^{III}(\eta^5\text{-}C_5H_4COOH)]_2^+$ in the iodide salt. The disorder of O1 and O2 is due to the necessity of optimizing the $O(H)\cdots O$ interactions within the $\mathbf{1}\cdot[Co^{III}(\eta^5\text{-}C_5H_4COOH)_2]^+$ unit. (Middle, bottom) space-filling views of the way the iodide ion is encapsulated between the super-cations.

4. SOLID-SOLID REACTIONS

In the context of our investigation of solid-state processes, [21] we have prepared hybrid organometallic-inorganic salts by reacting anhydrous **1**(solid) with a number of alkali salts MX (M = K^+, Rb^+, Cs^+, NH_4^+; X = Cl^-, Br^-, I^-, PF_6^- though not in all permutations of cations and anions, see below). As in the cases discussed above, exact information about the solid state structures of the reaction products were obtained by single-crystal X-ray diffraction experiments carried out on crystals obtained from the reaction powders. Information on the hydrogen bonding nature and on the relationship between structures in solution and those obtained in the solid-state by mechanical grinding were obtained by a combination of solution and solid state NMR.

In view of the analogies in preparation and the likelihood of the structures obtained by solid-state complexation, the supramolecular complex $[Co^{III}(\eta^5\text{-}C_5H_4COOH)(\eta^5\text{-}C_5H_4COO)]_2\cdot Cs^+I^-$, $\mathbf{1}_2\cdot Cs^+I^-$ can be used as an example.

Compound $\mathbf{1}_2\cdot Cs^+I^-$ is isostructural with the members of the family of hexafluorophosphate salts $[Co^{III}(\eta^5\text{-}C_5H_4COOH)(\eta^5\text{-}C_5H_4COO)]_2\cdot M^+[PF_6]^-$, $\mathbf{1}_2\cdot M^+[PF_6]^-$ (M = K^+, Rb^+, Cs^+, $[NH_4]^+$) previously

obtained from the cationic acid $[Co^{III}(\eta^5\text{-}C_5H_4COOH)_2][Co^{III}(\eta^5\text{-}C_5H_4COOH)(\eta^5\text{-}C_5H_4COO)]^+[PF_6]^-$ by treatment with MOH or ammonia. Compound $\mathbf{1}_2\cdot Cs^+I^-$ is thus characterized by the presence of a supramolecular cage formed by four zwitterionic molecules encapsulating the Cs^+ cations. The cage is sustained by $O\text{-}H\cdots O$ hydrogen bonds between carboxylic –COOH and carboxylate –$COO^{(-)}$ groups, and by $C\text{-}H\cdots O$ bonds between –CH_{Cp} and –CO groups, while the I^- anions form layers in between the cationic complexes, as shown in **Figure 10**. The structure determination was instrumental to the identification and characterization of the product obtained by solid-state grinding. **Figure 10b** shows a comparison between the XRPD patterns of polycrystalline $\mathbf{1}_2\cdot Cs^+I^-$, obtained by grinding the reagents together, and that calculated on the basis of the single crystal structure described above.
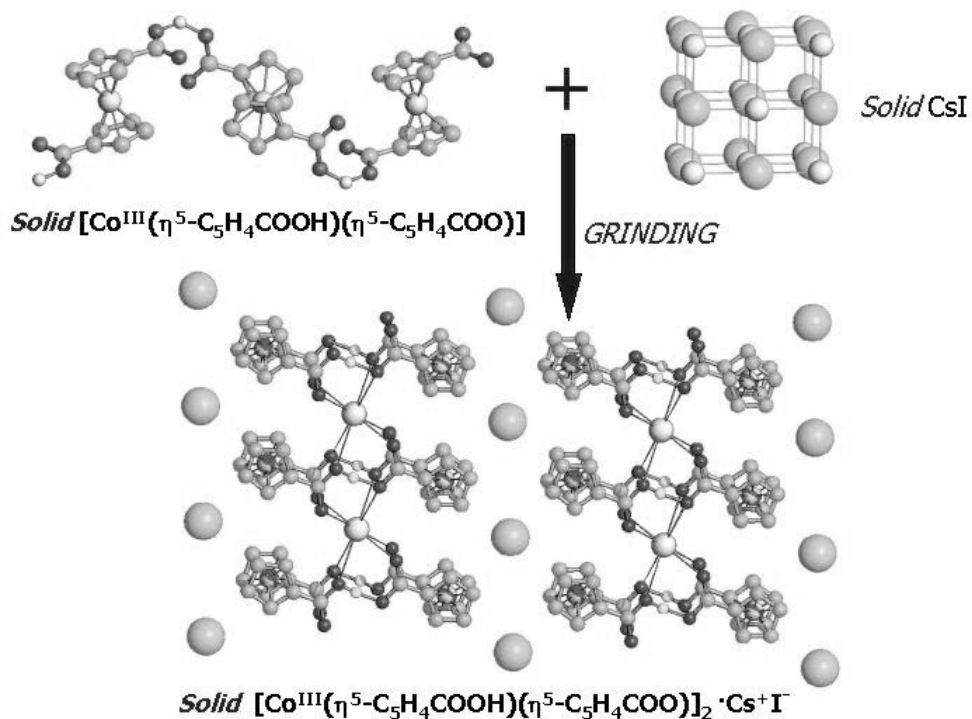

Figure 10. (a) The structure of the Cs adduct $\mathbf{1}_2\cdot Cs^+I^-$, (b) shows a comparison between the XRPD patterns of polycrystalline $\mathbf{1}_2\cdot Cs^+I^-$, obtained by grinding the reagents together, and that calculated on the basis of the single crystal structure.

The organometallic zwitterion **1** has also been utilized recently in the mechanochemical reaction with the solid base 1,4-diazabicyclo[2.2.2]octane $[C_6H_{12}N_2]$. The 1:2 reaction generates quantitatively the hydrated 1:2 adduct $[C_6H_{12}N_2H_2]^{2+}[Co^{III}(\eta^5\text{-}C_5H_4COO)_2]_2^{2-}\cdot 1.5H_2O$. The solid-solid reaction does not occur *via* formation of eutectic phases. Structural characterization (see below) allows us to see that the formation of the hybrid organic-organometallic compound imply proton transfer from the acid to the base, breaking and forming of the hydrogen bonding network in **1** and is accompanied by a profound structural rearrangement.

The mechanochemical preparation was carried out by manual grinding in an agata mortar of equimolar quantities of the two solid reactants (see Experimental section). After grinding, the polycrystalline material was used as such for powder diffraction experiments. In separate experiments (i) the zwitterion and base were dissolved in methanol in 2:1 and the solvent was allowed to evaporate at room temperature and (ii) small portions of the ground samples were dissolved in the minimum amount of solvent, in order to act as *seeds* and allow growth of single crystals suitable for X-ray diffraction experiments. By comparison with the diffractograms measured on the raw reactants, it was possible to ascertain whether the starting materials had been completely converted into products. The structure of the compound obtained mechanochemically is the same as the one obtained from solution crystallization.

Grinding of the zwitterion with the base in stoichiometric amounts other than 1:2 (i.e. 1:1, and 2:1) does not appear to lead to formation of different compounds, rather a mixture of the 1:2 products and of unreacted base or acid (as ascertained by X-ray powder diffraction) was invariably observed.

Figure 11 (top) shows that the adduct is characterized by the presence of a $[C_6H_{12}N_2H_2]^{2+}$ dication acting as a bridge between two $[Co^{III}(\eta^5\text{-}C_5H_4COO)_2]^-$ anions in *transoid* conformation, with formation of *charge-assisted* $^{(-)}O \cdots H\text{-}N^{(+)}$ hydrogen bonding interactions. **Figure 11** (bottom) shows how one of the water molecules (oxygen O5) is used to link together the $[C_6H_{12}N_2H_2]^{2+}[Co^{III}(\eta^5\text{-}C_5H_4COO)_2]_2^{2-}$ adducts.
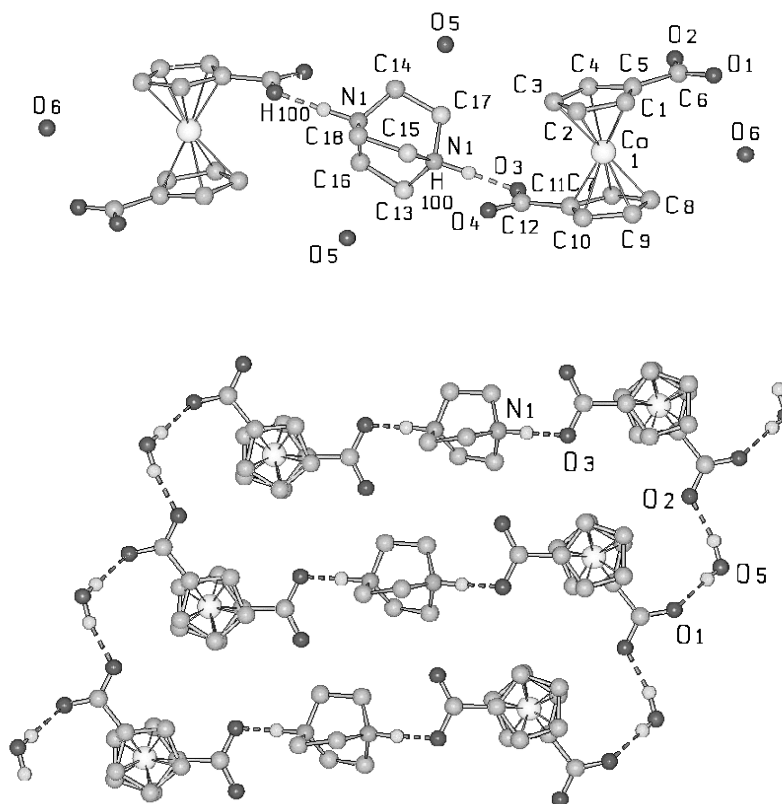
Figure 11. (Top) the adduct $[C_6H_{12}N_2H_2]^{2+}[Co^{III}(\eta^5\text{-}C_5H_4COO)_2]_2^{2-}$ is characterized by the presence of a $[C_6H_{12}N_2H_2]^{2+}$ dication acting as a bridge between two $[Co^{III}(\eta^5\text{-}C_5H_4COO)_2]^-$ anions in *transoid* conformation; (bottom) water molecules link together the $[C_6H_{12}N_2H_2]^{2+}[Co^{III}(\eta^5\text{-}C_5H_4COO)_2]_2^{2-}$ adducts. Relevant hydrogen bond parameters are N(1)···O(3) 2.580(6), O(5)···O(2) 2.733(7), O(5)···O(1) 2.766(7) Å.

5. EXPERIMENTAL SECTION

All the starting materials were purchased from Aldrich and used without further purification. Reagent grade solvents and bidistilled water were used.

Mechanochemical and solution syntheses of $[C_6H_{12}N_2H_2]^{2+}[Co^{III}(\eta^5\text{-}C_5H_4COO)_2]_2^{2-}\cdot 1.5H_2O$. 20.2 mg (0.073 mmol) of **1** and 8.2 mg (0.073 mmol) of 1,4-diazabicyclo[2.2.2]octane were manually ground in an agate mortar for 5 min; single crystals of $[C_6H_{12}N_2H_2]^{2+}[Co^{III}(\eta^5\text{-}C_5H_4COO)_2]_2^{2-}\cdot 1.5H_2O$ suitable for single crystal X-ray diffraction were obtained by slow evaporation of a solution obtained dissolving 23.2 mg (0.084 mmol) of **1** and 9.4 mg (0.084 mmol) of 1,4-diazabicyclo[2.2.2]octane in 3 mL of methanol 99.8% seeded with 5 mg of the ground sample.

Crystal structure determination. X-ray diffraction data for **1**·[Co^{III}(η^5-C$_5$H$_4$COOH)$_2$]$^+$I$^-$ and [C$_6$H$_{12}$N$_2$H$_2$]$^{2+}$ [Co^{III}(η^5-C$_5$H$_4$COO)$_2$]$_2$$^{2-}$· 1.5H$_2$O were collected at room temperature on a Nonius CAD-4 diffractometer. Crystal data and details of measurements are summarized in Table 1. Common to both compounds: MoKα radiation, λ = 0.71073 Å, monochromator graphite, ψ-scan absorption correction. The SHELXL97 [23a] package was used for structure solution and refinement based on F^2. All non-H atoms were refined anisotropically. The I$^-$ anion in **1**·[Co^{III}(η^5-C$_5$H$_4$COOH)$_2$]$^+$I$^-$ is located on an inversion center, while the neutral and cationic moieties are related by a second inversion center; despite the good data quality, it was not possible to locate the three hydrogen atoms belonging to the -COOH groups. The anion in [C$_6$H$_{12}$N$_2$H$_2$]$^{2+}$[Co^{III}(η^5-C$_5$H$_4$COO)$_2$]$_2$$^{2-}$·1.5H$_2$O is disordered over two positions, with 50:50 occupancy ratio; one of the two water molecules [O(6)] is also disordered around an inversion center, and was assigned an occupancy factor of 0.5. H$_{(CH)}$ atoms were added in calculated positions. In [C$_6$H$_{12}$N$_2$H$_2$]$^{2+}$[Co^{III}(η^5-C$_5$H$_4$COO)$_2$]$_2$$^{2-}$·1.5H$_2$O the H$_{(NH)}$ atom and the hydrogen atoms belonging to the water molecule that is not disordered were located from a difference Fourier map and not refined. The program SCHAKAL99 [23b] was used for all the graphical representations. The program PLATON [23c] was used to calculate the hydrogen bonding interactions. In all cases, correspondence between the structures determined by single crystal X-ray diffraction and that of the bulk materials precipitated from solution was confirmed by comparing the experimental powder diffractograms obtained from the bulk material with those calculated on the basis of the single crystal structures.

Table 1
Crystal Data and Details of Measurements for
***1**·[Co^{III}(η^5-C$_5$H$_4$COOH)$_2$]$^+$I$^-$ and [C$_6$H$_{12}$N$_2$H$_2$]$^{2+}$ [Co^{III}(η^5-C$_5$H$_4$COO)$_2$]$_2$$^{2-}$·1.5H$_2$O*

	1·[Co^{III}(η^5-C$_5$H$_4$COOH)$_2$]$^+$I$^-$	[C$_6$H$_{12}$N$_2$H$_2$]$^{2+}$[Co^{III}(η^5-C$_5$H$_4$COO)$_2$]$_2$$^{2-}$ ·1.5H$_2$O
formula	C$_{24}$H$_{19}$Co$_2$IO$_8$	C$_{30}$H$_{36}$Co$_2$N$_2$O$_{11}$
M$_W$	680.15	718.46
system	Triclinic	Triclinic
space group	P-1	P-1
a [Å]	6.898(3)	6.081(3)
b [Å]	7.704(2)	10.605(4)
c [Å]	11.161(2)	12.776(6)
α [°]	87.87(1)	113.77(4)
β [°]	81.71(1)	90.07(4)
γ [°]	72.17(1)	103.83(4)
V [Å³]	558.7(2)	727.7(6)
Z	1	1
F(000)	**334**	744
μ(Mo$_{K\alpha}$) [mm^{-1}]	2.917	2.414
measured reflns	2064	2662
unique reflns	1955	2539
parameters	161	218
GOF on F^2	1.134	0.979
R1 (on F [I >2σ(I)])	0.0285	0.0432
wR2 (on F^2,all data)	0.0763	0.1255

6. CONCLUSIONS

The paradigm of crystal engineering is the "bottom-up" construction of crystalline assembly from components and the exploitation of the resulting crystalline materials for physical and chemical applications. The "bottom-up" paradigm, derived from supramolecular chemistry [22], implies the ability to assemble molecular or ionic components into the desired architecture by engineering a target network of supramolecular interactions.

Since the focus of crystal engineering is *making* crystals, methods of choice to exploit crystal engineering strategies invariably (and inevitably) end up with the problem of obtaining crystals. The desired material needs to be *by definition* in the crystalline form and is usually obtained by a crystallization method, whether from solution, melt or from more forcing hydrothermal syntheses. We have argued that reactions between solids and between solids and vapors can represent alternative ways to prepare crystals. Since reactions involving solid reactants or occurring between solid and gases do not generally require recovery, storage and disposal of solvents, they are of interest in the field of the so-called "green chemistry" where environmentally friendly processes are actively sought [10]. Furthermore solvent-less reactions often lead to very pure products and reduce the formation of solvate species.

In this paper we have discussed how crystal engineering strategies can be exploited to design and construct molecular crystals to take part in solvent-free solid-gas or solid-solid reactions with molecules or molecular aggregates. When the solid state process proceeds *via* breaking and forming of non-covalent interactions (such as hydrogen bonds), the crystalline product is the result of the supramolecular association of two or more units and can be regarded as a *supramolecular reaction* between solid supermolecules.

We have focused on the behavior of the zwitterionic organometallic molecule $[Co^{III}(\eta^5\text{-}C_5H_4COOH)(\eta^5\text{-}C_5H_4COO)]$, **1**, which has proved to be very versatile thanks to its amphoteric acid-base behavior and its coordinating capacity. The solid-gas and solid-solid processes discussed above rely on the possibility of 'switching' between O-H---O hydrogen bonds between molecules of **1** and charge-assisted $^{(+)}$O-H---X$^{(-)}$ or O$^{(-)}$---[H-NR$_3$]$^{(+)}$ hydrogen bonds with cations and anions. In the case of the solid-gas reaction with formic acid, HCOOH, a third possibility has been ascertained: adduct formation without proton transfer. It is worth pointing out that these gas-solid reactions do not differ conceptually from gas-solid solvation. The main difference is in the energetic ranking of the interactions (whether covalent or non-covalent) that are broken or formed through the processes.

It is generally believed that molecular crystals held together only (or mainly) by hydrogen bonding interactions cannot compete with covalent or ionic inorganic solids in terms of cohesion and stability. In this paper we have shown that an organometallic molecule, such as **1**, easy to prepare and relatively inexpensive, can withstand both reversible gas-solid reactions with vapors of acidic and basic substances and mechanically activated reactions with inorganic salts and molecular crystals.

There are still several open issues, which we plan to address in the near future. For instance, we need to explore the effect of particle size and surface on the *kinetics* of the reactions as well as the relationship between composition of the vapor phase and exposure time in gas-solid reactions of **1** and the effect of the grinding time and of humidity on the product formation in the solid-solid reactions of **1**.

7. ACKNOWLEDGMENTS

8. REFERENCES

[1]   a) G. R. Desiraju, *Crystal Engineering: The Design of Organic Solids*, (Elsevier: Amsterdam, 1989); b) D. Braga, F. Grepioni, and G. R. Desiraju, Chem. Rev. **98** (1998) , 1375; c) D. Braga, F. Grepioni, and A. G. Orpen, eds., *Crystal Engineering: from Molecules and Crystals to Materials*,

(Kluwer Academic Publishers, Dordrecht, 1999); d) A. J. Blake, N. R. Champness, P. Hubberstey, W. S. Li, M. A. Withersby, M. Schroder *Coord. Chem. Rev.* **183** (1999), 117; e) L. Brammer, D. Zhao, F. T. Ladipo and J. Braddock-Wilking, *Acta Crystallogr., Sect. B*, **51** (1995), 632; f) C. B. Aakeröy, *Acta Crystallogr*., *Sect. B*, **53** (1997), 569; g) M. W. Hosseini, *Coord. Chem. Rev.,* **240** (2003), 157; h) *Proceedings of the Dalton Discussion on Inorganic Crystal Engineering, J. Chem. Soc. Dalton Trans.,* (2000), 3705. the whole issue; i) B. Moulton and M. J. Zaworotko, *Chem. Rev.,* **101** (2001), 1629;   j) D. Braga, G. R. Desiraju, J. Miller, A. G. Orpen and S. Price, *CrystEngComm*, **4** (2002), 500; l) M. D. Hollingsworth, *Science* **295** (2002), 2410; m) D. Braga, *Chem. Commun.*, (2003), 2751.

[2]   a) A.M. Beatty, *CrystEngComm* (2001); b) M.W. Hosseini and A. De Cian, *Chem. Commun.,* (1998), 727; c) C.B. Aakeröy and K.R. Seddon, *Chem. Soc. Rev.*, (1993), 397; d) T. Maris ; J.D. Wuest *J. Org. Chem.,* **69** (2004), 1776.

[3]   *The Crystal as a Supramolecular Entity. Perspectives in Supramolecular Chemistry.* G. R. Desiraju, Ed.; Wiley: Chichester, 1996.

[4]   a) G. R. Desiraju, *Angew. Chem. Int. Ed.,* **34** (1995), 2311; b) G. Gilli and P. Gilli, *J. Mol. Struc.*, **552** (2000), 1; c) D. Braga, L. Maini, F. Grepioni, F. Mota, C. Rovira, and J. J. Novoa, *Chem. Eur. J.*, **6** (2000), 4536; d) D. Braga, E. D'Oria, F. Grepioni, F. Mota, and J.J. Novoa, *Chem. Eur. J.,* **8** (2002), 1173; e) T. Steiner, *Angew. Chem. Int. Ed.*, **41** (2002), 48; f) G. R. Desiraju, *Acc. Chem. Res.*, **35** (2002), 565.

[5]   a) S. R. Batten and R. Robson, *Angew. Chem. Int. Ed.,* **37** (1998), 1461; b) S. R. Batten, B. F. Hoskins and R. Robson, *Chem. Eur. J.,* **6** (2000), 156; c) N. L. Rosi, M. Eddaoudi, J. Kim, M. O'Keeffe and O. M. Yaghi, *Angew. Chem. Int. Ed.*, **41** (2001), 284; d) O. M. Yaghi, H. L. Li, C. Davis, D. Richardson and T. L. Groy, *Acc. Chem. Res.*, **31** (1998), 474; e) H. Li, M. Eddaoudi, M. O'Keeffe and O. M. Yaghi, *Nature,* **402** (1999), 276; f) M. Eddaoudi, J. Kim, N. Rosi, D. Vodak, J. Wachter, M. O'Keefe and O. M. Yaghi, *Science,* **295** (2002), 469; g) S. A. Bourne, J. Lu, B. Moulton and M. J. Zaworotko, *Chem. Commun.*, (2001), 861; h) B. Rather and M. J. Zaworotko, *Chem. Commun.*, (2003), 830; i) B. Moulton, H. Abourahma, M. W. Bradner, J. Lu, G. J. McManus and M. J. Zaworotko, *Chem. Commun.*, (2003), 1342; l) M. Fujita, *Chem. Soc. Rev.*, **27** (1998), 417; m) B. Olenyuk, A. Fechtenkötter and P. J. Stang, *J. Chem. Soc.*, *Dalton Trans.*, (1998), 1707; n) N. L. Rosi, M. Eddaoudi, J. Kim, M. O'Keeffe and O. M. Yaghi, *Cryst. Eng. Comm.*, **4** (2002), 401; o) N.L. Rosi, J. Eckert, M. Eddaoudi, D.T. Vodak, J. Kim, M. O'Keeffe and O. M. Yaghi, *Science*, **300** (2003), 1127; p) M. D. Ward, *Science*, **300** (2003), 1124; q) L. Pan, M. B. Sander, X. Huang, J. Li, M. Smith, E. Bittner, B. Backrush and J. K. Johnson, *J. Am. Chem. Soc.*, **126** (2004), 1309; r) G. Frey, M. Larches, C. Sere, F. Mélange, T. Roseau and A. Percheron-Guégan, *Chem. Commun.*, (2003), 2976.

[6]   a) F. A. Cotton, C. Lin and C. A. Murillo, *J. Chem. Soc.*, *Dalton Trans.*, (2001), 499; b) F. A. Cotton, C. Lin, and C. A. Murillo, *Chem. Commun.*, (2001), 11; c) M. E. Braun, C. D. Steffek, J. Kim, P. G. Rasmussen and O. M. Yaghi, *Chem. Commun.*, (2001), 2532; d) W. Mori and S. Takamizawa, *J. Solid State Chem.*, **152** (2000), 120; e) L. Carlucci, G. Ciani, D. M. Proserpio and S. Rizzato, *CrystEngComm*., **4** (2002), 121; f) L. Carlucci, G. Ciani and D. M. Proserpio, *CrystEngComm*., **5** (2003), 269; g) L. Carlucci, G. Ciani and D. M. Proserpio, *Coord. Chem. Rev.*, **246** (2003), 247.

[7]   See, for example: a) M. Albrecht, M. Lutz, A. L. Speck and G. van Koten, *Nature*, **406** (2000), 970; b) M. Albrecht, R. A. Gossage, M. Lutz, A. L. Speck and G. van Koten, *Chem. Eur. J.*, **6** (2000), 1431.

[8]   D. Braga and F. Grepioni, *Angew. Chem. Int. Ed. Engl.*, **43** (2004), 4002.

[9]   D. Braga, L. Maini, M. Polito, L. Mirolo and F. Grepioni, *Chem. Eur. J.*, **9** (2003), 4362.

[10]   P. T. Anastas and J. C. Warner, *Green Chemistry: Theory and Practice*, (Oxford University Press, New York, 1998).

[11]   D. Braga, L. Maini, M. Polito and F. Grepioni, *Organometallics*, **18** (1999), 2577.

[12]   D. Braga, G. Cojazzi, D. Emiliani, L. Maini and F. Grepioni, *Chem Commun.*, **21** (2001), 2272.

[13]   D. Braga, G. Cojazzi, D. Emiliani, L. Maini and F. Grepioni, *Organometallics*, **21** (2002), 1315.

[14]   D. Braga, L. Maini, M. Mazzotti, K. Rubini and F. Grepioni, *CrystEngComm*., **5** (2003), 154 .

[15]   D. Braga, Lucia Maini, M. Mazzotti, K. Rubini, A. Masic, R. Gobetto and F. Grepioni, *Chem. Commun.*, (2002), 2296.

[16]   a) D. Braga, G. Cojazzi, D. Emiliani, L. Maini, and F. Grepioni, *Chem. Commun.*, (2001), 2272; b) D. Braga, G. Cojazzi, D. Emiliani, L. Maini, and F. Grepioni, *Organometallics*, **21** (2002), 1315.

[17]   a) D. Braga, F. Grepioni, *Chem. Soc. Rev.,* **4** (2000), 229; b) D. Braga and F. Grepioni in *Crystal Design, Structure and Function. Perspectives in Supramolecular Chemistry*, (Vol. 7, Ed. G. R. Desiraju), (J. Whiley, Chichester, UK, 2003).

[18]   a) T. L. Threlfall, *Analyst,* **120** (1995), 2435; b) N. Kubota, N. Doki, M. Yokota and D. Jagadesh, *J. Chem. Eng. Japan.,* **35** (2002), 1063.

[19]   D. Braga, L. Maini, G. de Sanctis, K. Rubini, F. Grepioni, M. R. Chierotti and R. Gobetto, *Chem. Eur. J.*, **9** (2003), 5538.

[20]   D. Braga. D. Emiliani, G. Cojazzi, L. Maini, M. Polito, F. Grepioni *J. Mol. Struc.*, **647**, (2003), 113.

[21]   a) D. Bradley, *Chemistry in Britain*, (2002), 42; b) K. Tanaka, F. Toda, *Chem. Rev.*, **100** (2000), 1025; c) K. Tanaka, *Solvent-free Organic Synthesis*, (Wiley-VCH, 2003); d) G. W. V. Cave, C. L. Raston and L. Scott, *Chem. Commun.*, (2001), 2159; e) G. Rothenberg, A. P. Downie, C. L. Raston and J. L. Scott, *J. Am. Chem. Soc.*, **123** (2001), 8701; f) G. Kaupp, *CrystEngComm.,* **5** (2003), 117; g) V. V. Boldyrev and K. Tkacova, *J. Mat. Synth. Proc.*, **8** (2000), 121; h) L. R. MacGillivray, *CrystEngComm*., **4** (2002), 37; i) F. Toda, *CrystEngComm.,* **4** (2002), 215.

[22]   a) J. M. Lehn, *Supramolecular Chemistry: Concepts and Perspectives*, (VCH, Weinheim, 1995); b) J. W. Steed and J. L. Atwood, *Supramolecular Chemistry*, (Wiley & Sons, 2000).

[23]   a) G. M. Sheldrick, *SHELXL97, Program for Crystal Structure Determination*, (University of Göttingen: Göttingen, Germany, 1997); b) E. Keller, *SCHAKAL99, Graphical Representation of Molecular Models,* (University of Freiburg, Germany, 1999); c) A. L. Spek, *Acta Crystallogr.(Sect. A),* **46** (1990), C31.